DISSERTATION

Photocatalytic Carbon Dioxide Reduction with Ionic Liquids

ausgeführt zum Zwecke der Erlangung des akademischen Grades eines Doktors der Naturwissenschaften

unter der Leitung von

Univ. Prof. Dipl.-Ing. Dr. techn. Katharina Schröder

E163-03-5
Institut für Angewandte Synthesechemie

eingereicht an der Technischen Universität Wien

Fakultät für Technische Chemie

von

Lisa Eisele MSc, BSc

Matrikelnummer: **12102426**

Wien, Februar 2025

Acknowledgements

I want to thank all the people whom I met during the last four years of my PhD. First and foremost, I would like to express my gratitude to my supervisor, Prof. Dr. Katharina Schröder, for giving me the opportunity to pursue my PhD. I am very grateful for all the support and advice she gave me over the years of my PhD as well as the trust to explore things on my own and to contribute to the group's research endeavours.
I would also like to extend my appreciation to my co-supervisor, Prof. Dr. Dominik Eder, for all the guidance he provided in the field of materials chemistry.
Furthermore, I want to acknowledge and appreciate the contributions of Alexey Cherevan to my PhD journey, as he was always available for valuable advice and troubleshooting. His unwavering enthusiasm and creativity consistently served as a great source of inspiration.
I am very grateful to all my former and current lab colleagues: Philipp Mikšovsky, Fabian Scharinger, Kristof Stagel, Ádám Pálvölgyi, Prasad Kathe, Cornelia Büttner, Olga Lanaridi, Julia Piotrowska, Bletë Hulaj, Michael Weiser, Florian Ehrschwendtner, Dorottya Mikoczi, Giada Moroni and Laura Ielo for creating an exceptionally pleasant and professional atmosphere in the lab.
Additionally, I want to extend my acknowledgments to all the members of the Eder group for their fellowship welcoming me as a guest in their lab and their willingness to collaborate and share their experience. Special thanks in this matter go to Jakob Blaschke, Samar Batool, Stephen Nagaraju Myakala, Shaghayegh Naghdi, Dogukan Hazar Apaydin, Jasmin Schubert, Hannah Rabl and Pablo Ayala.
Finally, I want to thank my friends and family for supporting me during this journey. I am extremely thankful for my partner, Johannes who supported and encouraged me during these years.

Abstract

This thesis investigates the photocatalytic reduction of CO_2 to CO, a key intermediate in chemical production. Imidazolium-based ionic liquids (ILs), renowned for their CO_2 physi- and chemisorption properties, were studied for their cooperative effects to improve photocatalytic performance.

The work starts with a review of imidazolium-based ionic liquids for photocatalytic CO_2 reduction, providing a comprehensive overview of the state-of-the-art developments in the field. This is followed by three major studies that progressively develop the application of imidazolium-based ionic liquids, transitioning from homogeneous catalysis to heterogeneous photocatalysis and gas-phase photoreductions.

First, in homogeneous photocatalysis, a benchmark system consisting of a Ru-based photosensitizer and a Re-catalyst was investigated. The addition of imidazolium-based ionic liquids, specifically 1-ethyl-3-methylimidazolium acetate in DMF, resulted in a strong enhancement of CO formation, with up to 20-fold increase observed. Even small amounts of ionic liquid were effective, and a clear correlation between anion basicity and CO_2 activation was demonstrated. However, stability limitations necessitated further adaptations.

To further develop the system toward heterogeneous photocatalysis, the system was immobilized within a polymerized ionic liquid matrix. Vinyl-functionalized photosensitizer and catalyst components were co-polymerized with a vinyl-modified imidazolium ionic liquid monomer. Characterization confirmed the preservation of catalyst oxidation states and component integrity. This heterogeneous system extended operational stability to 4 hours with sustained CO selectivity, a significant improvement over the 40-minute stability was observed in the homogeneous system. Mechanistic studies confirmed light excitation of the Ru-sensitizer and subsequent electron transfer to the Re-catalyst.

Subsequently, the approach was extended to porous UiO-67 metal-organic frameworks (MOFs). The covalent incorporation of imidazolium groups was investigated to transfer the CO_2-activating properties of imidazolium functionalities to highly porous materials.

Finally, a photocatalytic gas-phase reactor system was developed for both batch and continuous flow conditions. Prototypes were designed to enable sampling and catalyst testing, with the goal of scaling up heterogeneous materials such as supported ionic liquid phase (SILP) catalysts and graphitic carbon nitride (gCN)-based photoactive supports.

Zusammenfassung

Diese Dissertation untersucht die photokatalytische Reduktion von CO_2 zu CO, einem wichtigen Zwischenprodukt in der chemischen Industrie. Imidazolium-basierte ionische Flüssigkeiten (ILs), die CO_2 gut über Physi- und Chemisorption aktivieren können, wurden hinsichtlich ihrer kooperativen Effekte zur Verbesserung der photokatalytischen Reduktion untersucht.

Die Arbeit wird mit einem zusammenfassenden Artikel über die Anwendung von Imidazolium-basierten ionischen Flüssigkeiten in der photokatalytischen CO_2-Reduktion eingeleitet. Der Artikel fasst wichtige und aktuelle Entwicklungen auf diesem Gebiet zusammen. Darauf folgen drei aufeinander aufbauende Hauptstudien, die die Anwendung von Imidazolium-basierten ionischen Flüssigkeiten in der photokatalytischen Reduktion von CO_2 untersuchen – beginnend mit homogener Katalyse über die heterogene Photokatalyse bis hin zu Gasphasen-Photoreduktionen.

Zunächst wurde ein homogenes photokatalytisches Referenzsystem untersucht, das aus einem Ru-basierten Photosensibilisator und einem Re-Katalysator besteht. Die Zugabe von Imidazolium-basierten ionischen Flüssigkeiten, speziell 1-Ethyl-3-methylimidazoliumacetat in DMF, führte zu einer starken Verbesserung der CO-Bildung, wobei ein bis zu 20-facher Anstieg beobachtet wurde. Bereits geringe Mengen an ionischer Flüssigkeit hatten einen stark positiven Einfluss, und es konnte eine Korrelation zwischen der Basizität des Anions und der CO_2-Aktivierung nachgewiesen werden. Die begrenzte Langzeitstabilität erforderte jedoch weitere Anpassungen.

Zur Weiterentwicklung des Systems in Richtung heterogener Photokatalyse wurden die Katalysatoren in einer polymerisierten ionischen Flüssigkeitsmatrix immobilisiert. Vinyl-funktionalisierte Photosensibilisator- und Katalysatorkomponenten wurden mit einem vinylmodifizierten Imidazolium-Monomer copolymerisiert. Durch Charakterisierung konnten die Oxidationszustände des Katalysators und die Integrität aller Teilkomponenten verifiziert werden. Dieses heterogene System verbesserte die Langzeitstabilität auf vier Stunden mit anhaltend hoher Selektivität für CO als Produkt, was eine deutliche Verbesserung gegenüber der 40-minütigen Stabilität des homogenen Systems darstellt. Mechanistische Studien bestätigten die Lichtanregung des Ru-Photosensibilisators und den anschließenden Elektronentransfer zum Re-Katalysator.

In weiterer Folge wurde das Konzept auf poröse metallorganische Gerüstverbindungen ("metal-organic frameworks", MOFs) übertragen. Die kovalente Einbindung von Imidazolium-Gruppen in MOFs wurde untersucht, um die CO_2-aktivierenden Eigen-

schaften der Imidazolium-Gruppe auf hochporöse Materialien zu übertragen.

Abschließend wurde ein photokatalytisches Reaktorsystem für Experimente in der Gasphase unter Batch- und Durchflussbedingungen entwickelt. Prototypen wurden entworfen, um Probenahme und Katalysatortests zu ermöglichen. Ziel ist es, heterogene Materialien wie geträgerte ionische Flüssigkeiten ("supported ionic liquid phases", SILPs) und Katalysatoren mit Kohlenstoff-Nitrid (gCN)-basierten photoaktiven Trägermaterialien zu untersuchen.

Contents

1. Introduction **13**

1.1. Carbon Capture and Utilization 13

1.1.1. Energy demand of conversion 14

1.1.2. The ERC project CARBOFLOW 15

1.2. Photocatalytic CO_2 reduction 16

1.2.1. Homogeneous photocatalysis 16

1.2.2. Heterogeneous photocatalysis 25

1.2.3. Hybrid systems 27

1.2.4. **REVIEW: Photocatalytic CO_2 Reduction with Imidazolium-based Ionic Liquids**

Submitted Manuscript 29

2. Aim of the thesis **49**

3. Results and Discussion **51**

3.1. **Boosting Visible-Light Carbon Dioxide Reduction with Imidazolium-Based Ionic Liquids**

ChemCatChem 16:e202301454 (2024) 51

3.2. **Polymerized ionic liquid co-catalyst driving photocatalytic CO_2 transformation**

RCS Sustainability 9, 2524–2531 (2024) 61

3.3. **Imidazolium modified UiO-67 metal-organic frameworks for CO_2 absorption**

Manuscript in Preparation 71

4. Outlook **89**

4.1. Photocatalytic gas-phase reactions 90

4.1.1. Reactor design and operation 90

4.1.2. In-operando DRIFTs 93

4.1.3. Catalyst development 94

4.2. Summary 98

Bibliography **101**

Appendix **109**

A. **Supplementary information** *ChemCatChem* 16:e202301454 (2024) . . 109

B. **Supplementary information** *RSC Sustainability* 9, 2524-2531 (2024) . 123
C. **Supplementary information** *Manuscript in Preparation* 131
D. General Appendix 139

List of Abbreviations

Abbreviation	Definition
4CzIPN	2,4,5,6-Tetra(9H-carbazol-9-yl)isophthalonitrile
9CNA	9-Cyanoanthracene
A	Acceptor
BNAH	Benzyl dihydronicotinamide
Benz-S	Benzylthiolate
BIH	Phenylbenzimidazoline
CCU	Carbon capture and utilisation
CO_2RR	CO_2 reduction reaction
COFs	Covalent organic frameworks
D	Donor
DMF	Dimethylformamide
DRIFTS	Diffuse reflectance infrared Fourier transform spectroscopy
FRET	Fluorescence resonance energy transfer
gCN	Graphitic carbon nitride
H_2A	Ascorbic acid
HOMO	Highest occupied molecular orbital
ISC	Intersystem crossing
LA-ICP-MS	Laser ablation-inductively coupled plasma-mass spectrometry
LUMO	Lowest unoccupied molecular orbital
MeCN	Acetonitrile
MFCs	Mass flow controllers
MLCT	Metal-to-ligand charge transfer
MOFs	Metal-organic frameworks
NHE	Normal hydrogen electrode
OERS	One electron reduced species
POM	Polyoxymethylene
PS	Photosensitizer
$ScCO_2$	Supercritical carbon dioxide
SCILL	Solid catalyst with ionic liquid layer
SET	Single electron transfer
SILP	Supported ionic liquid phase
SiO_2	Silicon dioxide
TEA	Triethylamine
TEOA	Triethanolamine
XPS	X-ray photoelectron spectroscopy

1. Introduction

1.1. Carbon Capture and Utilization

Facing the climate crisis, carbon dioxide (CO_2) emissions pose a serious threat to planetary health, demanding immediate and decisive action.[1] Achieving net-zero emissions is essential and requires the rapid development of innovative technologies that both reduce emissions and capture and utilize CO_2, supporting the establishment of a circular economy. Combining renewable energy sources to reduce emissions with effective CO_2 capture and recycling provides a sustainable pathway for the future (see Figure 1.1).[2–4]

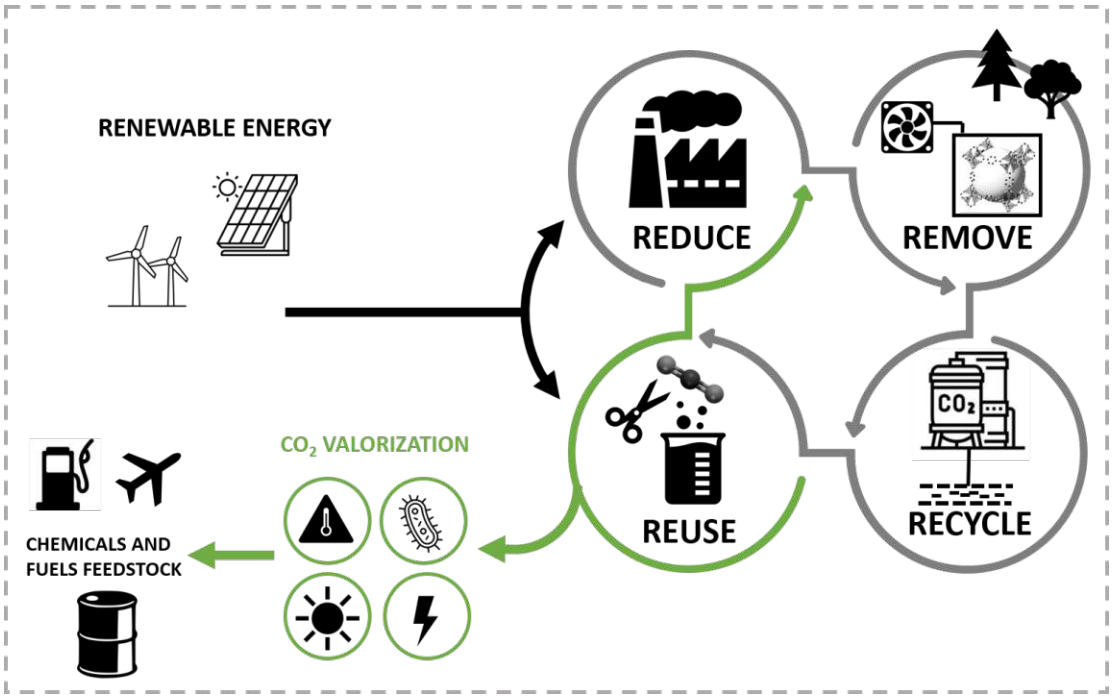

Figure 1.1. Schematic overview of the role of CO_2 valorisation toward carbon neutrality and a circular economy. Thermochemical, biochemical, photochemical, and electrochemical CO_2 valorisation strategies can be used to reuse emitted CO_2, forming building blocks that serve as intermediates for fuels and chemical feedstocks.

Carbon capture and utilization (CCU) technologies are vital for closing the carbon cycle and aligning with circular economy principles. Through CO_2 valorization, carbon dioxide can be converted into valuable resources. CO_2 is captured, transported, and finally transformed into small molecular building blocks through electrochemical, photochemical, thermal, or biochemical techniques.[5] Important C_1 products are carbon

monoxide (CO), formic acid (HCOOH), formaldehyde (HCHO), methanol (CH_3OH), and methane (CH_4). Furthermore, multicarbon chemicals such as oxalic acid ($H_2C_2O_4$), acetic acid (CH_3COOH), acetaldehyde (CH_3CHO), ethanol (CH_3CH_2OH), ethylene (C_2H_4) and ethane (C_2H_6) play an important role.[6] These building blocks can then serve as feedstocks for the chemical industry, enabling the sustainable production of chemical goods or use as synthetic fuels.[7]

Integrating renewable energy with carbon capture and CO_2 valorization presents a promising solution to both reduce emissions and generate valuable products, advancing critical environmental and economic objectives.

1.1.1. Energy demand of conversion

Carbon dioxide (CO_2) as end-product of combustion reactions represents the highest oxidation state of carbon (+IV). Consequently, all transformations to value-added products involve the reduction of carbon. The linear structure of CO_2 is highly stable, requiring significant energy to overcome the reaction barrier of injection of the first electron. Reducing CO_2 by a single electron yields an angled radical anion (see Figure 1.2), an energetically unfavorable process, as it occurs at a very negative potential (E° = -1.90 V vs. NHE at pH 7).[8,9]

Subsequently, reductions involving the transfer of 2, 4, 6, or 8 electrons, along with concurrent proton transfer, occur at less negative potentials (see Table 1.1). The complexity of the cascade necessary for multielectron reduction products comes at the cost of kinetic limitations. The use of catalysts is essential to enable selective reactions under mild conditions, especially given the high overpotentials and kinetic limitations involved.[10]

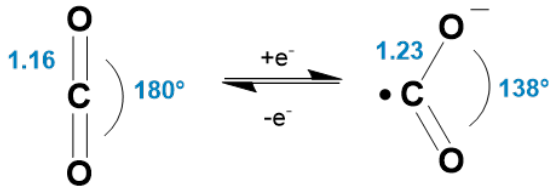

Figure 1.2. Structural description of CO_2 bond angle bending upon the injection of the first electron.[9]

Table 1.1. Half-reactions of CO_2 reduction and their redox potentials at pH= 7.[10]

Product	Reduction half-reaction	Redox potential (V)
CO_2^-	**$CO_2 + 1e^- \rightarrow CO_2^-$**	**-1.9**
CO	$CO_2 + 2e^- + 2H^+ \rightarrow CO + H_2O$	-0.52
$HCOO^-$	$CO_2 + 2e^- + H^+ \rightarrow HCOO^-$	-0.41
HCHO	$CO_2 + 4e^- + 4H^+ \rightarrow HCHO + H_2O$	-0.48
CH_3OH	$CO_2 + 6e^- + 6H^+ \rightarrow CH_3OH + H_2O$	-0.38
CH_4	$CO_2 + 8e^- + 8H^+ \rightarrow CH_4 + 2H_2O$	-0.24

1.1.2. The ERC project CARBOFLOW

Carbon monoxide (CO) is a crucial C_1 building block widely used in industrial processes for synthesizing both bulk and fine chemicals. Examples of industrially significant applications include the utilization of CO in alkene carbonylation, hydroformylation processes, and Fischer-Tropsch synthesis to produce alkanes and alkenes.[11–15] However, the bulk use of CO poses significant challenges due to its high toxicity, which raises safety concerns and handling difficulties in industrial settings. An innovative approach to mitigate these issues is to utilize carbon dioxide (CO_2) as a safer alternative feedstock, with CO formed either in-situ or ex-situ as a reaction intermediate. By integrating CO_2 reduction with carbonylation reactions, this approach aims to create a continuous flow-based process that combines safety and efficiency while supporting sustainable chemical production. The ERC project CARBOFLOW aims to develop efficient strategies to synthesize carbonylation products from CO_2 feedstock by integrating in situ CO_2 reduction with the synthesis of carbonylation products in a streamlined process (see Figure 1.3). To establish environmentally benign reaction conditions, ionic liquids, and supercritical CO_2 are combined to create a multifunctional reaction matrix that sequentially serves as a CO_2 pre-activation catalyst, substrate, solvent, and extraction medium. The project is structured around three main goals:

- Developing (photo-)catalytic CO_2 reduction systems selective for CO in ionic liquid media.
- Advancing parallel carbonylation reactions with CO/CO_2 mixtures.
- Integrating the outcomes of the first two goals to establish a fully streamlined and efficient process for high-value fine chemicals.

This thesis contributes to **Goal 1**, aiming at the development of photocatalytic CO_2 reduction in ionic liquid media.

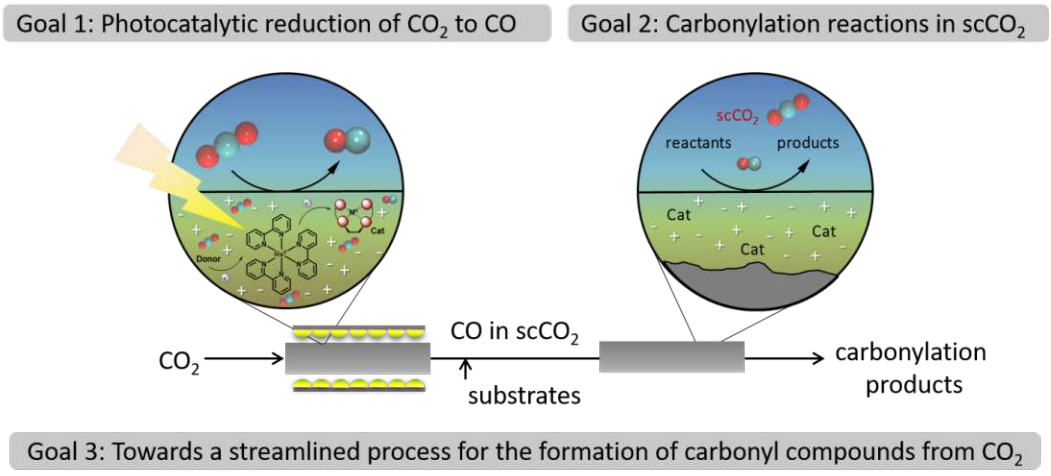

Figure 1.3. Schematic description of the ERC project CARBOFLOW. Reproduced from [16].

1.2. Photocatalytic CO_2 reduction

Photocatalysis presents a powerful method for overcoming high reaction barriers, enabling selective reactions. Unlike traditional thermochemical methods that require high temperatures or pressures, photocatalysis can proceed under mild conditions, which reduces energy costs and environmental impact. Inspired by natural photosynthesis — the essential process that supports life on earth by converting water and carbon dioxide into oxygen and carbohydrates using sunlight — photocatalysis similarly harnesses solar energy to transform CO_2 into valuable fuels and chemicals.[17]
The fundamental principle of photocatalysis is based on the absorption of photons by the photocatalyst, which generates reactive electron-hole pairs. These pairs, together with proton transfer, facilitate the reduction of substrates. In general, homogeneous and heterogeneous photocatalysis can be distinguished. Homogeneous photocatalysis involves catalysts in the same phase as the reactants and is typically performed in a solution. Advantages of this approach include uniform interaction with reactants and high selectivity due to well-defined reactive sights. In contrast, heterogeneous photocatalysis uses catalysts in a different phase, typically solid catalysts with gaseous or liquid reactants. Heterogeneous catalysis offers easier separation and recovery, as well as increased stability under reaction conditions. However, it may have lower selectivity and slower reaction rates as a result of limited surface interactions compared to homogeneous catalysis.[18]

1.2.1. Homogeneous photocatalysis

Homogeneous photocatalytic CO_2 reduction is based on metal-organic catalysts typically dissolved in organic solvents or water. Electrons for the reduction reaction are generated with metal-organic sensitizers or organic dyes by quenching the excited state. Certain requirements need to be fulfilled for a catalyst to facilitate selective CO_2 reduction reaction (CO2RR) with high yields. Catalysts can lower the activation energy of CO_2 transformation. This energy is defined by the overpotential of the electrochemical reaction. In order to facilitate reactions the redox potential of the catalyst should be close to the equilibrium potential of the reaction. As water reduction to H_2 is thermodynamically more favorable than CO2RR, the catalyst should not interact or reduce H_2. Furthermore, multiple electron reduction is facilitated by the accessibility of multiple redox states of both the metal and the ligands.
Common catalysts are based on Ruthenium, Rhenium, and Iridium. The development of metal-organic catalysts based on earth-abundant metals has emerged over the past years with the goal of finding alternatives to expensive and rare noble metal catalysts. Examples comprise, for example, Manganese, Nickel, and Iron complexes. Selected examples of both, noble and non-noble metal-organic catalysts, are shown in Figure 1.4.[19,20]

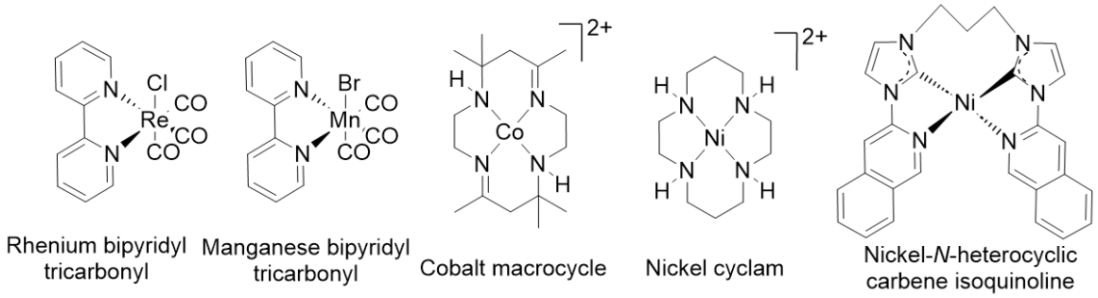

Figure 1.4. Catalysts selective for CO formation used in photocatalytic CO2RR.

The first step in the mechanism of photocatalytic CO2RR catalyzed by organometallic catalysts is based on the reduction of the catalyst to a low-valent state with an unsaturated binding site that can uptake CO_2. In homogeneous photocatalysis, electrons for the low-valent state are generated by the use of photosensitizers. The mechanism is described in Figure 1.5. The sensitizer is excited by light. The excited state can be reductively quenched by electron donors to form the one electron reduced state (OERS). The OERS of the photosensitizer can relax under the transfer of electrons to the catalyst initializing the catalysis mechanism.[20]

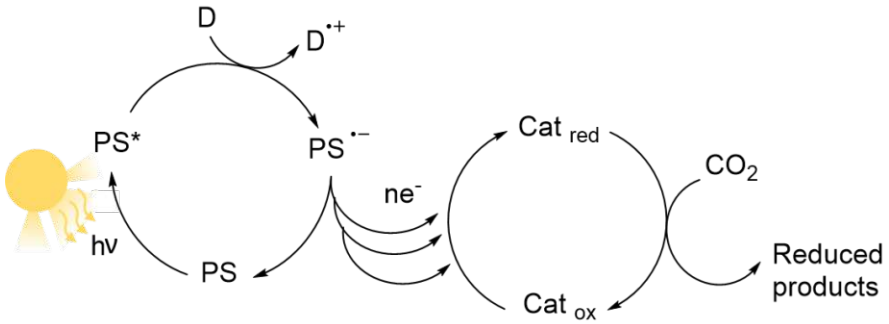

Figure 1.5. Principle of homogeneous photocatalytic CO2RR with photosensitizer and photocatalyst. Picture adapted from Kuramochi et al. [20].

The quenching by electron donors, also called sacrificial agents, resembles the oxidation counter-reaction to CO2RR. Alternatively to reductive quenching, the excited state of the photosensitizer can be quenched via oxidative quenching.[21] Both processes are described in Figure 1.6. The oxidative quenching mechanism operating under the direct transfer of electrons from the sensitizer to the catalyst and acceptance of holes by sacrificial agents is only rarely known. This can be explained by the highly negative reduction potentials that need to be battled with even higher reduction potentials of the excited state of the photosensitizer. It is worth mentioning that CO2RR to CO is a two-electron process, requiring the transfer of a second electron after the reduction of the catalyst. This step is kinetically slow as it requires a second electron source like a second sensitizer molecule or reduced catalyst undergoing a disproportion reaction. This kinetic limitation is also a reason why the oxidative quenching mechanism is unlikely to happen. The probability for quenching of the excited state by the abundantly

available donor molecule is higher than the interaction of catalyst and sensitizer.[20,22,23]

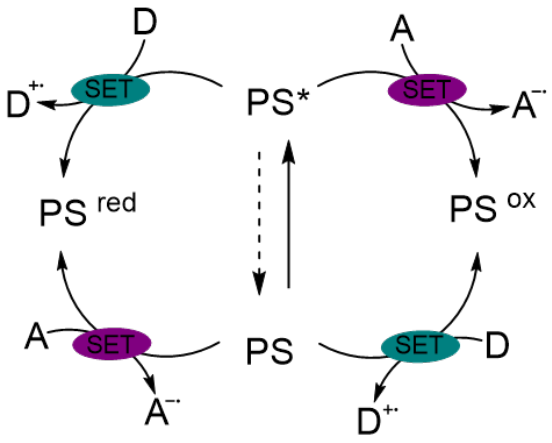

Figure 1.6. Mechanism of reductive and oxidative quenching of excited photosensitizer. Adapted from Zhu et al. [21].

Common sacrificial agents used in CO2RR are aliphatic amine-based agents like triethylamine (TEA) and triethanolamine (TEOA). Aromatic amines are used as well, such as benzyl dihydronicotinamide (BNAH) and dimethyl phenylbenzimidazoline (BIH). Furthermore, agents such as ascorbic acid H_2A, oxalate and thiols like benzylthiolate (Benz-S) find application. Corresponding structures are shown in Figure 1.7.[24]

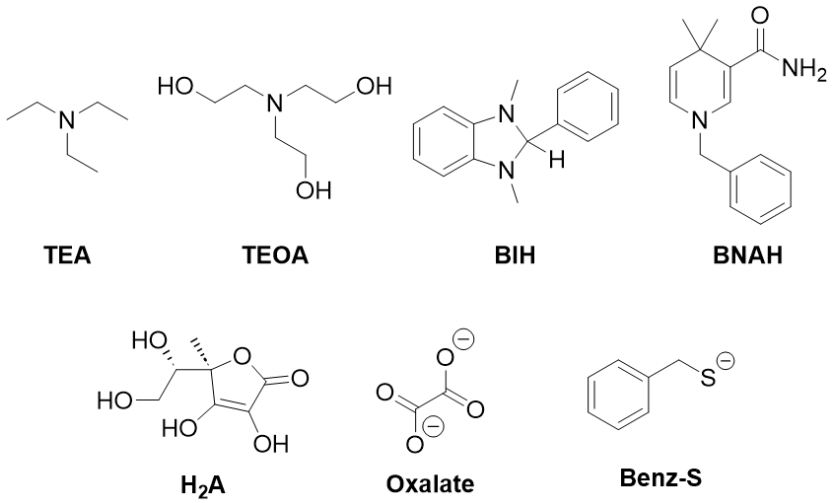

Figure 1.7. Sacrificial agents used in photocatalytic CO2RR.

Requirements for good photosensitizers are strong light absorption, enabling selective excitation of the sensitizer. Spectral overlaps with other components of the system should be avoided at the chosen excitation wavelength. Light emission in the visible light is beneficial as it allows for the utilization of sunlight. Furthermore, requirements for efficient generation of electron charges and transfer of charges in the system need to be fulfilled. The reactive excited state should be formed with a high yield, which

is influenced by the intrinsic quantum yield as well as by absorption cross-section dependent on molar absorptivity and molar concentration. Long excited-state lifetimes are required to facilitate an efficient reductive quenching process. This process is influenced by the diffusion kinetics of an excited sensitizer interacting with a donor molecule in a bimolecular reaction. The excited and ground-state redox potentials of the photocatalyst must provide for an exothermic (or, at worst, weakly endothermic) reaction. Strong oxidation power of the excited state is required to efficiently capture electrons from the sacrificial donor. Additionally, high stability of the OERS is required to transfer electrons to the catalyst. In terms of long-term stability, the reversibility of photophysical processes plays an important role. The photocatalyst must exhibit reversible electrocatalytic behavior to prevent photodegradation in the absence of a quencher.[20,22,23]
Common sensitizers are based on noble metals like Iridium, Ruthenium, and Osmium. Alternatively, purely organic sensitizers emerged over the last years. Examples of organic sensitizers are structures based on anthracenes and cyanoarenes like 4CzIPN and 9CNA.[22,25] Examples of metal-organic sensitizers as well as organic sensitizers are shown in Figure 1.8.

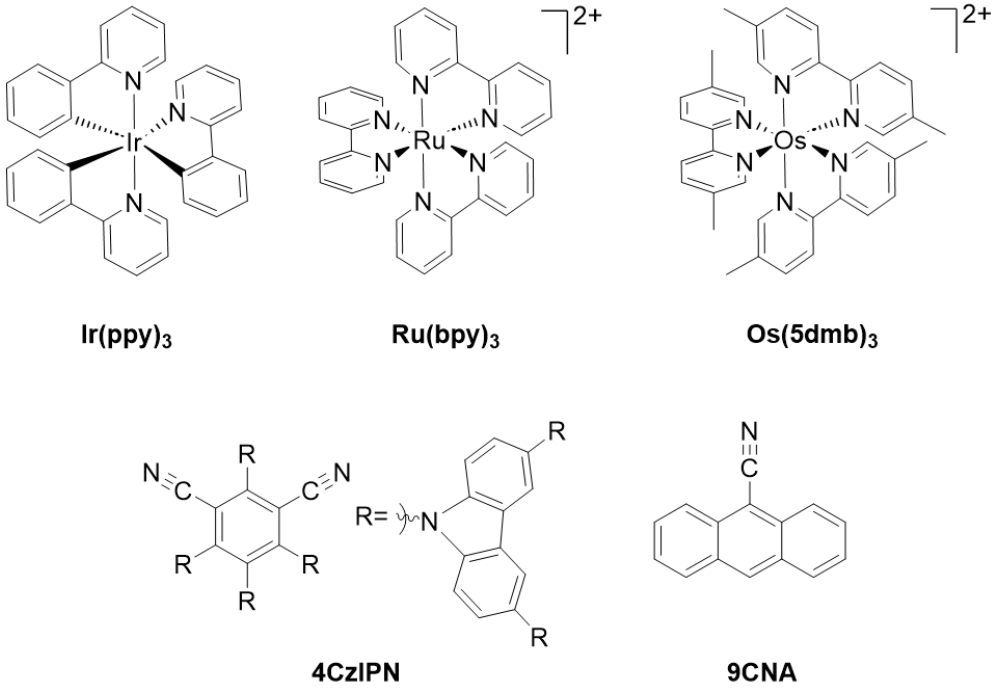

Figure 1.8. Sacrificial agents used in photocatalytic CO2RR.

Catalysis with Ruthenium sensitizer and Rhenium catalyst

The system based on the Ruthenium sensitizer $[Ru(bpy)_3]Cl_2$ and the Rhenium catalysts $[Re(bpy)(CO)_3Cl]$ was established over the past years as a well-investigated catalyst pair for photocatalytic CO2RR (see Figure 1.9). The Ru-sensitizer was first characterized in 1954 as a complex by Brandt, who further described the luminescence properties of the complex in 1968.[26–28] In the early 1980s, Jean-Marie Lehn, Raymond Ziessel, and Jeannot Hawecker pioneered the field of artificial photosynthesis investigating photocatalytic CO_2 reduction with metal-organic complexes. They studied $[Re(bpy)(CO)_3Cl]$ in photo- and electrocatalytic CO_2 reduction and employed $[Ru(bpy)_3]^{2+}$ as a sensitizer.[29–32] The Re-catalyst is renowned for its high selectivity toward CO production. Over the years, numerous applications in both photo- and photo-electrocatalysis have been reported, and the catalyst has been incorporated into more sophisticated catalytic systems, like supramolecular catalysts and organic-inorganic hybrid materials.[33–36] More recent developments in the field of synthetic photo-organic chemistry underline the relevance of $[Ru(bpy)_3]^{2+}$ as a sensitizer, which is now widely used in numerous transformations.[37] Groundbreaking work in this area was initiated by the groups of MacMillan and Yoon, who both published pioneering studies in 2008 that combined photocatalysis with organic synthesis. MacMillan developed photocatalyzed asymmetric alkylations, while Yoon introduced photocatalyzed cycloadditions.[38,39]
The sensitizing mechanism involving the Ru-sensitizer, as well as the mechanism of the CO2RR reduction reaction, have been thoroughly investigated. These details will be discussed further in the following chapter.

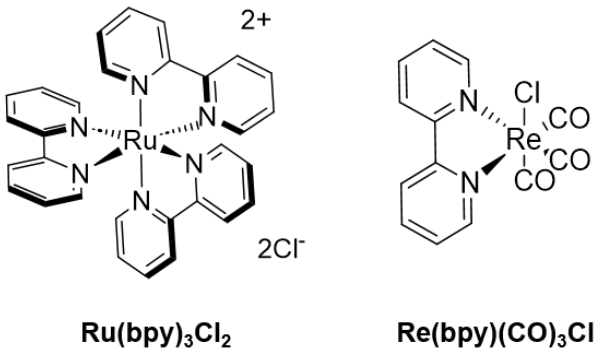

Figure 1.9. Photocatalytic system consisting of Ru-sensitizer and Re-catalyst investigated in this work.

The Ru-based sensitizer $[Ru(bpy)_3]^{2+}$ fulfils most of the above-mentioned criteria for a good sensitizer providing high rates of excited state formation, long excited state lifetimes, and reversible redox behavior. Furthermore, chemical modification of the ligands allows for fine-tuning of photophysical properties of the complexes. The absorption in the visible range around 450 nm can be assigned to the metal-to-ligand charge transfer (MLCT) of the complex (see Figure 1.10a). The MLCT is obtained from the simultaneous reduction of the metal centre and oxidation of the ligand facilitated by the redistri-

bution of electron charge within the complex, forming $[Ru(bpy)_3^{-\cdot}]^{2+*}$ as intermediate (see Figure 1.10b).[23,40]

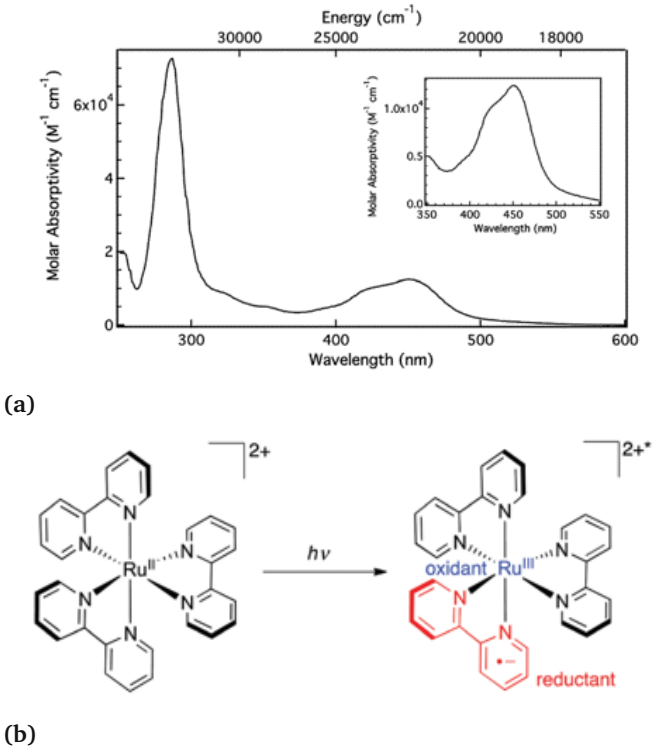

Figure 1.10. UV-Vis absorption of $[Ru(bpy)_3]^{2+}$ with MLCT at around 450 nm (a) and schematic description of internal charge separation upon excitation (b). Graphic taken from Arias-Rotondo and McCusker [23].

The photophysics of the excited state can be best described with potential energy surface diagrams (see Figure 1.11). The different processes are also described in equations (1)-(4). Upon irradiation by $h\nu_{abs}$ the sensitizer is excited to the ^{1}MLCT state with a spin multiplicity of 1 (see Equation (1)). This state is quickly relaxing by intersystem crossing (ISC) to the triplet state ^{3}MLCT (Equation (2)). The ^{3}MLCT can relax to the ground state via phosphorescence or non-radiative pathways (Equations (3) and (4)).

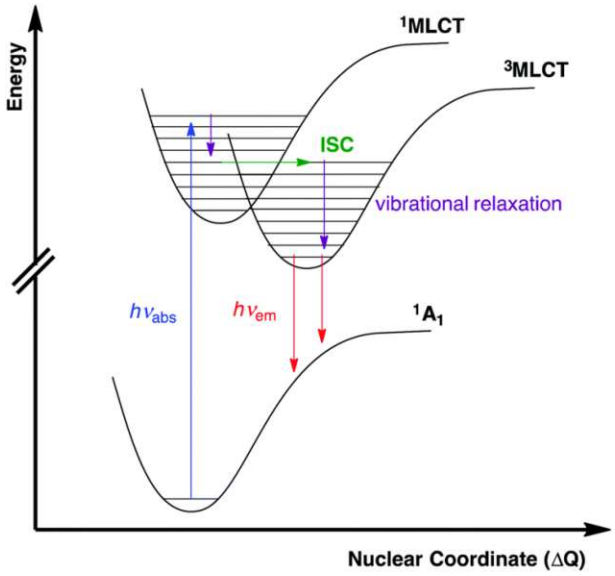

Figure 1.11. Mechanism of photocatalytic excitation described with potential well. Picture taken from Arias-Rotondo and McCusker [23].

$$[Ru^{II}(bpy)_3]^{2+} \xrightarrow{h\nu_{abs}} [Ru^{III}(bpy^-)(bpy)_2]^{2+*} \tag{1}$$

$$^1[Ru^{III}(bpy^-)(bpy)_2]^{2+*} \xrightarrow{k_{isc}} {}^3[Ru^{III}(bpy^-)(bpy)_2]^{2+*} \tag{2}$$

$$^3[Ru^{III}(bpy^-)(bpy)_2]^{2+*} \xrightarrow{k_{em}} [Ru^{II}(bpy)_3]^{2+} + h\nu_{em} \tag{3}$$

$$^3[Ru^{III}(bpy^-)(bpy)_2]^{2+*} \xrightarrow{k_{nr}} [Ru^{II}(bpy)_3]^{2+} + \text{heat} \tag{4}$$

The radiative relaxation leads to an emission spectra with a maximum around 620 nm. The as-described reactions illustrate steady-state emissions of the sensitizer. Building upon these considerations, quenching excited state reactivity of the ^{1}MLCT state is discussed.

The reactivity is based on the ability of the ^{1}MLCT state to act as an electron acceptor or an electron donor as described above in Figure 1.6 by single electron transfer (SET). Furthermore, energy transfer can occur through Förster or Dexter energy transfer (see Figure 1.12). Förster Energy Transfer, also known as Fluorescence Resonance Energy Transfer (FRET), is based on a dipolar mechanism. This mechanism takes place through space: Transition moment dipoles of donor and acceptor are coupled non-radiatively. On the contrary, Dexter electron transfer is based on the orbital overlap and can be described as energy transfer through bonds. Intramolecular Dexter Energy transfer is required as well as orbital overlap, and therefore, collision of acceptor and donor is necessary. Throughout the process, two electrons with opposite spin are exchanged.[41] In the case of the application of Ru-sensitizer with Re-catalyst energy transfer could lead

to the formation of Re-excited states.[23] In photocatalytic CO2RR the common mechanism is reductive quenching. *Ru(bpy)$_3^{2+}$ functions as an oxidant, accepting an electron from a sacrificial agent to give the reduced species Ru(bpy)$_3^{+}$. This Ru(I) intermediate is a good reductant ($E_{1/2} = -1.33V$ vs. SCE) and may donate an electron to an electron acceptor (Re) to afford the ground state species again.[37] The transfer mechanism is closely related to Dexter Energy transfer but with only one-electron transfer. The process of SET can be described by Marcus-theory and has lower distance dependency as dexter energy transfer, making SET more likely to occur.[23,42]

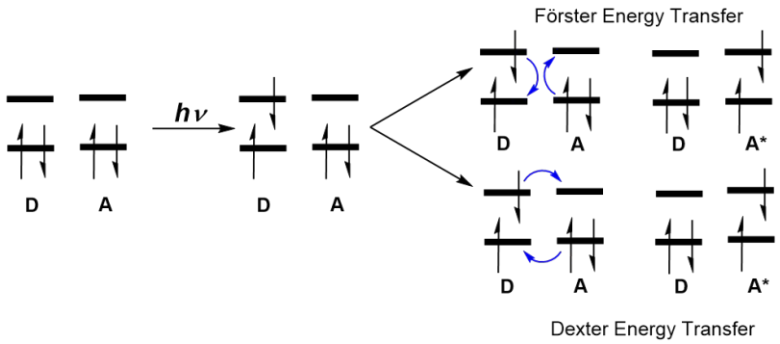

Figure 1.12. Schematic description of Förster and Dexter Energy Transfer. Scheme adapted from Arias-Rotondo and McCusker [23].

Stern-Vollmer-Quenching is a technique to investigate the nature of the quenching mechanism present. However, as the concentration of a quencher increases, *Ru(bpy)$_3^{2+}$ undergoes additional deactivation through electron-transfer pathways, leading to a reduction in the observed emission intensity at 615 nm.[37]

Photocatalytic CO_2 reduction with [Re(bpy)(CO)$_3$Cl] proceeds with high activity and extremely high selectivity for CO_2. The selectivity for CO_2 is maintained even in aqueous solutions. The reaction mechanism starting from the OERS of the Re-catalyst was intensively investigated (Figure 1.13). The mechanism proceeds with the loss of CO or Cl^- ligand. In-situ infrared spectroscopy showed that the elimination of halogen ligands is dominating.[32,43] The loss of the ligand leads to an open binding site that can interact with CO_2 or solvent. It is worth mentioning that the mechanism is strongly influenced by the reaction conditions, including the use of different solvents and additives. Depending on the solvent, interactions with the Re catalytic center can be stronger or weaker. Johnson et al. showed for example that MeCN can interact with the OERS of the Re-complex and stabilize the OERS radical.[44]

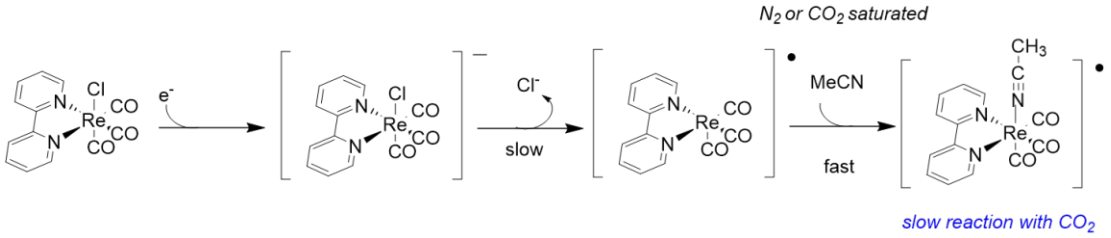

Figure 1.13. Ligand exchange after electron transfer to the Re-catalyst. Picture adapted from Kuramochi et al. [20].

Possible mechanisms starting from the solvent adduct of the OERS of the Re-complex are shown in Figure 1.14. A mechanism proposed by Gibson et al. proceeds via CO_2 coordination and proton-mediated dehydroxylation from the carboxylato complex $[Re(bpy(CO)_3(COOH)]$.[20,45] An alternative mechanism with CO_2 bridged Re-dimer complex was proposed by Hayashi et. al.[46]

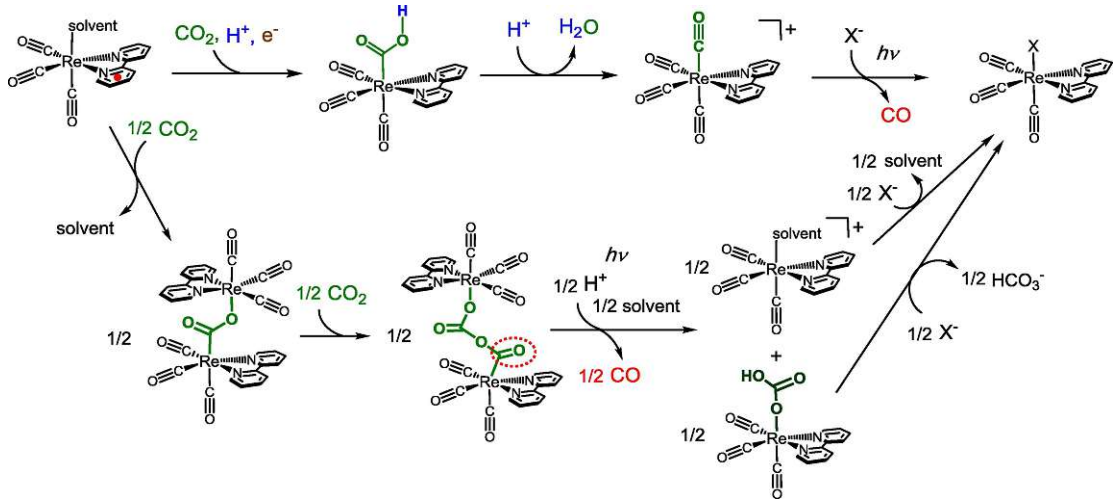

Figure 1.14. Mechanisms of photocatalytic CO2RR catalysed by Re complex. Graphic from Kuramochi et al. [20]

Furthermore, interaction with sacrificial agents like TEOA was observed, forming Re-CO_2-TEOA as intermediates. Similar effects were also reported for comparable complexes.[47–50]

A huge limitation of homogeneous photocatalysis lies in the deactivation of both catalyst and sensitizer. The process of degradation can be photoinduced as in the case of $[Ru(bpy)_3]^{2+}$ (see Figure 1.15). The OERS of the Ru-sensitizer is prone to the loss of one bpy ligand. The free coordination sites can interact with solvents. It was shown that the resulting complex can still catalyze CO2RR even in the absence of an additional catalyst. This mechanism can lead to changed product distribution.[20,51]

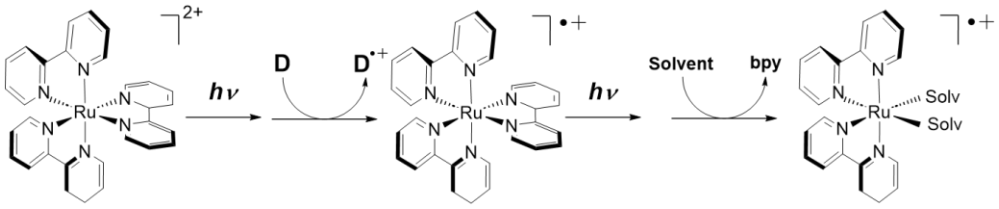

Figure 1.15. Photoinduced ligand loss of $[Ru(bpy)_3]^{2+}$. Picture adapted from Kuramochi et al. [20].

A common deactivation mechanism for metal-organic catalysts is degradation under the formation of dimers.[52,53] In the case of $[Re(bpy)(CO)_3Cl]$, dimer formation was observed in electrocatalytic experiments leading to the formation of Re^0 dimer complex $[Re(bpy)(CO)_3]_2$.[44,54]

1.2.2. Heterogeneous photocatalysis

Opposite to homogeneous photocatalysis, relying on molecular sensitizers and catalysts, classic heterogeneous catalysts are based on the use of inorganic semiconductor materials. The light-harvesting mechanism with semiconductors is based on the photoexcitation of electrons upon irradiation with light, transferring electrons from the valence band to the conduction band of the semiconductor (see Figure 1.16). The excitation is promoted by light with photon energies equal to or higher than the energy of the bandgap. The promotion of electrons leads to the formation of holes in the valence band of the semiconductor. The generated electron-hole pairs are transferred to the surface of the catalyst, facilitating parallel oxidation and reduction reactions. Parallel to CO2RR consuming the generated electrons, the oxidation of a reductant is promoted by the generated holes. In the ideal case, water oxidation can work as an oxidation counter-reaction.[10,55,56]

In order to facilitate the reaction, thermodynamic criteria need to be fulfilled. The reduction potential of the reduction half-reaction needs to be more positive than the energy of the conduction band, and the potential of the oxidation half-reaction needs to be more negative than the valence band. Catalytic sites on the surface of the semiconductor for CO2RR are required to facilitate the process from a kinetic perspective.[10,57]

Engineering of heterostructure catalysts is an efficient strategy to enhance charge separation and spectral responses in a broad range. P–n junction and Z-scheme heterojunction catalysts can be distinguished as two main classes of heterostructure catalysts (see Figure 1.16 a and b). In p-n heterojunction systems, electrons are transferred from the conduction band of a semiconductor with a higher energy level to the conduction band of a second semiconductor with a lower energy conduction band. Consecutively holes are transferred from the valence band of the semiconductor with the lower energy valence band to the valence band of the semiconductor valence band with more positive energy in the opposite direction as the electrons (see Figure 1.16a).

In a Z-Scheme heterostructure catalyst electrons generated in the material with a lower

valence band level are transferred from the conduction band to the valence band of the second material with higher conduction and valence band levels (see Figure 1.16b). Typical semiconductors are metal-oxides,[58,59] metal sulfides,[60] metal oxyhalides,[61] layered double hydroxides[62]as well as 2D structures like graphitic carbon nitride (gCN).[63,64] Further important materials are metals[65] and alloys[62] as well as metal-organic frameworks[66,67] and covalent organic frameworks (COFs).[68,69]

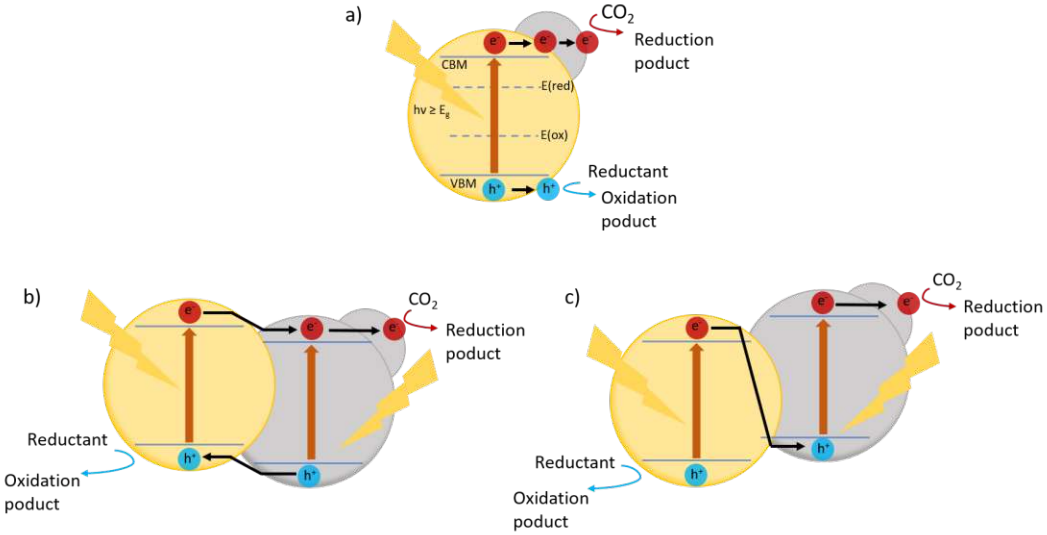

Figure 1.16. Principle of heterogeneous photocatalysis. Photocatalytic CO2RR in semiconductors (a) and semiconductor heterostructures (b) and (c). The principle of CO2RR with P-n heterojunction heterostructures (b) and Z-scheme heterojunctions (c) is described in detail. Picture adapted from Fang et al. [10].

Absorption of CO_2 on the surface of a heterogeneous catalyst is the first step to facilitate subsequent selective and efficient reduction (see Figure 1.17). The absorption leads to a partially charged species through the interaction with the catalyst's surface. The lone pairs of the CO_2 oxygen can donate electrons to Lewis acid surface atoms, and opposite Lewis basic surface atoms can donate electrons to the carbon atom of CO_2. The interaction leads to a change in bond angle, reducing the reaction barrier for the introduction of further electrons due to the lowering of the LUMO level in the bent molecule. The substrate can bind in different modes on the catalyst surface to promote the reduction via different pathways. Engineering strategies can be employed to enhance surface interactions and promote reactions. Examples are the increase of surface area, surface defect engineering, the introduction of basic sites as well as the introduction of co-catalysts.[70]

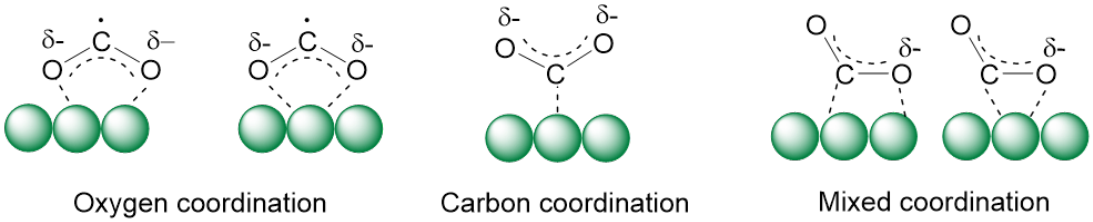

Figure 1.17. Possible coordination modes of $*CO_2$. Picture adapted from Chang et al. [70].

Various mechanisms have been described leading to the formation of different products.[71–73] An example of a mechanism selective for the formation of CO that proceeds via a surface bond -COOH intermediate is shown in Figure 1.18.

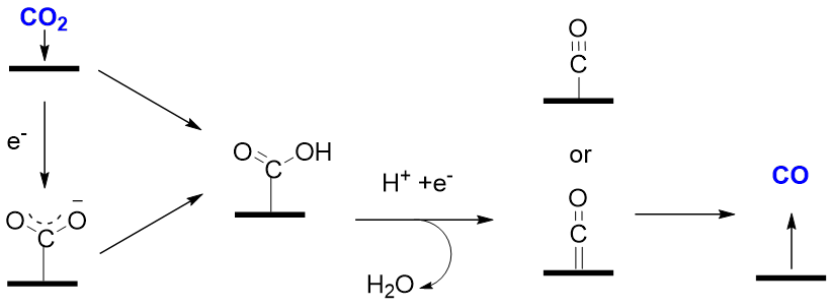

Figure 1.18. Example of a heterogeneous catalytic mechanism selective for CO. Picture adapted from Sun et al. [72].

1.2.3. Hybrid systems

A further possibility for producing efficient photocatalytic systems is the development of hybrid systems combining molecular catalysts with heterogeneous systems. Anchoring the molecular catalysts allows for the pairing of positive properties of both homogeneous and heterogeneous photocatalysis.

A heterogeneous photoactive support is used for charge generation and separation without the drawback of photodegradation that is known from organometallic molecular catalysts or from organic dyes. The homogeneous catalyst is immobilized via a linker and serves as an active-site reaction center with high selectivity.[74] This concept can be transferred to various supports such as gCN and TiO_2.[75–77] Figure 1.19 illustrates exemplary the mechanism of a photocatalytic hybrid system consisting of gCN heterogeneous photoactive support and a Re-complex with modified anchoring groups described by Nguyen et al.[76] forming a Z-scheme heterojunction. Furthermore, anchoring on porous materials like metall organic frameworks (MOFs) and covalent organic frameworks (COFs) is possible and increasingly investigated.[35,78,79]

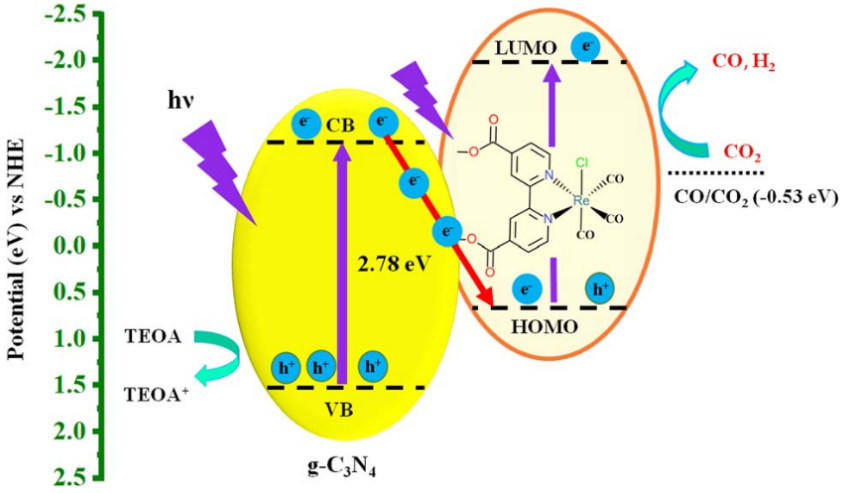

Figure 1.19. Z-Scheme heterojunction hybrid system for photocatalytic CO2RR build from gCN and Re-catalyst. Picture taken from Nguyen et al. [76].

1.2.4 Photocatalytic CO_2 Reduction with Imidazolium-based Ionic Liquids

Ionic liquids are salts in a molten state below a temperature of 100 °C. Their low melting points are attributed to a lack of local structural order within their ionic framework. This class of materials was first described by Paul Walden in 1914.[80]

Due to their high structural variability and the ability to combine various anions and cations, ionic liquids can be designed for specific tasks.[81] Common structural motifs for cations include heterocycles like pyrrolidinium, pyridinium, and imidazolium as well as phosphonium and ammonium derivatives. Typical anions are halides, acetate, alkyl sulfates as well as tetra- and hexafluoro derivatives (see Figure 1.20). Depending on the anion present, they can be classified as either hydrophilic or hydrophobic. Properties such as low vapor pressure, low flammability, high solvation capacity, and broad electrochemical windows make ionic liquids attractive for applications in fields like catalysis, separation, and more.[82]

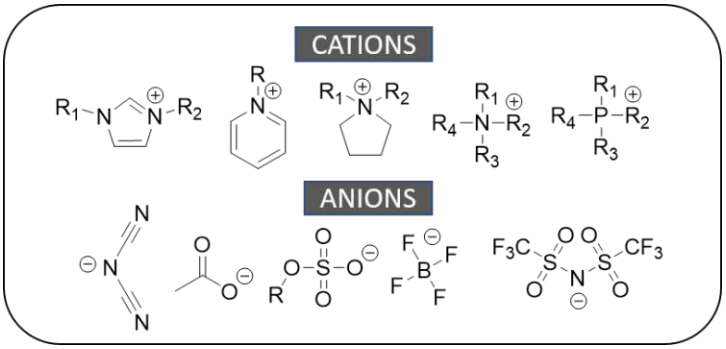

Figure 1.20. Structures of components for common ionic liquids.

Among the diverse types of ionic liquids, imidazolium-based ionic liquids are of particular interest due to their unique ability to both chemisorb and physisorb CO_2. The proton at the C_2 position exhibits an acidic character and can be abstracted in the presence of basic anions or an external base.[83,84] This proton abstraction leads to the formation of a free *N*-heterocyclic carbene, a well-known motif in organometallic catalysis. The resulting carbene can interact with CO_2, forming an imidazole-CO_2 complex. Electrochemical studies have shown that this complex can lower the high energy barrier associated with CO_2 reduction by reducing the overpotential of this reaction step.[85] Following fundamental work by Rosen et. al, the role of imidazolium-based ionic liquids has been investigated under various reaction conditions.

Complementary, the role of ionic liquids in heterogeneous photocatalysis was examined by multiple authors. In these systems, ionic liquids can be added as an additive or incorporated directly as an imidazolium structural motif. Recent developments have also explored systems that integrate ionic liquids with nanoparticles and highly porous materials, such as COFs and MOFs.

This subsection presents a review article that summarizes advances and state-of-the-art in photocatalytic CO_2 reduction assisted by ionic liquids in homogeneous and heterogeneous catalysis, with particular emphasis on mechanistic insights.

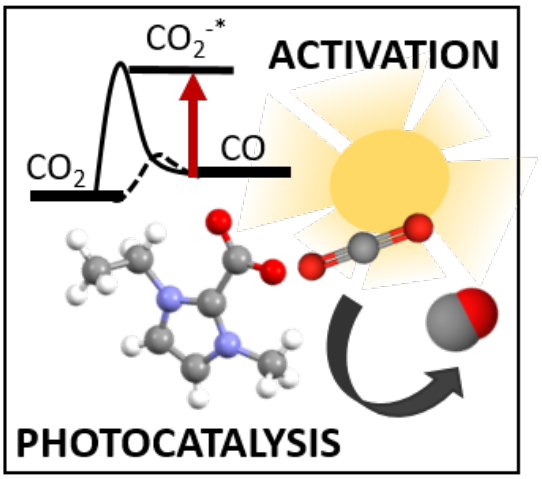

Figure 1.21. Graphical illustration on the role of imidazolium based ionic liquids in CO_2 activation for reduction.

The revised manuscript is currently submitted to the journal *ChemSusChem*. As the lead author, I conceptualized and wrote the manuscript.

REVIEW

Photocatalytic CO_2 Reduction with Imidazolium-based Ionic Liquids

Lisa Eisele, [a] and Katharina Bica-Schröder*[a]

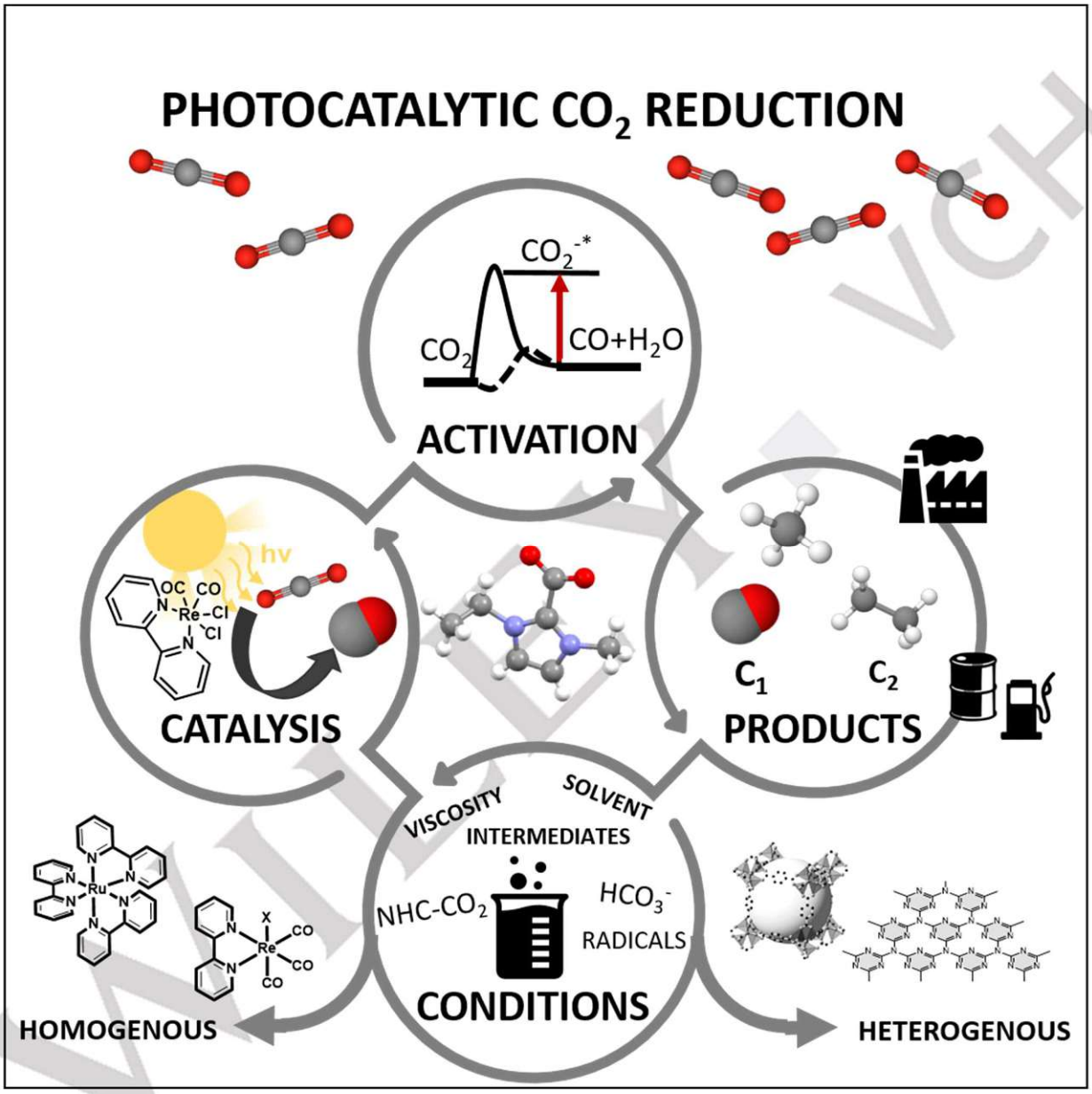

[a] L. Eisele, MSc, Prof. K. Bica-Schröder
Institute of Applied Synthetic Chemistry
TU Wien
Getreidemarkt 9/163 1060 Wien, Austria
E-mail: katharina.schroeder@tuwien.ac.at

Abstract: The growing urgency of addressing climate change caused by greenhouse gas emissions and dwindling fossil fuel supplies has heightened the need for effective strategies to capture and utilize carbon dioxide. Photocatalytic CO_2 conversion, inspired by natural photosynthesis, presents a viable approach for transforming CO_2 into useful C_1-C_3 chemical intermediates for industrial purposes. However, the inherent stability of CO_2 and the competing hydrogen evolution reaction (HER) introduce significant obstacles. Imidazolium-based ionic liquids can pre-activate CO_2, accelerate reaction kinetics, and act as eco-friendly solvents or additives. Systems employing ionic liquids with catalysts, such as homogeneous organocatalysts and heterogeneous materials like Metal-Organic Frameworks (MOFs) and quantum dots, offer potential solutions to these challenges. This review focuses on the role of ionic liquids in both homogeneous and heterogeneous photocatalytic processes, emphasizing their use in CO_2 reduction and highlighting recent mechanistic insights for imidazolium-based species.

1. Introduction

The urgent threat posed by greenhouse gas emissions and resulting climate change, along with the depletion of fossil resources, enhanced the development of effective carbon capture and utilization strategies[1–3]

Photocatalytic CO_2 reduction offers a promising approach for CO_2 valorization, mimicking natural photosynthesis to drive reactions that produce C_1 carbon building blocks like CO, CH_4, formic acid, and methanol.[4,5] This method is particularly attractive, as these building blocks can be used to synthesize value-added products of great interest to the chemical industry. Examples of significant industrial relevance include the valorization of CO in carbonylation reactions, hydroformylations, and Fischer Tropsch synthesis to alkanes and alkenes.[6–10]

An inherent challenge in CO_2 valorization is the molecule's high stability, as bending the bond angle—a key step in CO_2 activation—requires a high overpotential (Scheme 1a).[11] Additionally, the process is further complicated by the competing hydrogen evolution reaction (HER), which occurs at a lower potential than the CO_2 reduction reaction (CO_2RR).[12] The transformation of CO_2 goes along several consecutive steps, including CO_2 capture and pre-activation by angling of the molecule, alongside multielectron reduction steps that occur proton-coupled.[13,14]

The aforementioned challenges can be effectively addressed through the use of selective homogeneous organocatalysts or advanced heterogeneous photocatalysts.[15–19] These systems may feature materials such as metal-organic frameworks (MOFs)[20,21], covalent organic frameworks (COFs)[22,23], quantum dots, and plasmonic nanoparticles[24], often in composite forms.

Ionic liquids, particularly those based on imidazolium, can both chemisorb and physisorb substantial amounts of CO_2.[25] This capability makes them valuable for use in CO_2 pre-activation within various catalytic systems.[26–29] The usage of "CO_2 trapping agents" can facilitate the valorization of CO_2 from sources with low CO_2 partial pressure.[30,31] Additionally, their advantageous properties, such as extremely low vapor pressure, non-flammability, high thermal stability, and high solvation capacity, make them appealing as environmentally friendly solvents or additives.[32,33]

Initially used in homogeneous photocatalysis alongside metal-organic catalysts, it has been demonstrated that ionic liquids as solvents or additives can pre-activate CO_2 and drastically boost reaction rates. [34] Besides the introduction of ionic liquids as bulk material, imidazolium functionalities can be covalently linked to the catalytic system.[35–37] As the variety of tested catalytic systems involved more diverse and heterogeneous systems, it became evident that the role of ionic liquids extends beyond CO_2 activation and is highly dependent on the specific reaction conditions. For example, CO_2RR in water-ionic liquid mixtures was demonstrated through the direct excitation of ionic liquids via a radical mechanism.[38]

This review highlights the mechanistic understanding of the role of ionic liquids in both homogeneous and heterogeneous photocatalytic systems, with a particular focus on recent advancements in CO_2RR involving imidazolium ionic liquids or imidazolium structural motifs.

Lisa Eisele studied Chemistry at the University of Stuttgart and CPE Lyon and received her master's degree in 2020 in the field of Materials and Functional Molecules working at the Center for Solar Energy and Hydrogen Research Baden-Württemberg (ZSW). She joined the group of Katharina Schröder at TU Wien as a PhD student in 2021, focusing on ionic liquid-assisted photocatalytic CO_2 valorization within the ERC project CARBOFOW (864991).

Katharina Bica-Schröder received her PhD in 2006 from TU Wien and later joined the Queen's University Belfast/UK for a post-doctoral stay. Her research interest lie in sustainable organic chemistry, with a particular focus on novel catalytic processes for asymmetric synthesis, carbon capture and utilization, and on waste valorization. In 2019, she received the ERC consolidator grant. Since 2021 she holds a position as full professor for sustainable chemistry at the institute of Applied Synthetic Chemistry at TU Wien.

2. CO_2 activation by imidazolium-based ionic liquids

The biggest hurdle in CO_2 valorization is the high overpotential related to the transfer of the first electron and the bending of the CO_2 bond angle, rendering reactions highly energy-demanding (See Scheme 1a). [39,40]

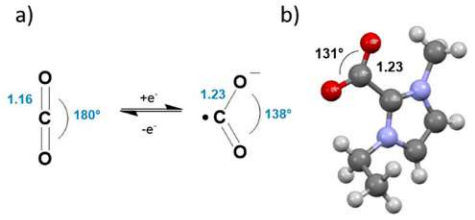

Scheme 1: Analogy between the change of bond angle for the first electron transfer in CO_2RR (a) and the angled geometry of the carbene complex formed between imidazolium-based ionic liquids and CO_2 [41–43].

A strategy to overcome this barrier is the development of a co-catalyst for the pre-activation of the CO_2 molecule. In the context of CO_2 capture and valorization technologies, various systems proved to be efficient in CO_2 capture based on chemisorption. Besides technologies such as aqueous alkanolamine solutions, switchable solvents, and deep eutectic solvents used for CO_2 capture from flue gas, ionic liquids have shown great potential in the field.[44–46]

Ionic liquids can both chemisorb and physisorb (i.e., solubilize) CO_2. Chemisorption in ionic liquids, in general, is based on interactions of CO_2 with either the ionic liquid anion or cation. It was shown that active sites for chemisorption in the ionic liquid core structure could enable CO_2 uptake to the equimolar level and higher, as necessary for the industrial application of CO_2 capture from flue gas. Strategies in the development of task-specific ionic liquids for CO_2 absorption further include the modification with amine side chains (Scheme 2, top). [47,48] However, amine functionalization leads to higher viscosity, which limits kinetics and, thus, application. Anions with strong basicity are equally suitable and comprise the incorporation of strong bases such as azolate or phenolate as anions (Scheme 2, bottom).[49,50]

Besides chemisorption, physisorption plays an important role, not activating CO_2 but enriching the reaction media with CO_2. This was considered the main mechanism for CO_2 solvation in unfunctionalized ionic liquids for a long time.

In general, ionic liquids can dissolve CO_2, exceeding the solubilities of permanent gases like N_2 or O_2.[51,52] The ability of ionic liquids (ILs) to solubilize CO_2 has a direct impact on reaction kinetics in CO_2 valorization processes, influencing the formation rate of reduction products. CO_2 physisorption in ionic liquids primarily depends on interactions between the cation and anion, with the anion playing a significantly stronger role than the cation. Studies from Brennecke and co-workers demonstrated that CO_2 solubility in [C_3mim]-based ionic liquids follows the order: [NO_3^-] < [$N(CN)_2$] < [BF_4^-] < [PF_6^-] < [OTf^-] < [Tf_2N^-] < [methide$^-$] (tris(trifluoromethylsulfonyl)methide).[53,54] However, it should be noted that the actual CO_2 solubility in a photocatalytic system is dependent on additives and ionic liquid concentrations.

Ionic liquids with fluorine-containing anions show greater affinity for CO_2 than those with non-fluorinated anions, with CO_2 solubility increasing as the number of fluorine groups on the anions rises. Additional factors affecting CO_2 solubilization include the length of the alkyl chains on the ionic liquids; longer alkyl chains enhance solubilization by increasing free volume. Fluorinated side chains and the presence of ester groups further boost CO_2 uptake.[55] Consequently, the high CO_2 solubility enables the conversion of CO2 even in low concentrations.[25,56–58] For a detailed overview of CO_2 solubilization by various classes of ionic liquids, including structural relationships and interactions, readers are referred to comprehensive review articles on CO_2 capture systems.[55,59], while the review by Dupont and co-workers [60] focuses on the diverse applications of ionic liquids in catalysis.

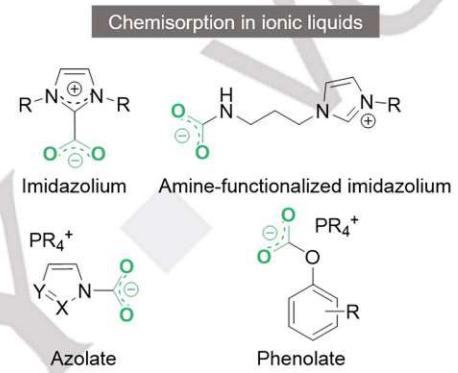

Scheme 2: Intermediates formed by chemisorption of CO_2 in imidazolium-based ionic liquids with optional amine functionalization (top) or in ionic liquids featuring strongly basic anions (bottom).

The outstanding reactivity of imidazolium-based ionic liquids mostly arises from the weak acidity of the proton at the C(2) position of the 1,3-dialkyl imidazolium ring, which can be abstracted under basic conditions. Reaction with CO_2 leads to the formation of a carbene complex, where CO_2 adopts an angled geometry (Scheme 1b) around 131° and longer bond lengths due to the lower s orbital character.[41,43] While initial studies suggested that C(2)-proton abstraction required the presence of added superbases[61,62], the group of Rogers demonstrated spontaneous deprotonation in the absence of a superbase[41], attributing it to the sufficient basicity of the counterion. The authors specifically investigated complex formation with the acetate anion. The investigation of the carbene-chalcogenide complex, including its isolation as a solid and structural elucidation via single-crystal X-ray diffraction, provided direct experimental evidence for the underlying mechanism of complex anion formation.

The absorption is facilitated by strong hydrogen bonding between the acetate anion and the C(2) proton of the imidazolium ring in pure 1-ethyl-3-methyl-imidazolium acetate [C_2mim][OAc] (Scheme 3a). In the presence of CO_2, the basic acetate anion plays a key role in the complexation of acetic acid, forming free *N*-heterocyclic carbene in equilibrium. This carbene is available to react with CO_2 to form the neutral zwitterion [C_2mim$^+$-COO$^-$], characterized by a C-O-C bond angle of 131°. It is also notable that the addition of water leads to the formation of [C_2mim][HCO_3], shifting the equilibrium away from the neutral zwitterion [C_2mim$^+$-COO$^-$] and possible carbene complex-centered reactions. Under water-free conditions, the CO_2 uptake of acetate-based imidazolium ionic liquids can reach 0.38 mol for [C_4mim][OAc][25] compared to in the uptake in pure water (0.0008 mol)[63] or ethanol (0.07 mol)[64].

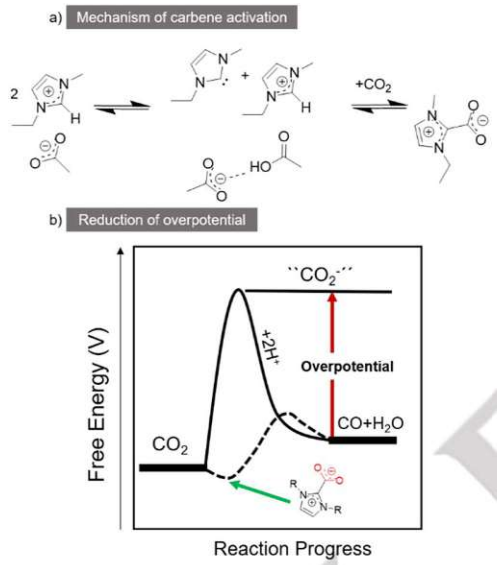

This Scheme 3: Mechanism of *N*-heterocyclic carbene-CO_2 complex formation (a) and reduction of overpotential by imidazolium based ionic liquids (b). Adapted from [41] and from [65]. Scheme 3a reprinted with permission from WILEY-VCH Verlag GmbH & Co. KGaA. Scheme 3b reprinted with permission from AAAS.

Rosen et al. have first demonstrated the ionic liquid-mediated reduction of overpotential in electrocatalytic CO_2RR selective for CO catalyzed by a silver electrode.[65] 1-Ethyl-3-methyl-imidazolium tetrafluoroborate [C_2mim][BF_4] was employed in an aqueous solution with a content of 18 mol%. The addition of ionic liquid led to a significant reduction of the overpotential to values below 0.2 V, operating with a faradaic efficiency greater than 96% (See Scheme 3b).[66] This remarkable result was seen as a breakthrough in the field of electrocatalytic CO_2RR. These findings lead to further investigations on ionic liquid co-catalyzed heterogeneous electrocatalysis.[67–70] Grills and coworkers transferred the concept to electrocatalysis with the well-established homogeneous catalyst [Re(bpy)$(CO)_3$]Cl (bpy=2,2′-bipyridine) in a neat ionic liquid 1-ethyl-3-methyl-imidazolium tetracyanoborate [C_2mim][$B(CN)_4$] for reduction of CO_2 to CO.[71] It was shown that the overpotential could be reduced by approximately 0.45 V in comparison to the reduction in acetonitrile. Furthermore, Lau et al. demonstrated through electrochemical experiments that an additional interaction between CO_2 and ionic liquids may occur when a substrate, such as an electrode, is involved.[72] By examining structure-activity relationships in a series of imidazolium ionic liquids with various substitution patterns at the C2, C3, C4, N1, and N2 positions in experiments with a silver electrode, it was shown that the C4 and C5-protons on the imidazolium ring could participate in CO_2 activation via H-bonding. This was evidenced by the low overpotential observed in experiments using imidazolium salts substituted at the C2 position. In this system, CO_2 can interact in three distinct modes, stabilizing the radical anion intermediate on the electrode surface. In these binding modes, the carbon atom interacts with the silver electrode, while the oxygen atoms form hydrogen bonds with the C4 and C5 protons (see Scheme 4). These interactions can occur either in a monodentate form or a bidentate form, involving hydrogen bonding with two imidazole molecules.

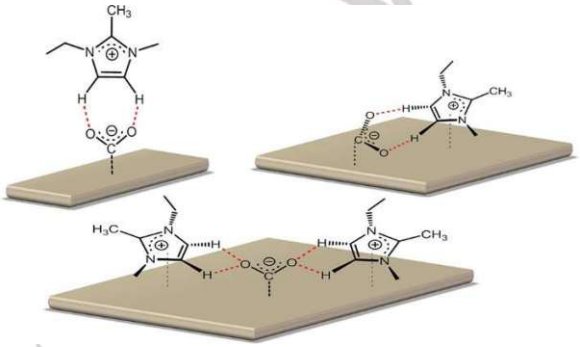

Scheme 4: Interaction of C4 and C5 protons of the imidazolium moiety in CO_2 activation on the surface of a Siver electrode. Reprinted with permission from [72]. Copyright © 2016 American Chemical Society.

This interaction mechanism necessitates a third binding site, in this case, the electrode surface. Notably, in electrocatalysis, the application of an external potential induces pre-organization effects, which can influence the interaction modes between ionic liquids and CO_2.[73]These fundamental findings from electrocatalysis also prompted the application of ionic liquids for CO_2 pre-activation in the field of photocatalysis using visible light as an energy source for the synthesis of chemical building blocks.

3. Ionic liquids in homogeneous photocatalysis

The following chapter examines recent advancements in homogeneous ionic liquid co-catalyzed photocatalytic CO_2 reduction reactions (CO_2RR). A summary of the reviewed studies is provided in Table 1 for easy comparison. Structures of all ionic liquids employed in the reviewed studies are provided in Scheme 5.

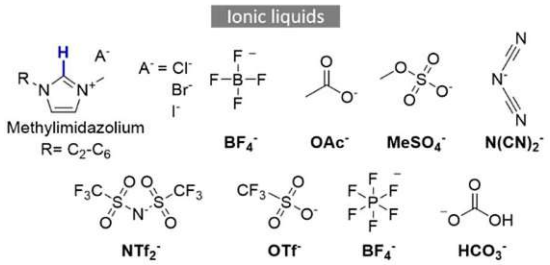

Scheme 5: Imidazolium-based ionic liquids employed in homogeneous CO_2RR.

3.1. Catalysis in the presence of noble metal sensitizer and catalyst

In 2013, Lin et al. presented the first studies on the use of ionic liquids in homogeneous photocatalysis, demonstrating that imidazolium-based structures interact cooperatively with the photocatalytic system, thereby enabling the photochemical reduction of CO_2 in various solvents under mild conditions.[34] The tested system consisted of $[Ru(bpy)_3]Cl_2$ (bpy = 2,2'-bipyridine) as the photosensitizer, $CoCl_2$ as the electron mediator, triethanolamine (TEOA) as a sacrificial agent, and a visible light source (see Scheme 6). Following the findings of Rosen et al. mentioned above, the ionic liquid $[C_2mim][BF_4]$ was selected for initial experiments in aqueous media.[65] Carbon monoxide (CO) formation was observed at a rate of 15.5 µmol•h^{-1}, while hydrogen was produced at a rate of 2.1 µmol•h^{-1}. Control experiments omitting individual components of the system confirmed both the reaction's photocatalytic nature and the ionic liquid's essential role in the reaction mechanism. A certain amount of water is necessary to kickstart the reaction by generating charged reaction partners for electrons and for holes, creating a media with enhanced conductivity. Overall, it was observed that the photocatalytic yield increased with the ionic liquid content. Experiments were repeated in organic solvents such as dimethylformamide (DMF) and acetonitrile (MeCN) to check on the general effect of ionic liquids. It was shown that adding ionic liquid increased CO formation in all tested solvents, whereas H_2 formation was suppressed. The highest yield was achieved using a MeCN-$[C_2mim][BF_4]$ mixture. Incorporating 15% water notably boosted the CO formation rate from 26.3 to 64.0 µmol•h^{-1}. Additionally, the type of counterion significantly impacted the efficiency of CO_2 photoreduction. The bis(trifluoromethane)sulfonamide (Tf_2N^-) anion demonstrated the most significant enhancement in the photocatalytic production of CO and H_2, outperforming other anions such as OAc^-, BF_4^-, dicyanamide ($N(CN)_2^-$), and trifluoromethylsulfonate (TfO^-). The Tf_2N^- anion's high structural symmetry is known to lower the viscosity, which favors reaction kinetics. The large ionic size and fluoroalkyl groups can increase the interaction between ionic liquid and CO_2.[74] Among a series of ionic liquids with different chain lengths in 1-position of the imidazolium core, varying from ethyl to octyl, CO yields decreased with increasing chain length. Longer carbon chains increase Van der Waals interactions, molecular weight, and viscosity, resulting in more significant steric hindrance and slowed catalytic kinetics. This initial study demonstrated a clear link between the chemical properties of ionic liquids, reaction conditions, and photocatalytic CO_2 reduction. However, mechanistic insights were not available at this stage.

Instead of using $CoCl_2$, a common approach in photocatalytic CO_2 reduction is the employment of metal-organic catalysts, which provide well-defined active sites and high selectivity. Catalysts investigated in context with ionic liquids in CO_2RR, as reviewed in this article, are described in Scheme 6.

Re(I) catalysts are particularly known for their high selectivity for CO in CO_2RR and have become benchmark catalysts. $[Re(bpy)(CO)_5]X$ (X = halide) catalysts, in this context, were extensively studied in combination with ionic liquids. [17,75]

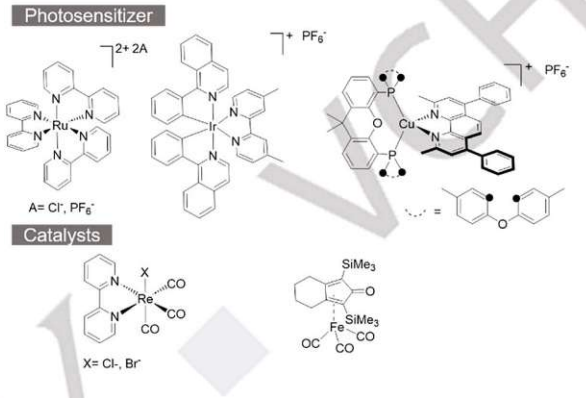

Scheme 6 Metal organic photosensitizers and catalysts employed in the reviewed papers.

Following previous work, Asai et al. reported photokinetics and mechanistic considerations using a system based on an iridium sensitizer and a rhenium catalyst.[76] To investigate photoexcitation and catalysis separately, $[Ir(piq)_2(dmb)](PF_6)$(Ir, piq = 1-phenylisoquinoline, dmb = 4,4′-dimethyl-bpy) sensitizer was combined with $[Re(bpy)(CO)_5]Br$ catalyst (see Scheme 6). The chosen catalysts were employed alongside BIH (1,3-dimethyl-2- phenyl-2,3-dihydro-1H-benzo[*d*]-imidazole), a well-known sacrificial agent with high reducing power that can transfer two electrons in consecutive steps.[77]

The system was tested in different ionic liquids employed as solvents. Results were compared to those in the solvent dimethylamine (DMA). In contrast to the study by Lin[34], experiments were conducted under the complete exclusion of water. Initial investigation of photophysical properties related to the Ir-sensitizer showed that the nature of the ionic liquid had only a marginal impact on parameters such as light absorption, light emission, emission lifetimes, and quantum yields. Some ionic liquids that show yellow color can absorb light and emit weak photoluminescence on their own. Quenching studies with BIH indicate that the quenching rate constants in imidazolium-based ionic liquids are lower than in DMA, likely due to the higher viscosity of the ionic liquids. Nevertheless, the fractions suggest that the Ir-sensitizer's photoexcitation and one electron-reduced species (OERS) formation occur with nearly identical efficiencies. Experiments with different imidazolium cation substitution and OTf^- anion reveal a strong impact of alkyl chain length and TON, leading to decreased yields in the presence of longer chains when sensitizer and catalyst are applied in a ratio of 100:1. This result

follows the findings by Lin.[34] However, it was shown that the choice of catalyst concentration might also play a role here. A detailed investigation suggests that for [C_2mim][OTf], the photocatalytic cycle is the rate-limiting step, unlike in [C_4mim][OTf] and [C_6mim][OTf], where the sensitizing cycle is limited. Additionally, it was indicated that the back electron transfer from the OERS of Ir-sensitizer to BIH is enhanced in ionic liquids, especially [C_2mim]][OTf], most likely due to solvent cage effects. On the other hand, the diffusion coefficients of the Re catalyst are highly dependent on viscosity and, therefore, the probability of sufficient electron transfer and collision with CO_2. Saturated solubilities for CO_2 in the tested ionic liquids are relatively similar and might, therefore, not be a crucial factor for the efficiency of CO_2RR. Cyclovoltametry experiments showed that the redox potentials of the Ir sensitizer does not strongly depend on the solvent properties. In contrast, the potential for [$Re(bpy)(CO)_5$]Br is slightly shifted towards positive values, increasing the driving force for electron transfer from OERS of Ir to the Re catalyst.

Unlike previous studies, which used ionic liquids as bulk solvents, our group focused on their application as low-level additives (0.5–20% (w/v)) to prevent effects related to viscosity or mass transfer issues.[78] The investigated system consisted of [$Ru(bpy)_3$](PF_6)$_2$ sensitizer and [$Re(bpy)(CO)_3$]Cl catalyst and was tested in the solvents MeCN, DMF, and dimethylsulfoxide (DMSO) without additional water. Initial investigations using the basic ionic liquid [C_2mim][OAc] in MeCN revealed concentration dependency of CO formation rates. In a series of experiments, varying ionic liquid content, ranging from 0% to 20% (w/v) of [C_2mim][OAc], CO formation increased from a TON of 16 at 0% (w/v) IL to a TON of 58 at 20% (w/v) ionic liquid. Further increases in ionic liquid content did not enhance the reaction. The suppression of H_2 production correlated with the amount of ionic liquid used. The most significant rise in CO formation was achieved with [C_2mim][OAc] in DMF, resulting in nearly a 20-fold increase in CO formation while simultaneously suppressing hydrogen production. Comprehensive studies on the influence of anions, using a range of imidazolium-based ionic liquids, reveal that CO yields can be correlated with the Kamlet-Taft parameters for solvent interactions in DMF and MeCN, although the trend was less pronounced in DMSO. Additionally, the effect of water on the reaction was thoroughly examined. NMR studies suggest that water promotes a shift in the mechanism toward the involvement of $[HCO_3]^-$, resulting in decreased selectivity for CO. In addition to the direct interaction between the ionic liquid, CO_2, and solvent cage effects, the coordination of the ionic liquid in the second coordination sphere of catalysts —whether CO_2 is present or absent— may also contribute to the reaction mechanism, potentially exhibiting a synergistic effect as described in the following section.

Matsubara et al. investigated thermodynamic aspects of ionic liquid co-catalyzed CO_2RR with a Re catalyst in electrocatalytic experiments, highlighting the role of ionic liquids in the second coordination sphere of the catalytic center.[79] It was postulated that 1-ethyl-3-methyl-imidazolium ($[C_2mim]^+$) cations could interact in an initial pre-coordination step with the reduced 5 ligand species of the rhenium complex, as well as with the CO_2-bound catalyst during the rate-determining step (Scheme 7a). Based on the work of Sung et al., who investigated the covalent attachment of ionic liquids in the secondary coordination sphere of a Re catalyst in electrocatalytic experiments, Chen et al. applied this concept to photocatalytic CO_2RR.[80,81] The Re catalyst was modified by introducing a covalently attached imidazolium moiety to the bipyridine ligand coupled via a C_1 linker, providing a po proximity to the reaction center (Scheme 7b). Opposite to results from electrochemistry suggesting that intramolecular C_2-H···Cl^- interactions may contribute to faster Cl^- dissociation enhancing electrocatalytic CO_2RR, it was shown that imidazolium modification of the linker did not have a beneficial impact in the sense of a synergistic effect on photocatalytic CO_2RR because of photophysical limitations. Due to the electron-deficient property of the imidazolium-modified complex, the light absorption is shifted to higher wavelengths. On the contrary, modification with less electron-deficient functional groups such as triethylamine (TEA) and triethanolamine (TEOA) serving as local proton sources had no negative impact on light absorption and led to improved TON, illustrating the powerful synergistic effect of this concept through the close proximity of reaction partners and active catalytic site.

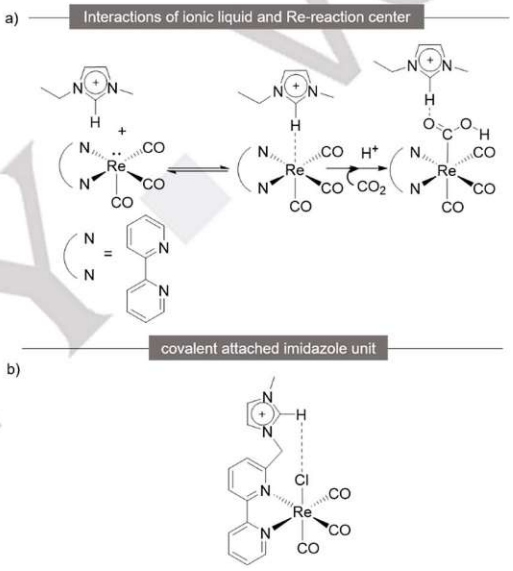

Scheme 7: Interaction of imidazolium based ionic liquids with Re catalyst in the presence and absence of CO_2 (a) and covalent attachment of ionic liquid to the Re catalyst (b). Adapted from [79] and [80] .

3.2. Catalysis in the presence of earth-abundant metal sensitizer and catalyst

Replacing noble metal catalysts with earth-abundant alternatives is a promising strategy for developing cost-effective reaction systems and addressing material shortages.[15] Forero-Cortés et al. transferred a photocatalytic system based on earth-abundant Cu and Fe to ionic liquid media.[82] In the investigated system, a newly developed Cu catalyst based on [Cu(bcp)(POP-xantphos)][PF_6]. and [Cu(bcp)(thixantphos)][PF_6] (bcp = 2,9-dimethyl-4,7-diphenyl-1,10-phenanthroline) was used in combination with the iron catalyst [Fe(cyclopentadienone)$(CO)_3$]. The system was tested in mixtures of ionic liquids and TEOA (4:1 *v*:*v*) under the addition of BIH. Among the tested ionic liquids based on imidazolium-, pyrrolidinium, and phosphonium-based ionic liquids, it was shown that selectivity and yield were highly dependent on the chosen ionic liquid. With the tested

imidazolium-based ionic liquid [C_2mim][NTf_2], hydrogen formation was enhanced. This effect might be related to the anion [NTf_2] as 1-butyl-1-methyl- pyrrolidinium bis(trifluoromethanesulfonyl)imide ([Bmpyrr][NTf_2]) and tri- butylmethylphosphonium bis(trifluoromethylsulfonyl)imide ([Tbmp][NTf_2]) had similar effects when compared to $[N(CN)_2)]^-$. Possible reasons might be interactions with the Fe catalyst or solvation behavior in the reaction mixture.

Based on the reviewed examples, the first two chapters of this review highlight the significant role of ionic liquids in photocatalysis, particularly in the presence of metal-organic sensitizers and catalysts. The results demonstrate how the ionic liquid's properties, including anion type and structure, influence the photocatalytic CO_2 reduction process, with some ionic liquids enhancing CO production while suppressing H_2 evolution. Additionally, the second coordination sphere of metal catalysts, especially investigated in the case of rhenium, can be influenced by ionic liquids, providing a synergistic effect that can improve photocatalytic efficiency.

Among various solvent conditions investigated, the impact of water has been explored, with water promoting the HCO_3^----based mechanism and enhancing H_2 evolution. Further investigations are necessary to fully understand the impact of protic solvents. This aspect is further discussed in the following chapter, where reactions in the absence of metal-organic catalysts or sensitizers are explored.

3.3. Catalysis in the absence of a metal-organic catalyst

As previously mentioned, certain ionic liquids possess intrinsic light absorption properties, which can be harnessed for direct photoexcitation. In this context, Qadir and Peng explored the photocatalytic reduction of CO_2 without the use of metal-organic photosensitizers or catalysts.[38,83] Qadir et al. specifically investigated the photoactivation of imidazolium-CO_2 adducts from [C_2mim][OAc] for CO production in an aqueous solution, in the absence of sacrificial agents or external catalysts. The presence of the carbene complex was demonstrated by NMR spectroscopy, while ESR experiments confirmed the radical nature of the reaction, which proceeds through the homolytic cleavage of the imidazolium cation-CO_2 adduct, generating CO_2 radicals (Scheme 8a). $CO_2^{\bullet-}$ radicals can undergo a cascade reaction to CO via a reaction mechanism comparable to the one reported for electrocatalytic experiments, featuring intermediates such as bicarbonate and hydrogen carbonate. When comparing ionic liquids with different counterions, it was shown that CO yields scale with the basicity of the counterion and, therefore, the ability to form the *N*-heterocyclic carbene. The reaction was selective for CO, as only traces of H_2 were detected.

Peng et al. conducted consecutive investigations into photocatalytic CO_2 reduction reactions (CO_2RR) under direct photoexcitation of ionic liquids in protic solvents. Based on the findings of Qadir et al., the authors explored the impact of UV-Vis absorption, anion properties, and the nature of the protic solvent. The results showed that UV-Vis absorption capacity was primarily related to the nature of the cation, determining whether the ionic liquid exhibited photocatalytic activity. In contrast, CO_2 activation was found to depend on the ionic liquid anion, as previously described by Qadir. A series of experiments in isopropanol with variable ionic liquid dilution demonstrated that the reaction mechanism is strongly influenced by the ratio between protic solvents and the ionic liquid. At low concentrations, the ions are present as contact ion pairs with strong interactions between ionic liquid cation and anion, hampering the formation of the *N*-heterocyclic carbene complex.

Under these conditions, no CO formation was observed. At higher dilutions, the ionic liquid aggregates are present as solvent-shared or solvent-separated ion pairs, and the interaction between basic ionic liquid anion and solvent becomes more prominent. The interaction of solvent and ionic liquid cation can hamper the formation of alkyl carbonate (Scheme 8b), shifting the reaction mechanism from cation-centered to solvent-centered. This intermediate can then undergo photoreduction with electrons provided by photoexcitation of the imidazolium cation. The concept was transferred to aqueous media under conditions of infinite dilution and a series of experiments with different ionic liquids. The ability of the counterion to interact with the solvent can be described using the Kamlet-Taft parameter (β). The higher the β value, indicating greater solvent interaction, the more HCO_3^- (or in isopropanol, RCO_3^-) was formed, leading to a more efficient reaction mechanism via the HCO_3^- pathway. In aqueous media, the HCO_3^- mechanism became dominant over the zwitterionic mechanism starting at a pH of 8. Despite the presence of H_2O, H_2 was only detected in traces.

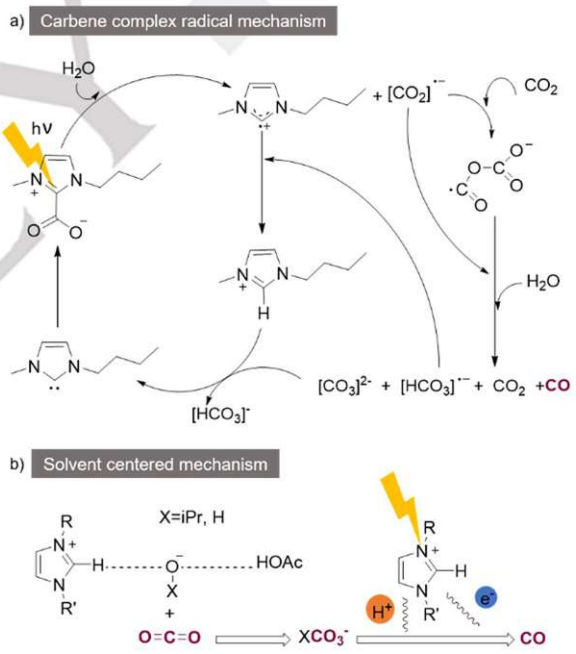

Scheme 8: Carbene complex radical mechanism suggested by Qadir (a) and solvent-centered mechanism suggested by Peng (b) Pictures adapted from [38] and [83]. Copyright Scheme a WILEY-VCH Verlag GmbH & Co. Copyright Scheme b © 2022 The Authors. Published by Elsevier B.V.

In summary, this chapter highlights the potential of ionic liquids as photocatalysts on their own due to their intrinsic light absorption properties, enabling CO_2 reduction without the need for external photosensitizers or catalysts. The findings reveal that the photocatalytic activity is influenced by the cation's UV-Vis absorption and the anion's basicity, which governs CO_2 activation

and the reaction pathway. Furthermore, the studies demonstrate how solvent interactions and ionic liquid concentration affect the reaction mechanism, with the shift from cation-centered to solvent-centered pathways offering new insights for optimizing CO_2RR in protic and aqueous media. These findings should also be considered in both homogeneous and heterogeneous systems featuring catalytic functionalities, where similar mechanistic influences may play a crucial role. Interestingly both discussed examples report only traces of H_2 formation.

prevent degradation processes, such as dimer formation, and enables continuous processes.[84,85] The use of imidazolium-based ionic liquids for CO_2 activation can be transferred to heterogeneous catalysis with different strategies: Ionic liquids can be employed as molecular units in polymerized or coordinated systems, or as active sites in composite materials.

The physical properties of ionic liquids in these cases differ significantly from those of bulk ionic liquids due to the confinement introduced by covalent bonds or surface interactions with

Table 1: Comparison of photocatalytic systems applied in homogeneous photocatalytic CO_2 reduction.

Photocatalytic system	Screened imidazolium based ionic liquids	Conditions	Selected results[b]	Reference
Metal-organic catalyst / Sensitizer				
$[Ru(bpy)_3]Cl_2$, $CoCl_2$	$[C_2mim]^+$ $[A]^-$, $[A]^{--}$=$[BF_4]^-$, $[L\text{-}L]^-$, $[OTf]^-$, $[N(CN)_2]^-$,$[OAc]^-$, $[Tf_2N]^-$; $[C_2\text{-}C_8mim][BF_4]$	3:1:1 solvent, ionic liquid, TEOA Solvents: H_2O, MeCN, DMF, THF, BTF 300W Xe-lamp (>420 nm)	17.4 µmol•h^{-1} CO, 5.5 µmol•h^{-1} H_2 in H_2O; $[C_2mim][Tf_2N]$	Lin et al.[34]
$[Ir(piq)_2(dmb)](PF_6)$, $[Re(bpy)(CO)_3Br]$	$[K]^+$= $[C_2mim^+$, $[C_4mim]^+$, $[C_6mim]^+$ $[A]^-$= $[OTf]^-$; $[Tf_2N]^-$, $[BF_4]^-$	Neat ionic liquid, BIH, TEOA mercury lamp (>370 nm),	TON=140 for CO in $[C_2mim][OTf]$	Asai et al.[76]
$[Ru(bpy)_3](PF_6)_2$ $[Re(bpy)(CO)_3Cl]$	$[C_2mim]^+$ $[A]^-$, $[A]^{--}$=Cl^-, Br^-, I^-, $[OAc]^-$,$[MeSO_4]^-$, $[NTf_2]^-$, $[N(CN)_2]^-$	MeCN, DMF, DMSO, TEOA, ionic liquid (0.5–20% (w/v)) 445 nm LED	5.4 µmol•h^{-1} CO in DMF; $[C_2mim][OAc]$	Eisele et al.[78]
$[Re(IL\text{-}bpy)(CO)_3Cl]$ IL=$[C_1MIM][Cl]$	$[C_1mim][Cl]$ covalent linked to catalyst	DMF TEOA 10:1 500 W Xenon lamp (>400 nm)	267 µmol•h^{-1} CO in DMF	Chen et al.[80]
$[Cu(N^N)(P^P)][PF_6]$ $[Fe(cyclopentadienone)(CO)_3]$	$[C_4mim][OTf]$	Neat ionic liquid, TEOA (4:1, v:v), BIH 400–700 nm (1.50 W)	34 µmol•h^{-1} CO, 34 µmol•h^{-1} H_2 in $[C_4mim][OTf]$, [b]	Forero-Cortés et al.[82]
Absence of metal-organic catalyst / Sensitizer				
none	$[C_4mim]^+$ $[A]^-$, $[A]^{--}$=$[N(CN)_2]^-$,$[PF_6]^-$, $[HCO_3]^-$, $[OAc]^-$, Cl^- ($[C_4mim]\text{-}CO_2$)[a] $[Bmim][OAc]$	H_2O 300 W Xe lamp	56 µmol•g^{-1}h^{-1} in H_2O with $[C_4mim]\text{-}CO_2$	Qadir et al.[38]
none	$[C_4mim]^+$ $[A]^-$, $[A]^{--}$=$[NTf_2]^-$; $[BF_4]^-$, $[N(CN)_2]^-$,$[OTf]^-$, Cl^-, $[OAc]^-$	H_2O /*i*PrOH/ protic ionic liquid	0.56 µmol•h^{-1} CO in $[C_4mim][OAc]$ *i*PrOH mixture	Peng et al. [83]

[a] Pre-reacted with CO_2, [b] If possible yields are reported in µmol• h^{-1}, [b] Calculated from reported TONs

4. Ionic liquids in heterogeneous photo-catalysis.

A key step in addressing the limitations of homogeneous metal-organic photocatalysis is the immobilization of metal-organic catalytic sites on heterogeneous supports. This approach helps to heterogeneous supports. Consequently, properties relevant to CO_2 solvation through physisorption may differ under such confined conditions compared to bulk systems.[86]

Examples involving ionic liquid sorption on porous supports, known as supported ionic liquid phases, have demonstrated increased CO_2 uptake due to enhanced surface area. This approach also addresses practical challenges, such as reducing the required amount and viscosity of ionic liquids for effective application.[26,29,87] Alternatively, imidazolium cations can be

incorporated via covalent linkage as functional groups or structural building blocks within highly porous materials, where the imidazolium single sites are sufficiently separated to prevent clathrate formation and, therefore, CO_2 solubilization by physisorption.[88] In addition to CO_2 sorption, heterogenized ionic liquids can play multiple roles within photocatalytic CO_2RR systems. The following examples highlight the role of ionic liquids as active sites for chemisorption and catalysis, as well as their function in charge mediation. The next chapter summarizes recent advances in the field of heterogeneous ionic liquid-assisted photocatalytic CO_2 reduction reactions (CO_2RR), as outlined in Table 2.

4.1. Polymerized ionic liquids for photocatalytic CO_2RR

One approach used for the heterogenization of homogeneous photocatalysts relies on immobilization in polymer frameworks.[89–91] In general, imidazolium-based polymerized ionic liquids (PILs) offer the advantage of high CO_2 absorption capacities.[92] In pioneering work by Zhou et al., a crosslinked polymer was synthesized through radical polymerization, incorporating a vinyl-modified Re-catalyst [(5,5′-divinyl-2,2′-bipyridine)Re(CO)$_3$Cl] and the polymerizable ionic liquid 3-ethyl-1-vinyl-imidazol-3-ium bromide.[93] The resulting polymer demonstrated high CO conversion rates of up to 40.1 mmol• g^{-1} and excellent selectivity for CO formation up to 95.5% over the time course of 12h, outperforming a polymer lacking the ionic liquid functionality, which was attributed to enhanced CO_2 uptake by the imidazolium motif.

Subsequent work by our group involved the incorporation of a ruthenium-based sensitizer into a polymerized ionic liquid matrix (Scheme 9). The study demonstrated that sensitizing with Ru species and consecutive electron transfer to the Re active site producing CO is feasible within the crosslinked polymer matrix.[37] These examples demonstrate the feasibility of transforming homogeneous photocatalytic systems based on metal-organic catalysis into heterogeneous polymerized systems. As a further step in this evolutionary process, the concept can be advanced toward systems with greater structural order, offering enhanced functionality and efficiency.

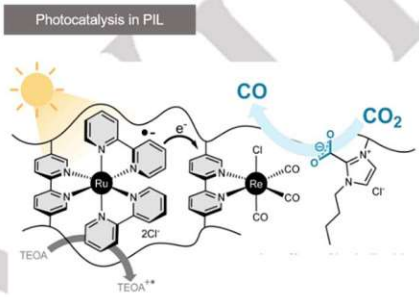

Scheme 9: Illustration of photocatalytic CO2RR in polymerized ionic liquid matrix (PIL) (a) and examples for monomers used in PIL photocatalysis (b). Reproduced from Ref. [37] with permission from the Royal Society of Chemistry.

4.2. Coordination frameworks for photocatalytic CO_2RR

Establishing heterogeneous catalytic porous systems, such as metal-organic frameworks (MOFs) and covalent organic frameworks (COFs) is highly appealing for photocatalytic CO_2 reduction due to their high porosity and large surface areas facilitating accessibility to reactive sides and gas permeability.

Ionic liquids can be embedded in metal-organic frameworks (MOFs) in different ways (Scheme 10a). This includes grafting to metal nodes or ligands (**A, B**) with different synthetic strategies or incorporation of ionic liquids into MOF pores (**C**). The cavity size of the MOF needs to be considered, as the size must be sufficiently large to host the ionic liquid. In the system described by Zhao and coworkers, the ionic liquid 1,3-bis(4-bromophenyl)-imidazolium bromide (BAMeImBr)is grafted via carboxylic acid groups to Zr-oxo clusters of porphyrinic MOF-526 framework (Scheme 10b).[94]

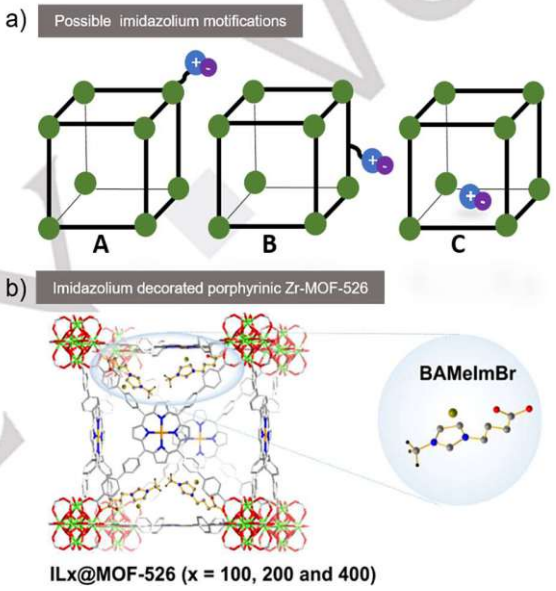

Scheme 10: Metal-organic frameworks (MOFs) and ionic liquids for photo-catalytic CO_2RR.Schematic illustration of covalent and non -covalent ionic liquid introduction strategies (a) and structural description of porphyrinic Zr-MOF-526 decorated with BAMIMBr ionic liquid covalently attached to Zr-oxo clusters. Scheme a adapted from [95]. Scheme b reprinted with permission from [94]. Copyright © 2024 American Chemical Society.

The modification decreased the surface area measured by N_2 uptake, whereas the CO_2 absorption capacity could be increased by ionic liquid modification. The MOF exhibits broad visible light absorption in the 499-800 nm range, which is attributed to the macrocyclic porphyrin, making external photosensitizer obsolete. Photocatalytic experiments were conducted in saturated MeCN solution with the sacrificial agent BIH. A clear correlation between CO_2 uptake and photocatalytic yield was observed. Experiments comparing anchored imidazolium motifs with ionic liquid added to the reaction solution clearly showed a beneficial effect of the anchoring strategy, illustrating that imidazolium motifs are not only involved in the CO_2 uptake of the system but also in modulating charge transfer. This was further reflected in a higher separation efficiency of photogenerated charges as evident from

transient photocurrent response and time-resolved photoluminescence spectroscopy. Examples from (photo-)electrochemistry studies further illustrate the beneficial effect of ionic liquids on MOF catalysis.[96]

Zhao et al. investigated a conjugated microporous polymer built from tetrakis(4-ethynyl phenyl)methane (TRPM) and imidazolium-based building blocks based on 1,3-bis(4-bromophenyl)-imidazolium bromide (ImI-CMP) (see Scheme 10a), providing a build-in electric field acting as a driving force for efficient charge separation and oriented transportation of photoelectrons.[97] The imidazolium motifs enable CO_2 chemisorption as shown by CO_2-temperature programmed desorption. Photocatalytic testing was performed on cobalt-nanoparticle-COF composite (ImI-CMP@CO) to support charge separation further. Experiments were conducted under 0.8 bar of CO_2 and visible light excitation using the external photosensitizer ($[Ru(bpy)_3]Cl_2$) and TEOA as sacrificial agents. The system reached a CO production rate of 2953 µmol• $g^{-1}h^{-1}$ and a turnover frequency of 30.8 h^{-1} over the time course of 35 min. This exceeds the results gained with a COF structure where imidazole-based units were replaced by an ethene bridge by far, indicating the important role of the imidazolium-based motif in the reaction mechanism. The system produced high amounts of H_2 as a side product, resulting in a gas stream in the ratio of traditional syngas. Zhao et al. suggested a mechanism where initially CO_2 is concentrated inside the COF pores, and TEPM segments can accept photogenerated electrons from Ru-sensitizer, while TEOA can consume electron holes (Scheme 11). Consecutively intramolecular charge transfer occurs in ImI-CMP

Table 2: Comparison of studies on heterogeneous photocatalysis assisted by imidazolium based ionic liquids.

Material	Ionic liquid/ Ionic liquid monomer	Conditions	Production rate[c]/TON main products	Reference
Polymerized ionic liquid				
Re-PIL	3-ethyl-1-vinylimidazolium bromide [a]	MeCN, TEOA, 500 W Xenon lamp (λ> 400 nm)	40.1 mmol• g^{-1} (12h), TON =30.9 for CO	Zhou et al. [93]
Ru-Re-PIL	1-butyl-3-vinylimidazolium chloride [a]	MeCN, TEOA, 445 nm LED	1.5 mmol• g^{-1} (15h), TON= 60 for CO	Eisele et al.[37]
Coordination polymers				
Pophyrin MOF-526	1,3-bis(4-bromophenyl)-imidazolium bromide[a]	MeCN, BIH; 420 nm LED	14.0 mmol g^{-1} (72h) for CO	Zhao et al.[94]
Conjungated-microporous polymer (ImI-CMP) with Co NP	1,3-bis(4-bromophenyl)-imidazol-3-ium bromide[a]	MeCN, TEOA visible light (λ > 420 nm)	5.4 mmol• g^{-1} (3.5h) for CO, (H_2:CO 2:1)	Zhao et al.[97]
Nanoparticles				
Co single atoms on boron-modified CN (*b*CN)	$[C_2mim][BF_4]$	Gasphase reaction, water vapor 300W Xenon lamp	81.0 µmol• g^{-1}(2h) for CO 12.6 µmol• g^{-1} (2h) for CH_4	Liu et al.[98]
Pd NP on *g*-CN	$[C_4mim][OAc]$	Ionic liquid *i*PrOH mixture, 300 W Xenon lamp (300-600 nm)	212.4 µmol• g^{-1} (3h) for CO	Peng et al.[99]
Au plasmonic particles	$[C_2mim][BF_4]$	Supported substrate in H_2O ionic liquid mixture; 520 nm (CW laser)	TOF= 4.91 for CH_4[b] (10 min) TOF= 1.26 for C_2H_4 TOF= 0.87 for C_2H_2 TOF= 0.63 for C_3H_6 TOF= 0.30 for C_3H_8	Yu et al. [42]

[a] Monomer/building block [b] TOF (NP h^{-1}), first cycle, [c] Yields are reported in µmol• g^{-1}wherever possible.

based on the built-in electric field where the segment with the imidazolium motif is electron deficient and can serve as an electron acceptor.

The electrons initially located at the Co site are further transferred to CO_2 to form the CO_2^- intermediate. This consecutively leads to the formation of the *N*-heterocyclic carbene complex with the imidazolium motif, which ultimately undergoes a facilitated CO_2RR.

In summary, the integration of imidazolium moieties into covalent organic frameworks (COFs) and metal-organic frameworks (MOFs) underscores their essential role in advancing the functionality of heterogeneous porous materials. Beyond significantly enhancing CO_2 uptake, these structural motifs actively contribute to charge modulation and separation, showcasing their potential to drive more efficient and sustainable catalytic processes.

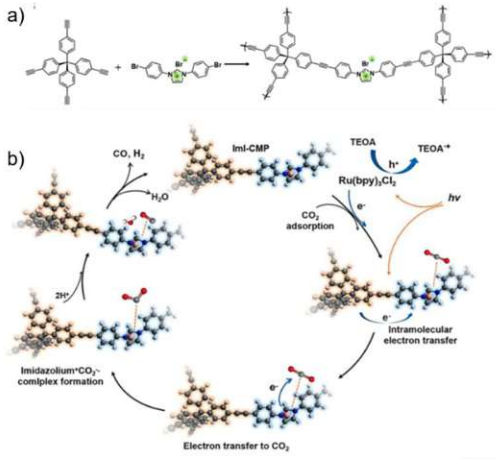

Scheme 11: Synthesis of mI-CMP (a) and suggested mechanism for photocatalytic CO2RR in Iml-CMP@CO by Zhao and coworkers (b). Reprinted with permission from [97]. Copyright 2022 Elsevier.

4.3 Nanoparticles and semiconductors

An alternative approach for heterogenized systems involves the combination of graphitic carbon nitride with nanoparticles. Graphitic carbon nitride (*g*-CN) acts as photoactive support without the drawback of photodegradation, while nanoparticles have a high surface charge-to-area ratio that can promote charge separation and enable selective photocatalysis.[100]

Liu et al. combined borate-anchored Co single atoms on boron-modified CN (*b*CN) with imidazolium-based ionic liquids (IL-*b*CN).[98] By using the composite system IL-*b*CN and the best performing ionic liquid, ethyl-3-methylimidazolium tetrafluoroborate ([C_2mim][BF_4]), they achieved a 9-42-fold increase of CO and CH_4 , respectively, for the photocatalytic CO_2 reduction in aqueous suspension compared to pure CN and *b*CN. Theoretical and experimental studies highlight the role of ionic liquids in the photocatalytic system: Ionic liquids seem to assist in the extraction of electrons initially generated by *g*CN and facilitate CO_2RR by acting as active sites (Scheme 12a and 12b). Meanwhile, Co single sites effectively trap holes, promoting efficient charge separation electron-hole pairs and catalyzing water oxidation. It was demonstrated that stoichiometric amounts of O_2 can be produced as a byproduct, confirming simultaneous CO_2 reduction and water oxidation, thus eliminating the need for sacrificial agents.

It can be assumed that the [C_2mim]-CO adduct as main intermediate in the reaction mechanism leading to CO formation, can further react to CH_4 by uptake of more electrons (Scheme 11b). It was demonstrated that the selection of ionic liquid affects the suppression of H_2 formation, which competes with CO_2 reduction. Specifically, the ionic liquid [C_2mim][BF_4] completely inhibited H_2 formation. A further advance worth mentioning here is the development of the reaction under gas phase conditions. The reaction protocol utilizes the catalyst in powder form, positioned on filter paper above a water reservoir. The humidity of the gas phase is regulated by bubbling CO_2 through water.

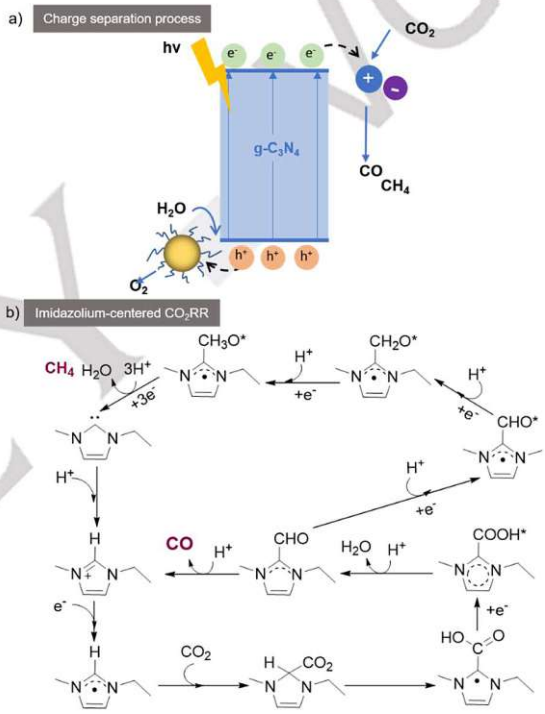

Scheme 12: Photocatalytic CO_2RR on boron modified g-CN. Schematic description of charge separation and parallel H_2O oxidation and CO2RR. (a) Proposed mechanism for CO and CH_4 formation on imidazole active side. Picture adapted with permission from [98].Copyright © 2023, The Author(s)

Peng et al. studied the impact of ionic liquid employed as solvent combined with protic co-solvent on a related system consisting of Pd nanoparticles on *g*CN, showing a clear correlation between the protic properties of the co-solvent and CO yield.[99] In the ionic liquid co-solvent mixtures, the co-solvents can serve as sacrificial agents, accepting generated holes and providing protons for CO_2 reduction. It was shown that the ionic liquid 1-butyl-3-methyl-imidazolium acetate ([C_4mim][OAc]) can pre-activate CO_2 by chemical sorption under the chosen reaction conditions to form the *N*-heterocyclic carbene species 1-butyl-3-methyl-imidazolium-2-carboxylate [C_4mim]-CO_2. Among the tested co-solvents such as H_2O, isopropanol (*i*PrOH), and the protic ionic

liquid 1-(2-hydroxyethyl)-3-methyl imidazolium bis(trifluoromethanesulfonyl)imide [C_1C_2(OH)Im][NTf_2], *i*PrOH demonstrated excellent performance for CO_2RR, achieving a CO formation rate of 70.81 μmol • $g^{-1}h^{-1}$ when included at a 0.2 volume fraction in the reaction mixture. NMR studies showed a clear correlation between the formation of [C_4mim]-CO_2 and the co-solvent fraction crucial for the pre-activation of the CO_2. Higher concentrations of protic solvent hamper the formation of HCO_3^- and CO_3^{2-} species. Control reactions in the absence of Pd-*g*CN or ionic liquid did not indicate CO formation. This observation is in contrast to results observed by Qadir et al., who achieved comparable high yields in a completely homogeneous system with a molar ratio H_2O/[C_2mim][OAc] >6000). The observations illustrate the complex interplay between CO_2-ionic liquid adduct and the presence of the sacrificial agent.

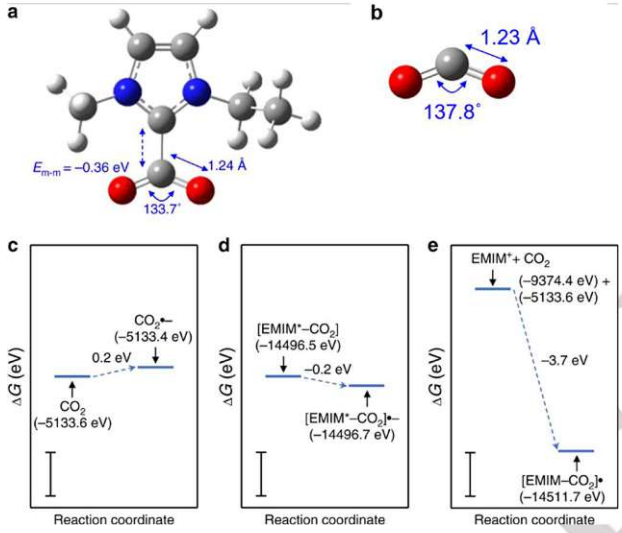

Scheme 13: DFT-optimized geometries of [EMIM*-CO_2](a) and $CO_2^{\bullet-}$(b). C, H, O, and N atoms are shown as gray, white, red, and blue spheres. Key bond lengths, bond angles, and the energy of intermolecular interaction, , are indicated for each of the complexes. DFT-computed free energy cost, ΔG, of formation of the 1e− adduct of CO_2 (c), 1e− adduct of [EMIM*-CO_2](d), and 1e− adduct of CO_2 in the presence of EMIM+ (e). In the latter case, the 1e− adduct of CO_2, $CO_2^{\bullet-}$, is stabilized by complexation with EMIM$^+$ as described by the net process: EMIM$^+$ + CO_2 + e^-→ [EMIM-CO_2]•.In c–e, the free energy of each species is indicated in parentheses. Scale bars are 1 eV in length. Reprinted with permission from [42]. Copyright © 2019 The Authors.

The application of plasmonic nanoparticles allows for photocatalysis without the necessity of an external photosensitizer or photoactive support.[24] Recently, Yu et al. reported a system based on Au plasmonic particles that have been employed in combination with [C_2mim][BF_4].[42] Light absorption is based on localized surface plasmon resonance (LSPR) using green LED light (520 nm). The reaction is selective for C_1, C_2, and even C_3 hydrocarbons (CH_4, C_2H_2, C_2H_4, C_3H_6, and C_3H_8), using water instead of traditional sacrificial agents.
These results are in strong contrast to electrocatalytic Au plasmonic particle experiments producing mainly CO, illustrating the significant impact of the ionic liquid. A clear correlation between ionic liquid content and product formation was observed with a peak product formation at 5 wt% of ionic liquid in H_2O. This is in good accordance with observations made by Peng et al., as well as on work done on homogeneous photocatalysis, showing that the formation of carbene complex in the reaction solution depends on proton concentration. As already concluded by Liu et al., Yu and coworkers found evidence by DFT calculations that the overpotential for injection of the first electron is drastically reduced if the CO_2 molecule is pre-configured for electron acceptance by the formation of the carbene complex (Scheme 13). In contrast to the high energetic demand for the drastic reorganization from linear CO_2 to the bent CO_2 that poses a major barrier for e− acceptance, the molecule can undergo complexation with the *N*-heterocyclic carbene, [C_2mim]*, formed from [C_2mim]$^+$ by abstraction of H^+. In the complex, the CO_2 is present in a bent configuration with an O=C=O angle of 133.7° and C=O bonds length of 1.24 Å resampling the geometry of bend $CO_2^{\bullet-}$ anion (see Scheme 13 a,b). The addition of one e^- to [C_2mim*-CO_2] is significantly more favorable than to molecular CO_2 (Scheme 13c, d), implying that [C_2mim].[BF_4]facilitates the transfer of photogenerated electrons from the Au nanoparticles to the adsorbed CO_2, addressing a key kinetic barrier in the photocatalytic reduction process. Additionally, it is likely that the $CO_2^{\bullet-}$ anion radical generated on the Au surface via photo-induced electron transfer exhibits an extended lifetime due to solvation or complexation with [C_2mim]$^+$ (Scheme 13e).
The role of ionic liquids in forming C_2 and C_3 products might be explained by the need for several carbene complexes available to undergo coupling to longer chain products. This hypothesis is supported by the trend of increased dependency of product formation on the availability of carbene correlating with the chain length of the product.
This chapter reviewed the progress of ionic liquids in photocatalysis with semiconductors and nanoparticles, emphasizing their role as active centers involved in the reaction mechanism. In the discussed examples, ionic liquids have been shown to inhibit H_2 evolution, thereby increasing the reaction's selectivity. Furthermore, their ability to alter reaction pathways compared to reactions in the absence of ionic liquids was demonstrated, particularly in the production of C_2 to C_4 products with plasmonic nanoparticles, overcoming the long-standing challenge of producing products with longer alkyl chains. The demonstration of parallel water oxidation in gas-phase reactions is a significant achievement, addressing the bottleneck caused by the use of sacrificial agents. These advancements underscore the transformative potential of ionic liquids in driving selective and sustainable photocatalytic processes.

5. Ionic liquid degradation

While the stability of metal-organic photosensitizers, particularly in the case of Ru-based species, is sometimes identified as bottleneck in the process, relatively little attention is typically spent on the stability of the imidazolium-based ionic liquid itself.
The purposeful degradation of ionic liquids was investigated in the context of pollutant removal from technological wastewater. However, their degradation in photocatalytic setups when used as additive has been scarcely studied. Stepnowski et al. explored various oxidative degradation mechanisms under conditions relevant to photocatalytic experiments.[101] They compared treatments using UV light alone, UV light with H_2O_2, and UV light

combined with TiO_2 in aqueous solution. The study revealed that the H_2O_2/UV system was the most effective for ionic liquid degradation. Under treatment with UV light or UV light in the presence of TiO_2, the stability of ionic liquids was found to correlate with the length of the alkyl chain on the N-1 alkyl substituent. Specifically, among 1-octyl-, 1-hexyl-, and 1-butyl-methylimidazolium compounds, the 1-octyl derivative was the most stable, while the 1-butyl compound exhibited the lowest stability. When illumination was combined with TiO_2, extending the alkyl chain on the N-3 position increased resistance to degradation. The impact of the long alkyl chains was attributed to various geometric intramolecular interactions in aqueous solutions. These interactions, such as flexing or strengthening, were influenced by solvation forces around the positively charged nitrogen atoms, ultimately enhancing resistance to photodegradation.

Conversely, under direct excitation (UV light alone), [C_2C_2im]-based ionic liquids were less stable than methylimidazolium-based counterparts. It was suggested that under these conditions, the higher polarization of nitrogen in the ethyl-substituted position compared to the methyl-substituted one might play a significant role. The most stable components exhibited losses of approx. 15% after 360 minutes of treatment.

Itakura et al. investigated the degradation of imidazolium-based ionic liquids using Pt-TiO_2 and TiO_2 as photocatalysts.[102] They achieved up to 99% degradation after 24 hours under UV light in an oxygen atmosphere. Ionic liquids with BF_4^- and PF_6^- counterions were found to be less stable compared to those with Br^- counterions.

A similar effect was found by Bedia et al., who studied photostability of different ionic liquids in water under solar light as well as the photocatalytic degradation of ionic liquids in water with TiO_2 under solar light.[103]In the absence of TiO_2, it was shown that imidazolium-based ionic liquids with a hydrophilic anion (Cl^-) were the most stable, exhibiting only 10 to 15% loss over the time course of 10h in comparison to hydrophobic anions like FAP (tris(pentafluoroethyl) trifluorophosphate). the authors claim that the lower light stability of this ionic liquid might be ascribed to the increased ion pair formation, which results in a different photophysical behavior compared to solvated ions, as indicated by differences in by DFT calculations. Additionally, the authors found that under the chosen conditions the absence of TiO_2 ionic liquids with shorter alkyl chains demonstrated greater stability against degradation compared to those with longer alkyl chains. This trend may be attributed to differences in the orbitals involved in the $S_0 \rightarrow S_1$ electronic excitation of the ionic liquids. These differences likely influence the reduction in electron density at the C4 and C5 atoms of the molecule upon irradiation, causing weakening of the covalent bond and contributing to degradation. Not surprisingly, the degradation rate was significantly faster when TiO_2 was present.

These findings demonstrate that ionic liquids are, apart from their role as co-catalysts, also prone to degradation, although the extent of this phenomenon is likely highly dependent on the reaction conditions and the chosen ionic liquid. While more information on degradation pathways is required, all studies underscore ionic liquid degradation as a potential challenge in photocatalytic CO_2 reduction reactions (CO_2RR) and emphasize the importance of addressing this issue in future research.

5. Summary and outlook

The reviewed studies highlight the versatile and impactful role of imidazolium-based ionic liquids in photocatalytic CO_2 reduction, functioning as CO_2 complexing agents, electron acceptors, and active radicals. These examples demonstrate the remarkable ability of ionic liquids to enhance photocatalytic CO_2 reactions in both homogeneous and heterogeneous systems, outperforming systems without ionic liquids.

Notably, both homogeneous and heterogeneous ionic liquid-based photocatalytic systems exhibit significant similarities in their underlying reaction mechanisms. Comparing results obtained under different reaction conditions reveals that factors such as concentration and viscosity of the reaction media significantly influence the mechanism. Additionally, the nature of the reaction center in homogeneous photocatalysis can play a critical role. In this context, considerable effort has been devoted to elucidating the reaction mechanisms in systems based on Re catalysts. Depending on the protic properties of the reaction solution, imidazolium-based ionic liquids can form CO_2-carbene complexes co-catalyzing the reaction. In the presence of proton sources HCO_3^- species are formed making the reaction less selective.

Coordination of imidazolium cations in the second coordination sphere of the catalytic center might also play a role. Furthermore, CO_2RR in the absence of metal-catalysts is possible. Depending on the ionic liquid concentration, protic properties of co-solvent and photoluminescence properties of the ionic liquid CO_2RR can occur either via radical mechanism or HCO_3^-/RCO_3^- centered mechanism. The development of systems that combine ionic liquids with earth-abundant metal-organic catalysts is particularly attractive and presents new opportunities in this field.

Furthermore, the extensive structural variety of MOFs and COFs, coupled with numerous modification strategies, opens up considerable possibilities for future innovations. Imidazolium moieties can be anchored to frameworks or included in the network as building blocks. First, studies prove the synergistic role in porous materials influencing charge separation and acting as active sites for CO_2RR. In the context of nanoparticles and nanoparticle composites, Co and Pd nanoparticles were combined with *g*CN as photoactive support and employed in combination with ionic liquids. As demonstrated with COFs and MOFs, ionic liquids facilitate the extraction of electrons, and carbene species act as active sites in CO2RR. The concept was transferred to catalysis with plasmonic nanoparticles, where C_1 - C_3 product formation was observed via a carbene-driven mechanism.

The field's evolution, from early proof-of-concept studies using metal-organic complexes to the use of imidazolium-based ionic liquids combined with advanced materials like MOFs and plasmonic nanoparticles, underscores the dynamics of this topic. The systems evolved from relying entirely on sacrificial agents towards the first examples that use water as a proton source. However, certain mechanistic details, such as the formation of C_2 and C_3 products, remain unclear.

Despite significant progress in the field, several open questions and challenges remain to be addressed. Future research should prioritize overcoming key obstacles to enhance the practicality and efficiency of ionic liquid-based systems. A critical focus lies in replacing sacrificial agents with water as a sustainable electron donor while deepening the mechanistic understanding needed to

design systems with high selectivity suppressing H_2 as a side product. While most systems sufficiently suppress H_2 formation, even in the absence of additional metal-organic catalysts, some systems produce product mixtures.

A further challenge awaiting is the synthesis of C2 and C3 building blocks as products, where notable first advancements were achieved by the application of plasmonic nanoparticles. Another crucial factor is ensuring the stability of ionic liquids under reaction conditions, which is vital for their long-term application and reusability and warrants further investigation. Finally, advancing scalable systems with robust, long-term stability will be pivotal for translating these technologies toward applications.

Building on the rapid achievements in the field and considering the remaining challenges, the development of new ionic liquid composites and hybrid materials offers exciting opportunities. The structural diversity in nanoparticle composites and MOF/COF systems is immense, and research into their complex mechanistic interactions is still in its early stages. Future progress may also involve exploring alternative reaction conditions, such as combining ionic liquids with supercritical CO_2 or developing continuous gas-phase reaction systems. Additionally, the advancement of innovative reaction platforms, including membrane-based systems and micro reactors, could further contribute to this field.[104]

Acknowledgments

This project has received funding from the European Research Council (ERC) under the European Union's Horizon 2020 research and innovation program (Grant Agreement No. 864991).

Keywords: Ionic liquids • CO_2 reduction • photocatalysis • cooperative effect

[1] United Nations, *State of the Global Climate 2023*, United Nations, **2024**.

[2] M. Carus, L. Dammer, A. Raschka, P. Skoczinski, *Greenh. Gases Sci. Technol.* **2020**, *10*, 488–505.

[3] F. Vidal, E. R. van der Marel, R. W. F. Kerr, C. McElroy, N. Schroeder, C. Mitchell, G. Rosetto, T. T. D. Chen, R. M. Bailey, C. Hepburn, C. Redgwell, C. K. Williams, *Nature* **2024**, *626*, 45–57.

[4] H. Dau, E. Fujita, L. Sun, *ChemSusChem* **2017**, *10*, 4228–4235.

[5] S. Fang, M. Rahaman, J. Bharti, E. Reisner, M. Robert, G. A. Ozin, Y. H. Hu, *Nat. Rev. Methods Prim.* **2023**, *3*, 61.

[6] R. Sang, Y. Hu, R. Razzaq, G. Mollaert, H. Atia, U. Bentrup, M. Sharif, H. Neumann, H. Junge, R. Jackstell, B. U. W. Maes, M. Beller, *Nat. Commun.* **2022**, *13*, 4432.

[7] S. Dabral, T. Schaub, *Adv. Synth. Catal.* **2019**, *361*, 223–246.

[8] A. Brennführer, H. Neumann, M. Beller, *Angew. Chem. Int. Ed* **2009**, *48*, 4114–4133.

[9] R. Franke, D. Selent, A. Börner, *Chem. Rev.* **2012**, *112*, 5675–5732.

[10] H. Schulz, *Appl. Catal. A Gen.* **1999**, *186*, 3–12.

[11] A. Álvarez, M. Borges, J. J. Corral-Pérez, J. G. Olcina, L. Hu, D. Cornu, R. Huang, D. Stoian, A. Urakawa, *ChemPhysChem* **2017**, *18*, 3135–3141.

[12] A. A. Peterson, J. K. Nørskov, *J. Phys. Chem. Lett.* **2012**, *3*, 251–258.

[13] S. Liang, L. Huang, Y. Gao, Q. Wang, B. Liu, *Adv. Sci.* **2021**, *8*, 2102886.

[14] K. P. Kuhl, T. Hatsukade, E. R. Cave, D. N. Abram, J. Kibsgaard, T. F. Jaramillo, *J. Am. Chem. Soc.* **2014**, *136*, 14107–14113.

[15] M. Khalil, J. Gunlazuardi, T. A. Ivandini, A. Umar, *Renew. Sustain. Energy Rev.* **2019**, *113*, 109246.

[16] K. A. Grice, *Coord. Chem. Rev.* **2017**, *336*, 78–95.

[17] Y. Kuramochi, O. Ishitani, H. Ishida, *Coord. Chem. Rev.* **2018**, *373*, 333–356.

[18] N. Vu, S. Kaliaguine, T. Do, *Adv. Funct. Mater.* **2019**, *29*, 1901825.

[19] M. E. G. Carmo, L. Spies, G. N. Silva, O. F. Lopes, T. Bein, J. Schneider, A. O. T. Patrocinio, *J. Mater. Chem. A* **2023**, *11*, 13815–13843.

[20] K. Guo, I. Hussain, G. Jie, Y. Fu, F. Zhang, W. Zhu, *J. Environ. Sci.* **2023**, *125*, 290–308.

[21] I. I. Alkhatib, C. Garlisi, M. Pagliaro, K. Al-Ali, G. Palmisano, *Catal. Today* **2020**, *340*, 209–224.

[22] B. B. Rath, S. Krause, B. V. Lotsch, *Adv. Funct. Mater.* **2023**, 2309060.

[23] L. Qin, C. Ma, J. Zhang, T. Zhou, *Adv. Funct. Mater.* **2024**, 2401562.

[24] F. Wang, Z. Lu, H. Guo, G. Zhang, Y. Li, Y. Hu, W. Jiang, G. Liu, *Chem. – A Eur. J.* **2023**, *29*, e202202716.

[25] A. Yokozeki, M. B. Shiflett, C. P. Junk, L. M. Grieco, T. Foo, *J. Phys. Chem. B* **2008**, *112*, 16654–16663.

[26] P. Mikšovsky, E. N. Horn, S. Naghdi, D. Eder, M. Schnürch, K. Bica-Schröder, *Org. Process Res. Dev.* **2022**, *26*, 2799–2810.

[27] J. Hu, J. Ma, L. Lu, Q. Qian, Z. Zhang, C. Xie, B. Han, *ChemSusChem* **2017**, *10*, 1292–1297.

[28] J. Sun, S. I. Fujita, F. Zhao, M. Arai, *Green Chem.* **2004**, *6*, 613–616.

[29] P. Mikšovsky, K. Rauchenwald, S. Naghdi, H. Rabl, D. Eder, T. Konegger, K. Bica-Schröder, *ACS Sustain. Chem. Eng.* **2024**, *12*, 1455–1467.

[30] D. Hospital-Benito, J. Lemus, C. Moya, R. Santiago, J. Palomar, *Chem. Eng. J.* **2020**, *390*, 124509.

[31] M. Aghaie, N. Rezaei, S. Zendehboudi, *Renew. Sustain. Energy Rev.* **2018**, *96*, 502–525.

[32] T. Welton, *Chem. Rev.* **1999**, *99*, 2071–2083.

[33] M. J. Earle, J. M. S. S. Esperança, M. A. Gilea, J. N. Canongia Lopes, L. P. N. Rebelo, J. W. Magee, K. R. Seddon, J. A. Widegren, *Nature* **2006**, *439*, 831–834.

[34] J. Lin, Z. Ding, Y. Hou, X. Wang, *Sci. Rep.* **2013**, *3*, 1056.

[35] J. Liang, Y. Q. Xie, X. S. Wang, Q. Wang, T. T. Liu, Y. B. Huang, R. Cao, *Chem. Commun.* **2018**, *54*, 342–345.

[36] L. G. Ding, B. J. Yao, W. L. Jiang, J. T. Li, Q. J. Fu, Y. A. Li, Z. H. Liu, J. P. Ma, Y. Bin Dong, *Inorg. Chem.* **2017**, *56*, 2337–2344.

[37] L. Eisele, B. Hulaj, M. Podsednik, F. Laudani, P. Ayala, A. Cherevan, A. Foelske, A. Limbeck, D. Eder, K. Bica-Schröder, *RSC Sustain.* **2024**, *2*, 2524–2531.

[38] M. I. Qadir, M. Zanatta, E. S. Gil, H. K. Stassen, P.

Gonçalves, B. A. D. Neto, P. E. N. de Souza, J. Dupont, *ChemSusChem* **2019**, *12*, 1011–1016.

[39] J. O. Bockris, J. C. Wass, *Mater. Chem. Phys.* **1989**, *22*, 249–280.

[40] K. Chandrasekaran, L. O. M. Bockris, *Surf. Sci.* **1987**, *185*, 495–514.

[41] G. Gurau, H. Rodríguez, S. P. Kelley, P. Janiczek, R. S. Kalb, R. D. Rogers, *Angew. Chem. Int. Ed* **2011**, *50*, 12024–12026.

[42] S. Yu, P. K. Jain, *Nat. Commun.* **2019**, *10*, 2022.

[43] K. Y. Cohen, R. Evans, S. Dulovic, A. B. Bocarsly, *Acc. Chem. Res.* **2022**, *55*, 944–954.

[44] P. G. Jessop, S. M. Mercer, D. J. Heldebrant, *Energy Environ. Sci.* **2012**, *5*, 7240–7253.

[45] J. Ruan, L. Chen, Z. Qi, *Green Chem.* **2023**, *25*, 8328–8348.

[46] J. Kim, K. Kim, H. Lim, J. H. Kang, H. S. Park, J. Park, H. Song, *J. Environ. Chem. Eng.* **2024**, *12*, 112664.

[47] S. Kang, Y. G. Chung, J. H. Kang, H. Song, *J. Mol. Liq.* **2020**, *297*, 111825.

[48] C. Wang, H. Luo, X. Luo, H. Li, S. Dai, *Green Chem.* **2010**, *12*, 2019–2023.

[49] C. Wang, H. Luo, D. E. Jiang, H. Li, S. Dai, *Angew. Chem. Int. Ed* **2010**, *49*, 5978–5981.

[50] X. M. Zhang, K. Huang, S. Xia, Y. Le Chen, Y. T. Wu, X. B. Hu, *Chem. Eng. J.* **2015**, *274*, 30–38.

[51] J. L. Anderson, J. K. Dixon, J. F. Brennecke, *Acc. Chem. Res.* **2007**, *40*, 1208–1216.

[52] C. Cadena, J. L. Anthony, J. K. Shah, T. I. Morrow, J. F. Brennecke, E. J. Maginn, *J. Am. Chem. Soc.* **2004**, *126*, 5300–5308.

[53] M. J. Muldoon, S. N. V. K. Aki, J. L. Anderson, J. K. Dixon, J. F. Brennecke, *J. Phys. Chem. B* **2007**, *111*, 9001–9009.

[54] E. K. Shin, B. C. Lee, *J. Chem. Eng. Data* **2008**, *53*, 2728–2734.

[55] S. Zeng, X. Zhang, L. Bai, X. Zhang, H. Wang, J. Wang, D. Bao, M. Li, X. Liu, S. Zhang, **2017**, DOI 10.1021/acs.chemrev.7b00072.

[56] Y. Yamazaki, M. Miyaji, O. Ishitani, *J. Am. Chem. Soc.* **2022**, *144*, 6640–6660.

[57] Q. Sun, Y. Zhao, W. Ren, C. Zhao, *Appl. Catal. B Environ.* **2022**, *304*, 120963.

[58] M. Liu, C. Ma, Q. Wang, R. Li, S. Yu, H. Chen, F. Liu, *Chem. Eng. J.* **2024**, *500*, 157099.

[59] G. Cui, J. Wang, S. Zhang, *Chem. Soc. Rev.* **2016**, *45*, 4307–4339.

[60] J. Dupont, B. C. Leal, P. Lozano, A. L. Monteiro, P. Migowski, J. D. Scholten, *Chem. Rev.* **2024**, *124*, 5227–5420.

[61] C. Wang, H. Luo, X. Luo, H. Li, S. Dai, *Green Chem.* **2010**, *12*, 2019–2023.

[62] H. Rodríguez, G. Gurau, J. D. Holbrey, R. D. Rogers, *Chem. Commun.* **2011**, *47*, 3222.

[63] G. K. Anderson, *J. Chem. Eng. Data* **2002**, *47*, 219–222.

[64] X. Gui, Z. Tang, W. Fei, *J. Chem. Eng. Data* **2011**, *56*, 2420–2429.

[65] B. A. Rosen, A. Salehi-Khojin, M. R. Thorson, W. Zhu, D. T. Whipple, P. J. A. Kenis, R. I. Masel, *Science* **2011**, *334*, 643–644.

[66] B. A. Rosen, J. L. Haan, P. Mukherjee, B. Braunschweig, W. Zhu, A. Salehi-Khojin, D. D. Dlott, R. I. Masel, *J. Phys. Chem. C* **2012**, *116*, 15307–15312.

[67] L. L. Snuffin, L. W. Whaley, L. Yu, *J. Electrochem. Soc.* **2011**, *158*, F155.

[68] J. L. Dimeglio, J. Rosenthal, *J. Am. Chem. Soc.* **2013**, *135*, 8798–8801.

[69] B. A. Rosen, W. Zhu, G. Kaul, A. Salehi-Khojin, R. I. Masel, *J. Electrochem. Soc.* **2013**, *160*, H138–H141.

[70] A. Salehi-Khojin, H. R. M. Jhong, B. A. Rosen, W. Zhu, S. Ma, P. J. A. Kenis, R. I. Masel, *J. Phys. Chem. C* **2013**, *117*, 1627–1632.

[71] D. C. Grills, Y. Matsubara, Y. Kuwahara, S. R. Golisz, D. A. Kurtz, B. A. Mello, *J. Phys. Chem. Lett.* **2014**, *5*, 2033–2038.

[72] G. P. S. Lau, M. Schreier, D. Vasilyev, R. Scopelliti, M. Grätzel, P. J. Dyson, *J. Am. Chem. Soc.* **2016**, *138*, 7820–7823.

[73] S. Noh, Y. J. Cho, G. Zhang, M. Schreier, *J. Am. Chem. Soc.* **2023**, *145*, 27657–27663.

[74] H. Lee, M. H. Cho, B. S. Lee, J. Palgunadi, H. Kim, H. S. Kim, *Energy and Fuels* **2010**, *24*, 6689–6692.

[75] J. Hawecker, J. M. Lehn, R. Ziessel, *J. Chem. Soc. Chem. Commun.* **1983**, 536–538.

[76] Y. Asai, H. Katsuragi, K. Kita, T. Tsubomura, Y. Yamazaki, *Dalton Trans.* **2020**, *49*, 4277–4292.

[77] Y. Pellegrin, F. Odobel, *Comptes Rendus. Chim.* **2016**, *20*, 283–295.

[78] L. Eisele, W. Chaikhan, S. Batool, A. Cherevan, D. Eder, K. Bica-Schröder, *ChemCatChem* **2024**, *16*, e202301454.

[79] Y. Matsubara, D. C. Grills, Y. Kuwahara, *ACS Catal.* **2015**, *5*, 6440–6452.

[80] K. Chen, N. Wang, Z. Yang, S. Xia, L. He, *ChemSusChem* **2020**, *13*, 6284–6289.

[81] S. Sung, D. Kumar, M. Gil-Sepulcre, M. Nippe, *J. Am. Chem. Soc.* **2017**, *139*, 13993–13996.

[82] P. A. Forero-Cortés, M. Marx, N. G. Moustakas, F. Brunner, C. E. Housecroft, E. C. Constable, H. Junge, M. Beller, J. Strunk, *Green Chem.* **2020**, *22*, 4541–4549.

[83] Y. Peng, K. C. Szeto, C. C. Santini, S. Daniele, *Chem. Eng. J. Adv.* **2022**, *12*, 100379.

[84] E. E. Benson, C. P. Kubiak, *Chem. Commun.* **2012**, *48*, 7374–7376.

[85] F. P. a Johnson, M. W. George, F. Hartl, J. J. Turner, *Organometallics* **1996**, *15*, 3374–3387.

[86] S. Zhang, J. Zhang, Y. Zhang, Y. Deng, *Chem. Rev.* **2017**, *117*, 6755–6833.

[87] A. I. Labropoulos, G. E. Romanos, E. Kouvelos, P. Falaras, V. Likodimos, M. Francisco, M. C. Kroon, B. Iliev, G. Adamova, T. J. S. Schubert, *J. Phys. Chem. C* **2013**, *117*, 10114–10127.

[88] S. P. Kelley, L. A. Flores, M. S. Shannon, J. E. Bara, R. D. Rogers, *Chem. – A Eur. J.* **2017**, *23*, 14332–14337.

[89] W. Zhang, H. Shimakoshi, N. Houfuku, X.-M. Song, Y. Hisaeda, *Dalton Trans.* **2014**, *43*, 13972–13978.

[90] H. Shimakoshi, M. Nishi, A. Tanaka, K. Chikama, Y. Hisaeda, *Chem. Commun.* **2011**, *47*, 6548–6550.

[91] A. S. Maier, C. Thomas, M. Kränzlein, T. M. Pehl, B. Rieger, *Macromolecules* **2022**, *29*, 29.

[92] S. Zulfiqar, M. I. Sarwar, D. Mecerreyes, *Polym. Chem.* **2015**, *6*, 6435–6451.

[93] Z.-H. Zhou, K.-H. Chen, S. Gao, Z.-W. Yang, L.-N. He, *Research* **2020**, *2020*, 9398285.

[94] X. Zhao, Q. Xu, J. Han, W. Zhang, H. Rao, D.-Y. Du, P. She, J.-S. Qin, *ACS Appl. Mater. Interfaces* **2024**, *16*, 26272–26279.

[95] S. Chen, N. Wang, H. Zhang, M. Qiu, L. Shi, Y. Xia, J. Zhang, Y. Huang, F. Cheng, P. Gu, X. Zhang, Q. Yi, *Ind. Eng. Chem. Res.* **2024**, *63*, 3443–3464.

[96] E. P. Delmo, Y. Wang, J. Wang, S. Zhu, T. Li, X. Qin, Y. Tian, Q. Zhao, J. Jang, Y. Wang, M. Gu, L. Zhang, M. Shao, *Chinese J. Catal.* **2022**, *43*, 1687–1696.

[97] W. Zhao, D. Zhai, C. Liu, D. Zheng, H. Wu, L. Sun, Z. Li, T. Yu, W. Zhou, X. Fang, S. Zhai, K. Han, Z. He, W. Deng, *Appl. Catal. B Environ.* **2022**, *300*, 120719.

[98] Y. Liu, J. Sun, H. Huang, L. Bai, X. Zhao, B. Qu, L. Xiong, F. Bai, J. Tang, L. Jing, *Nat. Commun.* **2023**, *14*, 1457.

[99] Y. Peng, K. C. Szeto, C. C. Santini, S. Daniele, *ChemPhotoChem* **2021**, *5*, 721–726.

[100] G. F. S. R. Rocha, M. A. R. da Silva, A. Rogolino, G. A. A. Diab, L. F. G. Noleto, M. Antonietti, I. F. Teixeira, *Chem. Soc. Rev.* **2023**, *52*, 4878–4932.

[101] P. Stepnowski, A. Zaleska, *J. Photochem. Photobiol. A Chem.* **2005**, *170*, 45–50.

[102] T. Itakura, K. Hirata, M. Aoki, R. Sasai, H. Yoshida, H. Itoh, *Environ. Chem. Lett.* **2009**, *7*, 343–345.

[103] J. Bedia, J. J. Rodriguez, D. Moreno, J. Palomar, C. Belver, *RSC Adv.* **2019**, *9*, 2026–2033.

[104] J. A. Piotrowska, C. Jordan, M. Harasek, K. Bica-Schröder, *ACS Sustain. Chem. Eng.* **2024**, *12*, 12236–12248.

Entry for the Table of Contents

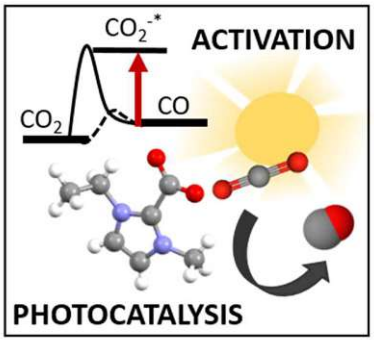

Addressing CO_2 emissions through photocatalytic conversion offers a sustainable route to produce C_1-C_3 chemical intermediates. Imidazolium-based ionic liquids play key roles in CO_2 pre-activation, enhancing reaction kinetics and acting as solvents or additives. Integrated with metal-organic catalysts, MOFs, and nanoparticles, they enable efficient CO_2 reduction, driving advancements in carbon capture and utilization under mild conditions.

2. Aim of the thesis

Addressing the pressing challenges of climate change and rising atmospheric CO_2 levels requires innovative solutions that align with the principles of carbon circularity. Carbon capture and utilization (CCU) offers a promising pathway to mitigate these issues by transforming CO_2 into value-added products, fostering environmental sustainability. Ionic liquids, renowned for their exceptional ability to chemisorb and physisorb CO_2, extend beyond their application in CO_2 capture. They also serve as cooperative agents in catalysis, enhancing the performance of catalysts and broadening their potential for transformative CO_2 conversion processes.

This thesis aims to investigate the impact of imidazolium-based ionic liquids on photocatalytic CO_2 reduction for the selective formation of CO, an important building block for chemical transformations in industry. Initially, the focus is on studying the role of imidazolium-based ionic liquids as co-catalysts in homogeneous photocatalysis to boost the reactivity. Building on this foundation, the research advances toward heterogeneous catalysis to enhance long-term stability and scalability with the ultimate goal of developing methodologies for imidazolium-based ionic liquid-catalyzed gas phase reactions.

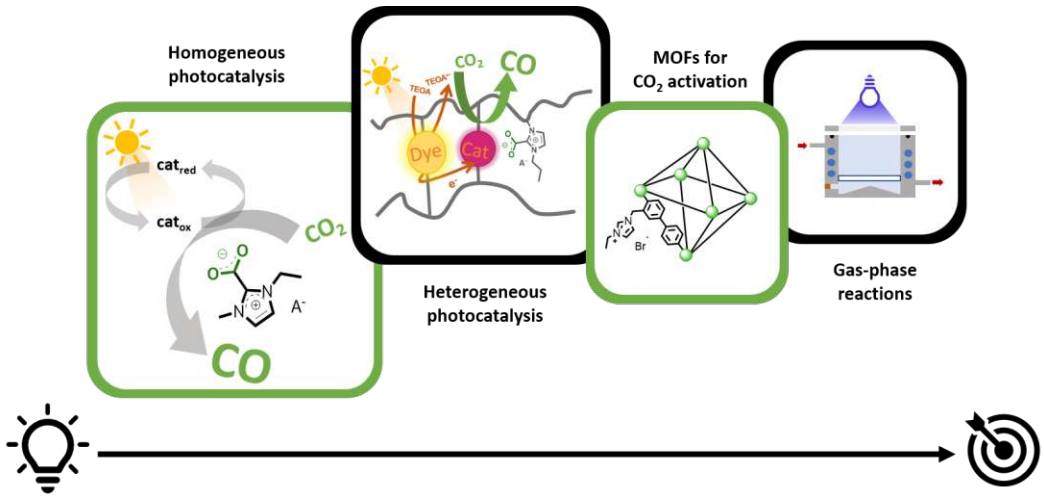

Figure 2.1. Outline of projects addressed in the thesis.

A critical step in this progression is the development of a heterogeneous ionic liquid matrix polymer that mimics the homogeneous photocatalysis system in an immobilized form. To further improve properties such as porosity and accessibility of active sites in heterogeneous systems, metal-organic frameworks modified with imidazolium groups are explored.

Finally, to enable gas-phase reactions, a prototype gas-phase photocatalytic reactor, capable of operating under batch and flow conditions, is constructed. This integrated approach seeks to address key limitations in photocatalytic CO_2 utilization and contributes to advancing sustainable CCU technologies.

3. Results and Discussion

Section 3.1:

Boosting Visible-Light Carbon Dioxide Reduction with Imidazolium-Based Ionic Liquids

ChemCatChem 16:e202301454 (2024)

Authors: Lisa Eisele, Wilaiwan Chaikhan, Samar Batool, Alexey Cherevan, Dominik Eder and Katharina Bica-Schröder

Imidazolium-based ionic liquids can both chemisorb and physisorb CO_2.[83,86,87] The effect of chemisorption occurs under the formation of the *N*-heterocyclic carbene-CO_2 complex, pre-activating the CO_2 and reducing the overpotential of CO_2 reduction as shown in electrochemical experiments.[85] This beneficial property can be used as a cooperative effect to further boost CO2RR when paired with photocatalytic CO2RR catalysts.

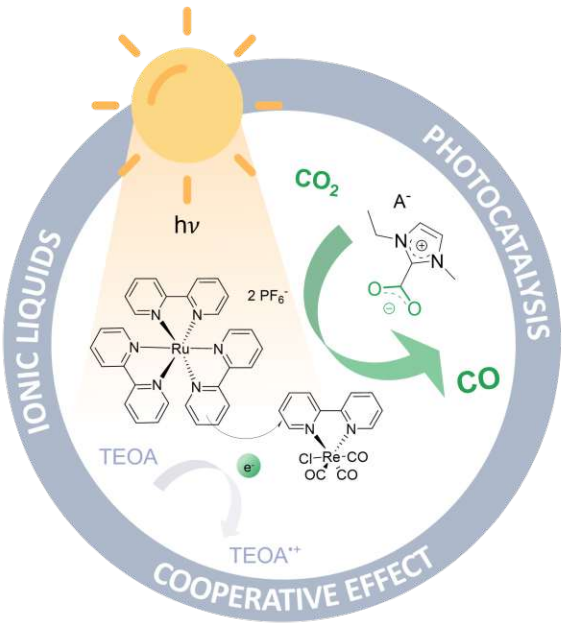

Figure 3.1. Graphical illustration of the cooperative effect of ionic liquids on photocatalytic CO_2 reduction reaction.

Due to the exceptional properties of ionic liquids consisting of ions, solvation in ionic liquids is featured by strong solvent-solvate and anion-cation interactions that may lead

to undesired effects such as solvent cage formation, high viscosity, and mass transfer limitations.[88] In contrast to previous works that focused on reactions in pure ionic liquids or their mixtures with small amounts of co-solvents, this study focuses on the addition of ionic liquids as a low-level additive to prevent the above-mentioned effects. We aimed to test this cooperative effect of ionic liquids in combination with a benchmark system for photocatalytic CO_2 reduction consisting of a Ru-sensitizer and Re-catalyst, aiming to investigate the influence of different ionic liquid anions.

It was shown that adding small amounts of ionic liquids (10% w/v) to traditional solvents significantly increased CO production, thus making it unnecessary to use ionic liquids as the bulk solvent. The impact of various counterions was analyzed using the Kamlet-Taft parameter β, which indicated a correlation between the nucleophilicity of the ionic liquid and the CO yield in DMF and MeCN. Out of the tested anions, the study provides evidence that the cooperative effect is strongest with the basic acetate anion, proving the formation of the CO_2-carbene complex. The study also explored the long-term performance of the photocatalytic system. While the addition of ionic liquids initially led to a rapid increase in the reaction rate, this rate decreased over time, suggesting potential limitations in the long-term stability of the photosensitizer.

As the main author, I conceptualized the experimental work and conducted the majority of the experiments. Additionally, I developed the analytical methods, designed the reaction setup, and drafted the original manuscript.

Boosting Visible-Light Carbon Dioxide Reduction with Imidazolium-Based Ionic Liquids

Lisa Eisele,[a] Wilaiwan Chaikhan,[a] Samar Batool,[b] Alexey Cherevan,[b] Dominik Eder,*[b] and Katharina Bica-Schröder*[a]

Efficiently generating C_1 building blocks from environmentally friendly carbon sources, such as through photocatalytic CO_2 reduction, is essential for fostering a sustainable circular economy. The pursuit of mild catalytic activation methods has yielded powerful catalysts that can be synergistically employed alongside various reaction media to enhance overall performance. Herein, we elucidate the influence of diverse imidazolium-based ionic liquids as additives for visible-light-driven CO_2 reduction with ruthenium(II)- and rhenium(I)-bipyridine complexes. Our investigation reveals that incorporating ionic liquids into traditional solvents at concentrations below 10% can markedly boost CO production while suppressing H_2 generation. The best results were obtained for the highly basic ionic liquid [C_2mim][OAc], resulting in a substantial rise in CO formation from 0.3 μmol/h to 5.4 μmol/h and an increase in turnover number from 3 to 59. This study underscores the cooperative influence of imidazolium-based ionic liquids on CO_2 photoreduction while circumventing their use as primary solvents, thus offering a promising avenue for sustainable chemical synthesis.

Introduction

Carbon fixation chemistry is a critical component of building a circular economy, especially in the face of rising atmospheric CO_2 levels and a shortage of natural resources. To make change happen, processes for converting CO_2 to chemical feedstocks must be developed, transforming chemical industries from petrol-based to renewable. This shift is essential for reducing our carbon footprint, mitigating climate change, and ensuring a more environmentally responsible future. By harnessing the power of carbon fixation chemistry, we can pave the way for a greener, more sustainable approach to chemical production, aligning with the principles of a circular economy and addressing the pressing challenges posed by climate change and resource scarcity.[1–3]

One potential pathway for CO_2 utilization follows the formation of C_1 building blocks, e.g. CO that can be used as a resource for making more complex molecules. Until today, the most extensive catalytic processes, e.g. Fischer-Tropsch synthesis, hydroformylations or methanol carbonylations, rely on CO as reactive and versatile feedstock. The replacement of CO with CO_2 as the prime feedstock in carbonylative transformations for fine chemical synthesis would thus be highly desirable. Before we can widely adopt CO_2-based platform chemicals, it's crucial to address the challenges associated with the demanding conditions needed to (photo)chemically reduce CO_2.[4–6]

The biggest challenge in CO_2 conversion is its activation, which typically requires harsh conditions and long reaction times owing to its high thermodynamic and kinetic stability. In this regard, nature can serve as a source of inspiration, as the conversion of CO_2 is a fundamental component of natural photosynthesis.[7–10] The search for mild catalytic activation strategies has led to a number of potent catalysts, mostly based on transition metal or organocatalytic species that can be optionally combined with different reaction media for a synergistic effect. Ionic liquids (ILs) are typical examples of such a cooperative media, as they can absorb large concentrations of CO_2 by physisorption and chemisorption and thus co-catalyze various reactions involving CO_2.[11–15] Moreover, the chemical interaction of many ionic liquids with CO_2 resembles the first step of CO_2 activation in the plant photosynthesis cycle. In particular, the chemisorption of CO_2 in ionic liquids has been shown to facilitate the bending of initial linear CO_2.[16] The interactions of ionic liquid and CO_2 can further lower the overpotential of CO_2 reduction, as proven in electrochemical experiments.[17,18]

As an alternative to purely chemical or electrochemical reductions, the exploitation of ubiquitous energy sources such as sunlight opens novel possibilities for the transformation of CO_2, stimulating research in non-conventional catalytic activation. In photocatalysis, the metal catalyst is paired with a photosensitizer (PS) that can be excited by light, generating an electron-hole pair, followed by reductive quenching with the help of an electron-donating agent to pass an electron to the catalyst, causing a low valent unsaturated state of the catalyst

[a] L. Eisele, W. Chaikhan, Prof. K. Bica-Schröder
Institute of Applied Synthetic Chemistry
TU Wien
Getreidemarkt 9/163 1060 Wien, Austria
E-mail: katharina.schroeder@tuwien.ac.at
[b] S. Batool, Dr. A. Cherevan, Prof. D. Eder
Institute of Materials Chemistry
TU Wien
Getreidemarkt 9/165 1060 Wien, Austria
E-mail: dominik.eder@tuwien.ac.at

Supporting information for this article is available on the WWW under https://doi.org/10.1002/cctc.202301454

that can interact with CO_2. The reduction of CO_2 to CO requires the transfer of two electrons, which can be facilitated by electron-donating sacrificial agents, such as triethanolamine (TEOA) and triethylamine (TEA).[19–21] As shown by Dupont and co-workers, ionic liquids possess the ability to stabilize localized charges and holes that can be generated electrochemically or by direct radiation. In case of suitable absorption properties, radical species are formed by homolytic cleavage of the imidazolium-CO_2 adduct even in the absence of an external photosensitizer, thus forming $CO_2^{-\bullet}$ and imidazolium$^{+\bullet}$ radicals in aqueous media.[15,22] However, as reported by Daniele et al., this mechanism is highly dependent on the pH value, since a HCO_3^- driven reaction is competing.[23]

The synergistic role of ionic liquids as co-catalysts for photocatalytic CO_2 reduction via formation of the imidazolium-CO_2 adduct was also demonstrated in aprotic solvents. Different imidazolium-based ionic liquids were added to the photocatalytic tandem system $[Ru(bpy)_3]Cl_2/CoCl_2 \cdot 6\ H_2O$ in different co-solvents by Lin *et al.*[24] The best results were observed for a mixture of 1-ethyl-3-methylimidazolium tetrafluoroborate ($[C_2mim]BF_4$) with acetonitrile in a ratio of 75% (v/v), resulting in an almost 3-fold increase in the reaction rate.[24] Furthermore, Asai *et al.* investigated the mechanism of CO_2 photoreduction in the presence of ionic liquids in more detail, using an Ir-based sensitizer and $[Re(bpy)(CO)_3]Cl$ as a catalyst. The ionic liquids were used in pure form without co-solvent, and a strong influence of their molecular structure on photosensitizing and catalytic cycles was observed. Ultimately, triflate (OTf^-) based ionic liquids were identified as most efficient species, thus highlighting their potential as valuable solvents for photocatalytic CO_2 reduction[7]

In here, we aim for a mild protocol for photocatalytic CO_2 reduction that benefits from the cooperative effect of imidazolium-based ionic liquids in combination with $[Ru(bpy)_3](PF_6)_2$ sensitiser and $[Re(bpy)(CO)_3]Cl$. In contrast to previous studies, we focused on the use of ionic liquids as a low-level additive (0.5–20% (w/v)) in three different aprotic solvents rather than using the ionic liquid as a bulk solvent, thus aiming for a systematic investigation of the cooperative effects of ionic liquids on visible light-driven CO_2 photoreduction and an understanding of the counterion effect.

Results and Discussion

The design of the catalyst plays a crucial role in controlling selectivity and efficiency. $[Re(bpy)(CO)_3]Cl$, first characterized by Lehn *et al.*, is known as a highly selective catalyst for CO formation and has been extensively investigated and established as a model catalyst in combination with visible light photosensitizer $[Ru(bpy)_3](PF_6)_2$. It was, therefore, chosen as a model system for the investigation of the impact of ionic liquids as additives.[25–28]

As a starting point, a set of imidazolium-based ionic liquids with variable counterions was examined in combination with the catalytic model system using the polar and aprotic solvents dimethylformamide (DMF), acetonitrile (MeCN), and dimethylsulfoxide (DMSO) that are often used solvents in photocatalysis with $[Re(bpy)(CO)_3]Cl$ (Figure 1).

To avoid issues from viscosity and miscibility and to keep the ionic liquid as low as possible, experiments were conducted with an ionic liquid content of 0.5–20% (w/v). The initial screening of the ionic liquid content was performed in MeCN with $[C_2mim][OAc]$ **1 d** (Table 1). Results indicate that the formation of CO is increasing when the ionic liquid content is increased up to 10% (w/v); however, a further increase to 20% (w/v) is not beneficial anymore. Moreover, with increasing ionic liquid content, the formation of H_2 is stronger suppressed. Consequently, we selected a concentration of 10% (w/v) ionic liquid as an additive for all future experiment, corresponding to a molar fraction of $1.0–5.0 \cdot 10^{-5}$, depending on the ionic liquid species.

For further insight in the role of the anion, various imidazolium-based ionic liquids were studied in MeCN (Figure 2). The most prominent and distinct influence on CO_2 reduction performance was found for $[C_2mim][OAc]$ **1 d**, which increased the yield of CO from 1.45 µmol to 5.19 µmol in MeCN. The observed CO formation corresponds to a rise in turnover number (TON) from 3 to 59. Within the halide series 1a-c, $[C_2mim][Cl]$ **1 a** performed best and substantially raised the CO yield. Additionally, there is a trend for a decrease in activity in the halide series (**1 a–c**) in the order $Cl^- > Br^- > I^-$. In case of $[C_2mim][MeSO_4]$ **1 e**, results are difficult to compare since the

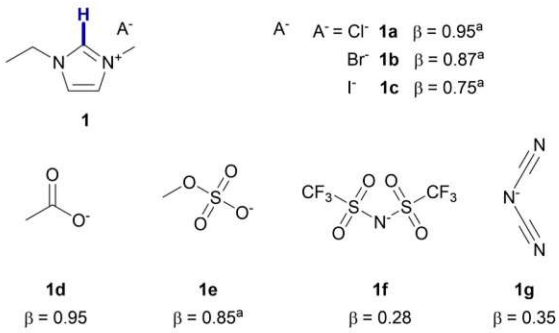

Figure 1. Structures and properties of the ionic liquids used in this study. The proton relevant for counterion interactions is highlighted in blue. Numbers indicate cations and a–g (letters) correspond to counteranions.[29] [a] Parameter β reported for the corresponding ionic liquid with $[C_3mim]^+$ cation.[30]

Table 1. Photocatalytic CO_2 reduction in the presence of various amounts of $[C_2mim][OAc]$ **1 d**.

Ionic liquid [wv]	CO [µmol]	H_2 [µmol]	TON[b]	Selectivity[c]
0	1.46 ± 0.43	0.06	16	96.1
0.5	2.63 ± 0.11	0.10	29	96.3
5	3.96 ± 1.08	0.02	44	99.4
10	5.19 ± 0.71	< 0.01	58	> 99.9
20	2.66 ± 0.15	< 0.01	30	> 99.9

Conditions: 0.6 mM $[Ru(bpy)_3](PF_6)_2$, 0.06 mM $[Re(bpy)(CO)_3]Cl$, 0.32 M TEOA, 0.1 g/mL $[C_2mim][OAc]$ in MeCN; t = 1 h, T = 22 °C. Results are reported as mean ± STD, n = 3. [b] Calculated for CO. [c] Selectivity for CO.

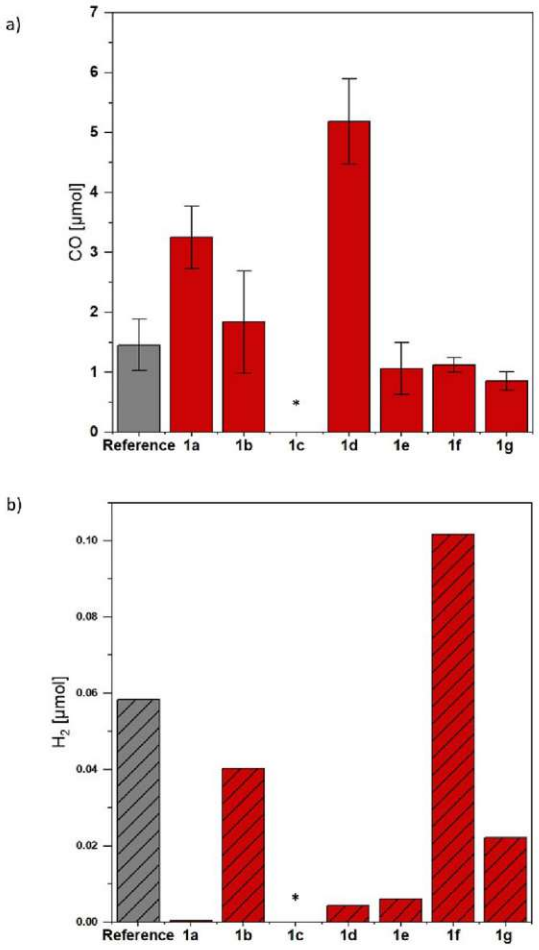

Figure 2. Formation of CO (a), and H_2 (b) in the photocatalytic screening of ionic liquids in the solvent MeCN. Conditions: 0.6 mM $[Ru(bpy)_3](PF_6)_2$, 0.06 mM $[Re(bpy)(CO)_3]Cl$, 0.32 M TEOA, 0.1 g/mL IL; t = 1 h, T = 22 °C.* not detected.

reaction became biphasic when performed in MeCN. In contrast, no positive effect could be observed for the ionic liquids $[C_2mim][NTf_2]$ **1 f** and $[C_2mim][N(CN)_2]$ **1 g**. In fact, CO formation decreased slightly in comparison to the reference values.

The addition of imidazolium-based ionic liquids also affects the selectivity towards CO formation. Except for the $N(Tf)_2^-$based species **1 f**, all ionic liquids made the photocatalytic reduction more selective for CO formation and suppressed the formation of by-products. In the case of the best-performing ionic liquid, **1 d**, the formation of H_2 was reduced by a factor of 13 from $5.8 \cdot 10^{-2}$ µmol to $4.3 \cdot 10^{-3}$ µmol in MeCN. Furthermore, CH_4 was only detected in negligible amounts in all samples.

The observed impact of the best performing ionic liquid **1 d** is not limited to MeCN as a solvent, and experiments were alternatively performed in the apolar solvents DMF and DMSO (ESI Table S1, Figure S2 & S3). In fact, the positive effect is even more pronounced in DMF, with a 20-fold increase in CO yield compared to the reference system without ionic liquid **1 d**. This observation might be attributed to differences in reaction mechanism.[31] The chosen solvents possess different ability to coordinate with the rhenium complex, resulting in a solvochromatic shift of the absorption spectra.[25] In general, MeCN is considered as the strongest coordinating solvent due to its additional ability for ligand exchange with Cl, thus stabilizing the 18-electron radical $[Re(bpy)(CO)_3(solvent)]$ as intermediate.[25,28] On the other hand the weaker coordination ability of DMF without ligand exchange was reported as beneficial aspect for the formation of the Re-TEOA-CO_2 adducts, which might be responsible for the increased reactivity.[20,32] In comparison, DMSO exhibits comparable polarity than MeCN, but showed less tendency for direct coordination with the Re complex, thus the observed enhancements in the reaction rate are less explicit.

Different factors and properties of ionic liquids may cause the observed enhancement in CO formation and influence the photocatalytic reduction of CO_2. The outstanding performance of the carboxylate-based ionic liquid **1 d** is not surprising, given its basic nature and known potential for interaction with CO_2. In general, the counterions' ability for interaction with the C-2 proton of the imidazole core can be described by the Kamlet-Taft parameters α (hydrogen bond donating ability), β (hydrogen bond acceptance) and π* (polarity/polarizability) derived from linear solvent energy relationships.[33–36] Corresponding C-2 protons are highlighted in Figure 1. The findings from photoreduction can, to some extent, be correlated with the parameter β, showing a relationship with photocatalytic yields for CO. Ionic liquids with high nucleophilicity and, therefore, high β values such as **1 d** or **1 f** increased CO formation compared to the reference reaction (Figure 1). The low yields obtained after the introduction of fluorinated alkyl groups, as in the cases of $N(Tf)_2$ anions (**1 f**), also correlates with lower values of the parameter β. It is interesting to note that an amino group in the side chain of the cation cannot compensate for the absence of a basic anion. This is evident from the comparison of the 1-ethyl-3-methylimidazolium-based ionic liquid **1 f** with the diisopropylamine-functionalized ionic liquid $[iPr_2N(CH_2)_2mim][N(Tf)_2]$ **2 f**, which both gave comparable yields for CO formation (ESI Table S2). The trend of anion basicity is also visible for the halide series (**1 a–c**) that follows the order $Cl^- > Br^- > I^-$. This is in accordance with the anions' affinity for interaction with the C-2 protons according to their charge per surface area ratio, as well as with the Kamlet-Taft parameter β.

The unique ability of the acetate-based ionic liquid in CO_2 capture and utilization may also be related to the spontaneous N-heterocyclic carbene formation.[37] Apart from several NHC-catalyzed reactions, *e.g.* benzoin condensations, that are known to occur in carboxylate-based ionic liquids, the interaction of the free carbene with CO_2 has been reported by several authors and is a key player in its activation.[16,38] To study the interaction of CO_2 with $[C_2mim][OAc]$ **1 d** as co-catalytic effect in the photocatalytic reduction, Fourier transform infrared spectroscopy (FT-IR) studies in transition mode were performed (Figure S3). A strong C=O stretching vibration at 1668 cm^{-1} was observed after purging the reaction mixture with CO_2 that corresponds to $[C_2mim\text{-}CO_2]^-$, thus proving the chemisorption

of CO_2 as a dominating interaction accompanied by bending of the CO_2 bond angle. Similarly, the formation of the CO_2-carbene complex is evident in ^{1}H NMR (Figure S5a), as indicated by the doubling of imidazole core proton signals due to the formation of $[C_2mim\text{-}CO_2]^-$ as the second species. The carbene complex formation is also evident from the appearance of an additional peak at 155 ppm that can be assigned to the CO_2^- carbon, along with a doubling of the remaining signals (ESI Figure S4).[39] Interestingly, the addition of TEOA as a sacrificial proton donor leads to the weakening or complete disappearance of the doubling of imidazole core proton signals (Figure S5), implying that TEOA as a protic agent interferes with the chemisorption mechanism. This is in line with literature studies, confirming that coordination of CO_2 with TEOA forming CO_2-TEOA or Re-TEOA-CO_2 intermediates plays a key role in the reaction mechanism of this reaction.[20,32]

A similar effect is found for the addition of 5% water (corresponding to molar ratio approx. 200:1 for ionic liquid to water) to the photoreduction, where a decrease in CO formation and an increase in H_2 formation was observed (Table 2). As evident in ^{13}C NMR, the addition of water leads to disappearance of the ^{13}C NMR signal at 155 ppm (Figure S6). An additional signal at 163 ppm is indicating the formation HCO_3^- and CO_3^- supporting the hypothesis that in protic reaction media the reaction might proceed via HCO_3^- intermediate[40] Still, the CO formation in **1 d** with 5% H_2O reached 3.96 µmol and TON of 44, which is higher compared to the reference value.

For further insight into the reaction mechanism, a set of control experiments was performed with the ionic liquid **1 d** in DMF as best-performing combination (Table 3). Peng et al. and Qadir et al. reported CO formation via the direct photoexcitation of imidazolium-based ionic liquids.[22,23] For this reason, the photocatalytic activity was also studied in the absence of $[Ru(bpy)_3](PF_6)_2$ and $[Re(bpy)(CO)_3]Cl$; however, the formation of CO was not observed under otherwise similar conditions. This observation is in accordance with UV-vis spectroscopy data of ionic liquid and catalyst (ESI Figure S8), indicating that absorption of the ionic liquid is very low in comparison to the catalyst at the chosen conditions. On the other hand, photoreduction using just $[Ru(bpy)_3](PF_6)_2$ resulted in low CO formation in the range of 0.06 µmol with a low selectivity of 90.3%, indicating H_2 formation to be much more prominent. As reported in literature, the presence of $[Re(bpy)(CO)_3]Cl$ as co-catalysts favors the formation of CO. It is interesting to note that a similar effect on selectivity can be observed with **1 d** instead of $[Re(bpy)(CO)_3]Cl$ – in both cases, the selectivity for CO reaches >99%. However, both Ru and Re-based species are required to observe the substantial increase in CO formation caused by the addition of **1 d**.

Photoluminescence (PL) studies were performed with **1 d** to verify the role of ionic liquid addition. In line with the observed improvements in CO_2 photoreduction yields, we observe pronounced PL quenching of the excited $[Ru(bpy)_3]^{2-*}$ state when in the presence of **1 d**, which speaks for a more rapid charge transfer between the components of the photocatalytic system (Figure 3).

Table 2. Photocatalytic CO_2 reduction in the presence and absence of water for three selected ionic liquids (**1 a**, **1 b** and **1 d**).

Conditions[a]	H_2O	CO [µmol]	H_2 [µmol]	TON[b]	Selectivity[c]
Reference	5%	2.31	0.16	26	93.6
	–	1.46	<0.01	16	>99.9
1 a	5%	2.23	0.02	25	99.0
	–	3.25	<0.01	36	>99.9
1 b	5%	0.67	0.20	7	77.5
	–	1.83	<0.01	20	>99.9
1 d	5%	3.96	0.04	44	99.1
	–	5.19	<0.01	57	>99.9

[a] Conditions: 0.6 mM $[Ru(bpy)_3](PF_6)_2$, 0.06 mM $[Re(bpy)(CO)_3]Cl$, 0.32 M TEOA, 0.1 g/mL IL; t = 1 h, T = 22 °C in MeCN. [b] Calculated for CO. [c] Selectivity for CO.

Table 3. Mechanistic study on the impact of $[C_2mim][OAc]$ **1 d**.

Photo-sensitizer[a]	Catalyst	IL	CO [µmol]	Selectivity%[b]
–	–	-	n.d	–
$[Ru(bpy)_3](PF_6)_2$	–	-	0.06	90.3
–	$[Re(bpy)(CO)_3]Cl$	-	0.26	>99.9
$[Ru(bpy)_3](PF_6)_2$	$[Re(bpy)(CO)_3]Cl$	-	0.28	>99.9
–	–	1d	n.d.	–
$[Ru(bpy)_3](PF_6)_2$	–	1d	0.06	>99.9
–	$[Re(bpy)(CO)_3]Cl$	1d	0.04	>99.9
$[Ru(bpy)_3](PF_6)_2$	$[Re(bpy)(CO)_3]Cl$	1d	5.93	>99.9

[a] Conditions: 0.6 mM $[Ru(bpy)_3](PF_6)_2$, 0.06 mM $[Re(bpy)(CO)_3]Cl$, 0.32 M TEOA, 0.1 g/mL IL; t = 1 h, T = 22 °C in DMF. [b] Selectivity for CO.

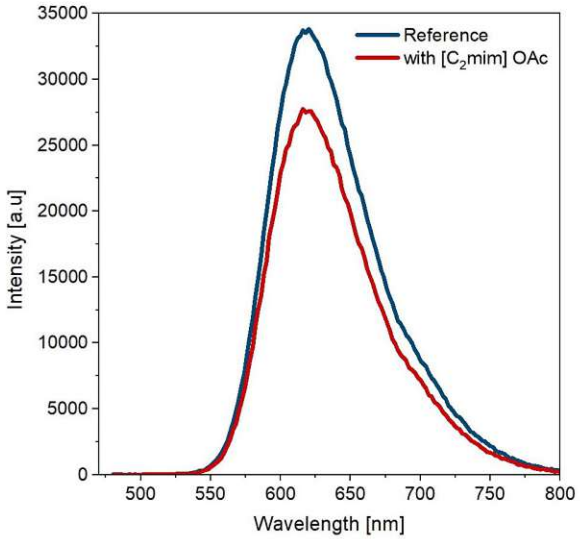

Figure 3. UV-Vis emission spectra of reaction mixture reference (blue) and mix with **1 d** (green). Excitation wavelength 445 nm, solvent DMF. 0.6 mM $[Ru(bpy)_3](PF_6)_2$, 0.06 mM $[Re(bpy)(CO)_3]Cl$, 0.32 M TEOA, 0.1 g/mL IL.

Finally, the performance of the photocatalytic system was further investigated for up to 2 hours of reaction time (Figure 4). The reference system showed a low turnover frequency of around 0.05, which increased only slightly to about seven after 120 minutes. In contrast, the TON of the photosystem with **1 d** increased rapidly up to 46 within only 45 minutes.

The rate dropped significantly afterwards to reach a stable rate of about 40, indicating that the higher reaction rate may impact the long-term stability of the catalytic system. Instant TOF indicates a complete inactivation of the catalytic system. This might be caused by the photolysis of $[Ru(bpy)_3](PF_6)_2$, which has been previously reported in literature for different biphenyl sensitizer systems.[41,42] Eventually, the increases in reaction rate are paid off by reduced stability of the photosensitizer, suggesting that other catalytic systems – such as those based on redox-stable solid-state absorbers[43,44] – are required to fully take advantage of the beneficial effect of ionic liquids in photocatalytic CO_2 reduction.

Conclusions

In this study, we explored the use of various imidazolium-based ionic liquids as additives in photocatalytic reduction of CO_2. We employed $[Re(bpy)(CO)_3]Cl$ as catalyst and $[Ru(bpy)_2](PF_6)_2$ as sensitizer. In comparison to literature that focuses on reactions in pure ionic liquids or their mixtures with low amount co-solvents, we focused on the addition of ionic liquids as low-level additive, thus avoiding viscosity or mass transfer issues. For a comprehensive understanding the model reaction was tested in solvents MeCN, DMF and DMSO with a set of imidazolium based ionic liquids.

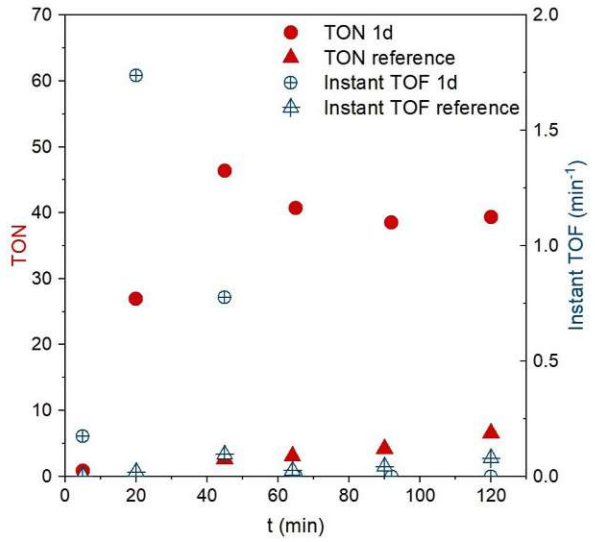

Figure 4. Turnover number (TON) and instant turnover frequency (TOF) for the reference sample and **1 d**. Time elapse of TON (red, left axis) and TOF (blue, right axis) is shown for the reference sample (triangle) and sample containing **1 d** (sphere). Conditions: 0.6 mM $[Ru(bpy)_3](PF_6)_2$, 0.06 mM $[Re(bpy)(CO)_3]Cl$, 0.32 M TEOA, 0.1 g/mL ionic liquid in DMF.

The results demonstrate that incorporating small amounts of 10% (w/v) of ionic liquids to conventional solvents could significantly enhance the production of CO, eliminating the need to use ionic liquids as the primary solvents. A gradual increase of **1 d** ionic liquid content from 0 to 10% (w/v) in MeCN lead to stepwise increase of CO formation and successively improved H_2 suppression, whereas a higher content was not beneficial. Notably, the addition of $[C_2mim][OAc]$ **1 d** in DMF led to nearly a 20-fold increase in CO yield. The impact of different counterions could be correlated with the Kamlet-Taft parameter β for solvent interactions in DMF and MeCN; however, this trend was less explicit in DMSO. Moreover, the inherent basicity of the C-2 proton in acetate-based ionic liquids allows for the chemisorption of CO_2 via formation of the carbene complex that goes along with bending the CO_2 bond angle to 138°, and thus pre-activation of CO_2. The addition of water favours a change of the mechanism towards the presence of the $[HCO_3^-]$ species, which is evident from ^{13}C NMR and a reduced selectivity for CO formation. Mechanistic investigations also revealed that all components of the system were crucial for efficient CO reduction, and photoluminescence measurements further proved that ionic liquids positively influence the quenching behavior of the excited state of the ruthenium sensitizer.

However, the long-term reaction rate of the photosystem appeared to decrease after an initial rapid increase, suggesting accelerated aging of the photosensitizer in the presence of ionic liquids. To fully harness the benefits of ionic liquids in photocatalytic CO_2 reduction, it seems that alternative catalytic systems may be necessary, and our ongoing research is focused on exploring these possibilities.

Experimental section

Materials: Solvents for photocatalytic experiments, including N, N-dimethylformamide (DMF, anhydrous, 99.8%), dimethylsulfoxide (DMSO, anhydrous, 99.9%), and acetonitrile (MeCN, anhydrous, 99.8%) were purchased from Sigma Aldrich Co. and stored over molecular sieve. CO_2 for application in all photocatalytic reactions was purchased from Messer Austria (>99.995%). Catalyst and catalyst precursors have been purchased from commercial suppliers if otherwise stated. The ionic liquids $[C_2mim][Cl]$, $[C_2mim][I]$, $[C_2mim][I]$, $[C_2mim][DCA]$ and $[C_2mim][OAc]$ have been purchased. $[C_2mim][Br]$, $[C_2mim][N(Tf)_2]$ and $[iPr_2N(CH_2)_2mim][N(Tf)_2]$ were synthesised according to standard literature procedure and analytical data was in accordance with literature[45,46] Ionic liquids were dried under high vacuum and stored under argon. The water content was checked to be lower than <3000 ppm by Karl Fischer titration before use. All reactions were conducted in an argon atmosphere unless explicitly stated as carried out under ambient conditions.

Sensitizer synthesis: Tris(2,2′-bipyridine)ruthenium(II) hexafluorophosphate was synthesised by dissolving tris(2,2′-bipyridine) ruthenium(II) chloride hexahydrate (0.30 g), 0.4 mmol in 150 mL water and adding 0.16 g (0.84 mmol) KPF_6. The solution turned immediately from red to bright orange. After sitting overnight, the solid material was filtrated, washed with water, and dried in vacuum to yield 0.28 g (81%) tris(2,2′-bipyridine)ruthenium(II) hexafluorophosphate. ^1H NMR (400 MHz, DMSO) δ 8.84 (d, J = 8.2 Hz, 1H), 8.25–8.10 (m, 1H), 7.73 (d, J = 5.6 Hz, 1H), 7.58–7.47 (m,

1H). 13 C NMR (101 MHz, DMSO) δ 156.54, 151.20, 137.92, 127.88, 124.47.

Methods: FTIR spectra (transmission mode) were recorded on a PerkinElmer spectrum 65 FTIR spectrometer. Diffusive reflectance spectroscopy in solution was measured using a JASCO 670 spectrometer. ^{1}H NMR spectra were recorded with a Bruker Advance UltraShield 600 MHz spectrometer, and chemical shifts were reported in ppm from TMS with a solvent resonance as the internal standard. Photoluminescence measurements (PL) were measured with a PicoQuant FluoTime 300 spectrophotometer using an Xe arc lamp (300 W power) as an excitation source and a double-grating monochromator. The detection system comprised a PMAHybrid 07 detector and a high-resolution double monochromator. The excitation wavelength utilised for steady-state measurements was 445 nm. The data was collected and later fitted using EasyTau2 software. GC analysis was performed with the SHIMADZU Nexis™ GC-2030 gas chromatograph equipped with a dielectric barrier discharge ionisation detector (BID) and 1 m ShinCarbon ST column (Restek Co.)

General procedure for photocatalytic CO_2 reduction: Photo experiments were carried out in a glass reactor with a total capacity of 3.7 mL, comprising 1.5 mL for the solution and 2.2 mL for the headspace (ESI Figure S7). The glass reactor is equipped with a septum, water cooling, and a stirring bar. A Solis high-power 445 nm LED, operated with a DC2200 - High-Power 1-Channel LED Driver at a brightness setting of 5%, served as the light source. The emission spectra of the lamp is depicted in ESI Figure S8, together with the absorption spectra of all relevant components of the system, Prior to the reactions, the reaction mixtures were purged with CO_2 for 3 minutes at a flow rate of 10 ml/min. The reaction temperature was set to 22 °C. Samples of gas aliquots were taken prior to reaction and in consecutive intervals. Drops of TON might be related to consecutive sampling of aliquots from the reactor headspace. The detection limit of the GC with regard to CO, which can be seen as a characteristic of the reliability of the reported data (both TONs and TOFs), is around 10 ppm. This value corresponds to TON of 0.01.

Acknowledgements

This project has received funding from the European Research Council (ERC) under the European Union's Horizon 2020 research and innovation program (Grant Agreement No. 864991). The authors gratefully thank Proionic for providing ionic liquid samples for this project. SB and AC acknowledge the Austrian Science Fund (FWF) (grant number P32801-N). The authors acknowledge TU Wien Bibliothek for financial support through its Open Access Funding Programme.

Conflict of Interests

The authors declare no conflict of interest.

Data Availability Statement

The data that support the findings of this study are available in the supplementary material of this article.

Keywords: photocatalysis · CO_2 reduction · ionic liquids · carbenes · cooperative effects

[1] J. B. Zimmerman, P. T. Anastas, H. C. Erythropel, W. Leitner, *Science* **2020**, *367*, 397–400.
[2] C. Hepburn, E. Adlen, J. Beddington, E. A. Carter, S. Fuss, N. Mac Dowell, J. C. Minx, P. Smith, C. K. Williams, *Nature* **2019**, *575*, 87–97.
[3] M. Cokoja, C. Bruckmeier, B. Rieger, W. A. Herrmann, F. E. Kühn, *Angew. Chem. Int. Ed.* **2011**, *50*, 8510–8537.
[4] R. Sang, Y. Hu, R. Razzaq, G. Mollaert, H. Atia, U. Bentrup, M. Sharif, H. Neumann, H. Junge, R. Jackstell, B. U. W. Maes, M. Beller, *Nat. Commun.* **2022**, *13*, 4432.
[5] S. Dabral, T. Schaub, *Adv. Synth. Catal.* **2019**, *361*, 223–246.
[6] H. Schulz, *Appl. Catal. A* **1999**, *186*, 3–12.
[7] Y. Asai, H. Katsuragi, K. Kita, T. Tsubomura, Y. Yamazaki, *Dalton Trans.* **2020**, *49*, 4277–4292.
[8] H. Dau, E. Fujita, L. Sun, *ChemSusChem* **2017**, *10*, 4228–4235.
[9] J. Schneider, H. Jia, J. T. Muckerman, E. Fujita, *Chem. Soc. Rev.* **2012**, *41*, 2036–2051.
[10] C. Vogt, M. Monai, E. B. Sterk, J. Palle, A. E. M. Melcherts, B. Zijlstra, E. Groeneveld, P. H. Berben, J. M. Boereboom, E. J. M. Hensen, F. Meirer, I. A. W. Filot, B. M. Weckhuysen, *Nat. Commun.* **2019**, *10*, 5330.
[11] S. Wang, X. Wang, *Angew. Chem. Int. Ed.* **2016**, *55*, 2308–2320.
[12] D. C. Grills, E. Fujita, *J. Phys. Chem. Lett.* **2010**, *1*, 2709–2718.
[13] Y. B. Wang, D. S. Sun, H. Zhou, W. Z. Zhang, X. B. Lu, *Green Chem.* **2015**, *17*, 4009–4015.
[14] A. Yokozeki, M. B. Shiflett, C. P. Junk, L. M. Grieco, T. Foo, *J. Phys. Chem. B* **2008**, *112*, 16654–16663.
[15] M. I. Qadir, J. Dupont, *Angew. Chem. Int. Ed.* **2023**, *62*, 202301497–202301498.
[16] G. Gurau, H. Rodríguez, S. P. Kelley, P. Janiczek, R. S. Kalb, R. D. Rogers, *Angew. Chem. Int. Ed.* **2011**, *50*, 12024–12026.
[17] L. Sun, G. K. Ramesha, P. V. Kamat, J. F. Brennecke, *Langmuir* **2014**, *30*, 6302–6308.
[18] B. A. Rosen, A. Salehi-Khojin, M. R. Thorson, W. Zhu, D. T. Whipple, P. J. A. Kenis, R. I. Masel, *Science* **2011**, *334*, 643–644.
[19] Y. Yamazaki, H. Takeda, O. Ishitani, *J. Photochem. Photobiol. C* **2015**, *25*, 106–137.
[20] R. N. Sampaio, D. C. Grills, D. E. Polyansky, D. J. Szalda, E. Fujita, *J. Am. Chem. Soc.* **2020**, *142*, 2413–2428.
[21] Y. Pellegrin, F. Odobel, *Comptes Rendus Chim.* **2017**, *20*, 283–295.
[22] M. I. Qadir, M. Zanatta, E. S. Gil, H. K. Stassen, P. Gonçalves, B. A. D. Neto, P. E. N. de Souza, J. Dupont, *ChemSusChem* **2019**, *12*, 1011–1016.
[23] Y. Peng, K. C. Szeto, C. C. Santini, S. Daniele, *Chem. Eng. J. Adv.* **2022**, *12*, 100379.
[24] J. Lin, Z. Ding, Y. Hou, X. Wang, *Sci. Rep.* **2013**, *3*, 1056.
[25] Y. Kuramochi, O. Ishitani, H. Ishida, *Coord. Chem. Rev.* **2018**, *373*, 333–356.
[26] B. Durham, J. V. Caspar, J. K. Nagle, T. J. Meyer, *J. Am. Chem. Soc.* **1982**, *104*, 4803–4810.
[27] J. Hawecker, J. M. Lehn, R. Ziessel, *J. Chem. Soc. Chem. Commun.* **1983**, 536–538.
[28] L. Rodríguez, M. Ferrer, O. Rossell, F. J. S. Duarte, A. Gil Santos, J. C. Lima, *J. Photochem. Photobiol. A* **2009**, *204*, 174–182.
[29] S. Zhang, X. Qi, X. Ma, L. Lu, Y. Deng, *J. Phys. Chem. B* **2010**, *114*, 3912–3920.
[30] R. Lungwitz, V. Strehmel, S. Spange, *New J. Chem.* **2010**, *34*, 1135.
[31] F. P. A. Johnson, M. W. George, F. Hartl, J. J. Turner, *Organometallics* **1996**, *15*, 3374–3387.
[32] T. Morimoto, T. Nakajima, S. Sawa, R. Nakanishi, D. Imori, O. Ishitani, *J. Am. Chem. Soc.* **2013**, *135*, 16825–16828.
[33] J. M. Lee, S. Ruckes, J. M. Prausnitz, *J. Phys. Chem. B* **2008**, *112*, 1473–1476.
[34] M. A. Ab Rani, A. Brant, L. Crowhurst, A. Dolan, M. Lui, N. H. Hassan, J. P. Hallett, P. A. Hunt, H. Niedermeyer, J. M. Perez-Arlandis, M. Schrems, T. Welton, R. Wilding, *Phys. Chem. Chem. Phys.* **2011**, *13*, 16831–16840.
[35] S. Zhang, X. Qi, X. Ma, L. Lu, Q. Zhang, Y. Deng, *J. Phys. Org. Chem.* **2012**, *25*, 248–257.
[36] W. Linert, R. F. Jameson, A. Taha, *Dalton Trans.* **1993**, 3181–3186.
[37] O. Hollóczki, D. Gerhard, K. Massone, L. Szarvas, B. Németh, T. Veszprémi, L. Nyulászi, *New J. Chem.* **2010**, *34*, 3004.
[38] B. A. Rosen, J. L. Haan, P. Mukherjee, rn Braunschweig, W. Zhu, A. Salehi-Khojin, D. D. Dlott, R. I. Masel, *J. Phys. Chem. C* **2012**, *116*, 59.

[39] K. R. Seddon, A. Stark, M.-J. Torres, *Pure Appl. Chem.* **2000**, *72*, 2275–2287.
[40] F. Mani, M. Peruzzini, P. Stoppioni, *Green Chem.* **2006**, *8*, 995–1000.
[41] J. Van Houten, R. J. Watts, *Chemistry (Easton).* **1978**, *17*, 3381.
[42] A. Soupart, F. Alary, J. L. Heully, P. I. P. Elliott, I. M. Dixon, *Inorg. Chem.* **2020**, *59*, 14679–14695.
[43] S. Batool, S. P. Nandan, S. N. Myakala, A. Rajagopal, J. S. Schubert, P. Ayala, S. Naghdi, H. Saito, J. Bernardi, C. Streb, A. Cherevan, D. Eder, *ACS Catal.* **2022**, *12*, 6641–6650.
[44] S. P. Nandan, N. I. Gumerova, J. S. Schubert, H. Saito, A. Rompel, A. Cherevan, D. Eder, *ACS Mater. Au* **2022**, *2*, 505–515.
[45] S. Weber, J. Brünig, V. Zeindlhofer, C. Schröder, B. Stöger, A. Limbeck, K. Kirchner, K. Bica, *ChemCatChem* **2018**, *10*, 4386–4394.
[46] C. C. R. Allen, C. J. Boudet, C. Hardacre, M. E. Migaud, *RSC Adv.* **2014**, *4*, 19916–19924.

Manuscript received: November 13, 2023
Revised manuscript received: January 15, 2024
Accepted manuscript online: January 25, 2024
Version of record online: February 23, 2024

Section 3.2:

Polymerized ionic liquid co-catalyst driving photocatalytic CO_2 transformation

RCS Sustainability 9, 2524–2531 (2024)

Authors: Lisa Eisele, Bletë Hulaj, Maximilian Podsednik, Francesco Laudani, Pablo Ayala, Alexey Cherevan, Annette Foelske, Andreas Limbeck, Dominik Eder and Katharina Bica-Schröder

To address the limited stability in photocatalytic CO_2 reduction under homogeneous conditions — particularly the catalyst instability that leads to the formation of Re-dimers — a common strategy is to immobilize the catalyst on a heterogeneous support.[54] Polymerized ionic liquids can serve as an effective heterogeneous support, separating and stabilizing reactive centers while preserving the beneficial properties of ionic liquids. Furthermore, this approach enables employment in flow chemistry and may facilitate catalyst recycling. For imidazolium-based polymerized ionic liquids, CO_2 chemisorption and physisorption properties are retained in the polymerized state, allowing for effective CO_2 absorption and activation.[89,90]

This work describes the synthesis and application of a polymerized ionic liquid framework incorporating immobilized Ruthenium sensitizer and Rhenium catalyst moieties to facilitate the selective photocatalytic reduction of CO_2 to CO. Special emphasis was placed on the role of photoexcitation of the Ru-sensitizer within the polymer matrix.

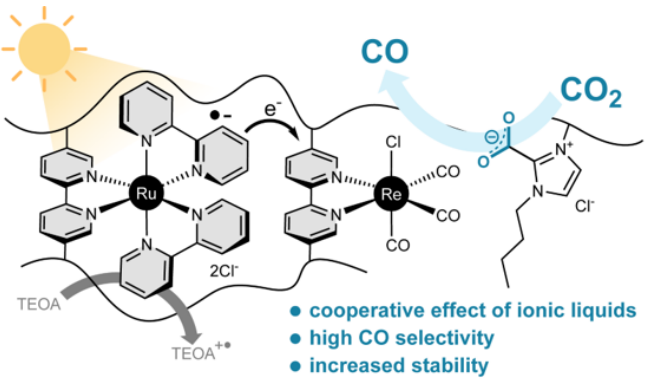

Figure 3.2. Schematic description of photocatalytic CO_2 reduction in polymerized ionic liquid matrix.

The desired polymers were synthesized through radical polymerization of vinyl-functionalized monomers using AIBN as the initiator. UV-Vis spectroscopy, IR, and XPS analyses confirmed the successful incorporation of ruthenium and rhenium moieties into the cross-linked polymer (CLP). Rhenium and Ruthenium contents were quantified using LA-ICP-MS, revealing immobilized rhenium contents between 0.34 and 0.65 wt%, with total rhenium contents reaching up to 6 wt%.

The CLP samples were evaluated for photocatalytic CO_2 reduction activity. The tested CLP showed high selectivity for CO production, achieving turnover numbers (TON) up to 60 and maintaining stable turnover frequencies (TOF) over 4 hours. The inclusion of the photosensitizer substantially increased CO_2 TON compared to samples without Rhenium, with CO TON linearly rising with the amount of sensitizer incorporated. Additionally, the heterogeneous system demonstrated improved long-term stability compared to homogeneous photocatalysis.

As the first author, I planned and conducted the experimental work and drafted the original manuscript. LA-ICP-MS measurements were carried out by Maximilian Podensnik, and XPS measurements were conducted by Francesco Laudani.

RSC Sustainability

ROYAL SOCIETY OF CHEMISTRY

PAPER

View Article Online
View Journal

Cite this: DOI: 10.1039/d4su00194j

Polymerized ionic liquid Co-catalysts driving photocatalytic CO_2 transformation†

Lisa Eisele, [a] Bletë Hulaj,[a] Maximilian Podsednik, [b] Francesco Laudani,[c] Pablo Ayala, [d] Alexey Cherevan, [d] Annette Foelske, [c] Andreas Limbeck, [e] Dominik Eder *[d] and Katharina Bica-Schröder *[a]

Received 23rd April 2024
Accepted 8th July 2024

DOI: 10.1039/d4su00194j

rsc.li/rscsus

Photocatalytic production of CO from CO_2 has the potential for safe and atom-economic production of feedstock chemicals *via in situ* carbonylation chemistry. We developed novel ionic liquid-based polymeric materials through radical copolymerisation of 1-butyl-3-vinylimidazolium chloride and photocatalytically active Re- and Ru-complexes that serve as the CO_2 reduction catalyst and photosensitiser, respectively. The crosslinked polymeric framework allows for the facile immobilisation of molecular organometallic complexes for use as heterogenised catalysts; moreover, the involved imidazolium core units co-catalyze the reduction of CO_2 *via* covalent interaction. The ratio of sensitiser and catalyst was analysed by laser ablation inductively coupled plasma mass spectroscopy (LA-ICP-MS) and set in relation to results from photocatalytic experiments. Ultimately, the heterogenous polymeric framework showed high selectivity for CO formation on photocatalytic CO_2 reduction with improved stability to the corresponding homogenous system.

Sustainability statement

Facing the challenges of climate crisis, there is an urgent demand for technologies that drive the advancement of a circular economy using CO_2 as a sustainable feedstock in chemical industries. Carbon dioxide can be reduced to CO, which serves as a feedstock for multiple processes. Combining photocatalyst with ionic liquids that can chemisorb and activate CO_2 opens new pathways to efficient systems. In this context, we envisioned the development of a heterogenous, polymerized ionic liquid framework bearing photocatalytic groups for efficient and selective photocatalytic CO_2 reduction. The aim of this work goes in line with the following UN Sustainable Development Goals: responsible consumption and production (SDG 12), climate action (SDG 13) and industry, innovation and infrastructure (SDG 9).

Introduction

In light of the escalating levels of atmospheric carbon dioxide and the pressing challenges posed by the climate crisis, there is an urgent demand for technologies that can drive the advancement of a circular economy using CO_2 as a sustainable feedstock.[1,2] A crucial technology in this endeavour involves producing C1 building blocks from CO_2, ultimately facilitating the formation of more intricate compounds.[3] Carbon monoxide (CO) produced by electro[4] or photochemical[5] means emerges as an attractive feedstock for hydroformylation,[6] Fischer–Tropsch synthesis[7] and synthesis of carbonylated platform chemicals.[8]

An essential stage in CO_2 reduction involves the challenging activation and first electron transfer, which requires a significant amount of activation energy and is accompanied by a change in the molecule's bond angle.[9] Moreover, CO_2 uptake is often limited by its solubility in the chosen reaction media.[10] Ionic liquids (ILs) demonstrate an exceptional capability to absorb substantial amounts of CO_2 through both physical (physisorption) and chemical (chemisorption) processes.[11,12] Particularly noteworthy is the role of chemisorption in imidazolium-based ionic liquids as it also plays a crucial role in the activation of CO_2.[13] The formation of a carbene complex between ionic liquids and CO_2 facilitates the bending of CO_2. For imidazolium-based ionic liquids, the interaction occurs at the C2-position of the imidazole core, leading to the formation of an N-heterolytic carbene (NHC)–CO_2 adduct.[14,15] This interaction between ionic liquids and CO_2 can efficiently reduce the overpotential of CO_2 reduction, as confirmed by electrochemical experiments.[16,17] To further reduce CO_2 into valuable building blocks such as CO, both organo-metallic and purely

[a]Institute of Applied and Synthetic Chemistry, TU Wien, Getreidemark 9/163, 1060 Wien, Austria. E-mail: katharina.schroeder@tuwien.ac.at
[b]KAI Kompetenzzentrum Automobil- und Industrieelektronik GmbH, Argentinierstraße 8, 1040 Wien, Austria
[c]Analytical Instrumentation Center, TU Wien, Lehargasse 6/Objekt 10, 1060 Wien, Austria
[d]Institute of Materials Chemistry, TU Wien, Getreidemarkt 9/165, 1060 Wien, Austria
[e]Institute of Chemical Technologies and Analytics, TU Wien, Getreidemarkt 9/164, 1060 Wien, Austria

† Electronic supplementary information (ESI) available: Additional analytical data and graphs. See DOI: https://doi.org/10.1039/d4su00194j

inorganic photocatalytic catalytic systems have been proven to be powerful tools using solar light for the reduction of CO_2.[5,18–21]

The combination of potent molecular systems with ionic liquid-based CO_2 absorption and activation enables the photoreduction of CO_2 with high selectivity under mild conditions, as our group and others have previously demonstrated for homogenous systems.[22–25] Transferring such systems into heterogeneous materials is crucial facing factors like stability of metal–organic catalysts and catalyst handling on bigger scales following the goal of developing gas phase reactions as a big milestone in the development of CO_2 capture and usage technologies.[26,27]

Out of a huge assortment of molecular systems consisting of metal–organic photosensitiser and catalysts systems ruthenium sensitizer and rhenium catalyst first introduced by Lehn have been established as a well-investigated benchmark system for CO_2 reduction selective for CO reduction despite all efforts of replacing noble metal complexes by base metal ones such as iron, nickel and cobalt systems.[5,28,29]

Different approaches to incorporate the catalyst system with ruthenium sensitiser and rhenium catalyst in a heterogeneous matrix have been investigated, such as polymer frameworks and highly coordinated structures like COF and MOF-based systems.[30–32] Direct polymerisation of vinyl-modified monomers is a straightforward method to incorporate ionic liquids into the polymer structure. Furthermore, special separation of transition metal reaction centres in heterogenous systems can be beneficial for long-term stability in comparison to homogenous systems, as dimer formation might be inhibited.[33]

Despite these obvious advantages, studies on immobilisation in a polymerizable ionic liquid matrix are rare. Zhang *et al.* studied materials based on styrene-linker functionalised catalyst with B12-catalyst and ruthenium tris-bipyridine sensitiser co-polymerized-IL for application in dechlorination reaction.[34] The application of crosslinked bipyridine linkers was shown to allow for facile polymerisation. Zhou *et al.* tested a system based on the catalyst $[Re(bpy)(CO)_3]Cl$ with divinyl functionalisation of the bipyridine ligand and 1-ethyl-3-vinyl imidazolium bromide ionic liquid in CO_2 reduction reaction and could prove high selectivity for CO. In this case, however, direct photoexcitation of the catalyst took place, leading to a limited light-harvesting capacity.[35] In contrary to this photosystem, the introduction of a separate sensitiser moiety is beneficial as it can lead to absorption of photons at higher wavelengths, and additionally, prevent the damage of the catalyst during the redox cycling.

We previously showed that imidazolium-based ionic liquids exhibit a strong co-catalytic effect in the photocatalytic reduction of CO_2 with an established photochemical system, consisting of a rhenium photocatalyst and a ruthenium photosensitiser. In this contribution, we integrate the advantageous attributes of imidazolium-based ionic liquids with this well-established photochemical system, consisting of a Re photocatalyst and a Ru photosensitiser, within an innovative crosslinked polymeric framework (CLP) to create an efficient method for selective visible-light CO_2 photoreduction under benign reaction conditions.

Results and discussion

The co-catalytic properties of the crosslinked polymer backbone are highly dependent on the design of the ionic liquid moiety. We selected ionic liquids with an imidazolium core structure since prior studies showed that such ionic liquids are capable of absorbing and activating high quantities of CO_2 *via* N-heterocyclic carbene (NHC) formation. A butyl side chain was introduced as a compromise to the long alkyl chains that offer increased CO_2 uptake and short chain derivates with lower viscosity and reduced steric hindrance.[24,36]

The anion plays a key role in the deprotonation of the acidic proton on the C2-position of the imidazolium ring and the consecutive formation of the NHC–CO_2 adduct. As previously shown, the co-catalytic effect of various imidazolium-based ionic liquids with different counter anions in CO_2 reduction with ruthenium sensitiser and rhenium catalyst correlates with the Kamlet–Taft parameter β of the ionic liquids, thus highlighting the importance of hydrogen bond acceptor properties of the anion.[37] Consequently, imidazolium-based ionic liquids with chloride as anion exhibited the best performance among all halogenides. Due to this superior performance and the presence of Cl as chlorido ligand in the ruthenium catalyst, we selected the ionic liquid 1-butyl-3-vinylimidazolium chloride (IL-1) as monomer for the design of the polymeric framework.[38]

The design of the catalyst relies on a cross-linked polymeric framework as illustrated in Fig. 1, where Ru centres can act as visible-light-absorbing moieties and transfer excited electrons

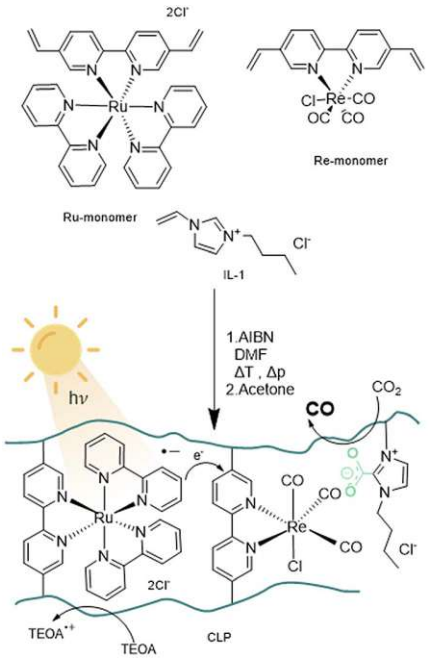

Fig. 1 Schematic representation of monomers used for the radical polymerisation of crosslinked polymers (CLP) with AIBN (azobisisobutyronitrile) towards a polymer framework for photocatalytic CO_2 reduction.

to the Re centres. For this purpose, the bipyridine ligands of the Re-containing photocatalyst monomer and the Ru-containing photosensitizer monomer, were modified with vinyl substituents *via* palladium catalysed Suzuki–Miyaru coupling mechanism.[39] The modified ligand was than introduced to the complex by ligand exchange from *cis*-bis(2,2′-bipyridine) dichloro ruthenium(II) and pentacarbonylchloro rhenium(I).[35]

With the desired monomers in hand, polymerisation was performed *via* free radical polymerisation with azobisisobutyronitrile (AIBN) as a radical starter under pressurized conditions. The ratio of monomers was chosen in variable ratios of catalyst and sensitiser with excess of ionic liquid, resulting in solid, hygroscopic crosslinked polymeric frameworks (CLP) that were isolated after precipitation with acetone (Table 1, Batch CLP-1 to CLP-4).

Material characterisation

Successful incorporation of Re-monomer and IL-1 was initially proven by Fourier transform infrared spectroscopy (FT-IR) *via* comparison of the spectral data recorded from IL-1, polymerized ionic liquid (PIL), Re-monomer and the polymer CLP-1 (Fig. S1†). Signals between 2025 and 1870 cm^{-1} (shaded area) correspond to the stretching vibrations of CO ligands of the Re complex and are visible in the spectra of the Re-monomer and the CLP. The vibration of the imidazole ring of the ionic liquid occurs at 1465 cm^{-1}, while the CH vibrations of the imidazole ring correspond to the signal peaks at 1542 and 1567 cm^{-1}. Therefore, it can be safely concluded that the Re-photocatalyst and ionic liquids are appropriately built into the polymer frameworks.

Thermogravimetric analysis (TGA) was performed on the polymerised ionic liquid (PIL) without Ru and Re, as well as polymer containing Re-monomer (CLP-3) and mixed polymer CLP-4 (Fig. S2†). All samples show an initial small mass loss starting at 100 °C, referring to the loss of absorbed water. From 240 °C, organic matter starts to decompose, leading to significant relative mass loss for all three samples. This loss is accordingly reduced in ruthenium or rhenium due to their higher inorganic content.

Table 1 Theoretical and experimental values for the composition of cross-linked polymers CLP-1 to CLP-4 with variable content of Ru and Re

Entry		Ratio		wt% Re		wt% Ru	
Batch	Theo.[a]	ICP-MS[b]	T-XRF[c]	Theo.	ICP-MS[b]	Theo.	ICP-MS[b]
CLP-1	1 : 10 : 90	19.31	14.23	0.77	0.58	4.17	6.03
CLP-2	1 : 0 : 90	0.00	0.00	1.08	0.34	0.00	0.00
CLP-3	1 : 10 : 90	8.10	7.61	0.77	0.55	4.17	2.42
CLP-4[d]	1 : 10 : 90	10.26	12.36	0.77	0.65	4.17	3.63

[a] Molar ratio of monomers Re-monomer : Ru-monomer : IL-1. [b] Measured by laser ablation inductively coupled plasma mass spectroscopy (LA-ICP-MS). Calculated from average of 6 lines scanned 3 times. Quantification with external standard set into relation to quantification of microwave digested aliquots of CLP-3. RSD ≤ 5%. [c] Calculated from total reflection X-ray fluorescence spectroscopy (T-XRF) measurements. [d] Upscaled preparation by factor 5.

UV-vis measurement on CLP-1 and monomer samples further proves the successful incorporation of photo redox-active monomers Ru-monomer and Re-monomer (Fig. 2). The broad signal between 400 and 500 nm can be attributed to the metal-to-ligand charge transfer (MLCT) transition of Ru-monomer.[40] The maximum of this transition is red-shifted by around 5 nm. The shoulder at around 350–400 nm can be attributed to Re MLCT, that is blue shifted compared to the free complex. Both red shift of Ru and blueshift of Re might be an indicator for spectral interaction between the two species within the polymer framework.

For a deeper understanding of the oxidation states of Ru photosensitizer and Re-catalyst in the samples, X-ray photoelectron spectroscopy (XPS) on CLP-1 and both Re-monomer and Ru-monomer was performed. The survey spectrum of CLP-1 clearly detects O 1s, C 1s, N 1s, Cl 2p and Re 4f along with Ru 3d (Fig. S3†). Comprehensive scans of Re 4f in Re-monomer reveal signals corresponding to Re $4f_{7/2}$ and $4f_{5/2}$ at 44.0 and 41.60 eV respectively, consistent with data reported for Re(I) oxidation state (Fig. 3a).[41] Comparing Re-monomer with CLP-1 the Re 4f signal is not shifted (<0.1 eV) (Fig. 3a). This evidence confirms the integrity of the catalytic site throughout the polymerization process. The clear separation of Ru $3d_{5/2}$ from C 1s is beneficial for the detection of Ru in the polymer framework. The peak maximum for Ru $3d_{5/2}$ can be detected at 281.1 eV for the Ru-monomer and CLP-1, which is in accordance with data from the literature for Ru(II).[42]

Scans of the Cl 2p peak show different positions for the two monomers due to the different bonding state (Fig. S4†). The Cl 2p scans for the Ru monomer show two different chemical states, which have been assigned as anionic and covalently bonded. The anionic component is quantitatively dominant and the peaks' positions perfectly match with the ones measured for the CLP-1 polymer (196.7 eV and 198.3 eV).[43,44] The Cl 2p peaks from the Re catalyst are shifted 1.0 eV higher due to their ligands bonding nature but they don't appear in the polymer scans. This is most likely due to a negligible

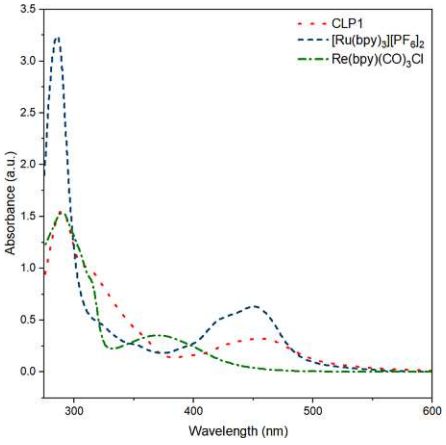

Fig. 2 UV-vis spectra of polymer CLP-1 (red, dot), and complexes $[Ru(bpy)_3][PF_6]_2$ (blue, dash) and $Re(bpy)(CO)_3Cl$ in MeCN (green, dash-dot).

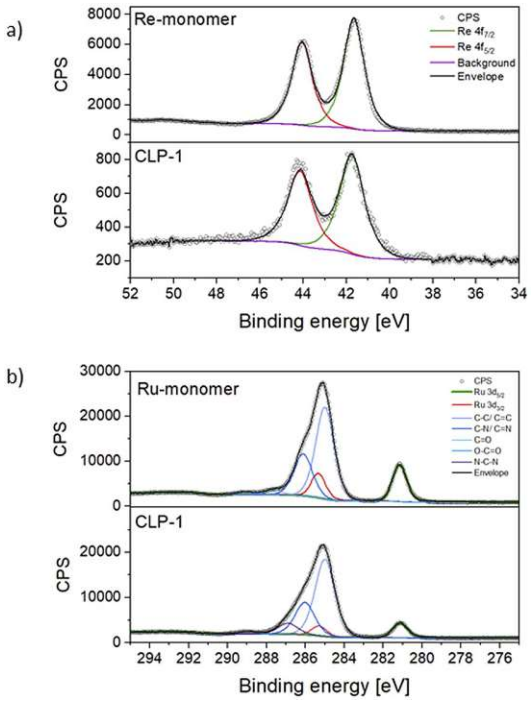

Fig. 3 Detailed XPS scans of CLP-1 and monomers. Re 4f (a) and C 1s together with Ru $3d_{5/2}$ (b).

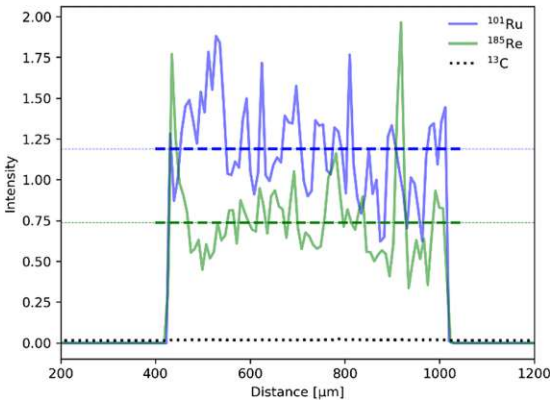

Fig. 4 LA-ICP-MS line scan for ^{101}Ru (red) and ^{185}Re (green) normalized to the ^{13}C isotope (black, dotted). Average intensity for each isotope is depicted as dotted line.

contribution coming from the much lower concentration of Re detected in XPS respect to the Ru one. Comparing the N 1s spectra of CLP-1 with those of both Re-monomer and Ru-monomer facilitates the distinct identification of nitrogen peaks originating from imidazole and bipyridines in the N 1s spectrum of CLP-1 (Fig. S5†). Bipyridine peaks can be identified at 400.1 eV (Re-monomer), 400.2 eV (Ru-monomer) and 400.1 eV (CLP-1) whereas the imidazole peak is shifted to higher binding energies (401.5 eV) in CLP-1.[45–47] The deviation between N 1s bipyridine peaks in CLP-1 and Ru-monomer can be explained by the measurement error in energy of 0.1.

Establishing the absolute Ru and Re contents in the polymer is crucial for the evaluation and benchmarking of catalytic properties of our CLP and was therefore further investigated by laser ablation inductively coupled plasma mass spectroscopy (LA-ICP-MS). The profile of the line scans reveals an even distribution of Ru and Re within the sample particles (Fig. 4). Scans of all elements are shown in the ESI (Fig. S6†). The uniformity of the particle morphology was further confirmed by scanning electron microscopy (SEM) (Fig. S7†), thus overall suggesting that the elements Ru and Re are evenly incorporated during the polymerization process. Exact quantification of Ru and Re in the samples was performed after standardisation with a sample completely dissolved by microwave digestion under acidic conditions. It is worth noticing that the Ru content varied in the range of 2–6 wt% for 3 polymer batches, whereas results for Re were far more consistent and averaged around 0.6 wt%. The ratio of Ru and Re was further confirmed by T-XRF (total reflection X-ray fluorescence spectroscopy) measurements (Table 1). The variability can be attributed to the inherent unpredictability of free radical polymerization, leading to inconsistent insertion of the monomers.

Photocatalytic CO_2 reduction

Photocatalytic testing was performed in a quartz glass reactor using organic solvents bubbled with CO_2 and the sacrificial agent triethanolamine (TEOA). The yield of CO, H_2 and CH_4 was traced by headspace gas chromatography under illumination with $\lambda = 445$ nm. Testing of CLP-1 in 15 h-long experiments revealed photocatalytic activity up to turnover numbers (TON) of 60, producing 0.7 µmol of CO in acetonitrile (MeCN) as solvent (Table 2). Comparing the performance of CLP-1 in dimethylformamide (DMF) showed that the reaction rate is significantly lower than in MeCN. A possible explanation for this observation could be the swelling behaviour of the polymer, affecting the accessibility of reaction centres.

A set of experiments with different illumination settings was further carried out to study the excitation mechanism of the system. Illumination at 445 nm leads to a TON of 60 and yields 0.7 µmol of CO. Repetition of the experiment under broad visible spectrum (see experimental part) using a 500 nm band-pass filter (emission range: 472–527 nm) yielded similar values (0.7 µmol and TON = 61), which further indicates that major excitation takes place *via* Ru centres. This is in line with the proposed excitation and charge transfer mechanisms (Fig. 1), where Ru is excited and quenched with TEOA to be the one-electron-reduced species. Electrons are then transferred from Ru-centres to Re-centres *via* orbital overlap through the partially conjugated backbone or trough collision of two units in close proximity in order to start the CO_2 reduction reaction on the Re-reaction centre. Reaction mechanisms relying on Re-excited states may play a less relevant role, as direct excitation of Re seems to be less efficient under the chosen conditions. Alternatively, Re-excited states might form upon energy transfer from Ru-excited states.

Table 2 Photocatalytic CO_2 reduction with cross-linked polymers

Entry	Batch	Cond.[a]	Ru [wt%]	CO[b] [μmol]	TON[c]	Sel. CO[d] [%]
1	CLP-1	445 nm, MeCN	6.03	0.70	60	97.7
2	CLP-1	445 nm, DMF	6.03	0.08	7	97.6
3	CLP-1	500 nm, MeCN[e]	6.03	0.71	61	97.8
4	CLP-1	445 nm, MeCN[f]	6.03	0.03	3	81.2
5	CLP-2	445 nm, MeCN	0.00	0.17	1	98.3
6	CLP-2	365 nm, MeCN	0.00	0.01	0	n.d.
7	CLP-3	445 nm, MeCN	2.42	0.33	28	>99

[a] Conditions: 0.3 mg mL^{-1} polymer, 0.32 M TEOA, $T = 22$ °C, $t = 15$ h, standard solvent MeCN, 5% brightness. [b] Yields calculated from headspace GC sampling. [c] Turnover number (TON) calculated for. [d] Selectivity calculated for CO. [e] Bandpass filter 500 nm adjusted photon flux. [f] Brightness mode 100% (20-fold photon flux of condition a).

Given the partial conjugation of the polymer backbone, we anticipate the potential for energy transfer through Fluorescence Resonance Energy Transfer (FRET) or Dexter transfer mechanisms for exchanges between Ru-monomer and Re-monomer. FRET involves a dipolar mechanism, where two dipoles are coupling non-radiatively, while Dexter energy transfer relies on electron transfer through orbital overlap *via* a conjugated system (intramolecular) or physical contact of reaction partners (intermolecular). FRET and Dexter mechanism differ in the length scale of the effects to occur. FRET can take place over a distance of 100 Å whereas intramolecular Dexter transfer is limited to a radius of 10 Å. Besides energy transfer the transfer of electrons can occur as well *via* a Dexter like mechanism over longer distances compared to energy transfer.[48] The ratio and quantity of ionic liquid will determine the average distance between the Re-monomer and Ru-monomer units. Based on the selected ratio, it is reasonable to conclude that the average distance between Re-monomer and Ru-monomer units within the framework exceeds the 10 Å radius required for intramolecular Dexter energy transfer to take place. Therefore, it can be assumed that FRET, as a mechanism operational over 10–100 Å, is the dominating mechanism for the transfer of excited electrons, as well as Dexter-like electron transfer *via* orbital overlap. A substantial decrease in the product yield with increased photon flux (20-fold increase) indicates the fragility of the sensitizer towards light-induced ageing and suggests that a balance between photoexcitation and redox charge transfer needs to be maintained to avoid degradation (Table 2). The effect of photosensitizer ageing seems to outperform possible kinetic limitations of CO_2/CO absorption and desorption as the rate-limiting step as the reaction rate of entry 1 couldn't be reached.

Additional experiments in the absence of Ru-monomer with CLP-2, at excitation wavelengths 365 nm and 445 nm led only to traces of CO and H_2, proving the crucial role of Ru monomer as a sensitizer. The impact of ruthenium content on the mechanism was investigated by comparing the performance of CLP-1 and CLP-3 samples, where CLP-3 has half the amount of Ru-monomer as measured by LA-ICP-MS. The increase in Ru-monomer from 2.42 wt% to 6.03 wt% led to the rise of TON per Re centre from 28 to 60, which strongly suggests that another balance between the number of Ru and Re centres needs to be established to achieve optimal charge utilization. A higher content of Ru-monomer within the polymer framework might lead to a shorter average distance between Ru and Re centres and a higher availability of electrons for photoreaction on the Re centres. Both samples exhibit excellent selectivity for CO.

The evolution of CO over time was further studied with the best-performing polymer CLP-1 over 6 hours (Fig. 5). Evaluation of instant TON and TOF reveal that the system is stable over 4 hours. It is interesting to compare this to results from homogenous photocatalysis that we carefully studied in our previous work.[25] There we also observed stable performance followed by a sudden deactivation, however this took place already after 40 min under the conditions otherwise similar (light, intensity, solvent). A possible explanation for the decrease in catalytic activity is the light-induced degradation of photosensitiser.[49] This fragility can be further confirmed by UV-vis spectroscopy of the reaction solution after illumination (Fig. S8†). A strong drop in absorption in the range from 440 to 445 nm accompanied by a red shift of the signal assigned to the MLCT indicates the degradation of Ru sensitizer. Additionally, the degrease in

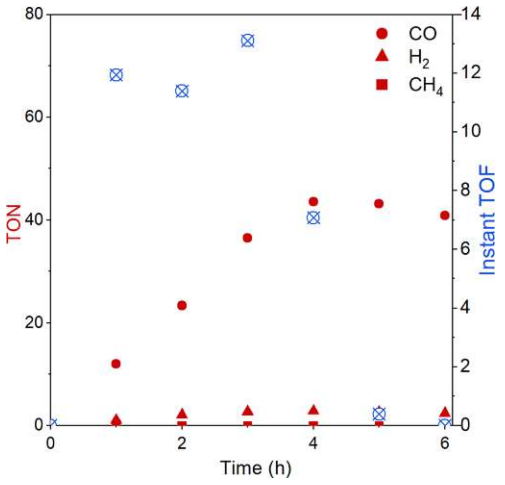

Fig. 5 Turnover number (TON) and instant turnover frequency (instant TOF) of CO_2 reduction reaction over the time course of 6 h with CLP-1.

absorption intensity below 380 nm indicates additional degradation of Re catalyst. Despite CLP-1 is ultimately deactivated, we see a positive effect of the catalyst heterogenization which is able to prolong the stable performance 5 times resulting in instant turnover frequencies up to 13 min^{-1}.

Conclusion

In this study, we present the successful synthesis of heterogeneous polymerized ionic liquid frameworks incorporating immobilized ruthenium sensitizers and rhenium catalyst moieties for the selective photocatalytic reduction of CO_2 to CO *via* radical polymerization with AIBN. The successful integration of ruthenium and rhenium moieties was confirmed through UV-vis spectroscopy, IR, and XPS analyses. Quantification of rhenium and ruthenium content was carried out using LA-ICP-MS, enabling facile determination of metal contents even on single crumbs of the sample. The immobilized rhenium content ranged from 0.34 to 0.65 wt%, with overall rhenium contents reaching up to 6 wt%. The synthesized samples were evaluated for their photocatalytic CO_2 reduction activity, revealing high selectivity towards CO with turnover numbers (TON) reaching up to 60 and stable turnover frequencies (TOF) sustained over 4 hours. Notably, the high selectivity persisted throughout the entire 4 hours duration. The introduction of photosensitizer led to a significant enhancement in CO_2 TON compared to samples lacking rhenium, with CO TON showing a linear increase corresponding to the amount of sensitizer incorporated into the polymer. Our future endeavours aim to develop systems with enhanced long-term stability, focusing on strategies applicable in the gas phase. Ongoing work in our laboratory is directed towards this objective.

Materials and methods

All chemicals purchased from commercial suppliers were used without further purification unless otherwise noted. Dry solvents intended for anhydrous reactions were pre-distilled and desiccated on Al_2O_3 columns (PURESOLV, Innovative Technology). Column chromatography was carried out on standard manual glass columns using silica gel from Merck (40–63 μm) with pre-distilled solvents. TLC analysis was performed on precoated aluminium-backed plates from Merck (silica gel 60 F254). UV active compounds were visualised at 254 nm.

Infrared (IR) spectra were recorded on a PerkinElmer Spectrum 65 FT IR spectrometer equipped with a particular MK II Golden Gate Single Reflection ATR unit. UV-vis spectroscopy was performed on a JASCO V-670 spectrophotometer with a spectral test range of 190 to 900 nm. Thermogravimetric analysis was conducted on a Netzsch STA 449 F1 system. The temperature was increased from 25 °C to 500 °C with a rate of 5 °C min^{-1}.

^1H and ^{13}C, NMR spectra were recorded on a Bruker Advance UltraShield 400 MHz spectrometer, and chemical shifts were reported in ppm using TMS (tetramethylsilane) as the internal standard. Coupling constants (*J*) are given in Hz. For NMR purposes, the multiplicities are reported using the following abbreviations: s = singlet, d = doublet, t = triplet, q = quartet, m = multiplet, dd = doublet of doublets, brs = broad singlet.

Headspace GC analysis was performed with the SHIMADZU Nexis™ GC-2030 gas chromatograph equipped with a dielectric barrier discharge ionisation detector (BID) and 2 m ShinCarbon ST column (Restek Co.)

Total-reflection X-ray fluorescence spectroscopy was performed using an Atomika 8030C X-ray fluorescence Analyser, which operates with a total reflection geometry using an energy-dispersive Si(Li)-detector. The measurements were performed with the tungsten continuous spectrum excitation mode (35 keV) at 50 kV and 47 mA for 100 s live time.

XPS Spectra were collected using a Physical Electronics PHI Versaprobe III with a hemispherical energy analyzer and a monochromatic aluminium Kα X-ray source (1486.6 eV).

In order to avoid contact with moisture and air sample transfer from the glove box into the vacuum of the XPS instrument was performed under argon atmosphere using a transfer vessel provided by PHI. Samples were attached to the sample stage with insulating double sided scotch tape. Charging was prevented through the instrument's charge neutralization system. Data were collected using a 200 μm, 50 W focused X-ray beam at a base pressure of 1×10^{-9} mbar, and a take-off angle of 45°. Survey scans were collected with a pass energy of 140.00 eV and a step size of 0.5 eV. High-resolution scans of peaks of interest were collected with a pass energy of 27.00 eV and a step size of 0.05 eV. Data were analyzed with CASA XPS software. All peaks were referenced to the C 1s aromatic component (285.0 eV). Peak fittings were performed with a Shirley-type background. Gaussian Lorentzian product (GL) and Lorentzian Asymmetric (LA) lineshapes have been used for the peak fittings: GL(50) (C 1s), LA(1.2,0.9,600) (Ru 3d), GL(80) (Re 4f), LA(80) (N 1s), LA(0.95,2,300) (Cl 2p). The pure monomers' fitted components have been used as a reference to constrain the same peaks in the polymer.

LA-ICP-MS measurements were performed using the "imageGEO193", an ArF laser ablation system equipped with a "TwoVol3" ablation chamber from Elemental Scientific Lasers (Bozeman, MT, USA), coupled *via* a PTFE tubing to the "iCAP-Q" from ThermoFisher Scientific (Marietta, OH, USA). An 800 mL min^{-1} helium carrier flow was employed for the analysis, and samples were fixated on a microscope slide using adhesive tape. The samples were ablated using line scans across the polymer crumbs with the following laser parameters: 0.5 J cm^{-2} laser fluence, 20 μm spot size, 50 Hz frequency, and 100 μm s^{-1} scan speed. The ICP-MS was operated in standard mode, recording the following isotopes: ^{13}C, ^{100}Ru, ^{101}Ru, ^{102}Ru, ^{104}Ru, ^{185}Re, and ^{187}Re. For the measured isotopes, a dwell time of 10 ms was used, and all the results were normalized to ^{13}C. Before all experiments, the instrument was tuned to maximum intensity using SRM NIST126. An in-house prepared matrix-matched standard was used to quantify the Ru and Re content.

Synthesis of monomers

1-Butyl-3-vinyl imidazolium chloride (IL-1) was synthesized according to literature.[38]

5,5′-Divinyl-2,2′-bipyridine. 5,5′-Dibromo-2,2′-bipyridine (4, 250.0 mg, 0.796 mmol, 1.0 equiv.), potassium vinyltrifluoroborate (397.8 mg, 2.95 mmol, 3.7 equiv.), palladium(II) acetate (3.6 mg, 0.016 mmol, 0.02 equiv.), triphenylphosphine (11.1 mg, 0.042 mmol, 0.05 equiv.) and caesium carbonate (726.4 mg, 2.23 mmol, 2.8 equiv.) were sealed in a 20 mL microwave vial equipped with a stirring bar and placed under Ar atmosphere. Degassed THF (13 mL) and water (0.53 mL) were added *via* syringe. The reaction mixture was stirred under reflux for 24 h. After cooling to room temperature, water (14 mL) was added, and the mixture was extracted with EtOAc. The combined organic layers were dried over anhydrous sodium sulfate, after which the solvent was removed under reduced pressure. The resulting crude was charged on silica and purified *via* column chromatography (4 : 1 : 0.25 = PE : EtOAc : TEA, R_f = 0.4). The desired product was obtained as a colourless powder (116.6 mg, 70%).

^{1}H NMR (400 MHz, $CDCl_3$): δ 8.67 (s, 2H, H-arom), 8.37 (d, J = 8.3 Hz, 2H, H-arom), 7.86 (dd, J = 8.3, 2.3 Hz, 2H, H-arom), 6.77 (dd, J = 17.1, 11.0 Hz, 2H, –CH=CH_2), 5.90 (d, J = 17.7 Hz, 2H, =CH_2), 5.42 (d, J = 11.0 Hz, 2H, =CH_2). ^{13}C NMR (400 MHz, $CDCl_3$): δ 155.19 (C-arom), 147.95 (C-arom), 133.60 (-CH=CH_2), 133.46 (C-arom), 133.11 (C-arom), 120.92 (C-arom), 116.47 (=CH_2). FT-IR (ATR, ν cm^{-1}): 3000, 1627, 1589, 1465, 1363, 1024, 910 (C=C), 843.

Re-monomer. 5,5′-Divinyl-2,2′-bipyridine (41.0 mg, 0.197 mmol, 1.0 equiv.), pentacarbonylchlororhenium(I) (71.3 mg, 0.197 mmol, 1.0 equiv.) and toluene (20 mL) were mixed under inert conditions in a single-neck flask equipped with a stirring bar. The reaction mixture was stirred under reflux for 16 hours. After cooling to room temperature, the solid was filtered off and washed with dry toluene.

The desired product was obtained as a yellow powder (81.3 mg, 80%) ^{1}H NMR (400 MHz, DMSO): δ 8.98 (s, 2H, H-arom), 8.75 (d, J = 8.6 Hz, 2H, H-arom), 8.55 (dd, J = 8.6, 2.1 Hz, 2H, H-arom), 7.03 (dd, J = 17.8, 11.2 Hz, 2H, –CH=CH_2), 6.29 (d, J = 17.7 Hz, 2H, =CH_2), 5.68 (d, J = 11.2 Hz, 2H, =CH_2). ^{13}C NMR (400 MHz, DMSO) δ 153.97, 151.09, 136.35, 135.74, 131.24, 124.30, 120.91. FT-IR (ATR, ν cm^{-1}): 2017 (CO), 1875 (CO), 1478, 1377, 1251, 915 (C=C), 856.

Ru-monomer. 5,5′-Divinyl-2,2′-bipyridine (35.4 mg, 0.170 mmol, 1.0 equiv.), *cis*-bis(2,2′-bipyridine) dichloro ruthenium(II) hydrate (9, 123.5 mg, 0.255 mmol, 1.5 equiv.) were sealed in a 20 mL microwave vial equipped with a stirring bar and placed under argon atmosphere. Dry ethanol (8.2 mL) and water (0.82 mL) were degassed and added *via* syringe. The reaction mixture was stirred under reflux for 16 h. After cooling to room temperature, the solvent was removed under reduced pressure. The resulting crude was dissolved in acetonitrile (5 mL) and precipitated in diethyl ether (100 mL). The solid was separated and dissolved in double-distilled water (5 mL). Insoluble residues were separated through a sintered glass filter. Acetonitrile (5 mL) was added to the filtrate, and then the solvent was removed under reduced pressure. The solid was dried over phosphorus pentoxide for 48 h to afford the desired product as a dark violet solid (115.1 mg, 98%).

^{1}H NMR (400 MHz, MeOD): δ 8.73 (d, J = 9.3 Hz, 4H, H-arom), 8.65 (d, J = 8.5 Hz, 2H, H-arom), 8.27 (dd, J = 8.6, 2.0 Hz, 2H, H-arom), 8.18–8.12 (m, 4H, H-arom), 7.91–7.80 (m, 4H, H-arom), 7.68 (d, J = 2.0 Hz, 2H, H-arom), 7.56–7.48 (m, 4H, H-arom), 6.59 (dd, J = 17.7, 11.1 Hz, 2H, –CH=CH_2), 5.88 (d, J = 17.6 Hz, 2H, =CH_2), 5.48 (d, J = 11.1 Hz, 2H, =CH_2) ^{13}C NMR (151 MHz, MeOD) δ 158.46, 157.12, 152.74, 150.38, 139.31, 138.51, 135.24, 132.45, 129.00, 125.70, 120.91.

General procedure for polymerisation

The required amounts of monomers, AIBN and DMF were sealed in an 8 mL screw-cap vial equipped with a stirring bar in the glovebox. The reaction was carried out in the autoclave purged with N_2 for 24 h, at 100 °C, at elevated pressures. After cooling to room temperature, the product was precipitated in anhydrous acetone and dried *in vacuo* yielding red solids.

Photocatalytic experiments

Photocatalysis was performed using a glass reactor built in house with a total volume of 3.7 mL, equipped with a septum, water-cooling system, and a stirring bar. A Solis High Power LED emitting light at 445 nm, powered by a DC2200 – High-Power 1-Channel LED Driver and set to a brightness of 5%, was employed as the light source. For experiments with 500 nm bandpass filter a Thor labs Solis 3c lamp was used in combination with a FBH500-40 hard-coated bandpass filter.

For photocatalytic experiments, polymer and TEOA were weighed into a Schlenk tube. The degassed and water-free solvent was added, and the sample was sonicated for three hours to dissolve the polymer completely. The solution was degassed *via* freeze–pump–thaw technique and transferred to the reactor. Before the reaction, reaction mixtures underwent CO_2 purging at a rate of 10 mL min^{-1} for 3 minutes. Reaction products were traced by Headspace GC analysis. All samples were checked for sufficient CO_2 saturation by GC detection of CO_2 at t = 0 h and t = 15 h. Detailed descriptions of calculations of reaction yield, TON and Instant TOF are provided in S9.†

Data availability

The data supporting this article have been included as part of the ESI.†

Conflicts of interest

There are no conflicts to declare.

Acknowledgements

This project has received funding from the European Research Council (ERC) under the European Union's Horizon 2020 research and innovation program (Grant Agreement No. 864991). The Austrian Research Promotion Agency (FFG) is gratefully acknowledged for funding of the XPS infrastructure (FFG project number: 884672). This research was funded in part by the Austrian Science Fund (FWF) [10.55776/DOC142] (TU-DX: Towards Applications of 2D Materials).

Notes and references

1 C. Hepburn, E. Adlen, J. Beddington, E. A. Carter, S. Fuss, N. Mac Dowell, J. C. Minx, P. Smith and C. K. Williams, *Nature*, 2019, **575**, 87–97.
2 S. Dabral and T. Schaub, *Adv. Synth. Catal.*, 2019, **361**, 223–246.
3 A. Sternberg, C. M. Jens and A. Bardow, *Green Chem.*, 2017, **19**, 2244–2259.
4 R. I. Masel, Z. Liu, H. Yang, J. J. Kaczur, D. Carrillo, S. Ren, D. Salvatore and C. P. Berlinguette, *Nat. Nanotechnol.*, 2021, **16**, 118–128.
5 Y. Yamazaki, H. Takeda and O. Ishitani, *J. Photochem. Photobiol., C*, 2015, **25**, 106–137.
6 R. Franke, D. Selent and A. Börner, *Chem. Rev.*, 2012, **112**, 5675–5732.
7 H. Schulz, *Appl. Catal., A*, 1999, **186**, 3–12.
8 A. Brennführer, H. Neumann and M. Beller, *Angew. Chem., Int. Ed.*, 2009, **48**, 4114–4133.
9 A. Álvarez, M. Borges, J. J. Corral-Pérez, J. G. Olcina, L. Hu, D. Cornu, R. Huang, D. Stoian and A. Urakawa, *ChemPhysChem*, 2017, **18**, 3135–3141.
10 Y. Tomita, S. Teruya, O. Koga and Y. Hori, *J. Electrochem. Soc.*, 2000, **147**, 4164–4167.
11 A. Yokozeki, M. B. Shiflett, C. P. Junk, L. M. Grieco and T. Foo, *J. Phys. Chem. B*, 2008, **112**, 16654–16663.
12 G. Cui, J. Wang and S. Zhang, *Chem. Soc. Rev.*, 2016, **45**, 4307–4339.
13 Z.-Z. Yang, Y.-N. Zhao and L.-N. He, *RSC Adv.*, 2011, **1**, 545.
14 G. Gurau, H. Rodríguez, S. P. Kelley, P. Janiczek, R. S. Kalb and R. D. Rogers, *Angew. Chem., Int. Ed.*, 2011, **50**, 12024–12026.
15 Y. B. Wang, D. S. Sun, H. Zhou, W. Z. Zhang and X. B. Lu, *Green Chem.*, 2015, **17**, 4009–4015.
16 B. A. Rosen, A. Salehi-Khojin, M. R. Thorson, W. Zhu, D. T. Whipple, P. J. A. Kenis and R. I. Masel, *Science*, 2011, **334**, 643–644.
17 M. Alvarez-Guerra, J. Albo, E. Alvarez-Guerra and A. Irabien, *Energy Environ. Sci.*, 2015, **8**, 2574–2599.
18 S. N. Habisreutinger, L. Schmidt-Mende, J. K. Stolarczyk, L. Schmidt-Mende, J. K. Stolarczyk and S. N. Habisreutinger, *Angew. Chem., Int. Ed.*, 2013, **52**, 7372–7408.
19 Y. Wang, C. Zhang and R. Li, *Trans. Tianjin Univ.*, 2022, **28**, 227–235.
20 X. Xiong, C. Mao, Z. Yang, Q. Zhang, G. I. N. Waterhouse, L. Gu, T. Zhang, X. Xiong, Z. Yang, T. Zhang, C. Mao, Q. Zhang, L. Gu and G. I. N. Waterhouse, *Adv. Energy Mater.*, 2020, **10**, 2002928.
21 X. Xiong, Y. Zhao, R. Shi, W. Yin, Y. Zhao, G. I. N. Waterhouse and T. Zhang, *Sci. Bull.*, 2020, **65**, 987–994.
22 Y. Peng, K. C. Szeto, C. C. Santini and S. Daniele, *ChemPhotoChem*, 2021, **5**, 721–726.
23 L. Sun, G. K. Ramesha, P. V. Kamat and J. F. Brennecke, *Langmuir*, 2014, **30**, 6302–6308.
24 J. Lin, Z. Ding, Y. Hou and X. Wang, *Sci. Rep.*, 2013, **3**, 1056.
25 L. Eisele, W. Chaikhan, S. Batool, A. Cherevan, D. Eder and K. Bica-Schröder, *ChemCatChem*, 2024, **16**, e202301454.
26 M. Schreck and M. Niederberger, *Chem. Mater.*, 2019, **31**, 597–618.
27 S. Fang, M. Rahaman, J. Bharti, E. Reisner, M. Robert, G. A. Ozin and Y. H. Hu, *Nat. Rev. Methods Primers*, 2023, **3**, 61.
28 Y. Kuramochi, O. Ishitani and H. Ishida, *Coord. Chem. Rev.*, 2018, **373**, 333–356.
29 J. Hawecker, J.-M. Lehn and R. Ziessel, *Chem. Commun.*, 1984, 328–330.
30 L.-S. Hornberger and F. Adams, *Polymer*, 2022, **14**, 2778.
31 H. Shimakoshi, M. Nishi, A. Tanaka, K. Chikama and Y. Hisaeda, *Chem. Commun.*, 2011, **47**, 6548–6550.
32 A. S. Maier, C. Thomas, M. Kränzlein, T. M. Pehl and B. Rieger, *Macromolecules*, 2022, **29**, 29.
33 E. E. Benson and C. P. Kubiak, *Chem. Commun.*, 2012, **48**, 7374–7376.
34 W. Zhang, H. Shimakoshi, N. Houfuku, X.-M. Song and Y. Hisaeda, *Dalton Trans.*, 2014, **43**, 13972–13978.
35 Z.-H. Zhou, K.-H. Chen, S. Gao, Z.-W. Yang and L.-N. He, *Research*, 2020, **2020**, 1–11.
36 M. Ramdin, T. W. de Loos and T. J. H. Vlugt, *Ind. Eng. Chem. Res.*, 2012, **51**, 8149–8177.
37 R. Lungwitz, V. Strehmel and S. Spange, *New J. Chem.*, 2010, **34**, 1135.
38 K. Qiao, F. Ono, Q. Bao, D. Tomida and C. Yokoyama, *J. Mol. Catal. A: Chem.*, 2009, **303**, 30–34.
39 H. J. Nie, J. Yao and Y. W. Zhong, *J. Org. Chem.*, 2011, **76**, 4771–4775.
40 D. W. Thompson, A. Ito and T. J. Meyer, *Pure Appl. Chem.*, 2013, **85**, 1257–1305.
41 S. Oh, J. R. Gallagher, J. T. Miller and Y. Surendranath, *J. Am. Chem. Soc.*, 2016, **138**, 1820–1823.
42 R. M. Leasure, W. Ou, J. A. Moss, R. W. Linton and T. J. Meyer, *Chem. Mater.*, 1996, **8**, 264–273.
43 D. G. Tisley and R. A. Walton, *J. Mol. Struct.*, 1973, **17**, 401–409.
44 L. Yang, A. M. Ren, J. K. Feng, X. J. Liu, Y. G. Ma, M. Zhang, X. D. Liu, J. C. Shen and H. X. Zhang, *J. Phys. Chem. A*, 2004, **108**, 6797–6808.
45 D. Weingarth, A. Foelske-Schmitz, A. Wokaun and R. Kötz, *Electrochem. Commun.*, 2011, **13**, 619–622.
46 J. S. Stevens, L. K. Newton, C. Jaye, C. A. Muryn, D. A. Fischer and S. L. M. Schroeder, *Cryst. Growth Des.*, 2015, **15**, 1776–1783.
47 J. D. Bartl, C. Thomas, A. Henning, M. F. Ober, G. Savasci, B. Yazdanshenas, P. S. Deimel, E. Magnano, F. Bondino, P. Zeller, L. Gregoratti, M. Amati, C. Paulus, F. Allegretti, A. Cattani-Scholz, J. V. Barth, C. Ochsenfeld, B. Nickel, I. D. Sharp, M. Stutzmann and B. Rieger, *J. Am. Chem. Soc.*, 2021, **143**, 19505–19516.
48 D. M. Arias-Rotondo and J. K. McCusker, *Chem. Soc. Rev.*, 2016, **45**, 5803–5820.
49 A. Soupart, F. Alary, J. L. Heully, P. I. P. Elliott and I. M. Dixon, *Inorg. Chem.*, 2020, **59**, 14679–14695.

Section 3.3:

Imidazolium modified UiO-67 metal-organic frameworks for CO_2 absorption

Manuscript in Preparation

Authors: Lisa Eisele, Jakob Blaschke, Shaghayegh Naghdi, Dominik Eder and Katharina Bica-Schröder

Heterogeneous catalytic porous systems, such as MOFs, are highly appealing materials for photocatalytic CO_2 reduction due to their high porosity and large surface areas that facilitate gas permeability and access to reactive sides. Consisting of inorganic building units like metal ions or metal clusters combined with organic linkers, these structures offer large structural variety. For example, pore volume can be controlled by the length of the linker and the connectivity of metal nodes. This wide structural variety has led to applications across numerous fields, such as gas separation, catalysis,[91] wastewater treatment,[92] sensing,[93] and drug delivery.[94] Building on the structural variety, existing frameworks can be modified by functionalization of linkers, metal nodes, or pores, using the framework as a scaffold.[95] Structural modifications can be introduced by different strategies. Common approaches are synthesis from modified building blocks or post-modification strategies like ligand exchange processes. For applications in catalysis, MOFs can be modified with catalysts known from homogeneous photocatalysis. Benefits of the immobilization can be for example the stabilization of molecular integrity of the catalysts and cooperative effects such as size exclusion within the pores.[96–98] Furthermore, the framework can be used for photoexcitation and for the transfer of photo-generated charges.[99] In the context of pore modification, MOFs with ionic liquid-loaded pores are already established materials for applications in gas storage and separation.[100,101] Ionic liquids can be introduced to the pores by impregnation as post-synthetic modification like capillary action-, ship-in-a-bottle- or wet-impregnation-method, or through ionothermal synthesis applying ionic liquids as solvents in the synthesis process.[102,103]

UiO-67, named after the University of Oslo and first described in 2008, is a Zr-based metal-organic framework consisting of Zirconium-oxo clusters linked by diphenyl dicarboxylic acid (see Figure 3.3). The inorganic building blocks consist of $Zr_6O_4(OH)_4$-clusters that can be described as Zr-octahedrons where the triangular faces of the Zr_6-octahedron are alternatively capped by $\mu 3$-O and $\mu 3$-OH groups. The polyhedron edges formed by this cluster are capped with carboxyl groups originating from the carboxylic acid functionalities of the linker, forming $Zr_6O_4(OH)_4(CO_2)_{12}$ units.

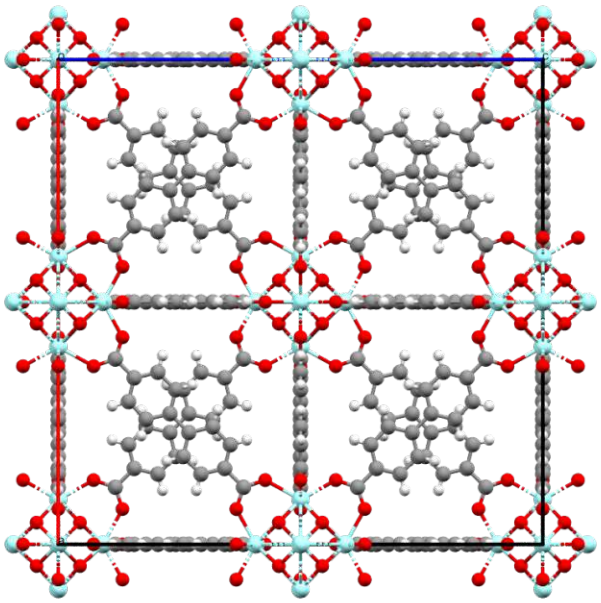

Figure 3.3. Crystal structure of UiO-67. Atoms are depicted in the following colors: Zr (blue), O (red), C (black), H (white).

Overall, each cluster is therefore connected to 12 linkers forming micropores. The framework bears micropores in centric octahedral and corner tetrahedral geometry, where each centric octahedral cage is surrounded by eight corner tetrahedral cages. UiO-67 is known for its high stability originating from the high connectivity in the Zirconium clusters with strong Zr-O bonds and the ability of the Zr_6-cluster to rearrange reversibly upon removal or addition of μ3-OH groups, without changes in connectivity to carboxylate units.[104]

MOFs are typically synthesized from metal salts and organic linkers under solvothermal conditions using microwave- or autoclave synthesis. The synthesis often requires the use of modulators like acids to control the formation of the framework by controlling the number of coordination sites of metal clusters.[105–108] In the case of UiO-67, standard synthesis is based on $ZrCl_4$, diphenyl dicarboxylic acid in the solvent DMF using acetic acid as the modulator. The incorporation of functional and catalytic units into the linker structure of UiO-67 is well-established. Specifically, the introduction of the $Re(bpy)(CO)_3Cl$ moiety has demonstrated efficient photocatalytic CO_2 reduction.[35,109,110] This modification can be achieved either through a post-synthetic modification route or by using pre-modified ligands, as illustrated in Figure 3.4. Examples for both modification of the linker and the metal node are known in the literature for different applications.[111,112]

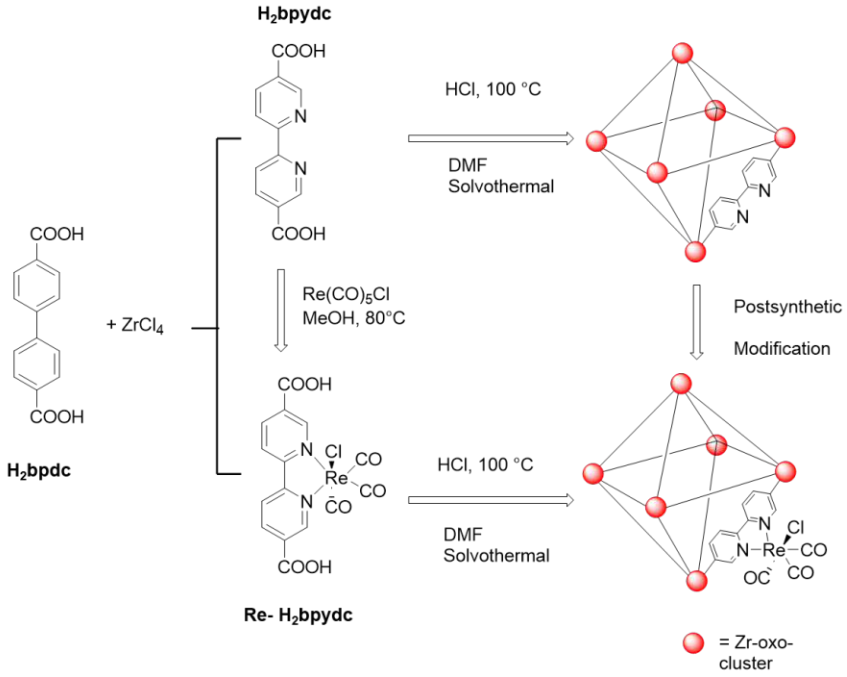

Figure 3.4. Stategies for synthesis of mixed-ligand UiO-67 with Re-modification.

Building on this state-of-the-art approach, the integration of Re-modified UiO-67 with imidazolium-based ionic liquids presents a promising strategy to harness the synergies of ionic liquid-mediated CO_2 activation. Our future objective is to design MOF structures capable of incorporating both imidazolium moieties and Re-active sites, thereby creating reaction centers with a fixed geometry that positions both functionalities in close proximity. Through this approach, we seek to extend the cooperative effects of imidazolium-based ionic liquids to heterogeneous photocatalysis in porous materials.

As an initial step, we focused on synthesizing imidazolium-modified UiO-67 and explored chemisorption and interaction with CO_2. (see Figure 3.5).

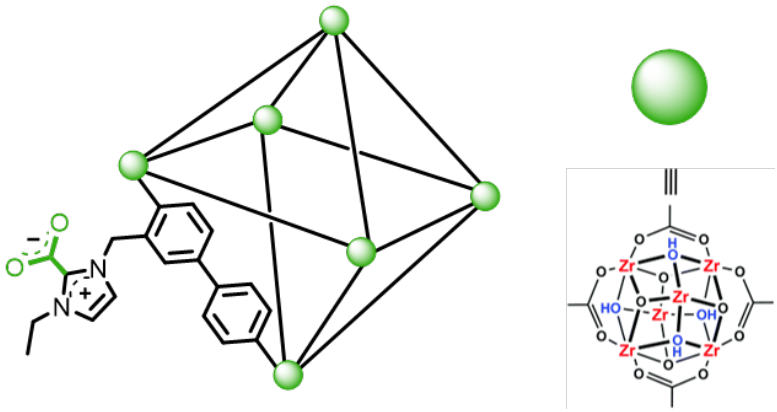

Figure 3.5. UiO-67 MOF modified with imidazolium functionality for chemisorption and preactivation of CO_2. Depiction of Zirkonia cluster adapted from Lawrence et al. [113].

This section contains unpublished work with results describing the synthesis and characterization of MOFs with imidazolium modification for the efficient chemisorption of CO_2 investigating the effect on chemisorption in the MOF framework. As the first author, I planned and conducted the experimental work and drafted the original manuscript.

Imidazolium modified UiO-67 metal-organic frameworks for CO_2 absorption

Lisa Eisele,[†] Jakob Blaschke,[‡] Shaghayegh Naghdi,[‡] Dominik Eder,[*,‡] and Katharina Bica-Schröder[*,†]

[†]*Institute of Applied Synthetic Chemistry, TU Wien, Getreidemarkt 9, 163 1060 Wien*

[‡]*Institute of Materials Chemistry, TU Wien, Getreidemarkt 9, 165 1060 Wien*

E-mail: dominik.eder@tuwien.ac.at; katharina.schroeder@tuwien.ac.at

Abstract

This study investigates the CO_2 sorption properties of the Zirconium-based MOF UiO-67 and its imidazolium-functionalized derivative, Im-UiO-67. Imidazolium motifs, known for their ability to pre-activate CO_2 through chemisorption, were introduced via side-chain functionalization of biphenyl dicarboxylate (bpd) linkers, thus enhancing interactions with CO_2. The crystalline materials were synthesized using microwave-assisted methods and characterized by X-ray diffraction, infrared spectroscopy, and diffusive reflectance infrared Fourier transform spectroscopy (DRIFTS). Chemisorption measurements revealed enhanced CO_2 uptake in Im-UiO-67 compared to UiO-67. Furthermore, DRIFTS studies indicated that CO_2 chemisorption involves interactions with the hydroxyl groups of Zirconia clusters. This strategy demonstrates significant potential for catalytic CO_2 pre-activation, paving the way for advanced applications in carbon capture and utilization.

Introduction

Facing rising atmospheric CO_2 concentrations and pressing consequences for the climate, innovative technologies for CO_2 capture and utilization is necessary.[1,2] Imidazolium-based ionic liquids are salts molten at low temperature with the ability for chemi- and physisorption of CO_2. Chemisorption is based on the weak acidity of the proton in C-2 position of the imidazolium core that can be abstracted under basic conditions.[3–5] The *N*-heterocyclic carbene (NHC) can interact with CO_2 and bind CO_2 in angled geometry. The observed bond angle resembles the geometry of the intermediate CO_2^{*-} radical obtained after one-electron transfer; thus, the formation of the NHC complex allows pre-activation of CO_2 for reductive transformations. In fact, imidazolium-based ionic liquids show a cooperative effect photo- and electrochemical CO_2 reduction overcoming the reaction barrier for the introduction of the first electron.[6–8] Previous studies showed a clear correlation between the basicity of the anion of the ionic liquid and the ability to form the *N*-heterocyclic carbene complex.[3,9,10]

Metal-organic frameworks (MOFs) are well-known for their high porosity and large surface area, attributes that arise from their unique three-dimensional structures composed of metal ions or nodes connected by organic linkers. These properties, combined with high structural variety and facile synthesis, make MOFs highly versatile, enabling their application in diverse fields such as catalysis, gas separation, sensing, and more. MOFs have also been firmly established in the field of carbon capture and sequestration (CCS), demonstrating CO_2 adsorption capacities that are comparable to or even exceed those of commonly used adsorbents such as zeolite 13X and activated carbon.[11,12] CO_2 interactions can be based on interactions between the quadrupole moment of CO_2 and open metal sites as well as interactions with organic linkers. Examples of CO_2 absorption based on linkers are interactions with basic NH_2 groups and interactions with imidazolate units in the MOF ZIF-8.[13–15]

The Zirconium-based MOF UiO-67 is constructed from Zirconium-oxo clusters linked by biphenyl dicarboxylic acid (see Figure 1). The inorganic building blocks consist of $Zr_6O_4(OH)_4$-clusters, which can be described as Zirconium octahedra, where the triangular faces of the

Zr_6-octahedron are alternately capped by μ3-O and μ3–OH groups. The edges of the polyhedron formed by this cluster are capped with carboxyl groups derived from the carboxylic acid moieties of the linker, forming $Zr_6O_4(OH)_4(CO_2)_{12}$ units. Consequently, each cluster is connected to 12 linkers, creating a microporous framework (see Figure 1). Infrared spectroscopy revealed that the chemisorption in UiO-67 and UiO-66 is based on interactions by bonding with μ3–OH groups on the MOF nodes and through dispersive interactions.[16,17]

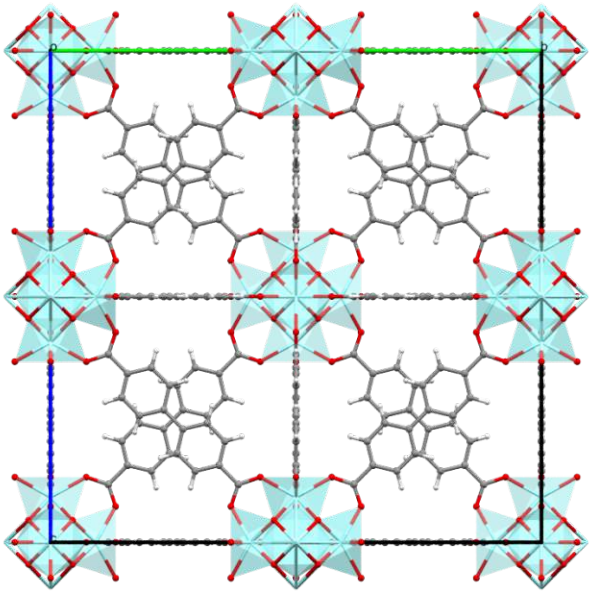

Figure 1: Structure of UiO-67.

Combining the advantages of porous MOF materials with imidazolium structural motifs for CO_2 activation offers a synergistic enhancement of CO_2 activation properties while improving the accessibility of active sites within the heterogeneous support. The concept of transferring CO_2 chemisorption via imidazolium motifs, originally used in homogeneous catalysis with ionic liquids, to porous materials is appealing, as it allows applications in the gas phase. Additionally, the well-organized geometry of the framework facilitates the design of reactive centers that integrate catalytic sites and imidazolium moieties for CO_2 activation, positioned in close proximity with precise steric control. This approach holds the potential

for numerous catalytic applications in the field of carbon utilization.

Examples of imidazolium-modified MOFs, particularly imidazolium-modified UiO-67, have demonstrated utility in CO_2 cycloaddition and metal-organic-framework glasses.[18,19] However, to the best of our knowledge, the chemisorption properties specifically related to imidazolium motifs in MOFs have not been thoroughly investigated.

In this study, we present the modification of UiO-67 with an imidazolium-functionalized linker for CO_2 activation in a heterogeneous porous material, investigating chemisorption sights in the framework.

Results and discussion

The synthesis of the imidazolium-modified linker, Im-bpd, is based on a Suzuki cross-coupling reaction and consecutive alkylation (see the supporting information for details). The bpd core was synthesized through a coupling reaction between 4-bromo-2-methylbenzoic acid methyl ester and 4-methoxycarbonyl phenylboronic acid yielding the corresponding ester, followed by the introduction of a bromide group via bromination with *N*-bromosuccinimide (NBS), yielding bpd-e-Br (ESI Figure 1). Both reactions were adapted from established literature protocols.[19,20]

The subsequent synthesis of the imidazolium-modified linker, starting from bpd-e-Br, is illustrated in Figure 2. The imidazolium motif was introduced through an alkylation reaction with ethyl imidazole (Im-bpd-e).[21] This was followed by cleavage of the ester group via acidic treatment with HBr, resulting in the imidazolium-modified linker, Im-bpd, with a Br^- counterion, isolated as a white precipitate.

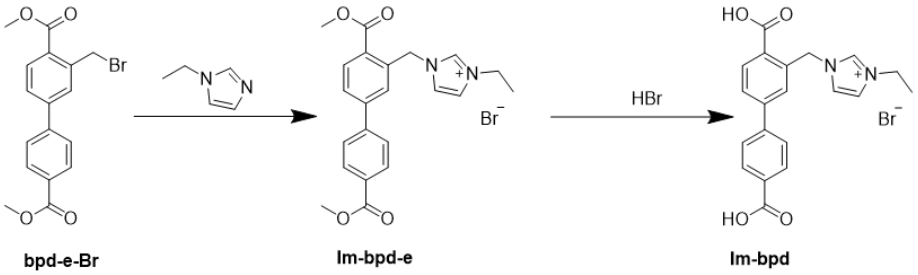

Figure 2: Synthesis of imidazolium modified ligand.

The modified linker Im-bpd was used to synthesize the imidazolium-modified MOF (Im-MOF) (see Figure 3). The synthesis was performed under solvothermal conditions using a microwave reactor. The imidazolium-functionalized linker (Im-bpd) was combined at a 10% ratio with unmodified bpd. $ZrCl_4$ was used as the Zirconium precursor, and the reaction was carried out in dimethylformamide (DMF) with acetic acid as a modulator. The obtained material washed with methanol and activated at 120°C under vacuum.

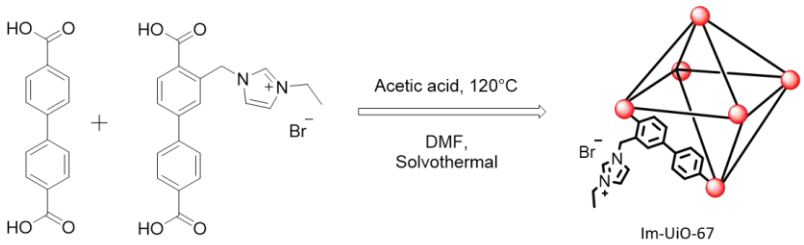

Figure 3: Solvothermal synthesis of Im-UiO-67 from mixed ligands.

The synthesized material was analyzed by powder X-ray diffraction (PXRD) as shown in Figure 4. The diffraction pattern of both UiO-67 and Im-UiO-67 show great accordance with reference data from the simulated pattern, confirming the successful synthesis of crystalline material with a 10% modified linker. The successful incorporation of linker was further confirmed by infrared spectroscopy (IR) shown in ESI Figure 3. The introduction of the imidazolium moiety is evident by vibrations at 2162 cm^{-1} and 1098 cm^{-1} assigned to $\nu_{C=N}$ and ν_{C-C-N}.

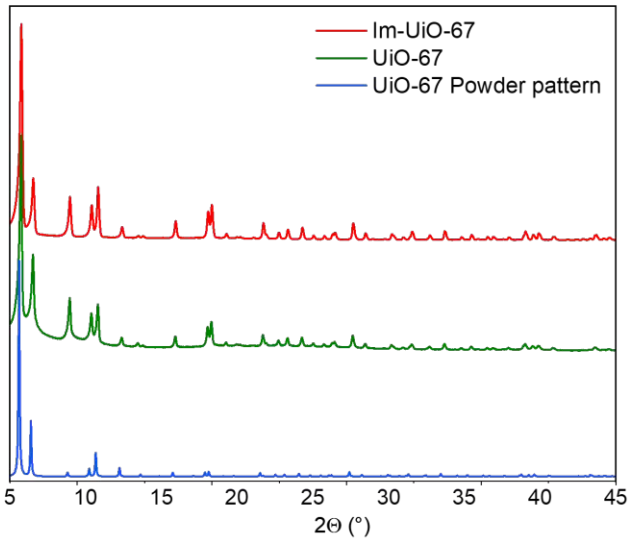

Figure 4: XRD pattern of UiO-67 and Im-UiO-67 in comparison to the simulated pattern.

The obtained material was further analyzed for chemisorption properties and thermal stability. Thermogravimetric analysis was carried out under air and CO_2 atmosphere (see Figure 5). The initial weight loss can be attributed to adsorbed solvents. The sample Im-UiO-67 exhibits mass loss under CO_2 starting from lower temperatures compared to TGA heating under air atmosphere. However, both samples exhibit thermal stability up to 400 °C in both atmospheres.

The chemisorption properties were further investigated through CO_2 temperature-programmed desorption (TPD) measurements using the Belcat II system. Detailed measurement parameters are provided in the supporting information. The sample was first pre-heated under a flow of Helium to remove adsorbed solvent. Subsequently, the samples were exposed to CO_2, followed by a second Helium purge to ensure that only adsorbed CO_2 remained in the measurement matrix. The sample was then heated at a fixed rate of 10 °C min^{-1} to release the attached CO_2.

To account for the weight of the sample, the measured signal was divided by the mass of the investigated sample (see Figure 6). Both samples exhibited CO_2 release starting at 170 °C, as indicated by an increase in the TCD signal. The observed onset temperatures for

CO_2 loss were below the decomposition temperatures measured by TGA, which started at 400 °C, thus ruling out material decomposition as the source for gas production.

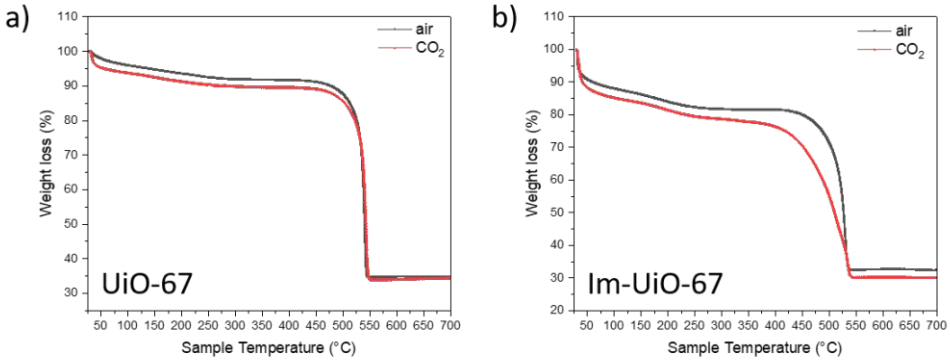

Figure 5: TGA measurements of UiO-67 (a) and Im-UiO-67 under synthetic air (black) and CO_2 atmosphere (red).

The slower release of CO_2, indicated by a broader TCD signal (green) in the Im-UiO-67 sample, could be attributed to stronger interactions between the framework and CO_2 due to the imidazolium functionalization. A comparison of the integrals of the measurement signals suggests that more CO_2 was adsorbed in the imidazolium-modified sample.

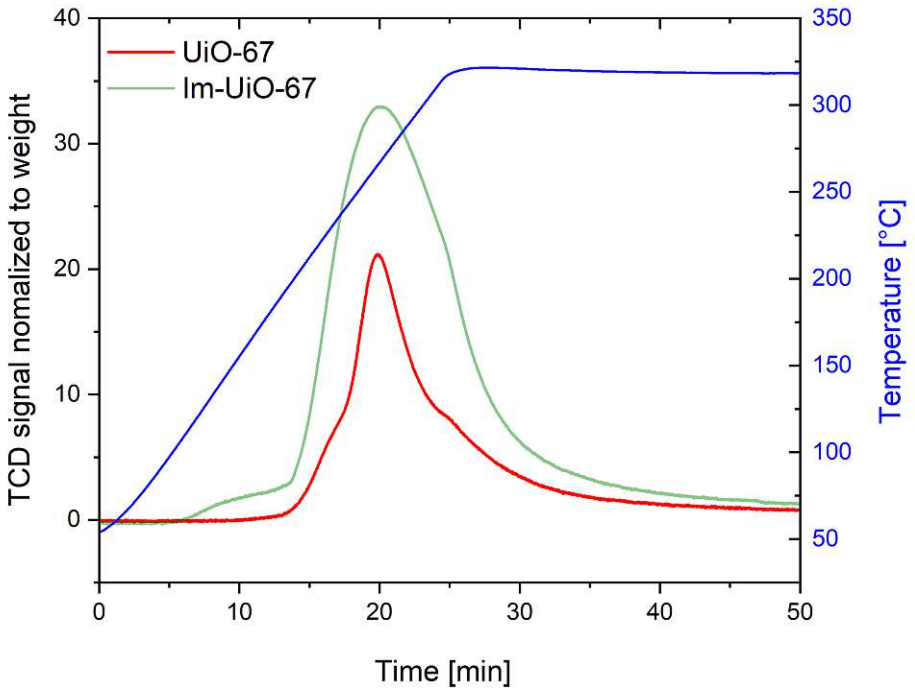

Figure 6: Carbon dioxide TPD chemisorption experiment with Im-Uio-67 (green) and UiO-67 (red) using a Bellcat II.

The chemisorption behavior of UiO-67 was studied further using in-situ diffuse reflectance infrared Fourier transform spectroscopy (DRIFTS) under CO_2 atmosphere, employing a reaction cell with precise temperature control. Details of the experimental setup are provided in the supporting information (see ESI Figure 4). The sample was exposed to a CO_2 pulse, and changes in surface chemistry were monitored through continuous IR measurements. The resulting overview spectra are presented in ESI Figure 5.

Weaker interaction of CO_2 with the framework is indicated by linear absorbed CO_2 in the region of 2300 cm^{-1} corresponding to ν_{as}(O-H) vibrations (see ESI Figure 5). Further features can be observed in the region of 3600 cm^{-1} indicative of ν(O-H) vibrations. The free μ_3-OH groups in Zirconia clusters are known to interact via hydrogen bond formation with guest molecules. In the absence of CO_2, the vibration for free μ_3-OH is detected at 3674 cm^{-1}.

Upon exposure to CO_2, time-resolved measurements under CO_2 atmosphere reveal additional vibrational bands at 3724, 3700, 3624, and 3600 cm^{-1}(see Figure 7). These bands can be assigned to CO_2 overtones and most likely OH stretching of bicarbonate species.[22] In addition to these symmetric features, a vibration at 3643 cm^{-1} is detected, which can be interpreted as a shift of the μ_3-OH vibration, related to a decrease in the force constant caused by CO_2 donating electron density to the σ antibonding orbital of the O-H bond, indicating chemical interaction between Zirkonia clusters and CO_2. Similar behavior is reported in the literature for UiO-66.[16]

The process is reversible. Upon purging with Helium, the vibrational signals disappear again (see Figure S6).

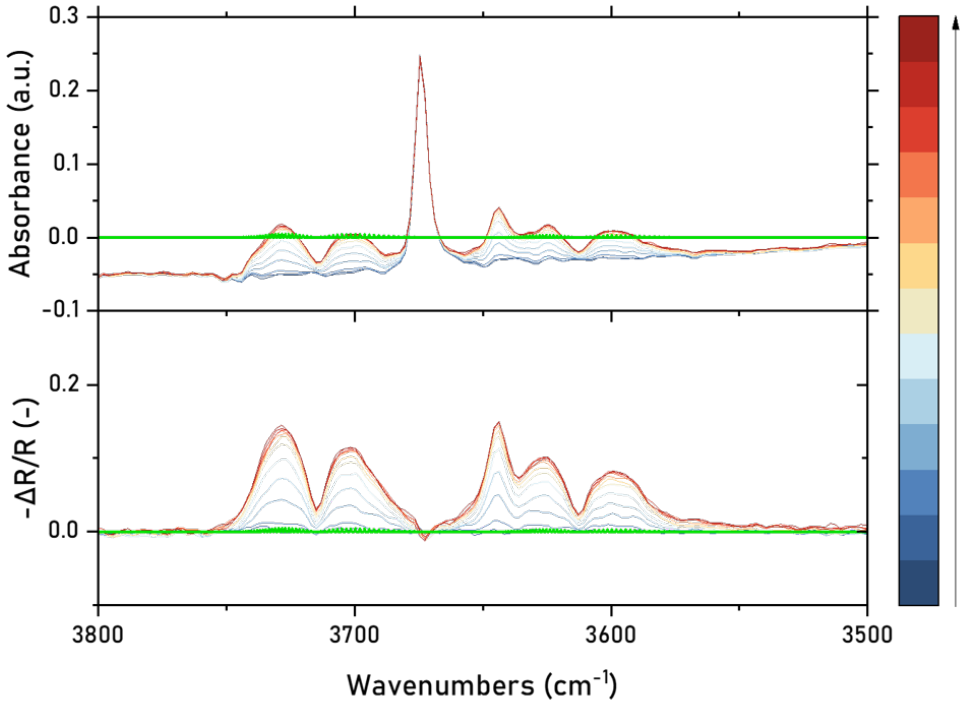

Figure 7: Time-resolved DRIFTS spectra of UiO-67 in the range from 3800 cm^{-1} to 3500 cm^{-1} exhibiting features related to ν_{as}(O-H) vibrations. Conditions: 5% CO_2 in He 10 mL min^{-1}, T= 30°C, timescale: 10 min, reference spectra of gas phase CO_2 is shown in green.

Conclusion

In this work, we investigated the CO_2 sorption properties of the Zirconium-based MOF UiO-67 and its imidazolium-modified derivative, Im-UiO-67. The imidazolium motif was introduced to enhance CO_2 interactions with the framework, providing an active chemisorption site for CO_2 activation, which could be advantageous in catalytic applications. The modification was achieved through side-chain functionalization of the bpd ligand, where the imidazolium group was incorporated via alkylation with ethylimidazol. Subsequently, Im-UiO-67 was synthesized using a mixture of ligands containing 10% imidazolium-modified linkers through microwave-assisted synthesis.

The obtained samples exhibited good crystallinity, and the successful incorporation of the imidazolium motif was confirmed by infrared spectroscopy.

Temperature-programmed desorption (TPD) measurements revealed that CO_2 interactions were enhanced in Im-UiO-67 most likely due to the introduction of imidazolium motifs. Furthermore, the CO_2 uptake was enhanced in imidazolium-modified UiO-67 compared to the reference system. DRIFTS spectroscopy demonstrated that chemisorption in UiO-67 is primarily associated with interactions involving the Zirconia-oxo clusters.

These preliminary results highlight the significant potential of this strategy, paving the way for further research objectives. As a future goal, we aim to explore the influence of different counterions on the positively charged imidazolium moiety, for example via the more basic acetate anion. Additionally, we intend to investigate Im-UiO-67 in the context of photocatalytic CO_2 reduction by integrating the system with modified linkers bearing catalytic groups selective for CO_2 conversion. Work in this direction is currently ongoing in our group.

Acknowledgement

This project has received funding from the European Research Council (ERC) under the European Union's Horizon 2020 research and innovation program (Grant Agreement No. 864991).

Supporting Information Available

Supporting Information is available in the Appendix.

References

(1) United Nations *State of the Global Climate 2023*; United Nations, 2024.

(2) Vidal, F.; van der Marel, E. R.; Kerr, R. W.; McElroy, C.; Schroeder, N.; Mitchell, C.; Rosetto, G.; Chen, T. T.; Bailey, R. M.; Hepburn, C.; Redgwell, C.; Williams, C. K. Designing a circular carbon and plastics economy for a sustainable future. *Nature* **2024**, *626*, 45–57.

(3) Gurau, G.; Rodríguez, H.; Kelley, S. P.; Janiczek, P.; Kalb, R. S.; Rogers, R. D. Demonstration of Chemisorption of Carbon Dioxide in 1,3-Dialkylimidazolium Acetate Ionic Liquids. *Angewandte Chemie International Edition* **2011**, *50*, 12024–12026.

(4) Gurkan, B. E.; De La Fuente, J. C.; Mindrup, E. M.; Ficke, L. E.; Goodrich, B. F.; Price, E. A.; Schneider, W. F.; Brennecke, J. F. Equimolar CO_2 absorption by anion-functionalized ionic liquids. *Journal of the American Chemical Society* **2010**, *132*, 2116–2117.

(5) Cui, G.; Wang, J.; Zhang, S. Active chemisorption sites in functionalized ionic liquids for carbon capture. *Chemical Society Reviews* **2016**, *45*, 4307–4339.

(6) Yu, S.; Jain, P. K. Plasmonic photosynthesis of C_1–C_3 hydrocarbons from carbon dioxide assisted by an ionic liquid. *Nature Communications* **2019**, *10*, 1–7.

(7) Rosen, B. A.; Salehi-Khojin, A.; Thorson, M. R.; Zhu, W.; Whipple, D. T.; Kenis, P. J.; Masel, R. I. Ionic liquid-mediated selective conversion of CO_2 to CO at low overpotentials. *Science* **2011**, *334*, 643–644.

(8) Asai, Y.; Katsuragi, H.; Kita, K.; Tsubomura, T.; Yamazaki, Y. Photocatalytic CO_2 reduction using metal complexes in various ionic liquids. *Dalton Transactions* **2020**, *49*, 4277–4292.

(9) Eisele, L.; Chaikhan, W.; Batool, S.; Cherevan, A.; Eder, D.; Bica-Schröder, K. Boosting Visible-Light Carbon Dioxide Reduction with Imidazolium-Based Ionic Liquids. *ChemCatChem* **2024**, *16*, e202301454.

(10) Yokozeki, A.; Shiflett, M. B.; Junk, C. P.; Grieco, L. M.; Foo, T. Physical and chemical absorptions of carbon dioxide in room-temperature ionic liquids. *Journal of Physical Chemistry B* **2008**, *112*, 16654–16663.

(11) Maia, R. A.; Louis, B.; Gao, W.; Wang, Q. CO_2 adsorption mechanisms on MOFs: a case study of open metal sites, ultra-microporosity and flexible framework. *Reaction Chemistry & Engineering* **2021**, *6*, 1118–1133.

(12) Sumida, K.; Rogow, D. L.; Mason, J. A.; McDonald, T. M.; Bloch, E. D.; Herm, Z. R.; Bae, T. H.; Long, J. R. Carbon dioxide capture in metal-organic frameworks. *Chemical Reviews* **2012**, *112*, 724–781.

(13) Torrisi, A.; Mellot-Draznieks, C.; Bell, R. G. Impact of ligands on CO_2 adsorption in metal-organic frameworks: First principles study of the interaction of CO_2 with functionalized benzenes. II. Effect of polar and acidic substituents. *Journal of Chemical Physics* **2010**, *132*, 44705.

(14) Sun, D.; Fu, Y.; Liu, W.; Ye, L.; Wang, D.; Yang, L.; Fu, X.; Li, Z. Studies on Photocatalytic CO_2 Reduction over NH_2-UiO-66(Zr) and Its Derivatives: Towards a Better Understanding of Photocatalysis on Metal–Organic Frameworks. *Chemistry – A European Journal* **2013**, *19*, 14279–14285.

(15) Banerjee, R.; Furukawa, H.; Britt, D.; Knobler, C.; O'Keeffe, M.; Yaghi, O. M. Control of Pore Size and Functionality in Isoreticular Zeolitic Imidazolate Frameworks and their Carbon Dioxide Selective Capture Properties. *Journal of the American Chemical Society* **2009**, *131*, 3875–3877.

(16) Grissom, T. G.; Driscoll, D. M.; Troya, D.; Sapienza, N. S.; Usov, P. M.; Morris, A. J.; Morris, J. R. Molecular-Level Insight into CO_2 Adsorption on the Zirconium-Based Metal-Organic Framework, UiO-66: A Combined Spectroscopic and Computational Approach. *Journal of Physical Chemistry C* **2019**, *123*, 13731–13738.

(17) Lawrence, M. C.; Spoel, A. M.; Katz, M. J. Pore Perfection vs Defect Design: Examining the Complex Relationship between Pore Structure and Carbon Dioxide Adsorption in Zr-Based MOFs. *Journal of Physical Chemistry C* **2024**, *128*, 10698–10704.

(18) Xue, W. L. et al. Melt-quenched glass formation of a family of metal-carboxylate frameworks. *Nature Communications* **2024**, *15*, 1–13.

(19) Ding, L. G.; Yao, B. J.; Jiang, W. L.; Li, J. T.; Fu, Q. J.; Li, Y. A.; Liu, Z. H.; Ma, J. P.; Dong, Y. B. Bifunctional Imidazolium-Based Ionic Liquid Decorated UiO-67 Type MOF for Selective CO_2 Adsorption and Catalytic Property for CO_2 Cycloaddition with Epoxides. *Inorganic Chemistry* **2017**, *56*, 2337–2344.

(20) Schumacher, W. T.; Mathews, M. J.; Larson, S. A.; Lemmon, C. E.; Campbell, K. A.; Crabb, B. T.; Chicoine, B. J.; Beauvais, L. G.; Perry, M. C. Organocatalysis by site-isolated N-heterocyclic carbenes doped into the UIO-67 framework. *Polyhedron* **2016**, *114*, 422–427.

(21) Zou, Y. H.; Wu, Q. J.; Yin, Q.; Huang, Y. B.; Cao, R. Self-Assembly of Imidazolium-Functionalized Zr-Based Metal-Organic Polyhedra for Catalytic Conversion of CO_2 into Cyclic Carbonates. *Inorganic Chemistry* **2021**, *60*, 2112–2116.

(22) Proaño, L.; Tello, E.; Arellano-Trevino, M. A.; Wang, S.; Farrauto, R. J.; Cobo, M. In-situ DRIFTS study of two-step CO_2 capture and catalytic methanation over Ru,Na_2O/Al_2O_3 Dual Functional Material. *Applied Surface Science* **2019**, *479*, 25–30.

4. Outlook

In the preceding chapters, the cooperative effects of ionic liquids on photocatalysis with organometallic catalysts was studied with the benchmark system consisting of $Re(bpy)(CO)_3Cl$ and $Ru(bpy)_3PF_6$. Investigations under homogeneous conditions demonstrated the potential of imidazolium-based ionic liquids as low-level additives to strongly enhance CO production in photocatalytic CO_2 reduction systems, mitigating issues of high viscosity and mass transfer and avoiding the need to use ionic liquids as primary solvents. Notably, the addition of $[C_2mim][OAc]$ in DMF resulted in a nearly 20-fold increase in CO yield. However, the long-term reaction rate of the photosystem stagnated after an initial rapid increase, indicating limited long-term stability, likely due to photosensitizer degradation.
In the next step, the system was transferred to a heterogeneous photocatalytic process through immobilization of photosensitizer and catalyst in a polymerized imidazolium-based ionic liquid framework via radical polymerization from vinyl group-bearing monomers. XPS measurements confirmed the maintenance of the redox state of Ruthenium sensitizer and Rhenium catalyst after polymerization, and quantification was carried out by Laser Ablation-Inductively Coupled Plasma-Mass Spectrometry (LA-ICP-MS). This study successfully demonstrated the integration of Ruthenium and Rhenium moieties into a heterogeneous polymer-based framework that acted as co-catalyst in the photocatalytic reduction of CO_2. The system achieved high selectivity for CO production with sustained turnover frequencies over 4 hours, thus outperforming the long-term stability of the homogenous system. The addition of the photosensitizer significantly enhanced CO turnover numbers, which scaled linearly with sensitizer concentration.
Furthermore, the concept of imidazolium structural motifs for CO_2 interaction was extended to MOFs for CO_2 activation. Imidazolium functionalities were incorporated through side-group modifications of the linkers, creating CO_2 activation sites within the highly ordered porous network. This strategy aimed to construct reactive centers with well-defined geometries for photocatalytic applications, offering catalytic single sites close to imidazolium functionalities for CO_2 pre-activation. Chemisorption measurements showed increased CO_2 uptake in imidazolium-modified UiO-67 compared to the reference system. Additionally, DRIFTS spectroscopy indicated that chemisorption in UiO-67 is mainly driven by interactions with the Zirconia-oxo clusters.

The next steps of this research project aim to advance these reactions toward gas-phase reactions in continuous flow, aiming for a high-throughput process with hetero-

geneous catalysts that are accessible, scalable, and offer improved long-term stability towards photodegradation.
The first result of these ongoing developments, as well as future perspectives are presented in the following section.

4.1. Photocatalytic gas-phase reactions

Compared to homogeneous and slurry-phase heterogeneous photocatalysis in the liquid phase, gas-phase heterogeneous photocatalysis offers several advantages. By overcoming the limitation of CO_2 solubility in diverse solvents, gas-phase conditions enable improved catalyst exposure to CO_2. Light utilization efficiency is also enhanced, as gas-phase systems avoid light scattering commonly observed in homogeneous solutions.[10]

When comparing reactions in batch and continuous flow, re-adsorption and undesirable back- or side reactions are common in batch reactors. This is a result of the constant build-up of products, which can lead to reduced yields. In contrast, reactions in a flow set-up maintain a continuous flow of reactants and products. This minimizes product accumulation but requires the adaption and tuning of flow rates to optimize residence times.[114] To gain a thorough understanding of gas-phase reactions under continuous flow, experiments are planned in two parallel setups.

- One newly constructed setup enables gas-phase photocatalytic reactions and in-line gas analysis with catalyst loadings ranging from 10 to 100 mg. A significant portion of this PhD research has been dedicated to building and establishing this reaction system for gas-phase studies, which will be described in detail in the following chapter.

- In parallel, diffuse reflectance infrared fourier transform spectroscopy (DRIFTS) will be used to further elucidate mechanistic details in gas phase under continuos flow. A brief introduction to DRIFTS measurements is provided in subsection 4.1.2, and detailed studies are currently ongoing in collaboration with Jakob Blaschke.

- Eventually, first approaches towards supported ionic liquid phase (SILP) catalysts based on a Re-catalyst immobilized within the ionic liquid layer on gCN as heterogeneous support and photosensitizer for gas-phase photoreductions.

4.1.1. Reactor design and operation

Inspired by gas-phase reactors from the literature, a new reaction setup was constructed to facilitate gas-phase reactions in both batch and flow modes. The system comprises a tailor-made reactor connected to gas supply and analytic devices.[115,116] The schematic of the reactor prototype is presented in Figure 4.1. The main body of the reactor consists of alumina with a built-in heating/cooling mantle and connections to the gas inlet and

outlet for purging and evacuation. The interior of the alumina body provides space for a conventional glass filter frit that can be filled with catalyst material. The bottom of the inner reactor body is designed with a circular gutter, allowing for the introduction of sacrificial agents that can be evaporated and controlled by the reactor temperature. The top part of the reactor is covered with a lid made of quartz glass, held in place with a rubber seal, allowing for illumination from above. Four screws and a Teflon seal secure the lid. Additionally, the reactor chamber includes a built-in septum that can be used to draw samples with a gas-tight syringe when operated in batch mode.

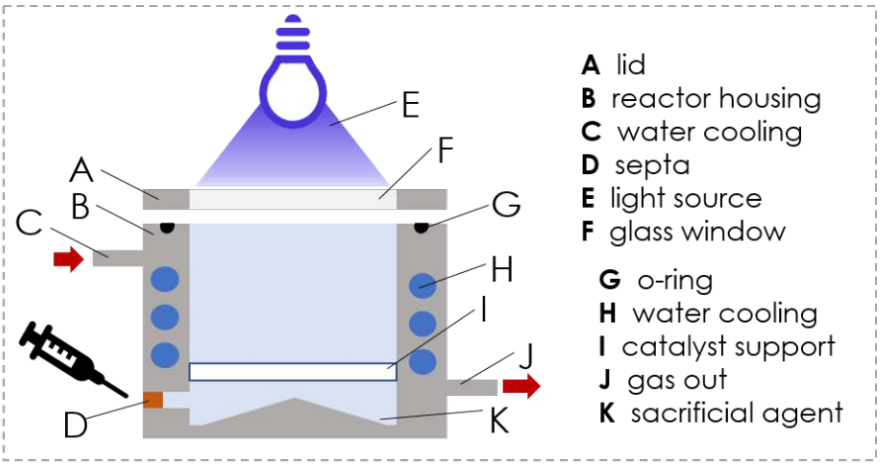

Figure 4.1. Schematic description of the developed gas-phase reactor.

Due to limitations faced by corrosion of alumina arising from basic sacrificial agents such as TEOA and TEA, a second prototype was constructed consisting of Polyoxymethylene (POM) (see Figure 4.2). To overcome limitations in heat transfer originating from the very low heat coefficient, the reactor design was changed to a layout with a heating/cooling circuit that features thinner lines but a higher number of circumambulations around the center of the reactor. The appendix provides heat transfer simulations (see Appendix Figure 4.3) and technical drawings of the reactor prototypes Appendix 4.4, 4.5, and 4.6. However, simulations suggest that heat transfer is still very limited in the system, and further reactor development might be necessary.

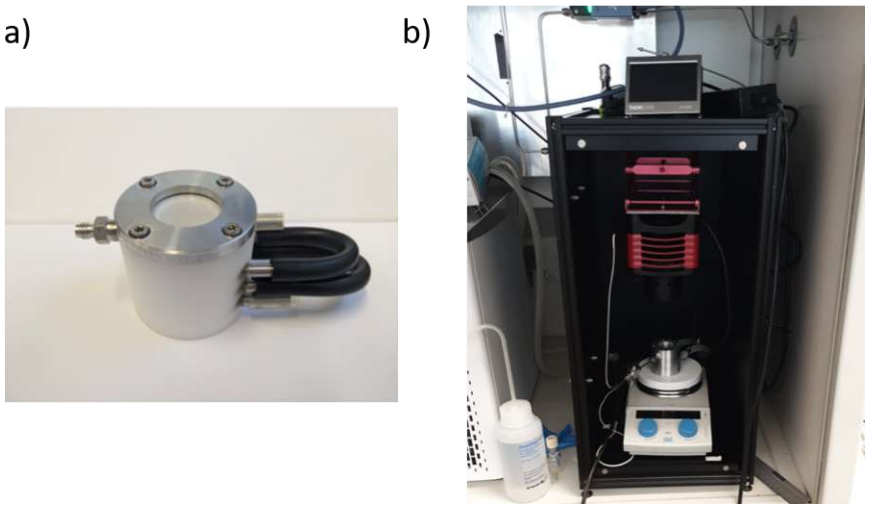

Figure 4.2. Pictures of POM gas-phase reactor prototype (a) and reaction setup installed into a black box (b).

The overall reaction setup can be used in batch mode with closed inlet and outlet valves. In this case, samples can be withdrawn via the septa, and sacrificial agent/water is provided by deposition of the latter on the bottom of the reactor chamber. Furthermore, the setup includes installations for continuous operation (see Figure 4.3).

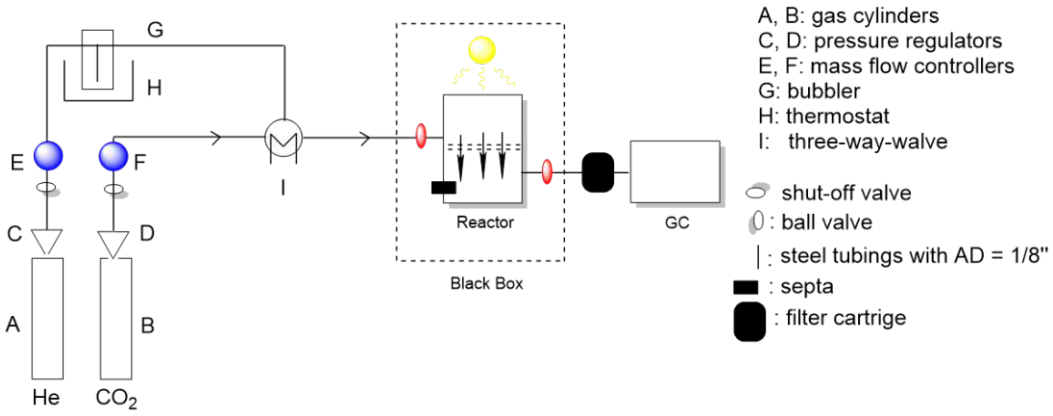

Figure 4.3. Schematic description of gas-phase setup in continuous flow mode.

The reactor inlet is connected to mass flow controllers (MFCs) for both CO_2 and He, allowing precise adjustment of gas mixtures. To address limitations caused by the gradual evaporation of sacrificial agents within the reactor chamber and to achieve greater control over gas-phase vapor saturation, the gas stream can be directed through a bubbler unit, enriching it with a sacrificial agent or water vapor. The vapor concentration is controlled by adjusting the temperature of the bubbler, which is mounted on a thermostat. Incorporating the bubbler requires heating lines around the metal tubing for gas transfer, preventing condensation of the sacrificial agent or water within the tubing, and avoiding potential damage to gas chromatography (GC) equipment. The reactor can be connected to a sampling line linked to a headspace GC (Shimadzu Nexis

GC-2030) equipped with a sampling loop and a Vici Valco valve for inline sampling. To further protect the GC, particularly the column, from damage, a cartridge was constructed for installation in the gas stream; it can be filled with silica beads for water absorption. As continuous flow reactions might require long residence times, the MFCs can be controlled with software that features stopped-flow mode.

4.1.2. In-operando DRIFTs

To gain further insights into the reaction mechanisms of CO2RR with heterogeneous catalysts in gas phase, diffuse reflectance infrared Fourier transform spectroscopy (DRIFTS) provides a powerful tool for in-operando investigations. Figure 4.4 shows a schematic of the reaction setup.

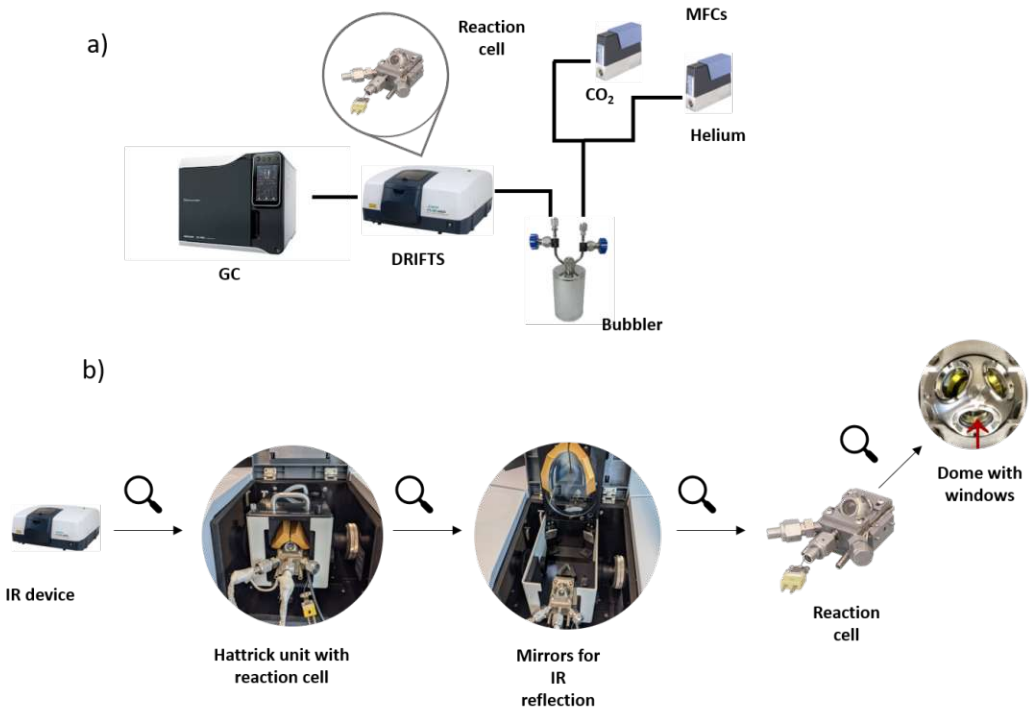

Figure 4.4. Schematic description of the in-operando DRIFTS setup consisting of DRIFTs reaction cell connected to a GC (a) and close-up of reaction cell mounted into IR device (b).

The setup consists of an IR device with a built-in Hattrick cell that hosts the sample. The sample can be deposited on a frit in the center of the cell, equipped with Peltier elements for heating. Additionally, the cell surroundings are cooled by an external water cooling system. The inner part of the cell can be purged with controlled flows of CO_2 and Helium using mass flow controllers (MFCs). The cell also features a dome-shaped cap with three windows: Two for IR reflectance and one for direct illumination of the sample using an external light source.

The Hattrick cell is installed under the bowl-shaped mirrors of the IR device to capture the reflectance of the IR beam from diffuse reflectance. The IR device is continuously

purged with dry air to prevent interference from changes in the gas space. The measurement cell is also connected to a gas chromatograph (GC) for in-line sampling. Water vapor can be introduced via a He-purged bubbler unit. To prevent water condensation, all gas tubings were lined with external heating.
Typical overall sample loads do not exceed 5 mg. Additionally, sample dilution is necessary to achieve a good signal-to-noise ratio for IR detection, which is done by mixing 10 wt% of the sample with diamond powder. However, this dilution limits the detection of gaseous products by in-line GC sampling. For this reason, the custom-made setup with a larger reaction chamber can be used for complementary studies on photocatalytic yields.

A typical experimental layout comprises purging of the reaction cell followed by control IR. Consequently, CO_2 gas flow is introduced to the chamber, and DRIFTS measurements monitor CO_2 absorption on the sample in the absence or presence of water vapor. For in-operando CO2RR experiments, water vapor is introduced to the gas stream, and the gas phase is sampled by headspace GC using an in-line sampling technique.

4.1.3. Catalyst development

A well-known approach for applying ionic liquids in catalysis relies on their immobilization on porous support, a concept that is also known as supported ionic liquid phase (SILP) technology. Ionic liquids can be efficiently immobilized on solid supports, such as mesoporous silica, through physisorption - a strategy that has been widely employed for various applications ranging from catalysis to separations.[117,118] The SILP technology integrates the benefits of both homogeneous and heterogeneous catalysis, offering short diffusion pathways within the ionic liquid film, as illustrated in Figure 4.5. This feature is particularly advantageous for overcoming mass transfer limitations commonly encountered in traditional liquid-liquid biphasic catalysis. The SILP catalyst concept is especially well-established for gas-phase reactions, including hydroformylations[119] and hydrogenations.[120] Additionally, successful applications have been demonstrated in combination with supercritical carbon dioxide ($scCO_2$). The high solubility of CO_2 in ionic liquids enhances mass transfer, mitigating the diffusion limitations observed in bulk ionic liquid phases.[121]

The supported ionic liquids can serve as catalysts themselves, for example in the conversion of CO_2 with epoxides to cyclic carbonates.[122] Alternatively, the ionic liquid can act as media for dissolving or dispersing a wide range of catalysts, including transition metal catalysts, organometallic catalysts, nanoparticles, or even biocatalysts such as enzymes.[118]Alternatively, the ionic liquid can be coated on a catalytically active solid catalyst as a protective layer; a concept, that is sometimes found under the term "solid catalyst with ionic liquid layer" (SCILL).[123]

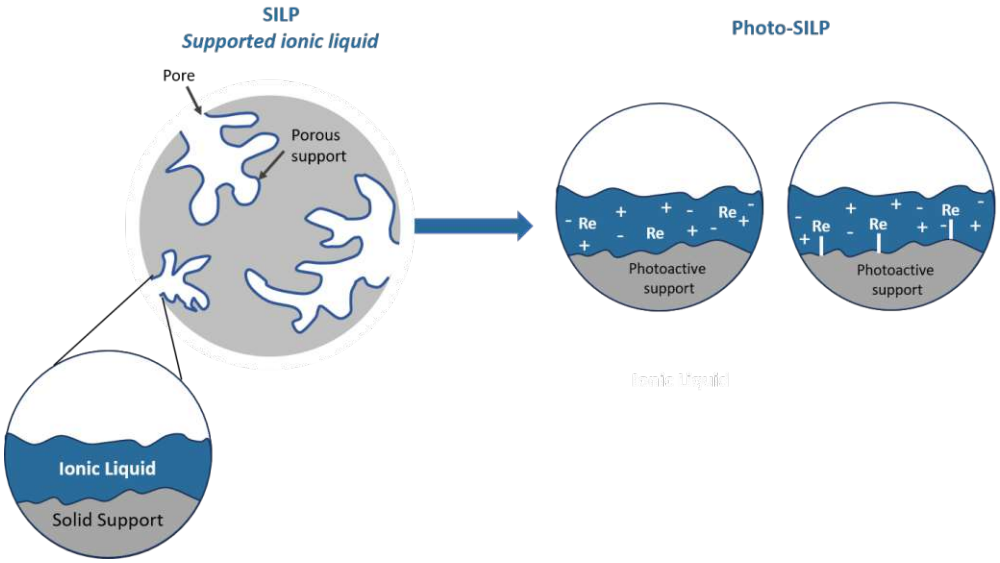

Figure 4.5. Concept of supported ionic liquid phases (SILPs) and its adaption for photocatalytic CO2RR with photoactive support and Rhenium single site catalyst.

Typical applications of SILP materials in catalysis rely on inert mesoporous materials, such as silicon dioxide (SiO_2), as supports. Alternatively, inorganic semiconductors such as TiO_2 could be used, although this is less common.[124,125] This would allow combining the role of the photosensitizer with the role of the support for the ionic liquid, thus providing a novel approach to heterogeneous mesoporous photocatalysts with simple preparation that can be easily scaled ("photocatalytically active supported ionic liquid phases, Photo-SILP". Furthermore, the catalytic system can be upgraded with additional catalytic species, e.g. Re-catalysts that are dissolved in the ionic liquid or covalently attached to the mesoporous photosensitizer (see Figure 4.5, right).

For a first approach to this novel strategy, we aimed to modify TiO_2 with $Re(bpy)(CO)_3Cl$ in combination with the best performing ionic liquids from our studies under homogenous conditions. Initial experiments in the batch mode were performed with a TiO_2-derived Photo-SILP using water as a proton source and sacrificial in the previously described reactor prototype with alumina housing. However, the experiments showed very low yield and selectivity. Although CO was detected on a low level, a comparison of samples modified with the Re-catalyst showed no significant increase in photocatalytic activity. Most likely, surface-attached carbon might play a role here. This carbon can desorb and react under the chosen reaction conditions, indicating that high-purity conditions would be required.[126–128]

Alternatively, we looked at graphitic carbon nitride (gCN) as photoactive heterogeneous support for SILP catalysis (see Figure 4.6).[64] This polymeric semiconductor material is derived from organic precursors and is mainly composed of carbon and nitrogen. The structure is formed from tri-s-triazine units.

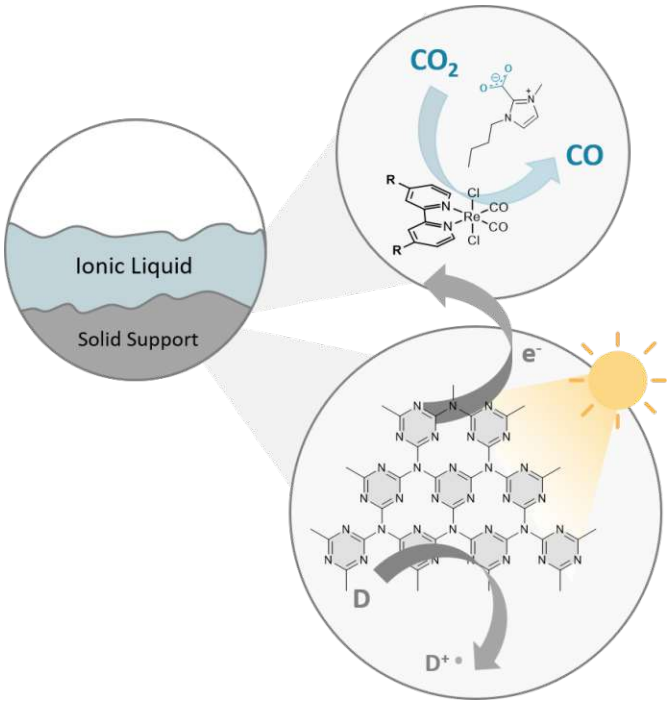

Figure 4.6. Concept of CO2RR photo-SILP catalysis with gCN heterogeneous photoactive support, ionic liquid and Re-catalyst.

Initial slurry-phase studies on the photocatalytic reduction of CO_2 were performed in a mixture of DMF and TEOA with excitation at 445 nm investigating the combination of unmodified Re-catalyst and gCN by adding both gCN and catalyst to a reaction mixture in water. A detailed description of the procedure is described in the Appendix subsubsection D. Results are shown in Table 4.1. Compared to pure gCN, a significant increase in CO yield was measured when gCN and Re catalyst were combined.

Table 4.1. Preliminary photocatalytic results for gCN sensitized photocatalysis.

System	CO [μmol]	Standard Error	Selectivity
gCN	0.00	0.00	25.6
Re	4.09	0.80	99.7
gCN+Re	4.50	0.43	99.9

Reaction conditions: 3 mg mL^{-1} gCN, 0.3 mg mL^{-1} $Re(bpy)(CO)_3Cl$, DMF:TEOA 5:1, t=1h, T=22 °C, 445 nm, Brightness 95 %.

First experiments under continuous sampling of gaseous products with an EMERSON IR cell over 2 hours confirmed increased CO formation rate in the combined system compared to the used of Re-catalyst only (see Figure 4.7). However, the system degrades after 30 minutes of illumination.

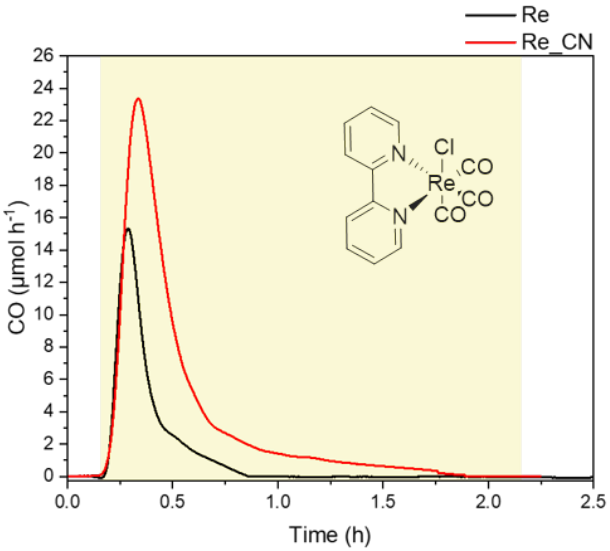

Figure 4.7. Experiment under continuous sampling of gaseous products with Re-catalyst and gCN in solution phase. Reaction conditions: 3 mg mL^{-1} gCN, 0.3 mg mL^{-1} $Re(bpy)(CO)_3Cl$, DMF:TEOA 5:1, t=2h, T=22 °C, 445 nm, Brightness 95%.

With this initial proof of the feasibility of combining gCN and Re-catalyst for a photo-SILP concept in hand, future steps will address stability issues and investigate modified Re- complexes in combination with gCN, aiming to further enhance the reaction through improved electron transfer. To enhance surface interactions between gCN and Re-catalyst, the bpy ligand can be optionally modified with phosphate or ester groups to promote interactions with NH_2-defects in the gCN layers (see Figure 4.8).[75,76]

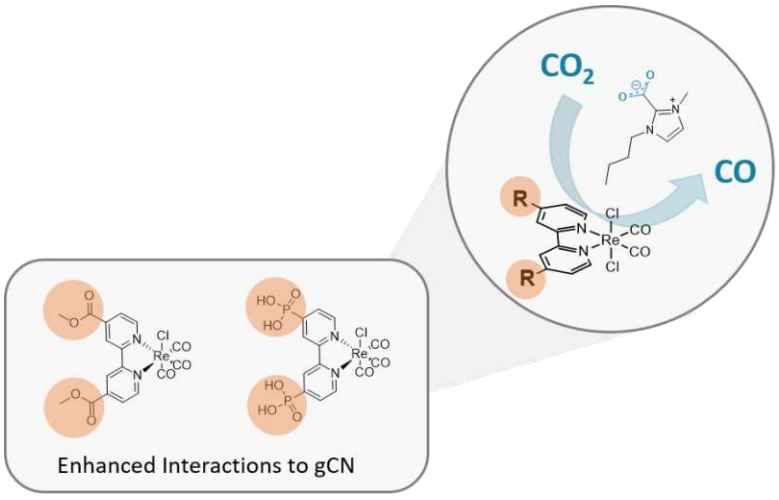

Figure 4.8. Modification of bpy ligand with ester and phosphate groups to enhance electron transfer from gCN.

Work on the synthesis of Re-complexes and their photocatalytic testing is ongoing.

4.2. Summary

Driven by the urgent need to shift chemical production towards a circular carbon economy using CO_2 as a feedstock, this work explores the transformation of CO_2 into CO, a crucial building block in the chemical industry. Photocatalysis provides a powerful method for achieving this transformation under mild conditions and can be paired with imidazolium-based ionic liquids, which chemisorb CO_2 to create a cooperative effect.

In the first part of this thesis, the impact of imidazolium-based ionic liquids on photocatalytic CO_2 reduction was investigated. Starting with a review of the state-of-the-art research on the role of these ionic liquids in photocatalytic CO_2 reduction, three studies were conducted to investigate their interaction with CO_2 and their cooperative effect on catalysis. The undertaken studies cover work on homogeneous and heterogeneous photocatalysis towards the selective formation of CO, as well as the investigation of chemisorption properties of imidazolium-modified metal-organic frameworks. Consecutively, reactor design, advanced analytical strategies and catalyst development for continuous photocatalytic gas-phase reaction were presented in an outlook chapter.

In the initial investigation on homogeneous photocatalysis, imidazolium-based ionic liquids were used alongside an organometallic catalyst under homogeneous reaction conditions in organic solvents. The studied benchmark photocatalytic system consisted of a Ru-sensitizer and a Re-catalyst. Adding an ionic liquid led to a 20-fold increase in CO_2 formation when using 1-ethyl-3-methylimidazolium acetate [C_2mim][OAc] in DMF. It was shown that even small amounts, as low as 10 % (w/v), of ionic liquid could significantly boost CO formation. A correlation was observed between anion basicity and CO_2 activation, demonstrating the impact of anion basicity on CO_2 activation and highlighting the cooperative effect of ionic liquids. However, a drawback of homogeneous photocatalysis is its limited long-term stability.
Building on these results, the system was adapted for heterogeneous photocatalysis by immobilizing the reaction components within a polymerized ionic liquid matrix. The photosensitizer and catalyst were synthesized with vinyl-bearing ligands, enabling radical co-polymerization with a vinyl-modified imidazolium-based ionic liquid monomer. The synthesized polymer was characterized by X-ray photoelectron spectroscopy (XPS) and LA-ICP-MS, confirming that the oxidation states of both the sensitizer and catalyst were preserved throughout polymerization and allowing for quantification of the Ruthenium and Rhenium content. The material was tested for photocatalytic CO2RR in organic solvents, achieving CO formation up to 0.71 μmol over 15 hours with high selectivity. These experiments confirmed that the Ru-based photosensitizer retained its activity in the polymer matrix. Additionally, the long-term stability was extended to 4 hours, a significant improve compared to the 40-minute stability observed in the homogeneous system.

In a subsequent project, imidazolium-based ionic liquids were transferred to porous materials using UiO-67 MOFs. Initial experiments with Re-modified UiO-67 in an ionic

liquid suspension demonstrated the necessity of covalently immobilizing imidazolium motifs within the MOF structure. Consequently, the research objective was refined to develop MOFs containing both covalently attached imidazolium groups, aiming to create a sterically controlled reactive site with cooperative effects. Investigations were conducted on synthesizing imidazolium-modified frameworks, focusing on analyzing the chemisorption properties of the synthesized materials.

Eventually, the development of a photocatalytic setup for gas-phase reactions involved design and construction a reactor for photocatalytic gas-phase reactions in both batch mode and flow conditions. Prototypes of these reactors were built to accommodate various sacrificial agents and allow sampling via septa or in-line GC. Initial steps were also taken to develop materials for gas-phase reactions, focusing on creating straightforward catalysts to synthesize, which are easily scalable and based on heterogeneous photoactive supports. In this context, SILP catalysts with a Re-catalyst immobilized within the ionic liquid layer on gCN as heterogeneous semiconducting support were developed and initially tested. Future studies will build on these preliminary tests and optimize conditions, in combination with a detailed investigation of reaction mechanisms using the developed DRIFTS setup for in-operando studies in gas phase.

Bibliography

[1] United Nations, *State of the Global Climate 2023*, United Nations, 2024.

[2] X. G. Zhang, A. Buthiyappan, N. Z. Mohd Azmi and A. A. Abdul Raman, *Chemical Papers*, 2024, **78**, 7229–7238.

[3] F. Vidal, E. R. van der Marel, R. W. Kerr, C. McElroy, N. Schroeder, C. Mitchell, G. Rosetto, T. T. Chen, R. M. Bailey, C. Hepburn, C. Redgwell and C. K. Williams, *Nature*, 2024, **626**, 45–57.

[4] J. B. Zimmerman, P. T. Anastas, H. C. Erythropel and W. Leitner, *Science*, 2020, **367**, 397–400.

[5] O. S. Bushuyev, P. De Luna, C. T. Dinh, L. Tao, G. Saur, J. van de Lagemaat, S. O. Kelley and E. H. Sargent, *Joule*, 2018, **2**, 825–832.

[6] J. Albero, Y. Peng and H. García, *ACS Catalysis*, 2020, **10**, 5734–5749.

[7] J. Huo, Z. Wang, C. Oberschelp, G. Guillén-Gosálbez and S. Hellweg, *Green Chemistry*, 2023, **25**, 415–430.

[8] K. Y. Cohen, R. Evans, S. Dulovic and A. B. Bocarsly, *Accounts of Chemical Research*, 2022, **55**, 944–954.

[9] S. Yu and P. K. Jain, *Nature Communications*, 2019, **10**, 1–7.

[10] S. Fang, M. Rahaman, J. Bharti, E. Reisner, M. Robert, G. A. Ozin and Y. H. Hu, *Nature Reviews Methods Primers*, 2023, **3**, 1–21.

[11] R. Sang, Y. Hu, R. Razzaq, G. Mollaert, H. Atia, U. Bentrup, M. Sharif, H. Neumann, H. Junge, R. Jackstell, B. U. W. Maes and M. Beller, *Nature Communications*, 2022, **13**.

[12] R. Franke, D. Selent and A. Börner, *Chemical Reviews*, 2012, **112**, 5675–5732.

[13] S. Dabral and T. Schaub, *Advanced Synthesis and Catalysis*, 2019, **361**, 223–246.

[14] A. Brennführer, H. Neumann and M. Beller, *Angewandte Chemie International Edition*, 2009, **48**, 4114–4133.

[15] H. Schulz, *Applied Catalysis A: General*, 1999, **186**, 3–12.

[16] K. Schröder, *ERC Carboflow*, `https://info.ias.tuwien.ac.at/schroederlab/erc-carboflow/`, [Online; accessed 06-February-2025], 2023.

[17] H. Dau, E. Fujita and L. Sun, *ChemSusChem*, 2017, **10**, 4228–4235.

[18] S. Zhang, Q. Fan, R. Xia and T. J. Meyer, *Accounts of Chemical Research*, 2020, **53**, 255–264.

[19] H. Takeda, C. Cometto, O. Ishitani and M. Robert, *ACS Catalysis*, 2017, **7**, 70–88.

[20] Y. Kuramochi, O. Ishitani and H. Ishida, *Coordination Chemistry Reviews*, 2018, **373**, 333–356.

[21] B. Zhu, L. K. Yan, Y. Geng, H. Ren, W. Guan and Z. M. Su, *Chemical Communications*, 2018, **54**, 5968–5971.

[22] Y. Yamazaki, H. Takeda and O. Ishitani, *Journal of Photochemistry and Photobiology C: Photochemistry Reviews*, 2015, **25**, 106–137.

[23] D. M. Arias-Rotondo and J. K. McCusker, *Chemical Society Reviews*, 2016, **45**, 5803–5820.

[24] Y. Pellegrin and F. Odobel, *Comptes Rendus Chimie*, 2016, **20**, 283–295.

[25] C. F. Leung and T. C. Lau, *Energy and Fuels*, 2021, **35**, 18888–18899.

[26] W. W. Brandt, F. P. Dwyer and E. D. Gyarfas, *Chemical Reviews*, 1954, **54**, 959–1017.

[27] J. P. Paris and W. W. Brandt, *Journal of the American Chemical Society*, 1959, **81**, 5001–5002.

[28] D. M. Hedstrand, W. H. Kruizinga and R. M. Kellogg, *Tetrahedron Letters*, 1978, **19**, 1255–1258.

[29] J.-M. Lehn and R. Ziessel, *Proceedings of the National Academy of Sciences*, 1982, **79**, 701–704.

[30] J. Hawecker, J. M. Lehn and R. Ziessel, *Journal of the Chemical Society, Chemical Communications*, 1983, 536–538.

[31] J. Hawecker, J.-M. Lehn and R. Ziessel, *Journal of the Chemical Society, Chemical Communications*, 1984, 328–330.

[32] J. Hawecker, J.-M. Lehn and R. Ziessel, *Helvetica Chimica Acta*, 1986, **69**, 1990–2012.

[33] T. Tanaka, M. Shizuno, Y. Tamaki, K. Maeda and O. Ishitani, *ACS Catalysis*, 2024, 18615–18623.

[34] Y. Tamaki and O. Ishitani, *ACS Catalysis*, 2017, **7**, 3394–3409.

[35] R. Huang, Y. Peng, C. Wang, Z. Shi and W. Lin, *European Journal of Inorganic Chemistry*, 2016, **2016**, 4358–4362.

[36] C. Liu, K. D. Dubois, M. E. Louis, A. S. Vorushilov and G. Li, *ACS Catalysis*, 2013, **3**, 655–662.

[37] C. K. Prier, D. A. Rankic and D. W. MacMillan, *Chemical Reviews*, 2013, **113**, 5322–5363.

[38] D. A. Nicewicz and D. W. MacMillan, *Science*, 2008, **322**, 77–80.

[39] M. A. Ischay, M. E. Anzovino, J. Du and T. P. Yoon, *Journal of the American Chemical Society*, 2008, **130**, 12886–12887.

[40] L. Raju and E. Rajkumar, *Coordination compounds of iron, ruthenium and osmium*, Elsevier, 2023, pp. 135–203.

[41] C. Creutz and N. Sutin, *Inorganic Chemistry*, 1976, **15**, 496–499.

[42] R. A. Marcus, *Angewandte Chemie International Edition*, 1993, **32**, 1111–1121.

[43] B. P. Sullivan, C. M. Bolinger, D. Conrad, W. J. Vining and T. J. Meyer, *Chemical Communications*, 1985, 1414–1416.

[44] F. P. a. Johnson, M. W. George, F. Hartl and J. J. Turner, *Organometallics*, 1996, **15**, 3374–3387.

[45] D. H. Gibson, X. Yin, H. He and M. S. Mashuta, *Organometallics*, 2003, **22**, 337–346.

[46] Y. Hayashi, S. Kita, B. S. Brunschwig and E. Fujita, *Journal of the American Chemical Society*, 2003, **125**, 11976–11987.

[47] T. Morimoto, T. Nakajima, S. Sawa, R. Nakanishi, D. Imori and O. Ishitani, *Journal of the American Chemical Society*, 2013, **135**, 16825–16828.

[48] R. N. Sampaio, D. C. Grills, D. E. Polyansky, D. J. Szalda and E. Fujita, *Journal of the American Chemical Society*, 2020, **142**, 2413–2428.

[49] E. Fujita, D. C. Grills, G. F. Manbeck and D. E. Polyansky, *Accounts of Chemical Research*, 2022, **55**, 616–628.

[50] K. Ohkubo, Y. Yamazaki, T. Nakashima, Y. Tamaki, K. Koike and O. Ishitani, *Journal of Catalysis*, 2016, **343**, 278–289.

[51] J. M. Lehn and R. Ziessel, *Journal of Organometallic Chemistry*, 1990, **382**, 157–173.

[52] V. S. Thoi and C. J. Chang, *Chemical Communications*, 2011, **47**, 6578.

[53] D. L. DuBois, A. Miedaner and R. C. Haltiwanger, *Journal of the American Chemical Society*, 1991, **113**, 8753–8764.

[54] E. E. Benson and C. P. Kubiak, *Chemical Communications*, 2012, **48**, 7374–7376.

[55] J. L. White, M. F. Baruch, J. E. Pander, Y. Hu, I. C. Fortmeyer, J. E. Park, T. Zhang, K. Liao, J. Gu, Y. Yan, T. W. Shaw, E. Abelev and A. B. Bocarsly, *Chemical Reviews*, 2015, **115**, 12888–12935.

[56] S. N. Habisreutinger, L. Schmidt-Mende and J. K. Stolarczyk, *Angewandte Chemie International Edition*, 2013, **52**, 7372–7408.

[57] K. Li, B. Peng and T. Peng, *ACS Catalysis*, 2016, **6**, 7485–7527.

[58] L. Wan, Q. Zhou, X. Wang, T. E. Wood, L. Wang, P. N. Duchesne, J. Guo, X. Yan, M. Xia, Y. F. Li, F. M. Ali, U. Ulmer, J. Jia, T. Li, W. Sun and G. A. Ozin, *Nature Catalysis 2019 2:10*, 2019, **2**, 889–898.

[59] K. Zhong, P. Sun and H. Xu, *Small*, 2024, 2310677.

[60] M. F. Kuehnel, K. L. Orchard, K. E. Dalle and E. Reisner, *Journal of the American Chemical Society*, 2017, **139**, 7217–7223.

[61] Y. Shi, J. Li, C. Mao, S. Liu, X. Wang, X. Liu, S. Zhao, X. Liu, Y. Huang and L. Zhang, *Nature Communications*, 2021, **12**, 1–10.

[62] G. Chen, R. Gao, Y. Zhao, Z. Li, G. I. Waterhouse, R. Shi, J. Zhao, M. Zhang, L. Shang, G. Sheng, X. Zhang, X. Wen, L. Z. Wu, C. H. Tung and T. Zhang, *Advanced Materials*, 2018, **30**, 1704663.

[63] B. Ma, M. Blanco, L. Calvillo, L. Chen, G. Chen, T. C. Lau, G. Dražić, J. Bonin, M. Robert and G. Granozzi, *Journal of the American Chemical Society*, 2021, **143**, 8414–8425.

[64] Q. Lu, K. Eid, W. Li, A. M. Abdullah, G. Xu and R. S. Varma, *Green Chemistry*, 2021, **23**, 5394–5428.

[65] W. Shangguan, Q. Liu, Y. Wang, N. Sun, Y. Liu, R. Zhao, Y. Li, C. Wang and J. Zhao, *Nature Communications*, 2022, **13**, 1–11.

[66] S. Karmakar, S. Barman, F. A. Rahimi, D. Rambabu, S. Nath and T. K. Maji, *Nature Communications*, 2023, **14**, 1–13.

[67] Y. Chen, D. Wang, X. Deng and Z. Li, *Catalysis Science & Technology*, 2017, **7**, 4893–4904.

[68] Q. Zhang, S. Gao, Y. Guo, H. Wang, J. Wei, X. Su, H. Zhang, Z. Liu and J. Wang, *Nature Communications*, 2023, **14**, 1147.

[69] Q. Wu, R.-K. Xie, M.-J. Mao, G.-L. Chai, J.-D. Yi, S.-S. Zhao, Y.-B. Huang and R. Cao, *ACS Energy Letters*, 2020, **5**, 1005–1012.

[70] X. Chang, T. Wang and J. Gong, *Energy & Environmental Science*, 2016, **9**, 2177–2196.

[71] R. Kortlever, J. Shen, K. J. P. Schouten, F. Calle-Vallejo and M. T. Koper, *Journal of Physical Chemistry Letters*, 2015, **6**, 4073–4082.

[72] Z. Sun, T. Ma, H. Tao, Q. Fan and B. Han, *Chem*, 2017, **3**, 560–587.

[73] L. Wang, W. Chen, D. Zhang, Y. Du, R. Amal, S. Qiao, J. Wu and Z. Yin, *Chemical Society Reviews*, 2019, **48**, 5310–5349.

[74] T. M. Suzuki, H. Tanaka, T. Morikawa, M. Iwaki, S. Sato, S. Saeki, M. Inoue, T. Kajino and T. Motohiro, *Chemical Communications*, 2011, **47**, 8673–8675.

[75] R. Kuriki, K. Sekizawa, O. Ishitani and K. Maeda, *Angewandte Chemie International Edition*, 2015, **54**, 2406–2409.

[76] P. N. Nguyen, T. T. Tran, Q. A. Thi Nguyen, Y. Kawazoe, S. V. Vattikuti, L. V. Le, V. Q. Bui, T. M. Nguyen and N. N. Dang, *Journal of Materials Chemistry A*, 2023, **11**, 17145–17158.

[77] C. D. Windle, E. Pastor, A. Reynal, A. C. Whitwood, Y. Vaynzof, J. R. Durrant, R. N. Perutz and E. Reisner, *Chemistry – A European Journal*, 2015, **21**, 3746–3754.

[78] S. Y. Li, S. Meng, X. Zou, M. El-Roz, I. Telegeev, O. Thili, T. X. Liu and G. Zhu, *Microporous and Mesoporous Materials*, 2019, **285**, 195–201.

[79] L.-S. Hornberger and F. Adams, *Polymers*, 2022, **14**, 2778.

[80] P. Walden, *Bull. Acad. Imper. Sci. (St. Petersburg)*, 1914, **8**, 405–422.

[81] R. Giernoth, *Angewandte Chemie International Edition*, 2010, **49**, 2834–2839.

[82] N. V. Plechkova and K. R. Seddon, *Chemical Society Reviews*, 2007, **37**, 123–150.

[83] G. Gurau, H. Rodríguez, S. P. Kelley, P. Janiczek, R. S. Kalb and R. D. Rogers, *Angewandte Chemie International Edition*, 2011, **50**, 12024–12026.

[84] C. Wang, H. Luo, X. Luo, H. Li and S. Dai, *Green Chemistry*, 2010, **12**, 2019–2023.

[85] B. A. Rosen, A. Salehi-Khojin, M. R. Thorson, W. Zhu, D. T. Whipple, P. J. Kenis and R. I. Masel, *Science*, 2011, **334**, 643–644.

[86] C. Cadena, J. L. Anthony, J. K. Shah, T. I. Morrow, J. F. Brennecke and E. J. Maginn, *Journal of the American Chemical Society*, 2004, **126**, 5300–5308.

[87] G. Cui, J. Wang and S. Zhang, *Chemical Society Reviews*, 2016, **45**, 4307–4339.

[88] C. Hardacre, J. D. Holbrey, M. Nieuwenhuyzen and T. G. A. Youngs, *Accounts of Chemical Research*, 2007, **40**, 1146–1155.

[89] W. Zhang, H. Shimakoshi, N. Houfuku, X.-M. Song and Y. Hisaeda, *Dalton Transactions*, 2014, **43**, 13972–13978.

[90] S. Zulfiqar, M. I. Sarwar and D. Mecerreyes, *Polymer Chemistry*, 2015, **6**, 6435–6451.

[91] Q. Qian, P. A. Asinger, M. J. Lee, G. Han, K. Mizrahi Rodriguez, S. Lin, F. M. Benedetti, A. X. Wu, W. S. Chi and Z. P. Smith, *Chemical Reviews*, 2020, **120**, 8161–8266.

[92] H. Kaur, N. Devi, S. S. Siwal, W. F. Alsanie, M. K. Thakur and V. K. Thakur, *ACS Omega*, 2023, **8**, 9004–9030.

[93] J. F. Olorunyomi, S. T. Geh, R. A. Caruso and C. M. Doherty, *Materials Horizons*, 2021, **8**, 2387–2419.

[94] D. S. Khafaga, M. T. El-Morsy, H. Faried, A. H. Diab, S. Shehab, A. M. Saleh and G. A. Ali, *RSC Advances*, 2024, **14**, 30201–30229.

[95] D. Li, A. Yadav, H. Zhou, K. Roy, P. Thanasekaran and C. Lee, *Global Challenges*, 2024, **8**, 2300244.

[96] P. García-García, M. Müller and A. Corma, *Chemical Science*, 2014, **5**, 2979–3007.

[97] N. F. Suremann, B. D. McCarthy, W. Gschwind, A. Kumar, B. A. Johnson, L. Hammarström and S. Ott, *Chemical Reviews*, 2023, **123**, 6545–6611.

[98] X. Gao, B. Guo, C. Guo, Q. Meng, J. Liang and J. Liu, *ACS Applied Materials and Interfaces*, 2020, **12**, 24059–24065.

[99] R. Haldar, A. Ghosh and T. K. Maji, *Chemical Communications*, 2023, **59**, 1569–1588.

[100] I. Cota and F. Fernandez Martinez, *Coordination Chemistry Reviews*, 2017, **351**, 189–204.

[101] T. J. Ferreira, R. P. Ribeiro, J. P. Mota, L. P. Rebelo, J. M. Esperança and I. A. Esteves, *ACS Applied Nano Materials*, 2019, **2**, 7933–7950.

[102] W. J. Ji, Q. G. Zhai, S. N. Li, Y. C. Jiang and M. C. Hu, *Inorganic Chemistry Communications*, 2013, **28**, 16–19.

[103] F. P. Kinik, C. Altintas, V. Balci, B. Koyuturk, A. Uzun and S. Keskin, *ACS Applied Materials and Interfaces*, 2016, **8**, 30992–31005.

[104] J. H. Cavka, S. Jakobsen, U. Olsbye, N. Guillou, C. Lamberti, S. Bordiga and K. P. Lillerud, *Journal of the American Chemical Society*, 2008, **130**, 13850–13851.

[105] S. Diring, S. Furukawa, Y. Takashima, T. Tsuruoka and S. Kitagawa, *Chemistry of Materials*, 2010, **22**, 4531–4538.

[106] F. Azhari, D. W. Wulansari, W. Ciptonugroho, W. W. Lestari, A. Fitriyaningsih, U. S. Arrozi and Y. P. Budiman, *Research on Chemical Intermediates*, 2024, **50**, 5755–5779.

[107] F. Vermoortele, B. Bueken, G. Le Bars, B. Van De Voorde, M. Vandichel, K. Houthoofd, A. Vimont, M. Daturi, M. Waroquier, V. Van Speybroeck, C. Kirschhock and D. E. De Vos, *Journal of the American Chemical Society*, 2013, **135**, 11465–11468.

[108] A. Schaate, P. Roy, A. Godt, J. Lippke, F. Waltz, M. Wiebcke and P. Behrens, *Chemistry – A European Journal*, 2011, **17**, 6643–6651.

[109] A. H. Vahabi, F. Norouzi, E. Sheibani and M. Rahimi-Nasrabadi, *Coordination Chemistry Reviews*, 2021, **445**, 214050.

[110] K. Ling, M. M. Ogle, E. Flores, F. Godoy and A. A. Martí, *Journal of Photochemistry and Photobiology*, 2022, **11**, 100127.

[111] W. L. Xue, G. Q. Li, H. Chen, Y. C. Han, L. Feng, L. Wang, X. L. Gu, S. Y. Hu, Y. H. Deng, L. Tan, M. T. Dove, W. Li, J. Zhang, H. Dong, Z. Chen, W. H. Deng, G. Xu, G. Wang and C. Q. Wan, *Nature Communications*, 2024, **15**, 1–13.

[112] X. Zhao, Q. Xu, J. Han, W. Zhang, H. Rao, D.-Y. Du, P. She and J.-S. Qin, *ACS Applied Materials & Interfaces*, 2024, **16**, 26272–26279.

[113] M. C. Lawrence, C. Schneider and M. J. Katz, *Chemical Communications*, 2016, **52**, 4971–4974.

[114] E. Gong, S. Ali, C. B. Hiragond, H. S. Kim, N. S. Powar, D. Kim, H. Kim and S. I. In, *Energy & Environmental Science*, 2022, **15**, 880–937.

[115] S. Sorcar, Y. Hwang, C. A. Grimes and S. I. In, *Materials Today*, 2017, **20**, 507–515.

[116] S. Ali, M. C. Flores, A. Razzaq, S. Sorcar, C. B. Hiragond, H. R. Kim, Y. H. Park, Y. Hwang, H. S. Kim, H. Kim, E. H. Gong, J. Lee, D. Kim and S. I. In, *Catalysts*, 2019, **9**, 727.

[117] C. P. Mehnert, *Chemistry – A European Journal*, 2005, **11**, 50–56.

[118] R. Fehrmann, A. Riisager and M. Haumann, *Supported Ionic Liquids*, ed. R. Fehrmann, A. Riisager and M. Haumann, Wiley, 2014, pp. 1–474.

[119] M. Schörner, P. Rothgängel, K. Mitländer, D. Wisser, M. Thommes and M. Haumann, *ChemCatChem*, 2021, **13**, 4192–4200.

[120] C. P. Mehnert, R. A. Cook, N. C. Dispenziere and M. Afeworki, *Journal of the American Chemical Society*, 2002, **124**, 12932–12933.

[121] K. Stagel and K. Bica-Schröder, *European Journal of Organic Chemistry*, 2024, **27**, e202400917.

[122] P. Mikšovsky, E. N. Horn, S. Naghdi, D. Eder, M. Schnürch and K. Bica-Schröder, *Organic Process Research and Development*, 2022, **26**, 2799–2810.

[123] W. Schwieger, T. Selvam, M. Klumpp and M. Hartmann, *Supported Ionic Liquids: Fundamentals and Applications*, 2014, 37–74.

[124] J. Schneider, M. Matsuoka, M. Takeuchi, J. Zhang, Y. Horiuchi, M. Anpo and D. W. Bahnemann, *Chemical Reviews*, 2014, **114**, 9919–9986.

[125] S. Kreft, D. Wei, H. Junge and M. Beller, *EnergyChem*, 2020, **2**, 100044.

[126] A. Pougin, M. Dilla and J. Strunk, *Physical Chemistry Chemical Physics*, 2016, **18**, 10809–10817.

[127] M. Dilla, R. Schlögl and J. Strunk, *ChemCatChem*, 2017, **9**, 696–704.

[128] N. G. Moustakas and J. Strunk, *Chemistry – A European Journal*, 2018, **24**, 12739–12746.

Appendix A:

Supplementary information for

Boosting Visible-Light Carbon Dioxide Reduction with Imidazolium-Based Ionic Liquids

ChemCatChem 16:e202301454 (2024)

Authors: Lisa Eisele, Wilaiwan Chaikhan, Samar Batool, Alexey Cherevan, Dominik Eder, and Katharina Bica-Schröder

ChemCatChem

Supporting Information

Boosting Visible-Light Carbon Dioxide Reduction with Imidazolium-Based Ionic Liquids

Lisa Eisele, Wilaiwan Chaikhan, Samar Batool, Alexey Cherevan, Dominik Eder,* and Katharina Bica-Schröder*

Supporting information:

Boosting Visible-Light Carbon Dioxide Reduction with Imidazolium-Based Ionic Liquids

Lisa Eisele [a], Wilaiwan Chaikhan[a], Samar Batool [b], Alexey Cherevan [b], Dominik Eder [b] and Katharina Bica-Schröder *[a]

[a] L. Eisele, W. Chaikhan, Prof. K. Bica-Schröder
Institute of Applied Synthetic Chemistry
TU Wien
Getreidemarkt 9/163 1060 Wien, Austria
E-mail: katharina schroeder@tuwien.ac.at

[b] S. Batool, Dr. A. Cherevan, Prof. D. Eder
Institute of Materials Chemistry
TU Wien
Getreidemarkt 9/165 1060 Wien, Austria
E-mail: domink.eder@tuwien.ac.at

Table of contents

Calculations of yield in moles, TON and TOF: 2
Table S1: Overview Table 3
Figure S1: Photocatalytic CO_2 reduction in DMF 4
Figure S2: Photocatalytic CO_2 reduction in DMSO 5
Table S2: Side chain functionalized IL 6
Figure S3: IR of CO_2-saturated IL solution 6
Figure S4: NMR of **1d** in CO_2 -saturated solution 7
Figure S5: NMR of 1d and TEOA in CO_2 -saturated solution 8
Figure S6: ^{13}C NMR of 1d with TEOA and water bubbled with CO_2 9
Figure S7: UV-Vis spectra of all components and emission spectra of LED light source: .. 10
Figure S8: Reaction setup 9

Calculations of yield in moles, TON and TOF:

Reactor parameters:

Reactor volume (ml)	3.7
Reaction volume (ml)	1.5
Reactor headspace (ml)	2.2
Reaction time (sec)	3600

Conversion from ppm to Gas volume in mL:

$$Gas\ volume\ in\ mL = \frac{ppm \times Reactor\ headspace\ (mL)}{10^9}$$

Calculation of gas amount in moles by ideal gas law:

$$n(\mu mol) = \frac{pV}{RT}$$

With parameters:

P is pressure = 101.325 Pa

R is gas constant = 8.314 J mol^{-1} K^{-1}

T is temperature = 295 K

Turnover number (TON) is calculated as following:

$$TON = \frac{nomber\ of\ moles\ of\ CO}{number\ of\ moles\ of\ catalyst}$$

The turnover frequency (TOF) can be calculated from TON divided by the reaction time in minutes:

$$TOF\ (min^{-1}) = \frac{TON}{time\ [min]}$$

The instant TOF is defined as the first derivative (d) of TON against time:

$$Instant\ TOF(min^{-1}) = \frac{d\ (TON)}{d(time\ )}$$

Table S1: Overview Table

Table S1: CO, H_2 and CH_4 formation in solvents DMF, MeCN and DMSO.

Solvent	ionic liquid	CO [µmol]	H_2 [µmol]	TON[a]	Selectivity[b]
DMF	Reference	0.29	3.7E-03	3	98.75
	1a	3.53	2.0E-03	39	99.94
	1b	1.93	1.3E-02	21	99.30
	1c	0.01	0.0E+00	0	100.00
	1d	5.35	9.3E-04	59	99.98
	1e	1.24	8.7E-07	14	99.93
	1f	0.15	6.6E-04	2	99.34
	1g	0.06	0.0E+00	1	100.00
MeCN	Reference	1.46	5.8E-02	19	96.14
	1a	3.25	3.8E-03	17	99.88
	1b	1.84	4.0E-02	19	97.84
	1c	0.00	0.0E+00	5	46.47
	1d	5.19	4.3E-03	49	99.91
	1e	1.07	6.1E-03	35	99.43
	1f	1.12	1.0E-01	2	91.67
	1g	0.85	2.2E-02	1	97.45
DMSO	Reference	1.75	6.9E-03	16	98.89
	1a	1.56	3.1E-03	36	99.24
	1b	1.75	4.5E-03	20	99.45
	1c	0.49	9.5E-04	0	99.39
	1d	4.38	3.2E-03	58	99.87
	1e	3.14	9.1E-03	12	99.13
	1f	0.17	0.0E+00	12	99.61
	1g	0.10	0.0E+00	9	99.78

Conditions: 0.6 mM $[Ru(bpy)_3](PF_6)_2$, 0.06 mM $[Re(bpy)(CO)_3]Cl$, 0.32 M TEOA, 0.1 g/mL IL; t = 1 h, T = 22 °C. . [a] Calculated for CO. [b] Selectivity for CO

Figure S1: Photocatalytic CO_2 reduction in DMF

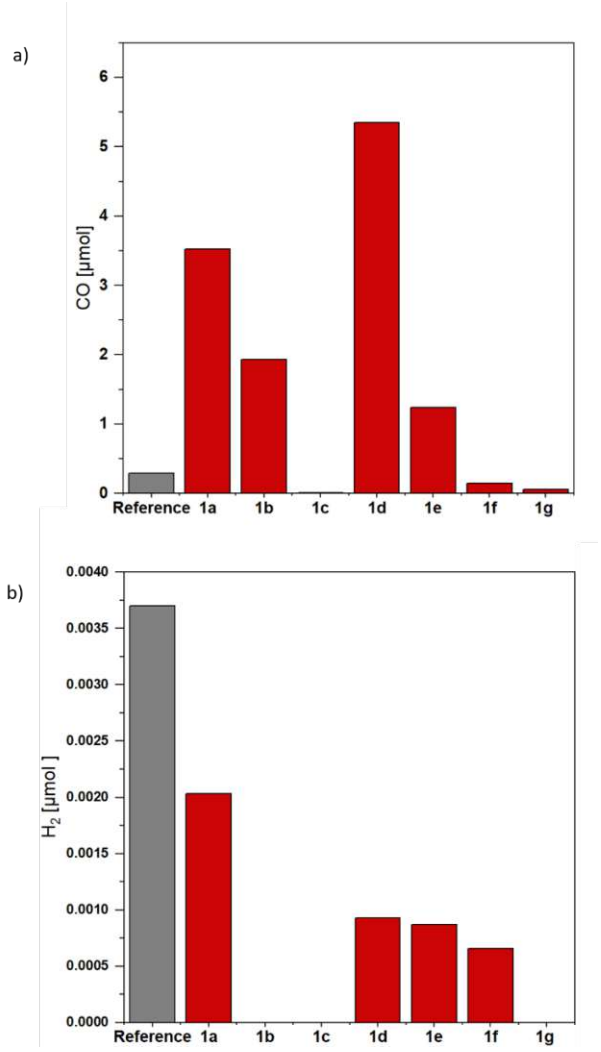

Figure S1: CO formation in the photocatalytic screening of ILs in the solvent DMF. Conditions: 0.6 mM $[Ru(bpy)_3](PF_6)_2$, 0.06 mM $[Re(bpy)(CO)_3]Cl$, 0.32 M TEOA, 0.1 g/mL IL; t = 1 h, T = 22 °C.

Figure S2: Photocatalytic CO_2 reduction in DMSO

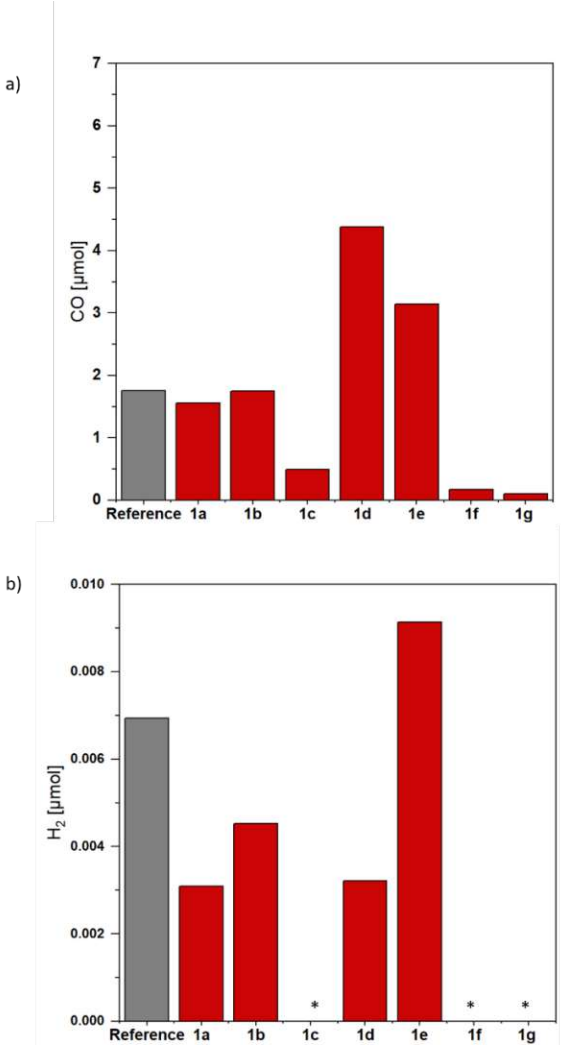

Figure S2: CO formation in the photocatalytic screening of ILs in the solvent DMSO. Conditions: 0.6 mM $[Ru(bpy)_3](PF_6)_2$, 0.06 mM $[Re(bpy)(CO)_3]Cl$, 0.32 M TEOA, 0.1 g/mL IL; t = 1 h, T = 22 °C.

Table S2: Side chain functionalized IL

Table S2: Photocatalytic yields with **2f**.

Solvent	CO [µmol]	H_2 [µmol]	CH_4 [µmol]
MeCN	0.47	0.18	0
DMF	1.46	0.01	0
DMSO	1.47	0	0

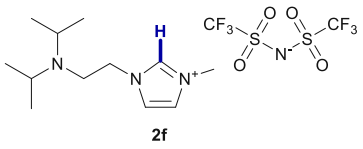

2f

Figure S3: IR of CO_2-saturated IL solution

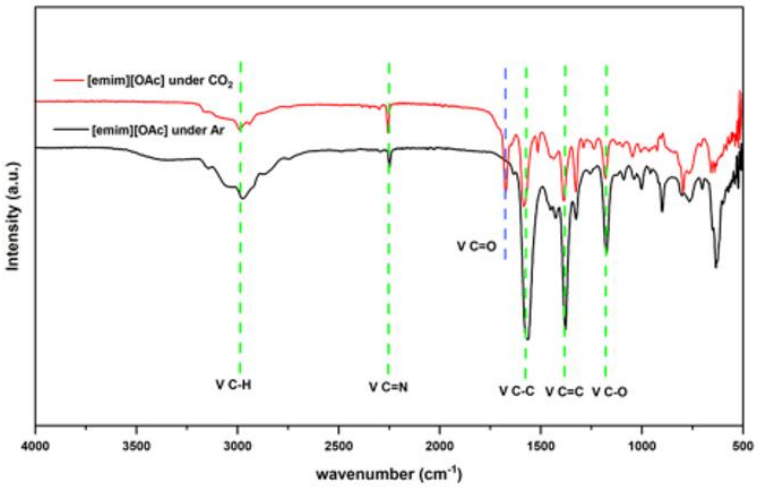

Figure S3: IR of CO_2 purged solution of **1d** in MeCN.

Figure S4: NMR of **1d** in CO_2-saturated solution

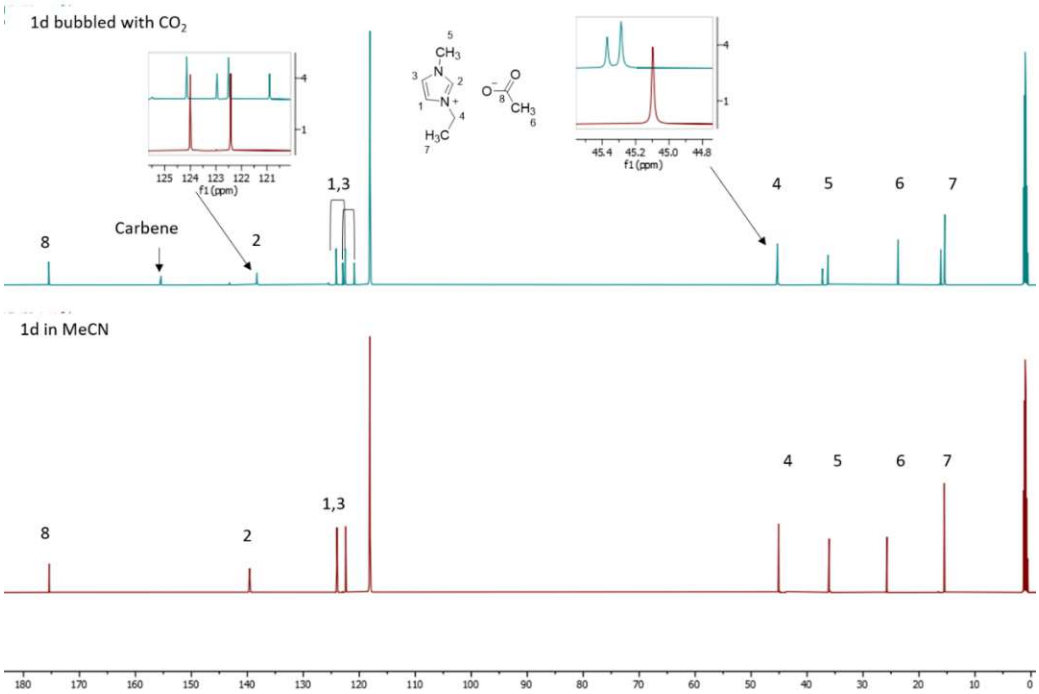

Figure S4: ^{13}C NMR of **1d** in MeCN (bottom) and CO_2 bubbled sample (top).

Figure S5: NMR of 1d and TEOA in CO_2 -saturated solution

a)

b)

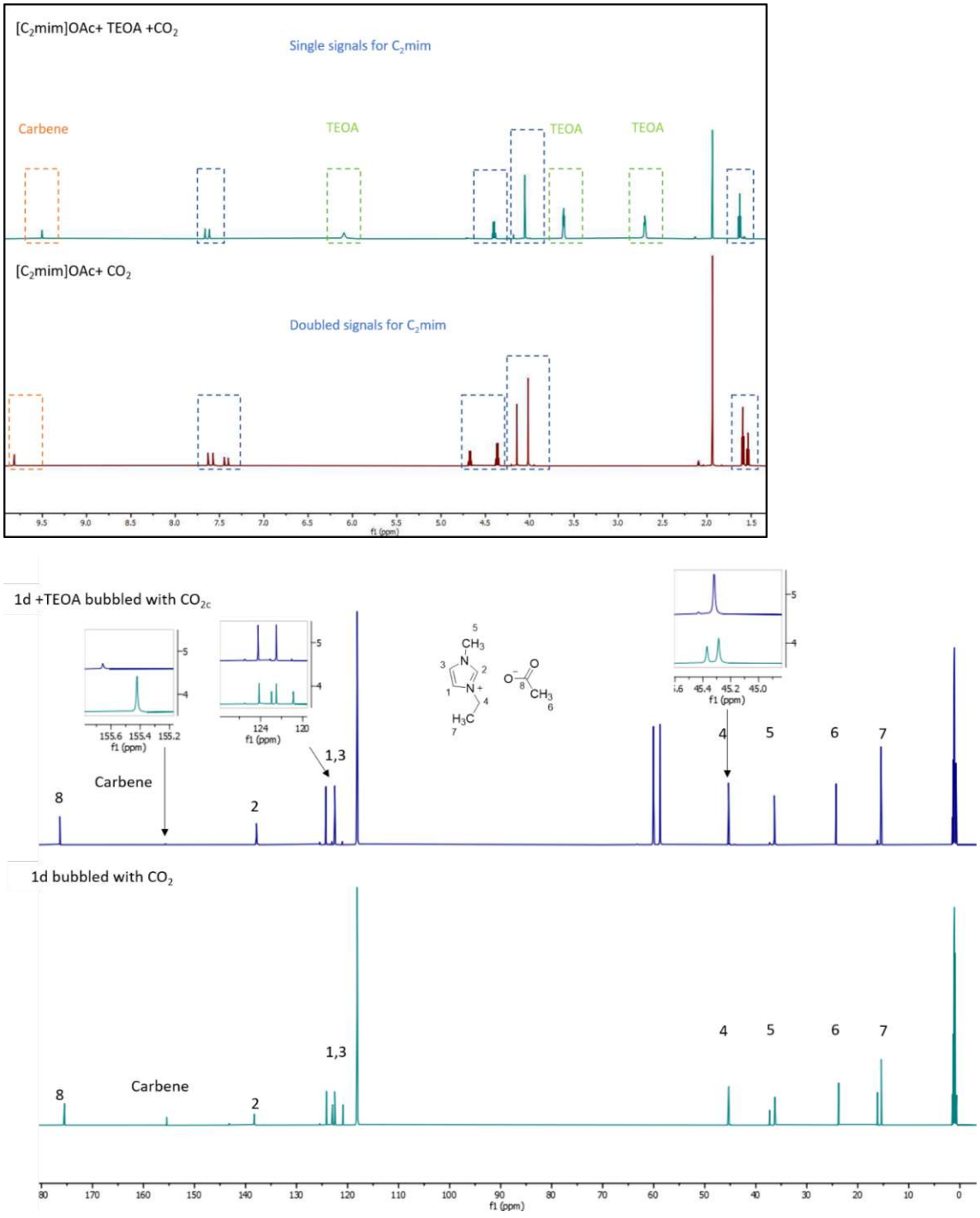

Figure S5: ^{1}H NMR of **1d** in CO_2 saturated solution (bottom) and **1d** and TEOA (top) in CO_2 saturated solution (a) and ^{13}C NMR of **1d** in CO_2 saturated solition (bottom) and **1d** and TEOA in CO_2 saturated solution (b).

Figure S6: ^{13}C NMR of 1d with TEOA and water bubbled with CO_2

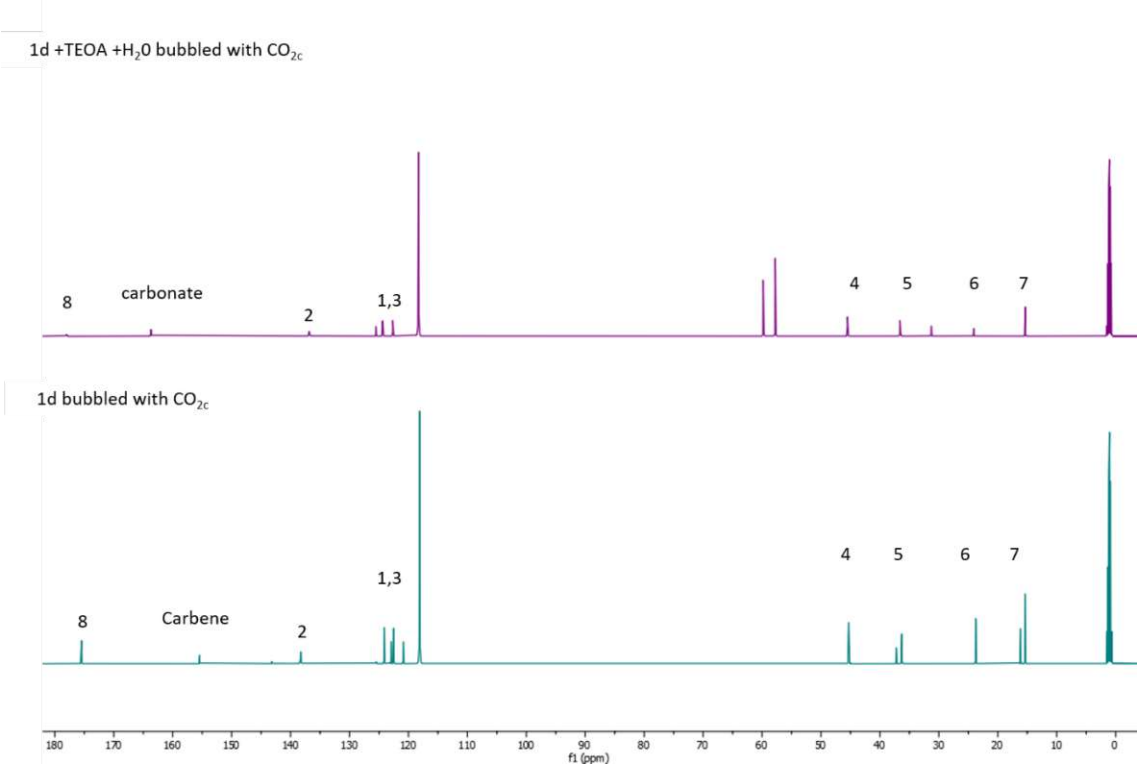

Figure S6: ^{13}C NMR of **1d** in MeCN, bubbled with CO_2 (bottom) compared with a sample that contains both **1d** TEOA and water bubbled with CO_2 (top).

Figure S7: Reaction setup

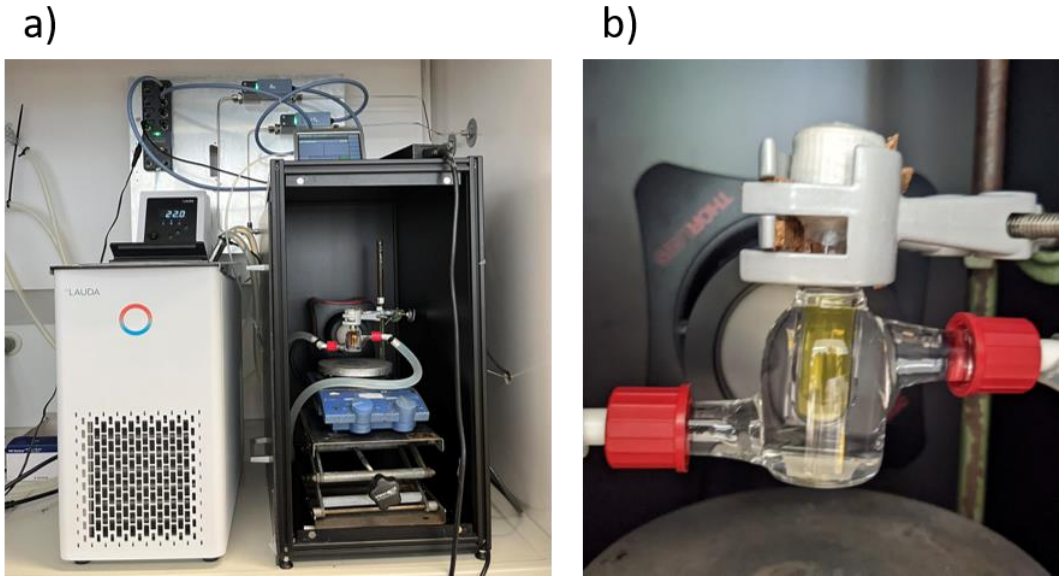

Figure S7: Photocatalytic CO_2 reduction setup (a) and a closeup of the reactor (b)

Figure S8: UV-Vis spectra of all components and emission spectra of LED light source:

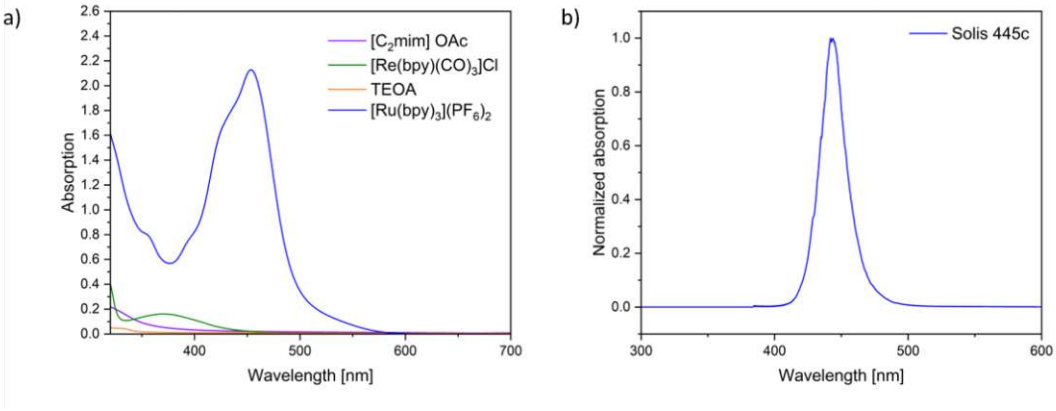

Figure S8: UV-Vis of $[Ru(bpy)_3](PF_6)_2$ (blue), $[Re(bpy)(CO)_3]Cl$ (green), $[C_2mim]OAc$ (violett), and TEOA (orange) (a) and (b) emission spectra of Solis 445c light source.

Appendix B:

Supplementary information for

Polymerized Ionic Liquid Co-Catalysts Driving Photocatalytic Carbon Dioxide Transformation

RSC Sustainability 9, 2524-2531 (2024)

Authors: Lisa Eisele, Blete Hulaj, Maximilian Podsednik, Franchesco Laudani, Pablo Ayala, Alexey Cherevan, Annette Foelske, Andreas Limbeck, Dominik Eder and Katharina Bica-Schröder

Polymerized Ionic Liquid Co-Catalysts Driving Photocatalytic CO_2 Transformation

Lisa Eisele [a], Bletë Hulaj [a], Maximilian Podsednik [b],Francesco Laudani [c], Pablo Ayala [d], Alexey Cherevan [d], Annette Foelske [c], Andreas Limbeck [e], Dominik Eder [d*] and Katharina Bica-Schröder [a*]

Contents

S1 Fourier transform infrared spectroscopy of synthesized materials: 2
S2 Thermogravimetric analysis of polymers: 2
S3 XPS Survey spectra of CLP-1: 3
S4 XPS detailed scans of Cl 2p: 3
S5 XPS detailed scans of N 1s: 4
S6 LA-ICP-MS scan lines: 4
S7 EDX scans of sample particles: 5
S8 UV-Vis spectroscopy of aged reaction solution: 5
S9 Calculations of Reaction parameters: 5

S1 Fourier transform infrared spectroscopy of synthesized materials:

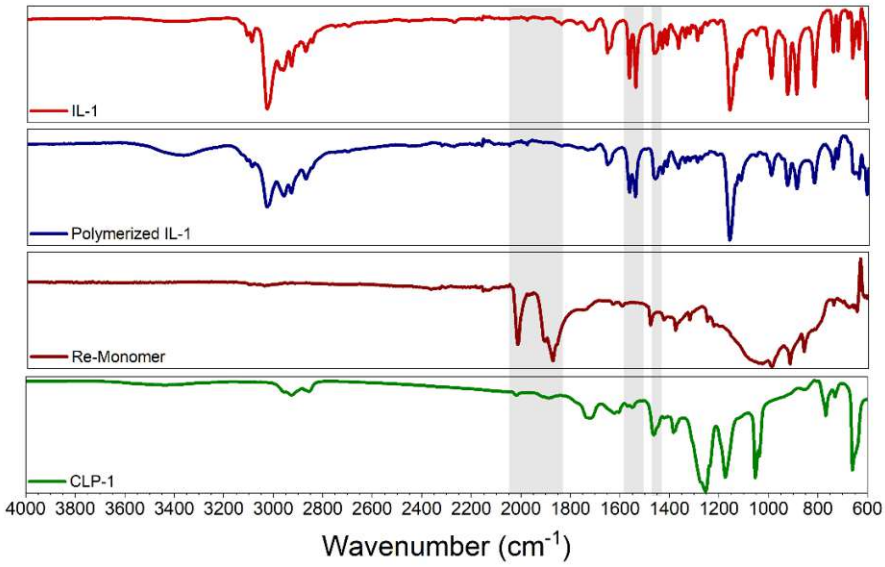

Figure S1: FT-IR spectroscopy of ionic liquid (IL-1)(red), polymerized ionic liquid (PIL) (blue), Re-Monomer (and CLP-1

S2 Thermogravimetric analysis of polymers:

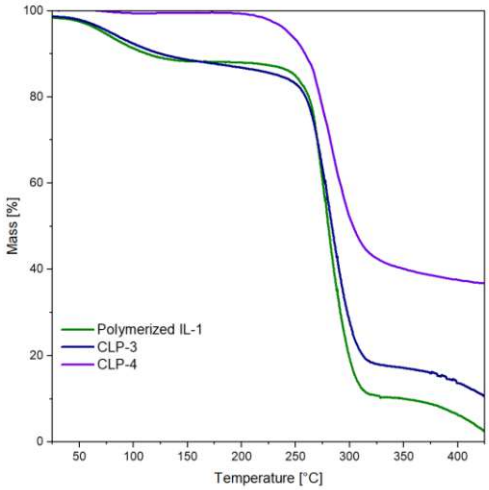

Figure S2: TGA of polymerized IL-1, CLP-3 and CLP-4

S3 XPS Survey spectra of CLP-1:

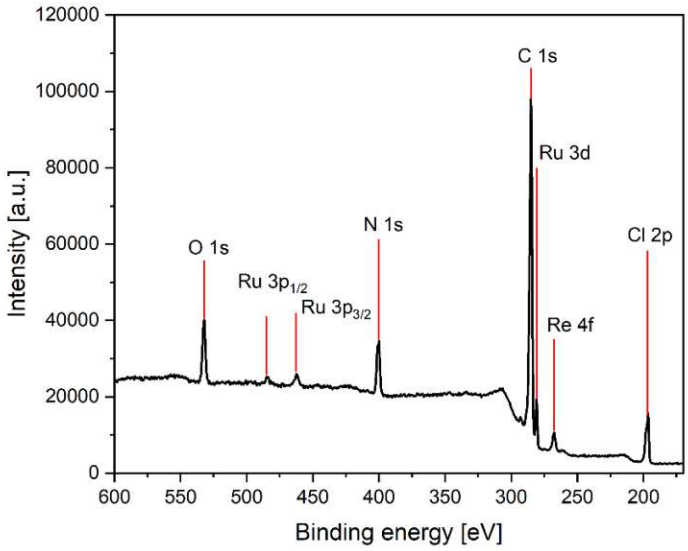

Figure S3: XPS Survey spectra of CLP-1.

S4 XPS detailed scans of Cl 2p:

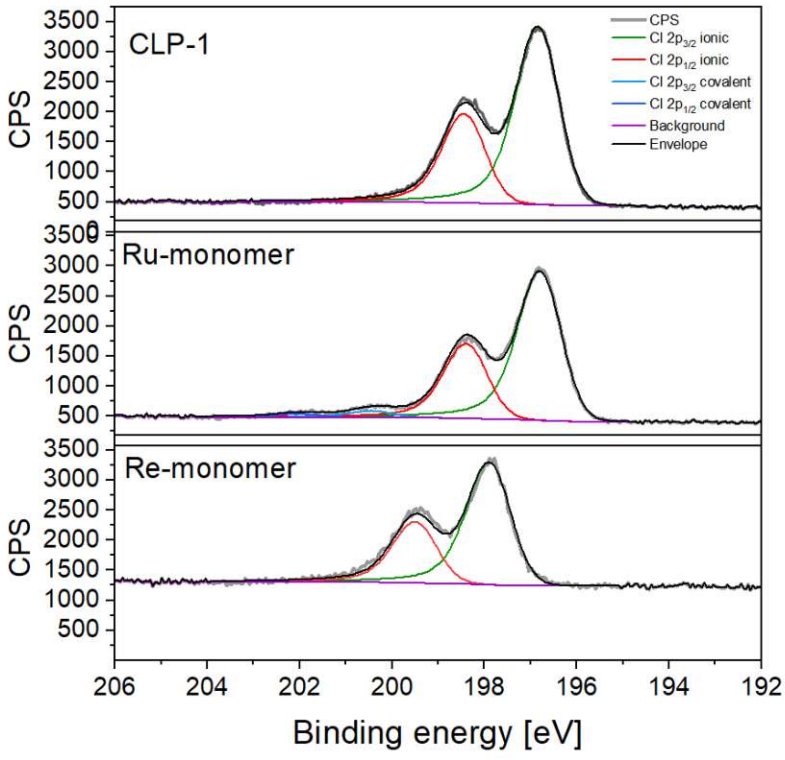

Figure S4: XPS detailed scans of Cl 2p.

S5 XPS detailed scans of N 1s:

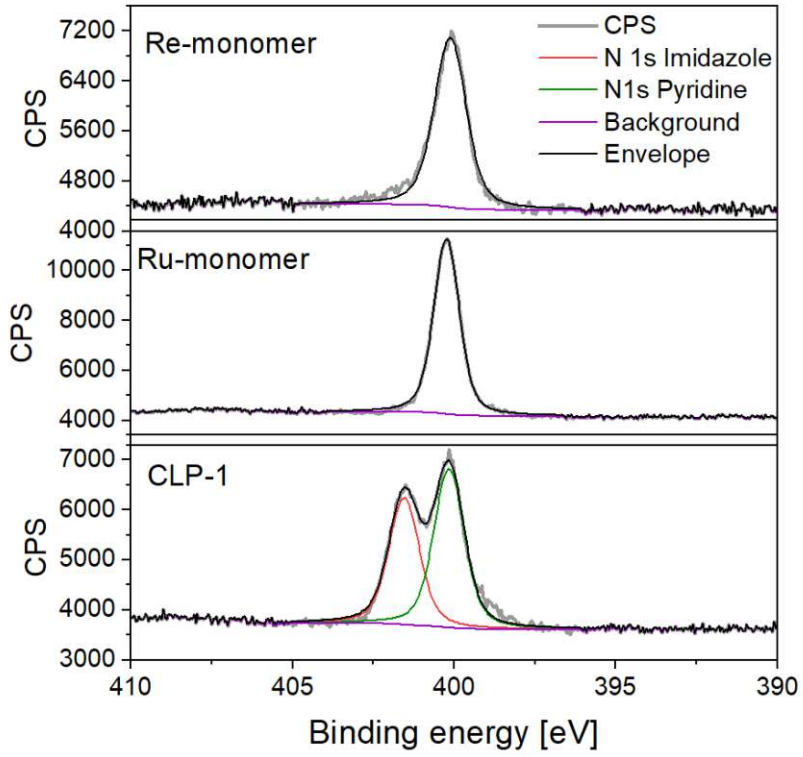

Figure S5: XPS scans of N 1s.

S6 LA-ICP-MS scan lines:

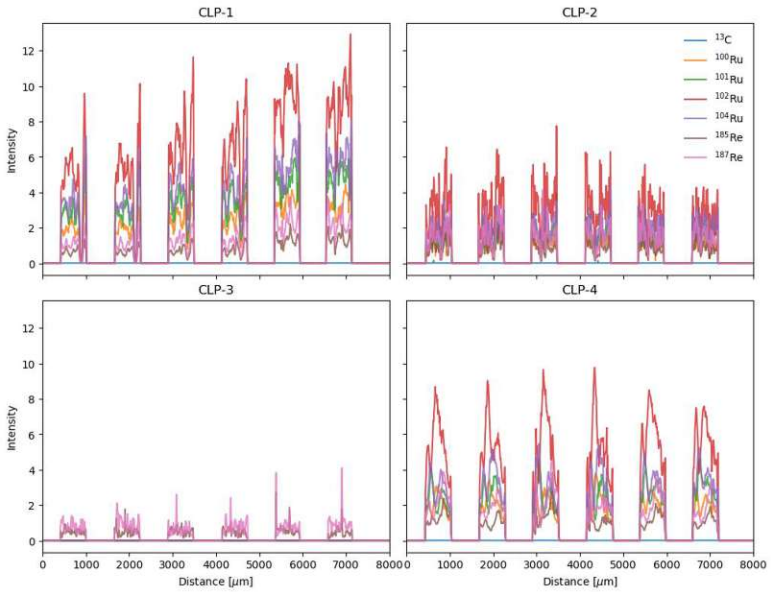

Figure S6: LA-ICP-MS Scans of isotopes in polymers CLP-1 to CLP-4

S7 EDX scans of sample particles:

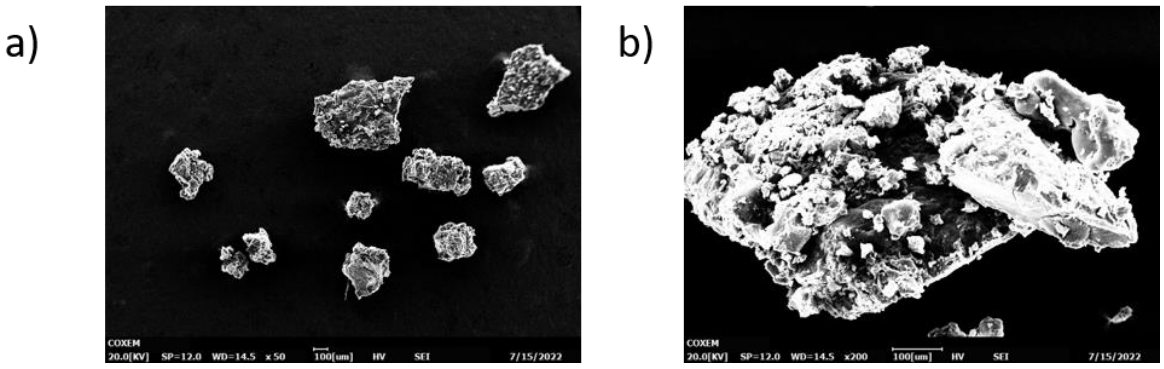

Figure S7: EDX Scans of sample particles of CLP-1. Several particles (a) and closeup (b).

S8 UV-Vis spectroscopy of aged reaction solution:

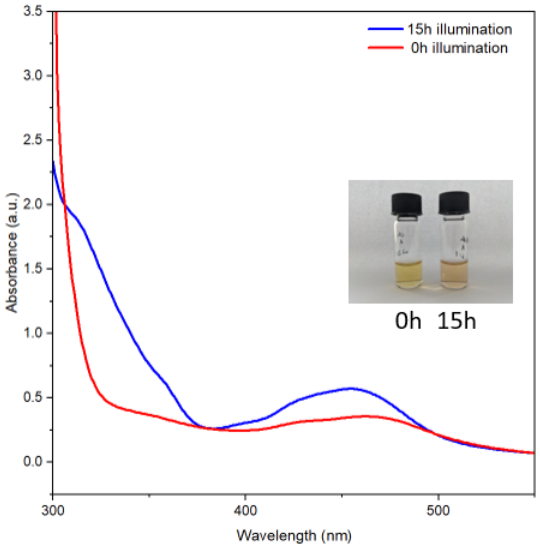

Figure 8: UV Vis spectra of reaction solution after 15h of illumination (blue) and 0h of illumination (red).

S9 Calculations of Reaction parameters:

Reactor parameters:

Reactor volume (ml)	3.7
Reaction volume (ml)	1.5
Reactor headspace (ml)	2.2
Reaction time (sec)	53000

Conversion from ppm to Gas volume in mL:

$$Gas\ volume\ in\ mL = \frac{ppm \times Reactor\ headspace\ (mL)}{10^9}$$

Calculation of gas amount in moles by ideal gas law:

$$n(\mu mol) = \frac{pV}{RT}$$

With parameters:

P is pressure = 101.325 Pa

R is gas constant = 8.314 J mol^{-1} K^{-1}

T is temperature = 295 K

Turnover number (TON) is calculated as following:

$$TON = \frac{nomber\ of\ moles\ of\ CO}{number\ of\ moles\ of\ catalyst}$$

The turnover frequency (TOF) can be calculated from TON divided by the reaction time in minutes:

$$TOF\ (min^{-1}) = \frac{TON}{time\ [min]}$$

The instant TOF is defined as the first derivative (d) of TON against time:

$$Instant\ TOF(min^{-1}) = \frac{d\ (TON)}{d(time\ )}$$

Appendix C:

Supplementary information for

Imidazolium modified UiO-67 metal-organic frameworks for CO_2 absorption

Manuscript in preparation

Authors: Lisa Eisele, Jakob Blaschke, Shaghayegh Naghdi, Dominik Eder and Katharina Bica-Schröder

Supporting Information

Lisa Eisele,[†] Jakob Blaschke,[‡] Shaghayegh Naghdi,[‡] Dominik Eder,[*,‡] and Katharina Bica-Schröder[*,†]

[†]*Institute of Applied Synthetic Chemistry, TU Wien, Getreidemarkt 9/163, 1060 Wien*

[‡]*Institute of Materials Chemistry, TU Wien, Getreidemarkt 9/165, 1060 Wien*

E-mail: dominik.eder@tuwien.ac.at; katharina.schroeder@tuwien.ac.at

Materials

The materials for the synthesis of ligands, including methyl-4-bromo-3-methylbenzoate and 4-methoxycarbonylphenylboronic acid, were purchased from commercial suppliers. $ZrCl_4$ was purchased from Fischer Scientific. All chemicals were used in analytical grade without further purification. The solvents dimethylformamide (DMF) and methanol (MeOH) were used in technical grade.

Methods

Microwave synthesis was carried out using a Monowave200 from Anton Paar with 30 mL reaction vessels.

FT-IR spectra in ATR mode were recorded on a PerkinElmer spectrum 65 FTIR spectrometer. ^{1}H NMR spectra were recorded with a Bruker Avance NEO 400 MHz spectrometer. Chemical shifts were reported in ppm from TMS with a solvent resonance as the internal standard.

Thermogravimetric analysis (TGA) was performed using a PerkinElmer TGA 8000 instrument. The samples were placed in Al_2O_3 crucibles and heated at a rate of 5 °C min^{-1} in air

and carbon dioxide atmospheres, over a temperature range of 25 to 700 °C.

Powder XRD spectra were obtained using a PANalytical X'Pert Pro MPD ($\Theta - \Theta$ diffractometer). The sample was prepared on a silicon sample holder and exposed to a copper X-ray source (8.04 keV, 1.5406 $\mathring{A}$) collecting data in Bragg–Brentano (Θ/Θ geometry over a 5 ° to 80 ° angular range using a semiconductor X'Celerator detector with a 2.1 ° detection angle.

Carbon dioxide chemisorption was investigated with a Belcat II chemisorption analyzer (MicrotracBEL Corp.) equipped with a thermal conductivity detector (TCD), performing temperature-programmed desorption experiments. In a typical experimental sequence, the sample was pre-heated to 150 °C for 1 h under Helium flow at a rate of 50 mL min^{-1}. The temperature was hold for 30 min. The preconditioned sample was cooled to 50 °C under He and the temperature was hold for 30 min, Conscecutiveley, the sample was exposed to CO_2 for 1h, and purged with He for another 30 min followed by heating to 300 °C with a heating rate of 10 °C min^{-1}.

Diffuse reflectance infrared Fourier transform spectroscopy (DRIFTs) was measured with an IR Tracer-100 under CO_2 atmosphere. The instrument was equipped with Praying Mantis™ High Temperature Reaction Chamber in a Praying Mantis™ Diffuse Reflection Kit Housing by Harrick Scientific Products. The reaction cell was equipped with a Peltier-Element for temperature control of the sample and water cooling of the surroundings. The housing was purged with dry air. The reaction chamber was connected to mass flow controllers (Burkert) providing Helium and CO_2 flow. A typical sequence started with a heat out of the sample (130 °C, 2h), followed by cooling to the measurement temperature of 30 °C. CO_2 was introduced by purging with a flow of 5% CO_2 in He with a flow rate of 20 mL min^{-1}.

Synthesis

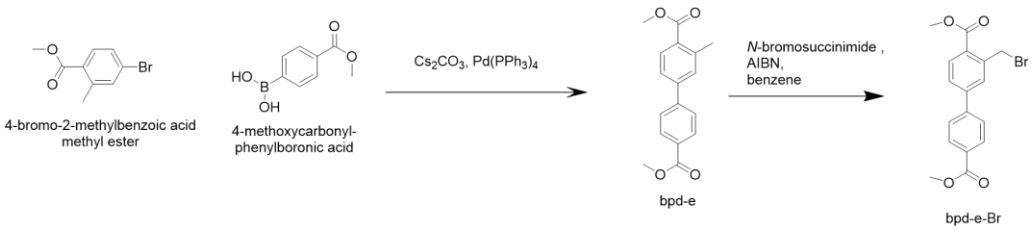

Figure 1: Synthesis of bpd-e and bpd-e-Br.

3-Methyl-4,4'-biphenyl dicarboxylic acid dimethyl ester (bpd-e)

4-bromo-2-methylbenzoic acid methyl ester (3.09 g, 1.3 mmol) and 4-methoxycarbonyphenyl-boronic acid (2.4 g, 1.3 mmol) were added under Argon to a microwave vial. Anhydrous DMF (40 mL) was added together with $Pd(PPh_3)_4$ (468 mg, 0.04 mmol) and Cs_2CO_3 (6.60 g, 2 mmol). The mixture was heated under Argon at 80 °C for 48h. After cooling to room temperature water (20 mL) and ethyl acetate (20 mL) were added and the aqueous phase was extracted with ethyl acetate . The organic layers were washed with brine and dried over sodium sulfate. The solvent was removed and the crude product was purified by column chromatography (PE:EE 10:1). The product bpd-e was isolated as a white solid (3.0 g, 77% yield).

^{1}H NMR (400 MHz, $CDCl_3$) δ 8.13 – 8.08 (m, 2H), 7.97 (d, J = 1.8 Hz, 1H), 7.91 (dd, J = 8.0, 1.7 Hz, 1H), 7.42 – 7.36 (m, 2H), 7.29 (d, J = 7.9 Hz, 1H), 3.94 (d, J = 4.8 Hz, 6H), 2.30 (s, 3H).

3-Methyl-4,4'-biphenyldicarboxylic acid dimethyl ester (bpd-e-Br)

The starting material bpd-e (0.84 g, 3 mmol) was combined with *N*-bromosuccinimide (0.6 g, 3.4 mmol), AIBN (0.05 g, 0.0.3 mmol) and benzene (20 mL) and stirred at 80°C overnight. After removal of the solvent under vacuum, the crude product was purified by column chromatography on silica using a light petrol -ethyl acetate (10:1 v/v) as the eluent. The product,

bpd-e-Br, was obtained as an orange solid (0.83 g, 78%).

^{1}H NMR (400 MHz, $CDCl_3$) δ 8.22 (d, J = 1.7 Hz, 1H), 8.16 – 8.12 (m, 2H), 8.02 (dd, J = 8.0, 1.8 Hz, 1H), 7.56 – 7.51 (m, 2H), 7.34 (d, J = 8.0 Hz, 1H), 4.42 (s, 2H), 3.96 (s, 6H).

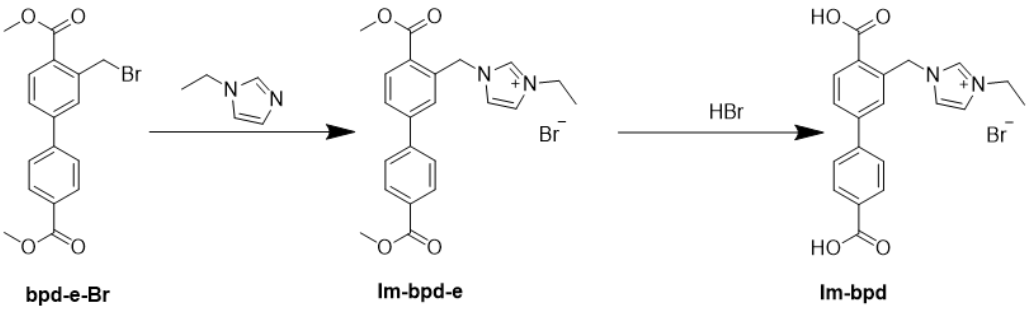

Figure 2: Synthesis of imidazolium-modified linker Im-bpd-e and Im-bpy.

Im-bpd-e and Im-bpd

The starting material bpd-e-Br (0.73 g, 2 mmol) was mixed with 1-methylimidazole (2 mmol, 0.19 g) in acetonitrile (30 mL) and stirred at 80°C overnight. The mixture was cooled to room temperature and the solvent was removed to obtain Im-bpd-e as a crude product. The crude was mixed with HBr in excess and refluxed for 12h to obtain Im-bpd as a colourless precipitate. The final product was dried under vacuum (90%, 0.63 g).

^{1}H NMR (400 MHz, DMSO) δ 8.78 (d, J = 1.7 Hz, 1H), 8.06 (dd, J = 7.9, 1.8 Hz, 1H), 8.04 – 7.97 (m, 3H), 7.68 (t, J = 1.8 Hz, 1H), 7.49 – 7.37 (m, 4H), 5.50 (s, 2H), 4.06 (q, J = 7.3 Hz, 2H), 1.28 (d, J = 7.3 Hz, 3H).

Im-MOF

Im-bpd (17.57 mg, 0.05 mmol) and bpd (109.0 mg, 0.45 mmol) were combined in a vial with 4 mL of DMF and sonicated in an ultrasonic bath. Concurrently, a 30 mL microwave vial was charged with $ZrCl_4$ (116,5 mg, 0.5 mmol), followed by the addition of 4 mL of DMF and 860 μL of acetic acid. The solution was then transferred into the microwave vial, and an additional 1 mL of DMF was added. The microwave vial was sealed and heated to 120°C

for 2 hours.

The resulting crude product was isolated using a microfiltration setup, followed by washing twice with 30 mL of DMF and three times with MeOH. The product was subsequently dried under vacuum at 60°C and activated under vacuum at 120°C.

Material characterization

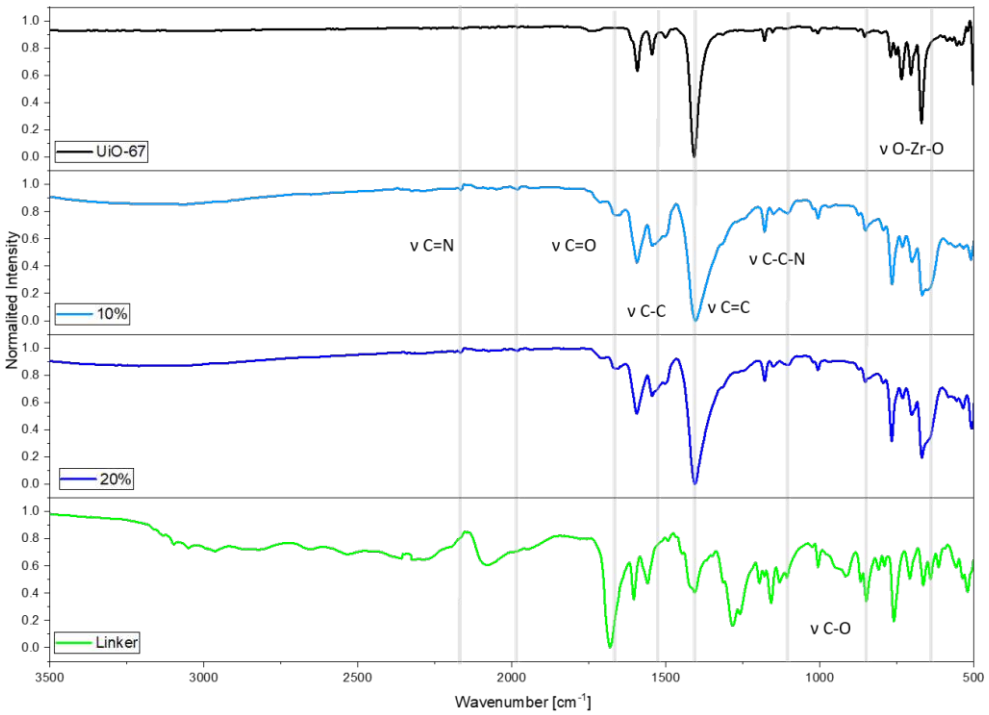

Figure 3: Infrared spectroscopy of synthesized MOFs.

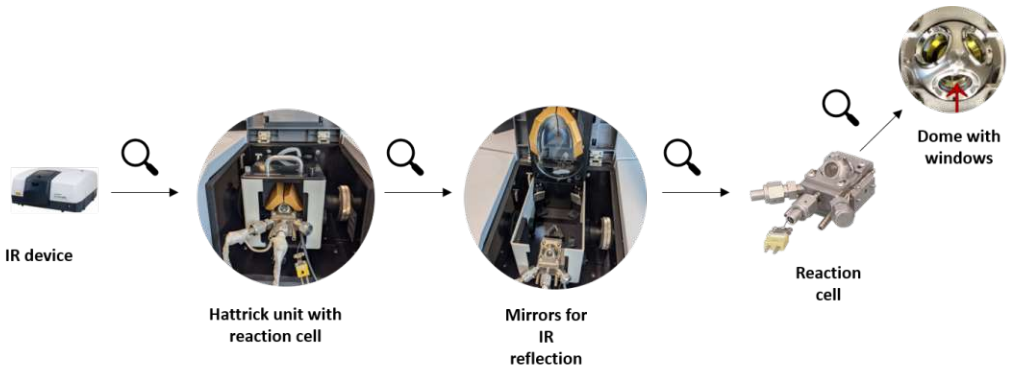

Figure 4: DRIFTS setup for in-situ characterisation.

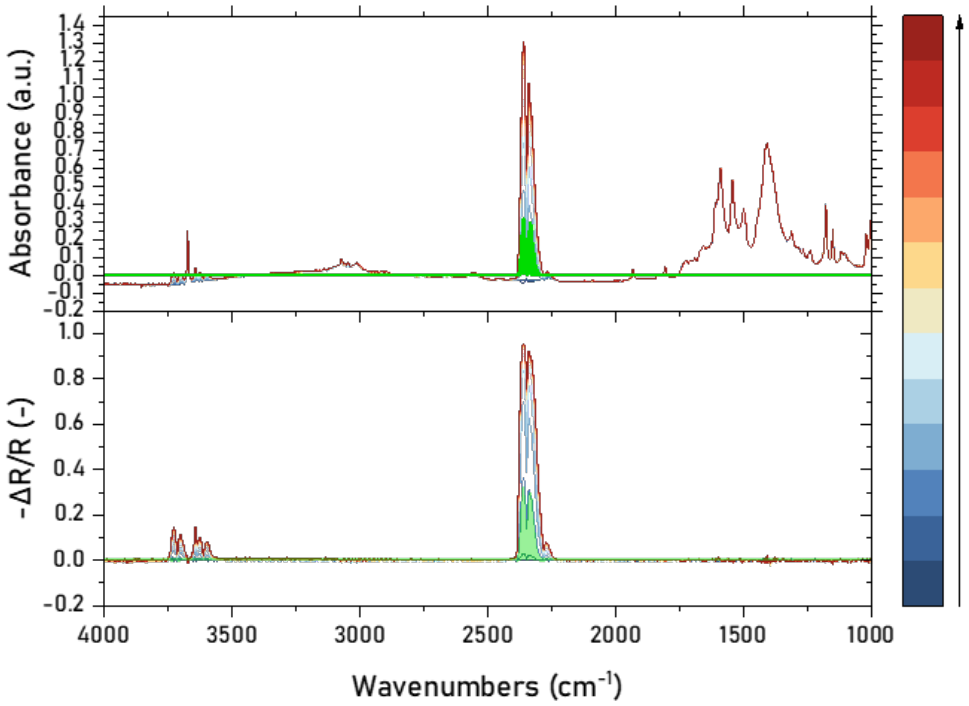

Figure 5: Overview DRIFTS spectra under CO_2 exposure. Conditions: 5% CO_2 in He 10 mL min $^{-1}$, T= 30°C, timescale: 10 min, reference spectra of gas phase CO_2 is shown in green.

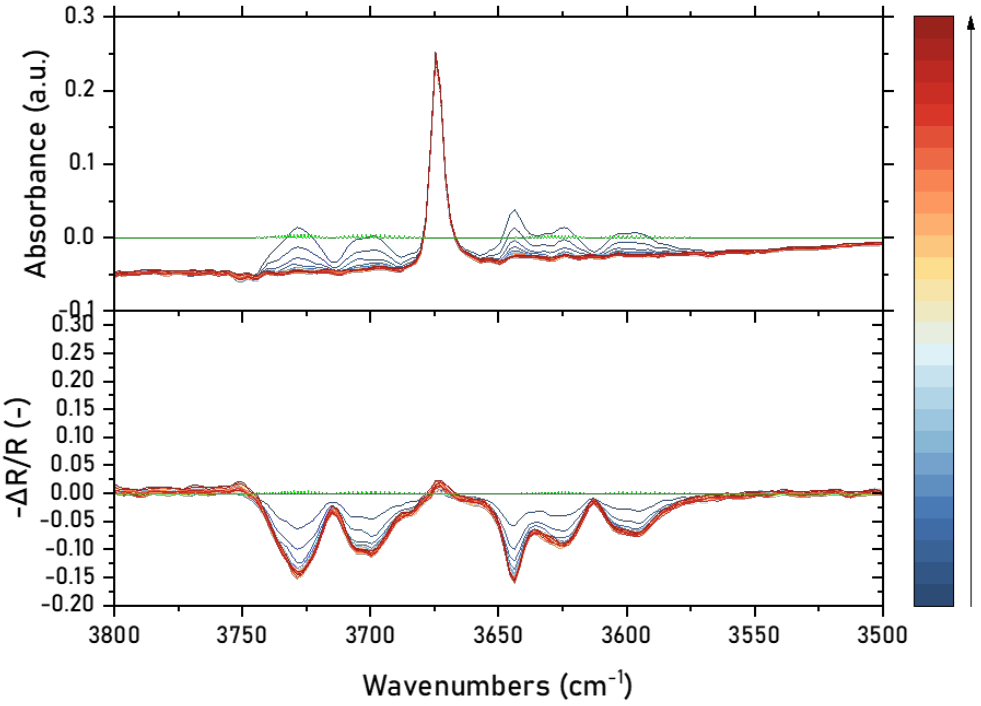

Figure 6: Time-resolved DRIFTS spectra of UiO-67 in the range from 3800 cm^{-1} to 3500 cm^{-1} exposed to CO_2 under He purge. The spectra exhibit features related to ν_{as}(O-H) vibrations, which decrease during He purging. Conditions: He at 10 mL min^{-1}, T = 30 °C, timescale: 1 h 30 min. The reference spectrum of gas-phase CO_2 is shown in green.

D. General Appendix

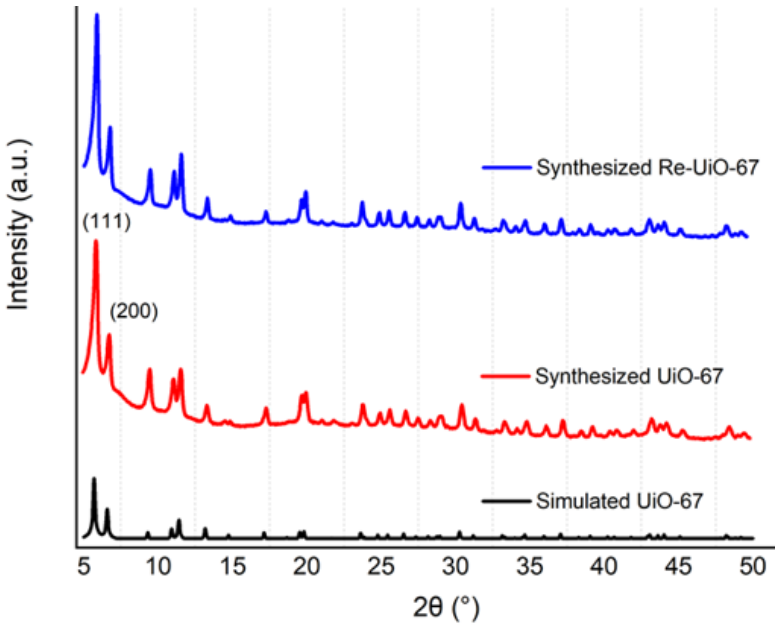

Figure 4.1. XRD of Re-UiO-67 and UiO-67.

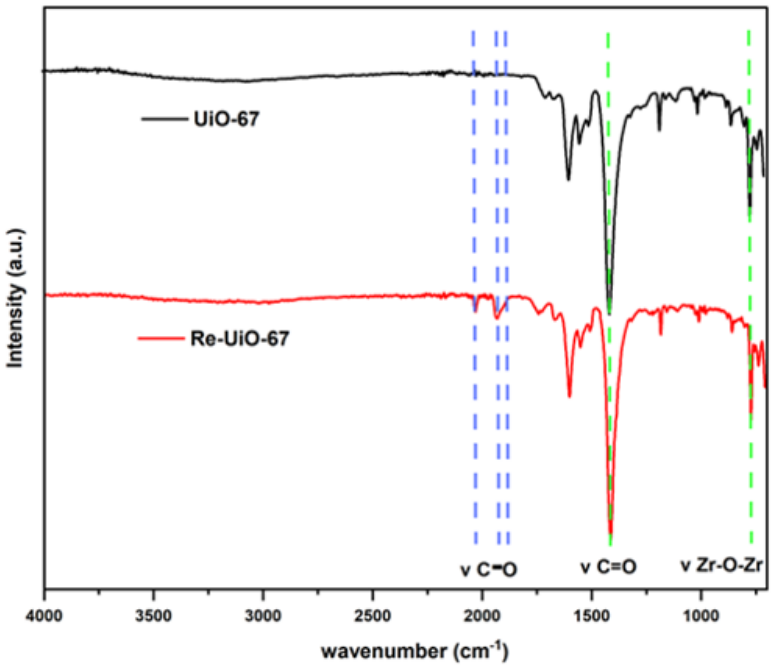

Figure 4.2. Infrared spectroscopy of UiO-67 and Re-UiO-67.

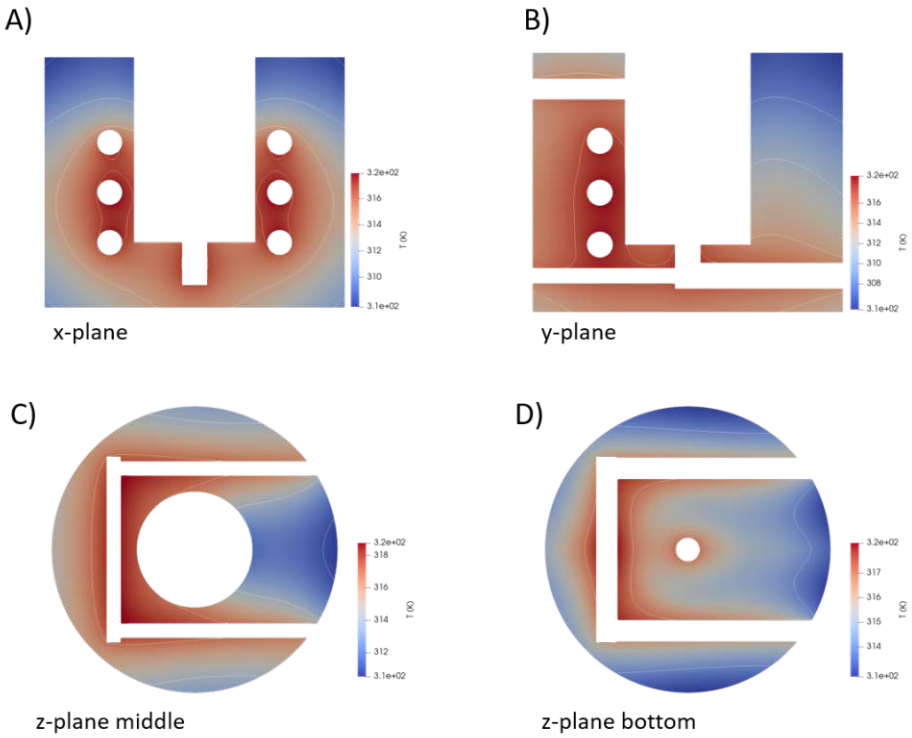

Figure 4.3. Simulation of temperature distribution in the reactor prototype made from POM with adapted geometry for a heating process from 293 K to 323 K over the time course of 1h with water heating.

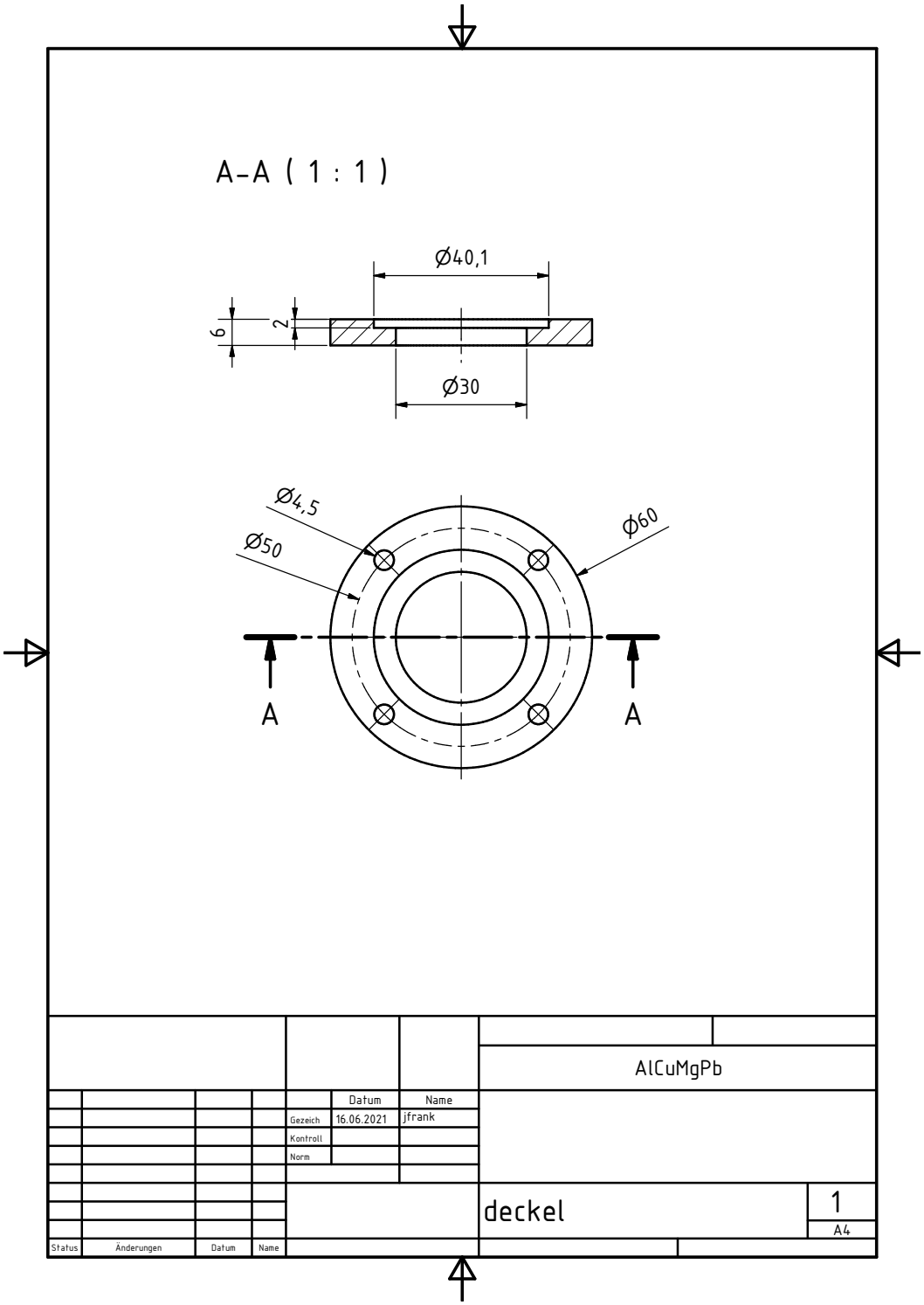

Figure 4.4. Technical drawing of the reactor lid.

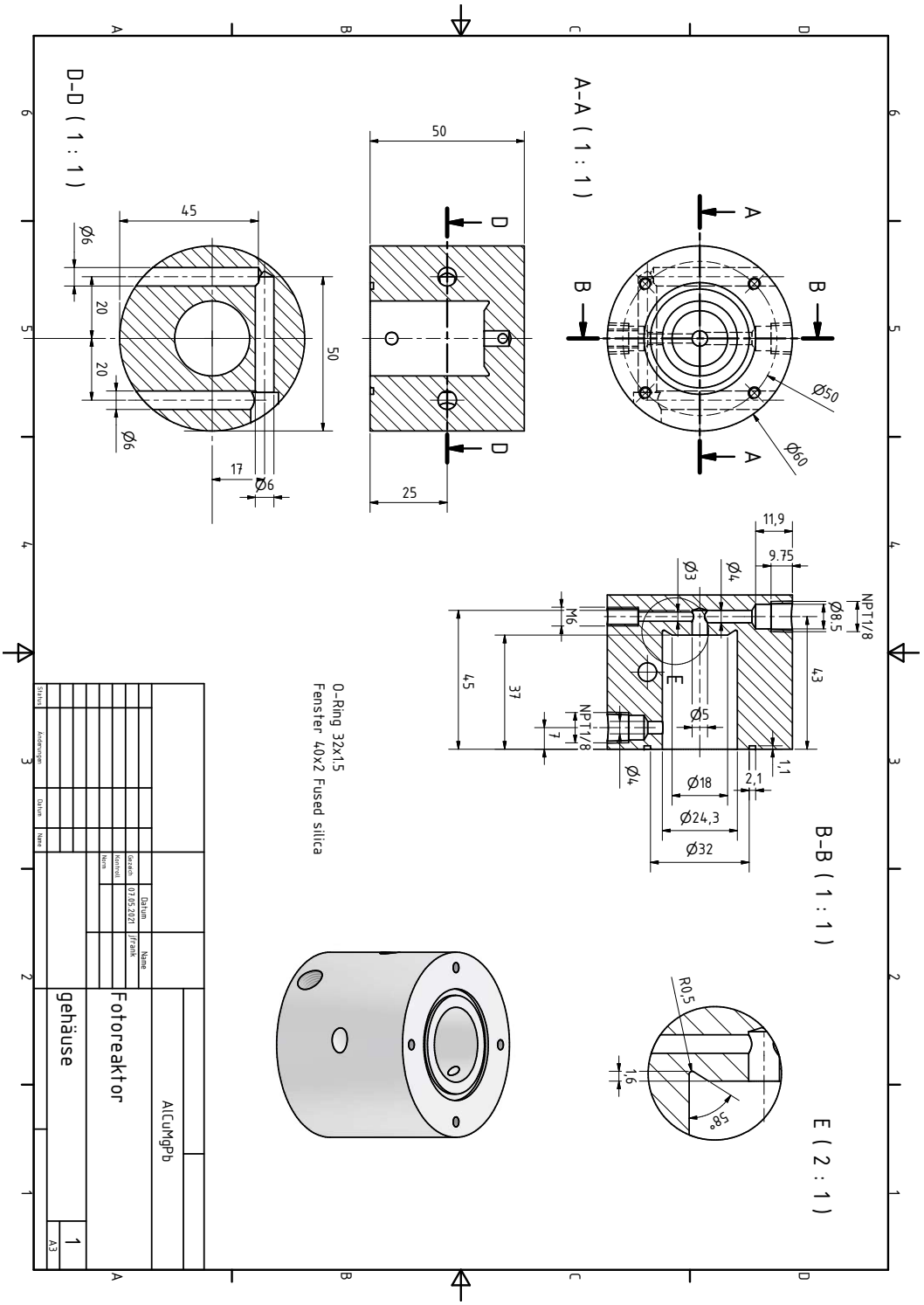

Figure 4.5. Technical drawing of the aluminium reactor prototype housing.

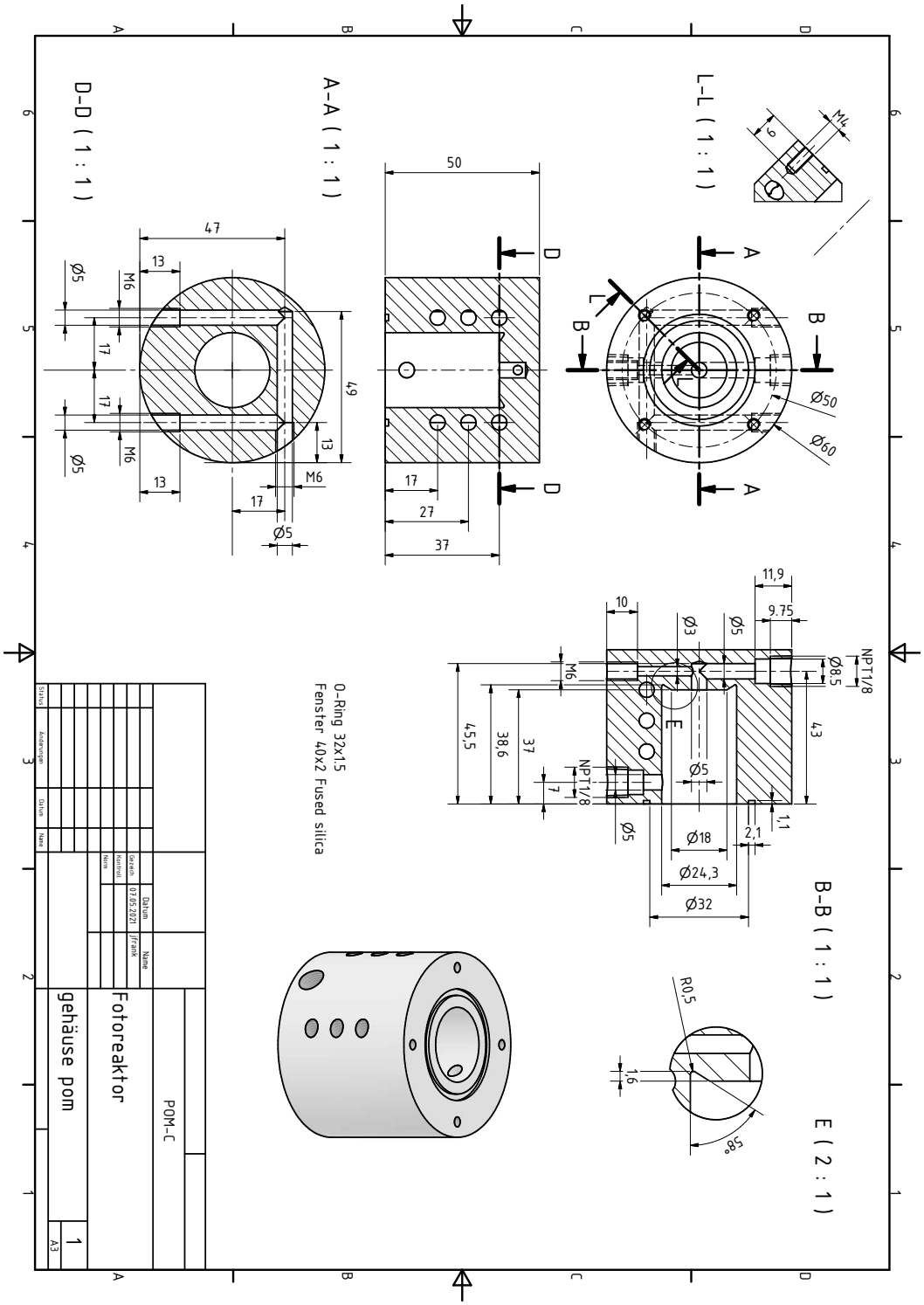

Figure 4.6. Technical drawing of the POM reactor prototype housing.

Experimental procedures for the Photo-SILP concept

Slurry phase reactions under GC sampling

Detailed description of the photoreactor and parameters of GC gas sampling are provided in chapter 3 in Section 1.

A stock solution of 3 mg mL^{-1} Re(bpy)$(CO)_3$Cl was prepared in a 5:1 mixture of DMF and TEOA. Graphitic carbon nitride (gCN) (6 mg) was mixed with 200 μL of stock solution and 1800 μL of the DMF and TEOA mixture. The suspension was sonicated for 10 minutes, and 1.5 mL of the mixture was transferred to the photoreactor. The reactor was purged for 5 minutes with a CO_2 flow of 10 mL min^{-1}. A reference sample of the reactor headspace was drawn and analyzed by headspace GC. The sample was illuminated for 1 hour with a 445 nm LED (Solis, Thorlabs) under water cooling at 22 °C. After 1 hour, illumination was terminated, and gaseous products were analyzed by headspace GC.

Photoreactions under continuous sampling with EMERSON flow cell

The reaction mixture was prepared as described above. The headspace of the septum sealed vial was purged with a mixture of 10% CO_2 in Argon at a gas flow of 30 mL min^{-1}. The reactor was connected to an EMERSON measurement cell (X-Stream XEGP) and the septum was sealed with wax. The gas flow was reduced to 15 mL min^{-1} for 45 minutes to equilibrate the baseline of the measurement cell. The reaction was illuminated at 445 nm (LED SOLIS Thorlabs) for two hours under water cooling at 15 °C. After two hours the LED was stopped and the detection of gaseous products was continued for another 30 min.